UNIVERSIDAD DE MÁLAGA

Programa de Doctorado en Biología Celular y Molecular

Departamento de Biología Molecular y Bioquímica

Facultad de Ciencias, Universidad de Málaga

TESIS DOCTORAL

Metabolic studies within the angiogenic microenvironment as a potential target for the treatment of cancer and other angiogenesis-dependent diseases

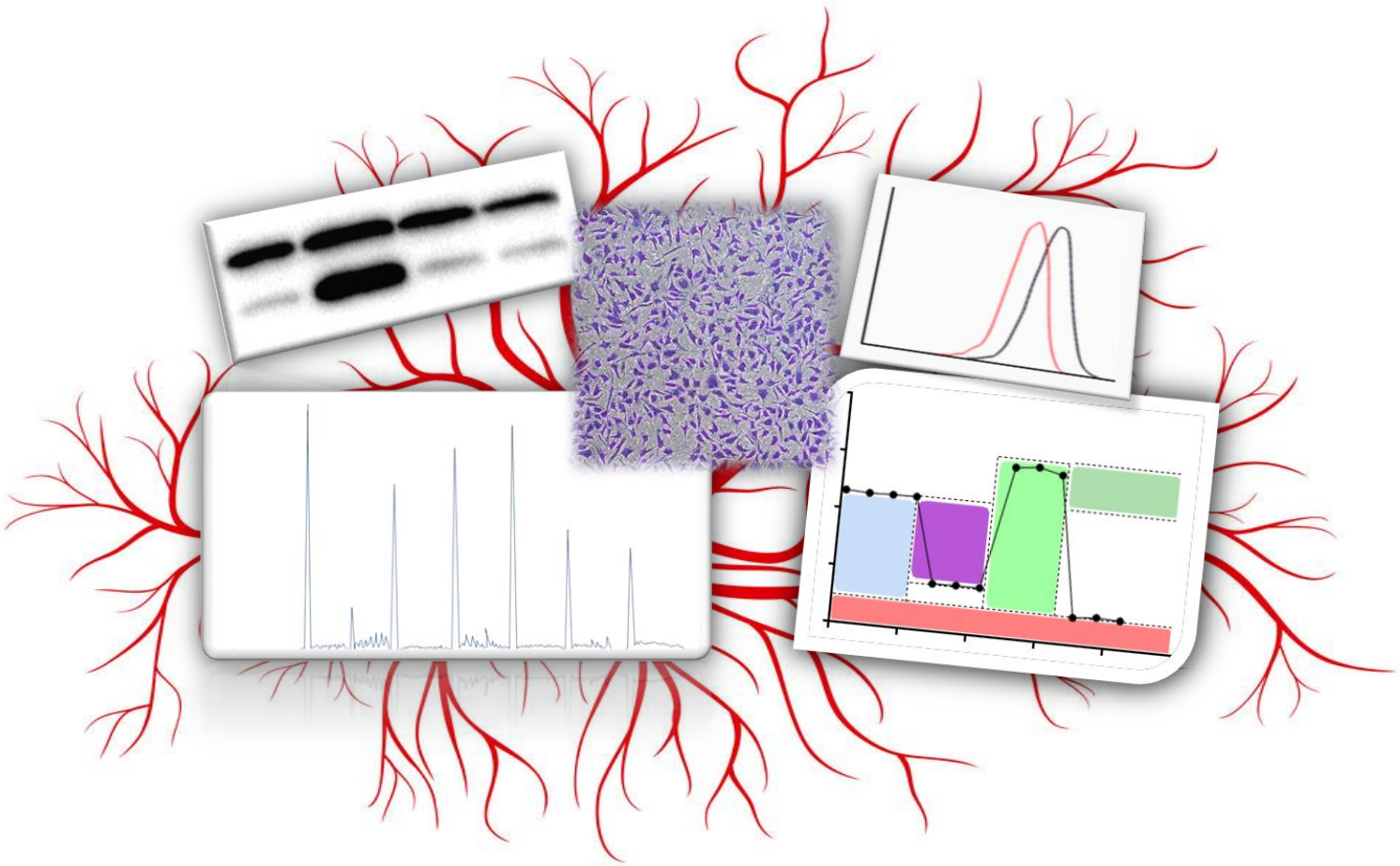

María del Carmen Ocaña Farfán

Director: Miguel Ángel Medina Torres

Marzo 2020

UNIVERSIDAD DE MÁLAGA

AUTOR: María del Carmen Ocaña Farfán

http://orcid.org/0000-0002-5468-5442

EDITA: Publicaciones y Divulgación Científica. Universidad de Málaga

UNIVERSIDAD DE MÁLAGA

Programa de Doctorado en Biología Celular y Molecular

Departamento de Biología Molecular y Bioquímica

Facultad de Ciencias, Universidad de Málaga

TESIS DOCTORAL

Metabolic studies within the angiogenic microenvironment as a potential target for the treatment of cancer and other angiogenesis-dependent diseases

María del Carmen Ocaña Farfán

Málaga, marzo de 2020

DECLARACIÓN DE AUTORÍA Y ORIGINALIDAD DE LA TESIS PRESENTADA PARA OBTENER EL TÍTULO DE DOCTOR

D./Dña MARÍA DEL CARMEN OCAÑA FARFÁN
Estudiante del programa de doctorado BIOLOGÍA CELULAR Y MOLECULAR de la Universidad de Málaga, autor/a de la tesis, presentada para la obtención del título de doctor por la Universidad de Málaga, titulada: METABOLIC STUDIES WITHIN THE ANGIOGENIC MICROENVIRONMENT AS A POTENTIAL TARGET FOR THE TREATMENT OF CANCER AND OTHER ANGIOGENESIS-DEPENDENT DISEASES

Realizada bajo la tutorización de MIGUEL ÁNGEL MEDINA TORRES y dirección de MIGUEL ÁNGEL MEDINA TORRES (si tuviera varios directores deberá hacer constar el nombre de todos)

DECLARO QUE:

La tesis presentada es una obra original que no infringe los derechos de propiedad intelectual ni los derechos de propiedad industrial u otros, conforme al ordenamiento jurídico vigente (Real Decreto Legislativo 1/1996, de 12 de abril, por el que se aprueba el texto refundido de la Ley de Propiedad Intelectual, regularizando, aclarando y armonizando las disposiciones legales vigentes sobre la materia), modificado por la Ley 2/2019, de 1 de marzo.

Igualmente asumo, ante a la Universidad de Málaga y ante cualquier otra instancia, la responsabilidad que pudiera derivarse en caso de plagio de contenidos en la tesis presentada, conforme al ordenamiento jurídico vigente.

En Málaga, a 6 de MARZO de 2020

Fdo.: MARÍA DEL CARMEN OCAÑA FARFÁN

A mi familia y amigos,

por todo su apoyo y compresión.

Caminante no hay camino,
se hace camino al andar.

(Antonio Machado)

El sentimiento es la raíz y el sustento de las ideas profundas.

(Eduardo Mendoza – Riña de gatos)

There is nothing like looking, if you want to find something.
You certainly usually find something, if you look,
but it is not always quite the something you were after.

(J.R.R. Tolkien – The hobbit)

UNIVERSIDAD
DE MÁLAGA

Por el presente documento, Don Miguel Ángel Medina Torres, catedrático del Departamento de Biología Molecular y Bioquímica de la Universidad de Málaga,

CERTIFICA

Que Dña. María del Carmen Ocaña Farfán, Licenciada en Biología por la Universidad de Málaga, ha realizado bajo su dirección el trabajo correspondiente a su Tesis Doctoral, que lleva por título «*Metabolic studies within the angiogenic microenvironment as a potential target for the treatment of cancer and other angiogenesis-dependent diseases*» en el Departamento de Biología Molecular y Bioquímica de la Universidad de Málaga.

Una vez revisado el trabajo, estimo que éste reúne contenido científico suficiente y las condiciones necesarias para ser presentado y defendido ante el tribunal correspondiente para optar al grado de Doctor Internacional.

Para que conste, a efecto de lo establecido en el Real Decreto regulador de los estudios de Tercer ciclo-Doctorado RD 99/2011, modificado por los Reales Decretos 534/2013, 43/2015 y 195/2016, AUTORIZO la presentación de esta Tesis Doctoral en la Universidad de Málaga.

Fdo: Miguel Ángel Medina Torres

Málaga, marzo de 2020

La presente Tesis Doctoral ha sido financiada por el proyecto BIO2014-56092-R (MINECO y FEDER) «Búsqueda de nuevas herramientas de intervención terapéutica para el control de la angiogénesis patológica», cuyo investigador principal es el Dr. Miguel Ángel Medina Torres; el proyecto P12 CTS 1507 (Junta de Andalucía) «Búsqueda y caracterización de nuevos fármacos inhibidores de la angiogénesis», cuya investigadora principal es la Dra. Ana Rodríguez Quesada; el proyecto UMA18-FEDERJA-220 (Junta de Andalucía y FEDER) «Estudio del potencial farmacológico de compuestos anti-angiogénicos para el tratamiento de la aterosclerosis», cuyos investigadores principales son Miguel Ángel Medina Torres y Beatriz Martínez Poveda; fondos del grupo BIO-267 (Junta de Andalucía y FEDER) y fondos del Plan Propio de Investigación y Transferencia (Universidad de Málaga). El director de la presente Tesis Doctoral es el líder del grupo U741 del CIBER de Enfermedades Raras (CIBERER). CIBERER es una iniciativa del Instituto de Salud Carlos III (ISCIII). La doctoranda María del Carmen Ocaña Farfán disfrutó de una ayuda para la formación de profesorado universitario (FPU) del Ministerio de Educación, Cultura y Deporte.

María del Carmen Ocaña Farfán realizó una estancia de una semana en el grupo de investigación de la Dra. Marta Cascante Serratosa en el Departamento de Bioquímica y Biomedicina Molecular de la Facultad de Biología de la Universidad de Barcelona (Barcelona, España), financiada por el proyecto BIO2014-56092-R (MINECO y FEDER), para llevar a cabo un estudio metabolómico en células endoteliales. Además, la doctoranda realizó una estancia de tres meses en el grupo de investigación del Dr. Ralph DeBerardinis en el *Children's Medical Center Research Institute* (CRI) de la Universidad de Texas SouthWestern (Dallas, Texas, Estados Unidos), financiada por las Ayudas de movilidad para estancias breves a beneficiarios del subprograma de formación del profesorado universitario (FPU) del Ministerio de Educación, Cultura y Deporte. Esta estancia le permitió aprender sobre técnicas de metabolómica y flujo metabólico utilizando espectrometría de masas, obteniendo resultados prometedores, así como optar a la obtención de la Mención Internacional de la presente Tesis Doctoral.

AGRADECIMIENTOS/ACKNOWLEDGES

Por fin ha llegado el momento de escribir esta parte de mi tesis, pues no solo significa que todo lo demás está hecho, sino que puedo agradecer a todos aquellos que habéis contribuido a que este libro sea una realidad. Porque todos sabéis que no ha sido fácil, que ha habido momentos buenos, momentos de celebración, pero también ha habido muchos momentos de estrés, de agobios, de fines de semana encerrada en el laboratorio, de vacaciones a medias o no vacaciones, y soy consciente de que algunos de vosotros habréis pagado el pato por mi estrés. Escriba lo que escriba en este libro no será suficiente para agradeceros la paciencia, el apoyo y la comprensión que habéis tenido conmigo durante estos casi cuatro años y medio.

No podría ser de otra manera que agradecer en primer lugar a la persona por la que puedo escribir estas palabras ahora mismo. Miguel Ángel, tú me acogiste cuando era una jovencísima alumna de carrera, hace ya más de siete años. Me diste la oportunidad de iniciarme en el mundo de los cultivos celulares y en la lectura crítica de artículos de investigación original. Gracias por confiar en mí, incluso en momentos en los que ni yo misma confiaba y en los que muchos otros me hubiesen abandonado. Siempre has intentado aumentar mi autoestima con alabanzas exageradas, has puesto plena confianza en mí, me has dado manga ancha en este camino el de la investigación y has apoyado y respetado todas mis decisiones. Para mí siempre serás mi padre científico. Gracias por todo.

Betty, llegaste al laboratorio como un ángel caído del cielo; siempre dispuesta a ayudar a esta pobre doctoranda llena de dudas. Has sido claramente una segunda directora de Tesis, aunque no conste oficialmente. Muchísimas gracias.

Gracias también a Ana R. Quesada, con la que siempre pude contar en momentos de necesidad. ¡Te deseo toda la suerte del mundo en tu aventura americana!

Y cómo no agradecer a todos aquellos con los que he estado, en mayor o menor medida, codo con codo en el laboratorio. José Joaquín, quien comenzó a enseñarme a «darle de comer» a mis celulitas. Paloma (Dra. Carrillo), hemos hecho la Tesis juntas de principio a fin, y siempre has sido de gran ayuda y apoyo; te deseo la mayor de las suertes con todo aquello que te propongas. José Antonio, nuestro hombretón en el laboratorio, incapaz de decir «no» y siempre lleno de buena voluntad y ganas de ayudar. A los *senior* que ya no están, pero que siempre han intentado ayudarme por correo si lo he necesitado: Mariavi, Melissa, Javi… A todos los técnicos/alumnos que han pasado

por el laboratorio, a los que he podido enseñar y/o que han podido enseñarme a mí: Laura, Alba, Clara, Cristina, Belén, Nicole, Ana D., Lorena... ¡Muchas gracias a todos por todo lo aprendido y por todas las risas compartidas!

Trabajar en las instalaciones del SCAI también me ha permitido conocer a otras personas maravillosas. Gracias por todas las conversaciones, las risas y el apoyo a otros usuarios de cultivos: Juan, Vicky, Virginia, Noela, Patri, Mamen, Lola, Baro… Gracias, Rosa (¡la próxima doctora serás tú, murciana!) y Yis. Gracias a Auxi, por mantener el servicio de cultivos de forma impecable, y por toda tu ayuda y soluciones a la infinidad de problemas que surgen en el camino. A Lara, por las risas y más risas, por tu infinita sinceridad, y por apoyarnos siempre a los que pasamos por el duro camino de la Tesis. Casimiro, no solo por el ensayo de proteómica ni por tu autógrafo, sino por transmitir siempre esa alegría que te caracteriza. David, nuestro MacGyver, ¡qué habría hecho yo sin tu ayuda con la citometría y la microscopía! Siempre tienes soluciones para todo. A Merche, Carolina, Reme, Sergio, Eli, y todos aquellos técnicos del SCAI que bien por utilizar sus servicios y/o bien por interesarse por cómo me iba han estado ahí.

Además, siempre he podido contar con algunos profesores de la Facultad para lo que necesitase. Gracias a José Luis Urdiales e Ignacio Fajardo, por aguantar todas mis dudas y echarme una mano en el laboratorio si lo necesitaba. Gracias a Ramón Muñoz-Chápuli, con quien pude tener un primer contacto como alumna interna cuando no tenía ni 20 añitos, y quien luego siempre estuvo dispuesto a resolver todas mis dudas. Manolo, gracias por toda tu ayuda con el pez cebra. Gracias a Nandi, por todas las maravillosas conversaciones que hemos tenido y por invitarme año tras año a enseñar lo que estaba en mi mano a sus alumnos. A José Manuel Matés, porque «me aproveché» de sus contactos y gracias a ello disfruté de una inolvidable experiencia.

I could not forget the amazing and rewarding experience I had during my three months fellowship in Dallas. Ralph, thank you so much for letting me stay in your lab; you are a magnificent researcher and a magnificent person. Chendong, I will never forget all the help you gave me in the lab; I learnt a lot from you and I could not have obtained all those results without you. Thanks to all the people in the lab who made my stay funnier: Bookyung, Aparna, Tracy, Cissy, Wen, Jerry… I miss you! And also thanks to the amazing people I met outside the lab: Rachael, Patrick, Michael and Uri. I hope we can see each other again some time!

Agradecer también a Marta Cascante por permitirme hacer el ensayo de Biocrates en su laboratorio. Muchas gracias, Silvia, por todo lo que aprendí de ti durante mi estancia en Barcelona.

Pero no todo en la vida es ciencia y laboratorio. También he contado con el apoyo de un montón de personas fuera del mundo de micropipetas y probetas. A algunos he tenido la suerte de conoceros durante mi paso por la facultad. Irene, Víctor y Bea, sois sin duda lo mejor que he sacado de la Licenciatura; Bea, gracias por todo lo vivido especialmente en los últimos dos años, y por cruzar el charco para verme. ¡Por muchos más viajes juntas! Fran, Jesús (Yisas) y Abel, mis bioquímicos, gracias por todo vuestro apoyo y ayuda, por todas las excursiones granaínas y malagueñas y por todas las que están por venir. Ana, la niña más dulce del universo, gracias por recibirme siempre en casa con una sonrisa. María, Eu(guay), Desi, Eu, gracias por seguir siempre ahí aunque me tire meses desaparecida.

Cómo olvidarme de a los que os conocí por otras maravillosas circunstancias de la vida. Jose (Platanito), mi compañero de penas, desgracias y alegrías de doctorandos, gracias por escucharme siempre. Gracias a mis amigos Carolina, Fran, Desi, Vampi, Rocío, Dani (Foley), Félix… Da gusto tener amigos como vosotros, con la paciencia que habéis tenido que tener para aguantarme durante estos años de Tesis.

Gracias a mi familia, especialmente a ti, mamá, por inculcarme desde pequeña la necesidad de formarme y de hacer lo que me gustara, sin importar lo que pensara la gente. Espero que estés orgullosa de ti, porque mis logros no son más que el reflejo de tu esfuerzo por intentar que sea la mejor versión de mí misma.

A Ángel, porque el último tirón sin ti hubiese sido aún más duro, pero estuviste ahí para hacerme la vida más fácil. No sabes la suerte que tengo de tenerte como compañero en la vida, sea cual sea la vida que elijamos.

ACC	Acetyl-Coenzyme A Carboxylase
Acetyl-CoA	Acetyl-Coenzyme A
ADMA	Asymmetric Dimethylarginine
ADORA2A	Adenosine A2a Receptor
Akt	Protein Kinase B
Alpha-AAA	Alpha-Aminoadipic Acid
ALT/GPT	Alanine Transaminase
AMD	Age-related Macular Degeneration
AMP	Adenosine Monophosphate
APS	Ammonium Persulfate
ARNT	Aryl-Hydrocarbon Receptor Nuclear Translocator
AST/GOT	Aspartate Transaminase
ATCC	American Type Culture Collection
ATP	Adenosine Triphosphate
BAEC	Bovine Aortic Endothelial Cell
βME	Beta-Mercaptoethanol
BrdU	5-Bromo-2'-Deoxyuridine
BSA	Bovine Serum Albumin
CAF	Cancer-Associated Fibroblast
CAM	Chorioallantoic Membrane
CA4P	Combretastatine 4-Phosphate
cDNA	Complementary Deoxyribonucleic Acid
CHC	α-Cyano-4-Hydroxycinnamate
CMP	Cytidine Monophosphate
CPT	Carnitine Palmitoyltransferase
Cq	Quantification Cycle
CVD	Cardiovascular Disease
DAG	Diglyceride
DCA	Dichloroacetate
DCFH-DA	2′,7′-Dichlorofluorescin Diacetate
dFBS	Dialyzed Fetal Bovine Serum
DFMO	Difluoromethylornithine
2-DG	2-Deoxyglucose

DHAP	Dihydroxyacetone Phosphate
DHFR	Dihydrofolate Reductase
DHODH	Dihydroorotate Dehydrogenase
DLL4	Delta Like Ligand 4
DMEM	Dulbecco's Modified Eagle Medium
DMF	Dimethyl Fumarate
DMSO	Dimethyl Sulfoxide
DNA	Deoxyribonucleic Acid
DOPA	Dihydroxyphenylalanine
Dpa	Days Post Amputation
DPBS	Dulbecco's Phosphate Buffer Saline
Dpm	Disintegrations Per Minute
EBM-2	Endothelial Cell Growth Basal Medium-2
EC	Endothelial Cell
ECAR	Extracellular Acidification Rate
ECGS	Endothelial Cell Growth Supplement
ECM	Extracellular Matrix
EdU	5-Ethynyl-2'-Deoxyuridine
EGF	Epithelial Growth Factor
EGM-2	Endothelial Growth Media-2
EHS	Engelbreth-Holm-Swarm
EMA	European Medicines Agency
EMEM	Eagle's Minimum Essential Medium
eNOS	Endothelial Nitric Oxide Synthase
EPC	Endothelial Progenitor Cell
ER	Estrogen Receptor
ERK	Extracellular Signal-Regulated Kinase
ETC	Electron Transport Chain
FABP	Fatty Acid Binding Protein
FAK	Focal Adhesion Kinase
FAO	Fatty Acid Oxidation
FAS	Fatty Acid Synthase
FAT	Fatty Acid Translocase

FBS	Fetal Bovine Serum
FCCP	Carbonyl Cyanide-4-(trifluoromethoxy)phenylhydrazone
FDA	Food and Drug Administration
FGF	Fibroblast Growth Factor
FIA	Flow Injection Analysis
FOXO1	Forkhead Box O1
GAPDH	Glyceraldehyde 3-Phosphate Dehydrogenase
GC/MS	Gas Chromatography/Mass Spectrometry
GDH	Glutamate Dehydrogenase
GFAT	Glutamine-Fructose-6-Phosphate Amidotransferase
GK	Glycerol Kinase
GLS	Glutaminase
GMP	Guanosine Monophosphate
GPAT	Glycerol-3 Phosphate Acyltransferase
G6PDH	Glucose 6-Phosphate Dehydrogenase
GPDH	Glycerol 3-Phosphate Dehydrogenase
GS	Glutamine Synthetase
GSH	Reduced Glutathione
GSR	Glutathione Reductase
GSSG	Oxidized Glutathione
HBP	Hexosamine Biosynthetic Pathway
HER2	Human Epidermal Growth Factor Receptor Type 2
HGF	Hepatocyte Growth Factor/Human Gingival Fibroblast
HIF	Hypoxia Inducible Factor
HK2	Hexokinase-II
HMEC	Human Microvascular Endothelial Cell
HMG-CoA	β-Hydroxy β-Methylglutaryl-CoA
Hpf	Hours Post Fertilization
HRE	Hypoxia Response Element
HRMS	High-Resolution Mass Spectrometry
HUVEC	Human Umbilical Vein Endothelial Cell
ICAM-1	Intercellular Adhesion Molecule-1
IC_{50}	Half Maximal Inhibitory Concentration

IDH	Isocitrate Dehydrogenase
iNOS	Inducible Nitric Oxide Synthase
ISV	Intersegmental Vessel
KLF2	Krüppel-Like Factor 2
LC3B	Light Chain 3B
LC/MS	Liquid Chromatography/Mass Spectrometry
LDH	Lactate Dehydrogenase
MAPK	Mitogen-Activated Protein Kinase
MCP-1/CCL2	Monocyte Chemoattractant Protein
MCT	Monocarboxylate Transporter
Met-SO	Methionine Sulfoxide
MMP	Matrix Metalloproteinase
mRNA	Messenger Ribonucleic Acid
MS	Mass Spectrometry
MSO	Methionine Sulfoximine
MTBSTFA	N-(Tert-Butyldimethylsilyl)-N-Methyltrifluoroacetamide
MT-MMP	Membrane-Type Matrix Metalloproteinase
MTT	3-(4,5-dimethylthiazol-2-yl)-2,5-Diphenyltetrazolium Bromide
NAC	N-Acetylcysteine
2-NBDG	2-(N-(7-Nitrobenz-2-oxa-1,3-diazol-4-yl)amino)-2-Deoxyglucose
NF-κB	Nuclear Factor Kappa B
nNOS	Neuronal Nitric Oxide Synthase
NO	Nitric Oxide
NOS	Nitric Oxide Synthase
Nrf2	Nuclear Factor Erythroid 2 (NF-E2)–Related Factor 2
OCR	Oxygen Consumption Rate
ODC	Ornithine Decarboxylase
OXPHOS	Oxidative Phosphorylation
oxPPP	Oxidative Pentose Phosphate Pathway
PAI	Plasminogen Activator Inhibitor
PBS	Phosphate Buffer Saline
PC	Pyruvate Carboxylase
PD-ECGF	Platelet-Derived Endothelial Cell Growth Factor

PDGFB	Platelet-Derived Growth Factor B
PDK	Pyruvate Dehydrogenase Kinase
PEDF	Pigment Epithelium Derived Factor
PFA	Paraformaldehyde
PFKFB	6-Phosphofructo-2-Kinase/Fructose-2,6-Biphosphatase
3-PG	3-Phosphoglycerate
PHD	Prolyl Hydroxylase
PHGDH	Phosphoglycerate Dehydrogenase
PhK	Phosphorylase Kinase
PHP	3-Phosphohydroxypyruvate
PI3K	Phosphoinositide 3-Kinase
PKC	Protein Kinase C
PKM2	Pyruvate Kinase M2
PlGF	Placental Growth Factor
PMA	Phorbol 12-Myristate 13-Acetate
PPP	Pentose Phosphate Pathway
PR	Progesterone Receptor
PRPP	Phosphoribosyl Pyrophosphate
PRPS1	Ribose-Phosphate Diphosphokinase
PSAT	Phosphoserine Aminotransferase
P-Ser	3-Phosphoserine
PSPH	Phosphoserine Phosphatase
PVDF	Polyvinylidene Difluoride
qPCR	Quantitative Polymerase Chain Reaction
R3-IGF-1	Recombinant Analog of Insulin-like Growth Factor-1
RNA	Ribonucleic Acid
RNase	Ribonuclease
ROS	Reactive Oxygen Species
RT	Room Temperature
SDMA	Symmetric Dimethylarginine
SDF-1/CXCL12	Stromal Cell-Derived Factor 1
SDS	Sodium Dodecyl Sulfate
SDS-PAGE	Sodium Dodecyl Sulfate-Polyacrylamide Gel Electrophoresis

SH2	Src Homology 2
SHMT	Serine Hydroxymethyltransferase
SGLT	Sodium-Glucose Linked Transporter
SLC	Solute Carrier
TAG	Triglyceride
TBS	Tris-Buffered Saline
TCA	Tricarboxylic Acid
TEMED	Tetramethylethylenediamine
TGFβ	Transforming Growth Factor Beta
THF	Tetrahydrafolate
TIC	Total Ion Current
TIMP	Tissue Inhibitor Metalloproteinase
TK	Tyrosine Kinase
TME	Tumor Microenvironment
TMP	Thymidine Monophosphate
TNBC	Triple Negative Breast Cancer
TNF-α	Tumor Necrosis Factor Alpha
tPA	Tissue Plasminogen Activator
TSP	Thrombospondin
UDP-GlcAn	Uridine Diphosphate-N-Acetylglucosamine
UMP	Uridine Monophosphate
uPA	Urokinase-Type Plasminogen Activator
uPAR	Urokinase-Type Plasminogen Activator Receptor
VCAM-1	Vascular Cell Adhesion Molecule-1
VEGF	Vascular Endothelial Growth Factor
VEGFR	Vascular Endothelial Growth Factor Receptor
VSMC	Vascular Smooth Muscle Cell

RESUMEN

INTRODUCCIÓN

1. El proceso angiogénico y enfermedades dependientes de angiogénesis

La angiogénesis es la formación de nuevos vasos sanguíneos a partir de un lecho preexistente, un proceso regulado por un balance de factores pro- y anti-angiogénicos secretados por las distintas células del microambiente angiogénico. Estas células incluyen células endoteliales, que son las responsables de la formación de estos vasos, y células del estroma, tales como pericitos, fibroblastos y células inmunes.

El proceso angiogénico se puede dividir en varias etapas: la activación del endotelio quiescente, la degradación de la matriz extracelular, la proliferación y migración de las células endoteliales y, por último, la morfogénesis y estabilización de los nuevos vasos sanguíneos. El diseño de fármacos inhibidores de angiogénesis implica la inhibición de al menos uno de estos pasos.

La activación de las células endoteliales se da por un balance a favor de los factores pro-angiogénicos, a menudo regulado por hipoxia. Las dos rutas de señalización más importantes en el proceso angiogénico son la ruta de VEGF/VEGFR2 y la de FGF-2/FGFR1. Éstas, a su vez, activan otras vías de señalización tales como ERK/MAPK y PI3K/Akt.

Para permitir la proliferación y migración de las células endoteliales, la matriz extracelular debe ser degradada. Las principales moléculas implicadas en la degradación de la matriz extracelular son el activador del plasminógeno tipo uroquinasa (uPA) y las metaloproteinasas de matriz extracelular (MMP). En concreto, la MMP-2 es la principal metaloproteinasa expresada por las células endoteliales. Por su parte, el uPA activa a las MMP. Por supuesto, es necesaria una regulación negativa de este proceso, que es llevada a cabo principalmente por los inhibidores tisulares de las MMP (TIMP) y los inhibidores del activador del plasminógeno (PAI).

Una vez degradada la matriz extracelular, las células endoteliales pueden adquirir dos fenotipos distintos: las células de la punta (*tip cells*) presentan una gran capacidad migratoria y van a la cabeza del frente, mientras que las células del tronco (*stalk cells*) son altamente proliferativas, establecen uniones adherentes y forman el lumen del nuevo vaso siguiendo a las células de la punta. La formación de estas células está regulada por las vías de señalización de Notch y DLL4, siguiendo un gradiente de VEGF. Además, la formación de uniones adherentes implica moléculas de adhesión tales como cadherina-VE, ICAM-1, VCAM-1 e integrinas.

Cuando los nuevos vasos sanguíneos están formados, se da un balance a favor de diversos inhibidores endógenos de la angiogénesis, las células endoteliales adquieren de nuevo un fenotipo quiescente, se sintetizan una nueva lámina basal y matriz extracelular y se reclutan a las células perivasculares.

Una desregulación en el balance entre factores pro- y anti-angiogénicos puede dar lugar a diversas patologías, conocidas como enfermedades dependientes de angiogénesis, bien por un defecto como por un exceso en el proceso angiogénico. El primer caso incluye enfermedades tales como la diabetes, el derrame cerebral, enfermedades neurodegenerativas, osteoporosis, isquemia o alopecia, mientras que en el segundo caso se recogen la artritis reumatoide, las retinopatías diabéticas, la endometriosis, la aterosclerosis, la degeneración macular asociada a la edad, la psoriasis, el cáncer y diversas patologías metabólicas, inflamatorias e infecciosas.

En el caso del cáncer, Judah Folkman estableció en 1971 que la angiogénesis era esencial para el desarrollo tumoral. De hecho, la angiogénesis se considera una de las señales distintivas del cáncer. El desarrollo de fármacos anti-angiogénicos podría, pues, emplearse en el tratamiento contra el cáncer. Sin embargo, a menudo esta aproximación terapéutica no es suficiente y se combina con radio-, quimio- o inmunoterapia. Más recientemente, se ha empezado a considerar el metabolismo de las células endoteliales como una diana potencial en el tratamiento de enfermedades dependientes de angiogénesis, incluyendo el cáncer.

2. Metabolismo en el microambiente angiogénico

El metabolismo de las células endoteliales ha cobrado importancia en investigación biomédica en los últimos años y ahora se considera una diana terapéutica en el tratamiento de enfermedades dependientes de angiogénesis. De hecho, se ha encontrado que varios compuestos moduladores del metabolismo presentan actividad anti-angiogénica. Es importante tener en cuenta que el metabolismo de las células endoteliales quiescentes difiere del de las células endoteliales activadas, estando mediado por factores de transcripción tales como FOXO1 y KLF2.

Basándonos en el metabolismo de las células endoteliales activadas, que son las que llevarán a cabo el proceso angiogénico, se sabe que estas células son altamente glucolíticas incluso en presencia de oxígeno (el conocido como efecto Warburg), tal y como ocurre en células tumorales. Es más, la inhibición de ciertos enzimas de la glucolisis, como la 6-fosfofructo-2-quinasa/fructosa-2,6-bisfosfatasa 3 (PFKFB3),

inhibe la angiogénesis. Por otra parte, la actividad glutaminasa (GLS) se considera sobreexpresada en células tumorales, y se ha visto que este enzima es importante también para el proceso angiogénico. En cuanto a los ácidos grasos, normalmente son utilizados para síntesis de lípidos en células tumorales, mientras que su oxidación es esencial para la proliferación y angiogénesis en células endoteliales. El lactato también puede oxidarse y, de hecho, existe un intercambio de metabolitos, incluyendo este ácido láctico, entre células tumorales y otras células del microambiente tumoral o incluso otras células tumorales. Sin embargo, se ha descrito que en células endoteliales el lactato extracelular puede incorporarse y regular vías de señalización implicadas en angiogénesis en lugar de usarse como sustrato oxidativo.

Además de estas rutas de obtención de energía, existen multitud de rutas metabólicas que generan distintos metabolitos esenciales para la correcta función celular. Por ejemplo, la glucosa 6-fosfato de la glucolisis puede destinarse a la vía de las pentosas fosfato (PPP), generando poder reductor en forma de NADPH, necesario en otras vías biosintéticas tales como la síntesis de lípidos, además de en la defensa contra el daño oxidativo. Además, mediante esta ruta se genera ribosa 5-fosfato, precursor del armazón principal en la síntesis de nucleótidos y coenzima A. El primer enzima de la ruta, la glucosa 6-fosfato deshidrogenasa (G6PDH), se considera esencial en el proceso angiogénico. Por otra parte, la glucosa 6-fosfato también puede utilizarse en la síntesis del glucógeno, cuyo metabolismo tiene cierta relevancia en células tanto tumorales como endoteliales. Otro intermediario de la glucolisis, la fructosa 6-fosfato, se utiliza en la ruta de síntesis de las hexosaminas (HBP), implicadas en la glucosilación de proteínas tales como VEGFR2, siendo, por tanto, una ruta metabólica esencial para la angiogénesis.

Si bien hay varios aminoácidos que se consideran esenciales y deben incorporarse con la dieta, hay otros que pueden sintetizarse a partir de estos u otros metabolitos. La alanina deriva del piruvato, mientras que el glutamato, la glutamina, la prolina, la arginina, el aspartato y la asparragina se producen a través de intermediarios del ciclo de Krebs o de otros aminoácidos. En el caso de la serina y la glicina, éstas se forman a partir del intermediario glucolítico 3-fosfoglicerato. El primer enzima de la ruta de síntesis de serina, la fosfoglicerato deshidrogenasa (PHGDH), es esencial en el proceso angiogénico. Además, serina y glicina participan en la síntesis de nucleótidos de base púrica, mientras que el aspartato lo hace en la de nucleótidos de base pirimidínica. Por tanto, estos aminoácidos tienen un papel esencial en la proliferación celular. La serina y

la glicina están, a su vez, implicadas en la síntesis de glutatión (GSH), molécula indispensable en la defensa contra el estrés oxidativo.

En cuanto a la síntesis de lípidos, la inhibición de varios enzimas implicados, tales como la ácido graso sintasa (FAS) y la acetil-CoA carboxilasa (ACC), afectan negativamente al proceso angiogénico. Por último, el metabolismo del colesterol se considera una diana terapéutica en el tratamiento de enfermedades dependientes de angiogénesis y cáncer.

MATERIAL Y MÉTODOS

1. Cultivos celulares y modelos animales

En esta Tesis Doctoral se han utilizado distintos tipos de células endoteliales, principalmente la línea endotelial microvascular humana HMEC, así como líneas tumorales, como la línea de cáncer de mama MDA-MB-231 y fibroblastos gingivales humanos, entre otras.

En cuanto a los modelos animales utilizados, se incluyen huevos de gallina fecundados, embriones de pez cebra transgénicos y adultos de pez cebra silvestres. En todos los casos se siguió la normativa ética establecida.

2. Ensayos *in vitro*

Los ensayos *in vitro* utilizados para la obtención de los resultados de la presente Tesis Doctoral incluyen ensayos de proliferación, supervivencia y ciclo celular. El ensayo MTT se utilizó para determinar la viabilidad celular tras la exposición a un compuesto o sustrato metabólico en diferentes condiciones experimentales. El efecto de distintos compuestos y/o sustratos metabólicos sobre la proliferación celular se estudió mediante la realización de curvas de crecimiento, así como mediante el uso del análogo de la timidina EdU en un ensayo de citometría de flujo. Por otra parte, el porcentaje de células en cada fase del ciclo celular pudo ser determinado también por citometría de flujo gracias al marcaje diferencial con yoduro de propidio.

2.1. Ensayos para el estudio de la angiogénesis

El estudio de la angiogénesis incluye multitud de aproximaciones experimentales *in vitro*. El ensayo de morfogénesis sobre Matrigel permite observar la inhibición, o no, en la formación de estructuras tubulares por parte de células endoteliales en cultivo. Una modificación de este ensayo discierne si dicha inhibición se causa por una disrupción de

las estructuras formadas. Para el estudio de la migración celular, se utilizaron dos experimentos distintos. El ensayo de la herida es una manera rápida y barata de observar un efecto sobre la migración celular. Debido a sus limitaciones, a menudo se acompaña de un ensayo de migración en cámara de Boyden, que posibilita alargar los tiempos de incubación y variar el estímulo para la migración de las células. La adición de Matrigel en el fondo de los insertos permite estudiar la capacidad invasiva de las células. Para la invasión, es necesario degradar la matriz extracelular, proceso en el que están implicadas diversas moléculas tales como la MMP-2 y el uPA. La producción y/o secreción de estas moléculas se puede determinar fácilmente mediante zimografías de gelatina y plasminógeno, respectivamente. Además, el receptor VEGFR2, que se activa mediante la fosforilación de residuos de tirosina, es esencial en el proceso angiogénico, y su activación se puede estudiar mediante el uso de kits comerciales, tales como el *VEGFR2 (KDR) Kinase Assay Kit* de BPS Bioscience.

2.2. Ensayos para el estudio del metabolismo

El estudio del metabolismo en células en cultivo se puede abordar de diferentes maneras. El analizador de flujo extracelular *Seahorse XF^{e}24* analiza dos parámetros: la tasa de consumo de oxígeno (OCR) y la tasa de acidificación extracelular (ECAR), correspondientes a la fosforilación oxidativa (OXPHOS) y a la fermentación láctica, respectivamente.

Ensayos más específicos incluyen estudios sobre la incorporación y/o utilización de sustratos metabólicos. En esta Tesis Doctoral se utilizaron aproximaciones experimentales mediante citometría de flujo, kits colorimétricos y fluorimétricos, metabolitos marcados con radioactividad (concretamente ^{14}C) y analizadores automáticos (como el NOVA) para estimar la incorporación de glucosa, glutamina y palmitato, así como la producción de lactato, glutamato y amonio. Además, la oxidación de glutamina se determinó gracias a la captura y medición de CO_2 marcado con ^{14}C procedente de glutamina radioactiva.

Otros experimentos más sofisticados permiten estudiar los niveles intracelulares de cientos de metabolitos en un único ensayo. Estos experimentos se basan en la utilización de técnicas de espectrometría de masas. Gracias a una breve estancia de cinco días en el grupo de Marta Cascante de la Universidad de Barcelona, se analizaron los niveles intracelulares de 188 metabolitos en células HMEC mediante el uso del *AbsoluteIDQ p180 kit* de la casa comercial Biocrates. Además, una estancia de tres

meses en el laboratorio de Ralph Deberardinis de la *University of Texas SouthWestern* (Dallas, Texas, Estados Unidos), permitió el análisis metabolómico y de flujo metabólico gracias al uso de metabolitos marcados con ^{13}C utilizando técnicas de espectrometría de masas acoplada a cromatografía de gases (GC/MS) o cromatografía líquida (LC/MS).

Además de todos estos ensayos, también se analizó la actividad enzimática de la PHGDH en extractos de células en cultivo gracias a un kit colorimétrico de la casa comercial BioVision. Por último, se midieron los niveles intracelulares de especies reactivas de oxígeno (ROS) mediante la detección fluorimétrica de diclorofluoresceína (DCF).

2.3. Ensayos de expresión de genes y proteínas

Tanto para el estudio de la angiogénesis como del metabolismo, es esencial determinar la expresión génica y/o de proteínas implicadas en estos procesos. En el caso de la expresión génica, se realizaron ensayos de PCR cuantitativa (qPCR), previa extracción del ARN mensajero y conversión a ADN complementario. Para la determinación de los niveles de proteínas, se realizó un estudio proteómico masivo mediante espectrometría de masas, llevado a cabo por el Servicio de Proteómica de la Universidad de Málaga. Para estudiar los niveles de proteínas concretas, se utilizó la técnica de *Western blot*, utilizando anticuerpos específicos para cada proteína.

3. Ensayos *in vivo*

En esta Tesis Doctoral también se realizaron ensayos de angiogénesis *in vivo*. En concreto, se estudió la angiogénesis en la membrana corioalantoidea (CAM) de huevos de gallina fecundados, así como la formación de vasos intersegmentales (ISV) utilizando embriones de pez cebra transgénicos que expresan una proteína fluorescente en células endoteliales. Adicionalmente, se utilizaron peces cebra silvestres adultos para el ensayo de regeneración de la aleta caudal.

RESULTADOS Y DISCUSIÓN

Capítulo 1: Estudios de preferencia metabólica en células tumorales

Los resultados recogidos en este capítulo forman parte del siguiente artículo:

- Mª Carmen Ocaña, Beatriz Martínez-Poveda, Ana R. Quesada, Miguel Ángel Medina (2020). Glucose favors lipid anabolic metabolism in the invasive breast cancer cell line MDA-MB-231. *Biology* 9(1), 16.

1. Introducción

El cáncer de mama es la segunda causa de muerte por cáncer en mujeres. Sin embargo, gracias a la investigación en este tipo de cáncer cada día la detección es más temprana y los tratamientos más eficaces. No obstante, no todos los tumores de mama son iguales. Su clasificación se basa, principalmente, en la expresión de determinados receptores: el receptor de estrógenos (ER), el receptor de progesterona (PR) y el receptor del factor de crecimiento epidérmico humano tipo 2 (HER2). Los tumores de mama que carecen de los tres receptores, los llamados tumores de mama triple negativo (TNBC de sus siglas en inglés), son a menudo los más agresivos y con peor pronóstico clínico. Un reciente estudio ha recopilado las diferencias metabólicas entre distintos tipos de cáncer de mama. Por tanto, el estudio del metabolismo de células tumorales de mama debe tener en cuenta los distintos subtipos existentes.

En esta Tesis Doctoral se ha elegido la línea de TNBC MDA-MB-231, que es altamente glucolítica, metastática e invasiva. En concreto, se ha estudiado su dependencia de glucosa y glutamina a largo plazo para la proliferación, y el uso de glucosa, glutamina y palmitato a corto plazo en diferentes escenarios de disponibilidad de sustrato, todo esto utilizando concentraciones fisiológicas de todos los sustratos metabólicos.

2. Resultados y discusión

Los resultados obtenidos en este capítulo pueden dividirse en dos apartados: los resultados de los ensayos a largo plazo y los de ensayos a corto plazo.

Los ensayos a largo plazo confirmaron el ya conocido efecto pro-apoptótico del palmitato en células MDA-MB-231 en ausencia de otros metabolitos que rescatan este efecto, como por ejemplo el oleato. Por ello, el uso de este ácido graso quedó relegado a ensayos a corto plazo. Por otra parte, estas células mostraron una total dependencia por glucosa y glutamina para su crecimiento, si bien la ausencia de glutamina causaba cambios morfológicos destacables en tan solo 24 h. Los resultados fueron similares con la línea de cáncer de mama ER positivo MCF7, aunque estas células podían crecer por un tiempo limitado en ausencia de glutamina pero no en ausencia de glucosa.

En cuanto a los ensayos a corto plazo, mediante distintas aproximaciones experimentales se confirmó la alta capacidad glucolítica de las células MDA-MB-231. El resultado más interesante fue el aumento en la tasa de incorporación de palmitato en presencia de glucosa extracelular, independientemente de su concentración. Este aumento se daba también en otras líneas de TNBC, como HCC1937 y MDA-MB-436, pero no en la línea ER positivo MCF7. Además, también aumentaba en otras líneas de cáncer invasivas como las células de adenocarcinoma de cuello de útero HeLa y las de neuroblastoma Kelly, mientras que no aumentaba en líneas no tumorales, como las endoteliales HUVEC. Estos resultados muestran una clara diferencia metabólica entre tumores de mama triple negativo y otros que no lo son.

Indagando en la posible causa para este aumento en la incorporación de palmitato, se vio que la ruta de señalización ERK, implicada en la disponibilidad en membrana de transportadores de lípidos como CD36 y FABP5, no se veía afectada por la presencia de glucosa. De hecho, esta glucosa debía ser metabolizada para ejercer su efecto sobre la incorporación de palmitato, ya que el inhibidor de la glucolisis 2-desoxiglucosa (2-DG) revertía el efecto. El inhibidor de la glicerol fosfato deshidrogenasa (GPDH) adipostatin A disminuía el efecto de la glucosa sobre la incorporación de palmitato, sugiriendo que la glucosa se metaboliza a glicerol 3-fosfato para la síntesis de triglicéridos y/o glicerofosfolípidos. La ausencia de fluorescencia en la membrana plasmática tras la incorporación de palmitato marcado con el marcador fluorescente BODIPY sugería que el palmitato incorporado en estas células se destinaba a triglicéridos.

Capítulo 2: Estudios de preferencia metabólica en células endoteliales

Fruto de los resultados contenidos en este capítulo se publicó un artículo de investigación original en la revista *Biomolecules*, indexada en *Journal Citation Reports* y perteneciente al primer cuartil.

- Mª Carmen Ocaña, Beatriz Martínez-Poveda, Ana R. Quesada, Miguel Ángel Medina (2019). Highly glycolytic immortalized human dermal microvascular endothelial cells are able to grow in glucose-starved conditions. *Biomolecules* 9:332.

1. Introducción

La relación entre angiogénesis y metabolismo endotelial ha llevado a un estudio exhaustivo de diferentes características metabólicas de células endoteliales. Sin embargo, en gran parte de los trabajos publicados se ha utilizado la línea de células

endoteliales macrovasculares HUVEC como modelo de estudio. Aunque es un modelo perfectamente válido, hay que tener en cuenta que la mayor parte de las patologías se deben a disfunciones a nivel de la microvasculatura. Además, se sabe que células endoteliales macrovasculares, de tamaño medio y microvasculares tienen diferentes características. En esta Tesis Doctoral se ha utilizado el modelo de célula endotelial microvascular HMEC, que facilita el trabajo al ser una línea inmortalizada, si bien ello conlleva analizar con cuidado los resultados obtenidos. Los efectos de distintos sustratos metabólicos, principalmente glucosa y glutamina, a largo y corto plazo han sido estudiados en estas células, así como su dependencia del lactato extracelular.

2. Resultados y discusión

Como ocurría con la línea tumoral MDA-MB-231, el palmitato también es tóxico para las células HMEC. Sin embargo, esta línea endotelial era capaz de crecer en ausencia de glucosa durante varios días incluso en condiciones de hipoxia, algo que no ocurría en otras líneas endoteliales y tumorales como BAEC o HeLa. Aumentar la concentración de glutamina o añadir piruvato al medio no favorecía el crecimiento de estas células. La ausencia de glucosa no afectaba a la distribución del ciclo celular ni a la migración en HMEC. Además, privar a las células de glucosa no inducía autofagia, con lo que algún mecanismo adicional debe ser el responsable para permitir el crecimiento de estas células en ausencia de glucosa.

Por otra parte, los resultados obtenidos para los experimentos a corto plazo sugieren que estas células son altamente glucolíticas, al igual que ocurre en el modelo macrovascular HUVEC. Además, ninguno de los tres principales sustratos metabólicos utilizados (glucosa, glutamina y palmitato) afectaba a la incorporación de los demás.

Respecto al metabolismo del lactato, se sabe que las células macrovasculares HUVEC presentan transportadores de incorporación de lactato MCT1. Sin embargo, su presencia en células endoteliales microvasculares solo se ha confirmado en tejidos oculares y de cerebro. Los resultados obtenidos en esta Tesis Doctoral apuntan a que las células HMEC no son capaces de incorporar lactato debido a la ausencia de transportadores MCT1 incluso en presencia de lactato extracelular. Por tanto, aunque se ha propuesto MCT1 como una diana terapéutica para enfermedades dependientes de angiogénesis, hay que tener en cuenta que no todas las células endoteliales podrían responder a este tratamiento.

Capítulo 3: Estudios de la posible actividad anti-angiogénica del fasentin, un inhibidor de GLUT1 y GLUT4

Los resultados de este capítulo forman parte de un manuscrito que se encuentra actualmente en una tercera fase de revisión en la revista *Scientific Reports*, perteneciente al primer cuartil de *Journal Citation Reports*.

- Mª Carmen Ocaña, Beatriz Martínez-Poveda, Manuel Marí-Beffa, Ana R. Quesada, Miguel Ángel Medina (2020). Fasentin diminishes endothelial cell proliferation, differentiation and invasion in a glucose metabolism-independent manner. *Scientific Reports* (en revisión).

1. Introducción

El fasentin (N-[4-cloro-3-(trifluorometil)fenil]-3-oxobutanamida) se ha descrito como un sensibilizador a los estímulos del receptor de muerte celular FAS. Se vio que este efecto es debido a una menor incorporación de glucosa en células tumorales. De hecho, un estudio *in silico* demostró que este compuesto se une físicamente al transportador de glucosa GLUT1, inhibiendo así su actividad. Sin embargo, la inhibición en la incorporación de glucosa era mayor en células que sobreexpresaban GLUT4, con lo que se consideró que el fasentin inhibía a ambos transportadores, GLUT1 y GLUT4, en células tumorales.

Se ha descrito que otros inhibidores de GLUT, como la silibinina, presentan actividad anti-angiogénica. Debido a la relación entre la angiogénesis y el metabolismo glucídico de células endoteliales, en esta Tesis Doctoral se estudió el posible efecto anti-angiogénico del fasentin.

2. Resultados y discusión

La primera aproximación experimental que se realizó fue un ensayo MTT para la determinación de la IC_{50} del fasentin en distintas líneas celulares. Este ensayo mostró un efecto inespecífico sobre la proliferación/muerte celular en líneas tumorales y endoteliales, siendo el efecto menor en fibroblastos. Mediante una modificación del ensayo MTT, así como la realización de curvas de crecimiento y un ensayo de proliferación utilizando el análogo de la timidina EdU, se confirmó que el fasentin inhibe la proliferación de células endoteliales de manera dependiente de concentración. Esta inhibición de la proliferación estaba acompañada de una parada en la fase G0/G1 del ciclo celular y una disminución del número de células en fase S.

Posteriormente, se eligieron varias dosis (25, 50 y 100 μM) para estudiar el posible efecto inhibidor de la angiogénesis del fasentin. Este compuesto inhibía la formación de estructuras tubulares sobre Matrigel totalmente a una dosis de 100 μM, pero no producía su disrupción. Su efecto *in vivo* es leve, provocando una desorganización de la vasculatura en el modelo CAM. Sin embargo, su efecto anti-angiogénico no pudo ser corroborado mediante el ensayo de formación de ISVs en el embrión de pez cebra, pues este compuesto a dosis iguales o superiores a 50 μM causaba efectos deletéreos o letales en el animal, y dosis menores no ejercieron ningún efecto. Aunque estas dosis también eran letales en el pez cebra adulto, el fasentin a 30 μM no afectaba a la viabilidad y disminuía la regeneración de la aleta caudal en este modelo.

Una vez corroborado el efecto del fasentin sobre la angiogénesis *in vitro* e *in vivo*, se procedió a estudiar las fases de la angiogénesis que se veían afectadas por este compuesto. Mientras que el fasentin no disminuía significativamente la capacidad migratoria de células endoteliales, sí que disminuía la producción de la MMP-2 y del uPA, moléculas directamente implicadas en la remodelación de la matriz extracelular. En consecuencia, el fasentin inhibía la capacidad invasiva de células endoteliales.

Sorprendentemente, el efecto del fasentin sobre la incorporación de glucosa era muy bajo en células HMEC. Esto podría explicarse por la presencia de transportadores GLUT14 en estas células, que podrían compensar la supuesta inhibición de GLUT1. Por tanto, otro mecanismo debe estar implicado en la inhibición, aún leve, de la angiogénesis por parte de este compuesto.

Se vio que el fasentin no afectaba a la actividad del receptor VEGFR2. En cuanto a dos de las rutas de señalización más estudiadas en el proceso angiogénico, el fasentin a 100 μM disminuía ligeramente la fosforilación de ERK, implicada mayormente en proliferación e invasión, mientras que este compuesto aumentaba la fosforilación de Akt de manera dependiente de concentración. Dado que la ruta de señalización de Akt también está implicada en el metabolismo de la glucosa, dando lugar a una mayor expresión de GLUT1, es posible que el fasentin, al inhibir GLUT1, provoque la activación de un mecanismo de compensación mediado por Akt. Sin embargo, el mecanismo concreto del fasentin sobre la angiogénesis de células endoteliales debe ser estudiado con mayor profundidad para poder sacar conclusiones.

Capítulo 4: Estudios de la posible actividad reguladora del metabolismo del dimetil fumarato

La mayor parte de los resultados contenidos en este capítulo constituyen un manuscrito ya elaborado y pendiente de ser enviado para su publicación en una revista de primer cuartil indexada en *JCR* a la mayor brevedad.

- Mª Carmen Ocaña, Chendong Yang, Beatriz Martínez-Poveda, Hieu S. Vu, Casimiro Cárdenas, José Antonio Torres-Vargas, Alba Subiri-Verdugo, Ralph DeBerardinis, Ana R. Quesada, Miguel Ángel Medina. The anti-angiogenic compound dimethyl fumarate inhibits the serine synthesis pathway and increases glycolysis in endothelial cells.

1. Introducción

El dimetil fumarato (DMF) es un derivado del ácido fumárico que constituye el principio activo del fármaco Tecfidera, utilizado en el tratamiento de la esclerosis múltiple, debido a su efecto inductor de la ruta de Nrf2. Además, este compuesto también se utiliza en el tratamiento de la psoriasis, una enfermedad inflamatoria que, además, es dependiente de angiogénesis. El DMF ha sido caracterizado como un compuesto anti-angiogénico gracias a la inhibición de VEGFR2. Asimismo, al poder metabolizarse en fumarato dentro de la célula este compuesto es capaz de alimentar al ciclo de Krebs y contribuir al metabolismo energético. Este hecho, sumado a la observada relación entre Nrf2 y la expresión de diversos genes del metabolismo y a la relación entre angiogénesis y metabolismo endotelial, sugiere que el DMF podría tener un efecto sobre el metabolismo energético de células endoteliales. Es más, se ha visto que este compuesto es capaz de inhibir la actividad del enzima gliceraldehído 3-fosfato deshidrogenasa (GAPDH) en macrófagos y de alterar el metabolismo energético de diversos tipos celulares de forma distinta. Por tanto, en este capítulo se recogen los resultados del estudio de los efectos del DMF sobre el metabolismo energético de la línea endotelial microvascular HMEC.

2. Resultados y discusión

Tras comprobar que el DMF era capaz de inhibir la formación de estructuras tubulares sobre Matrigel en la línea endotelial utilizada, se procedió a realizar un estudio de metabolismo energético general utilizando el analizador de flujo extracelular *Seahorse*. El DMF disminuía el consumo de oxígeno en estas células, mientras que

aumentaba su tasa glucolítica. Este aumento iba acompañado de una mayor incorporación de glucosa de manera dependiente de la dosis de DMF, que era sustancialmente mayor cuando las células eran tratadas con el compuesto durante una incubación larga, sugiriendo un efecto transcripcional. Este aumento en la incorporación de glucosa no era específico de células endoteliales, pues también se observó en células tumorales y en fibroblastos. Por otra parte, también se observó que en células endoteliales HMEC y HUVEC, así como en tumorales MDA-MB-231, la oxidación de glutamina era menor cuando las células habían sido tratadas previamente con DMF.

Gracias a un análisis proteómico se determinó que el DMF aumenta la expresión de los transportadores de glucosa GLUT1 y GLUT14 en HMEC, y una mayor expresión génica de *SLC2A1*, el gen que codifica para GLUT1, fue observada en células tratadas con DMF. Este aumento en la expresión de GLUT1 no se debía, sin embargo, a una regulación mediada por HIF-1α.

Un estudio metabolómico mostró que los niveles intracelulares de varios metabolitos se veían alterados tras un tratamiento con DMF. Entre ellos, destacan los menores niveles de aspartato, un metabolito esencial para la proliferación celular cuya síntesis se encuentra regulada por la cadena transportadora de electrones. Su síntesis a partir de glutamina se veía disminuida en células tratadas con DMF, como se pudo comprobar mediante un ensayo de flujo metabólico utilizando trazadores con ^{13}C.

Otro de los metabolitos cuyos niveles se veían afectados por el DMF es la glicina, presentando niveles ligeramente superiores. Sin embargo, la síntesis a partir de glucosa no solo de serina, sino especialmente la de glicina, se veía sustancialmente reducida en células tratadas con DMF, sin afectar a los niveles ni a la síntesis de 3-fosfoglicerato, el precursor glucolítico en la síntesis de estos aminoácidos. Esta disminución en la síntesis de serina y glicina se debía a una disminución en la actividad del enzima PHGDH, el primer enzima de la ruta de síntesis, en células tratadas con DMF, sin que se vieran afectados sus niveles de proteína ni el DMF afectase de forma directa a la actividad de la misma. Este resultado apunta a que la mayor tasa glucolítica no es un efecto directo de la inhibición de PHGDH, pues la línea de cáncer de mama MDA-MB-231 carece de este enzima, pero el DMF aumentaba su tasa de incorporación de glucosa. Además, las células endoteliales tratadas con DMF aumentaban la incorporación extracelular de serina y glicina, aunque los niveles de glicina eran menores que en el control en ausencia de serina extracelular, indicando que la glicina extracelular no es suficiente para suplir la inhibición en su síntesis.

El DMF inhibía drásticamente la capacidad proliferativa de estas células, en mayor medida en ausencia de serina y glicina extracelular, presentando una disminución en la tasa de síntesis de los nucleótidos de base púrica y, en menor medida, pirimidínica. El efecto en la proliferación no era rescatado por ácido fórmico, con lo que probablemente el enzima serina hidroximetiltransferasa (SHMT) no se vea afectada por el tratamiento con DMF.

Por otra parte, el DMF aumentaba el ratio glutatión reducido/glutatión oxidado (GSH/GSSG), sin disminuir los niveles de ROS, aunque la síntesis de GSH a partir de glucosa solo se veía afectada significativamente en ausencia de serina y glicina extracelular en células tratadas con DMF.

Por último, un análisis lipidómico permitió determinar que el DMF aumentaba los niveles de varios lípidos, especialmente de los glicerofosfolípidos, en estas células endoteliales, sin afectar a la incorporación de un ácido graso como es el palmitato.

Todos estos resultados apuntan a un importante efecto del DMF sobre el metabolismo energético no solo de células endoteliales, sino de varios tipos celulares. Sin embargo, el mecanismo exacto por el cual el DMF ejerce este efecto aún debe ser estudiado en profundidad.

INTRODUCTION

1. Angiogenesis

During the first steps of embryo development, blood vessels are created *de novo* by a process called vasculogenesis, in which the mesoderm differentiates into angioblasts, the endothelial precursor cells[1]. Once those blood vessels are formed, angiogenesis replaces vasculogenesis during the rest of embryo development, forming new blood vessels from the pre-vascular bed and thus expanding the vascular network[2,3]. This process is also given in adults in certain processes when nutrients and oxygen supply needs to be increased, such as wound healing, bone repair, and as a part of the reproductive cycle in women. However, it is important to take into account that in adults this process is transitory. The so-called angiogenic switch is fine-regulated by a balance of pro- and anti-angiogenic molecules secreted by several cells of the angiogenic microenvironment, composed by endothelial cells (ECs), stromal cells (mainly pericytes, fibroblasts and immune cells) and components of the extracellular matrix (ECM)[4-7]. A deregulation of this balance in favor of the anti-angiogenic molecules leads to an abnormal and permanently repressed angiogenesis, as is the case of ischemia, hypertension, cardiac failure, etc. In contrast, the prevalence of pro-angiogenic signaling results in an exacerbated, persistent and pathological angiogenesis, characteristic of several diseases, which will be further exposed later[8].

1.1. Physiology of angiogenesis

The angiogenic process is led by ECs. These cells are usually quiescent, but they can be activated by a prevalence of pro-angiogenic factors over anti-angiogenic signals. Then, these cells would degrade the ECM, proliferate, migrate and stabilize the new blood vessels. Due to this sequence of events, it could be considered that the angiogenic process is comprised by several steps that could be treated independently (**Figure 1**). The pharmacological treatment of angiogenesis is usually based on compounds that inhibit at least one of these steps[9].

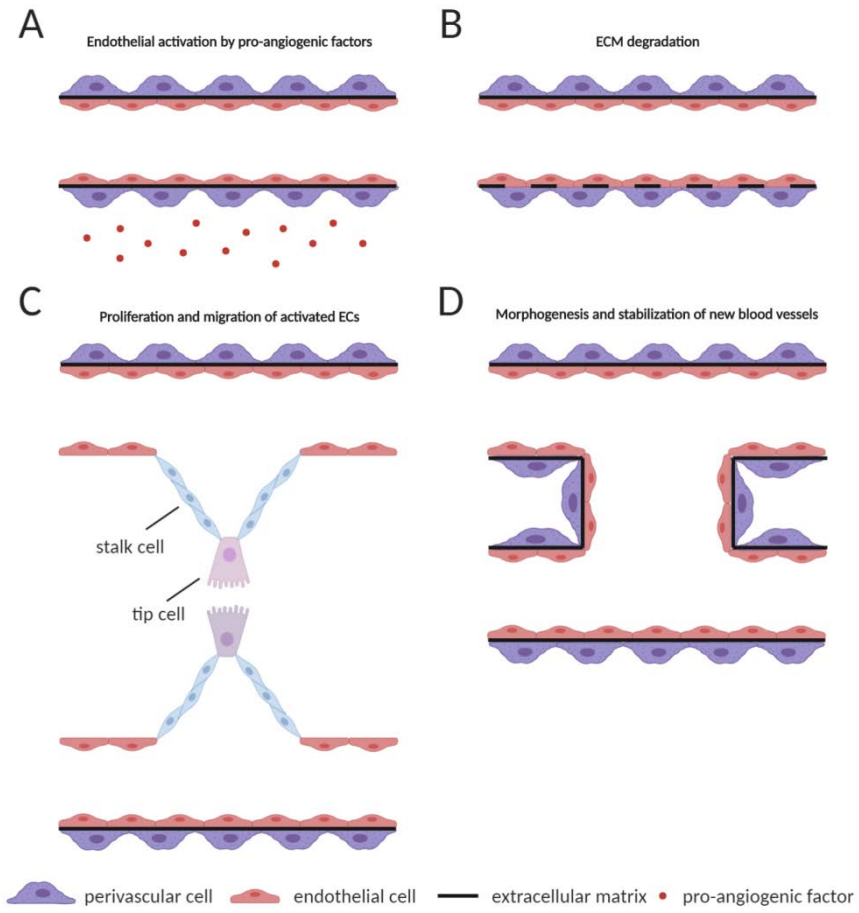

Figure 1. Physiology of angiogenesis. (A) Endothelial activation by pro-angiogenic factors. (B) Extracellular matrix (ECM) degradation. (C) Proliferation and migration of activated endothelial cells (ECs). (D) Morphogenesis and stabilization of new blood vessels. This figure was created with BioRender.com.

1.1.1. Endothelial cell activation

Under normal circumstances, ECs remain quiescent. However, after the angiogenic switch gets activated due to an unbalance in favor of pro-angiogenic factors the phenotype of these cells change in order to allow them to proliferate and migrate[4,7]. The acquisition of this specific phenotype of activated ECs would allow the design of anti-angiogenic drugs that recognize markers present specifically in these activated ECs but not in quiescent ECs. Some examples of these markers are HoxD3, integrin $\alpha_v\beta_3$, CD44, folistatin, monocyte chemoattractant protein (MCP-1) and thrombospondin (TSP-1). On the contrary, other molecules, such as the adhesion molecules E-selectin and ICAM-1, get repressed in these activated ECs[10].

1.1.1.1. Hypoxia

As mentioned above, the angiogenic process in adults gets triggered when the oxygen supply needs to be increased. Therefore, hypoxia is an important phenomenon involved in the activation of angiogenesis. Hypoxia inducible factor 1 (HIF-1) is the most known indicator of hypoxia. Indeed, in October of 2019 the discovery and association of HIF-1 to hypoxia, dated from 1995, was awarded the Nobel Prize in Physiology or Medicine[11]. This molecule is a heterodimer composed of an alpha and a beta subunit (HIF-1α and HIF-1β, respectively). HIF-1β (also known as ARNT –aryl hydrocarbon receptor nuclear translocator-) is constitutively expressed in cells, whereas HIF-1α is rapidly degraded in the presence of oxygen. Prolyl-hydroxylases (PHD) are the responsible of the labeling via hydroxylation of HIF-1α for its degradation in the proteasome in an oxygen-dependent reaction. Therefore, in the absence of oxygen or in hypoxia, PHD are unable to degrade HIF-1α, which translocates to the nucleus, binds HIF-1β and activates the transcription of several genes, including some involved in angiogenesis[12,13].

1.1.1.2. Angiogenic growth factors

During EC activation, several pro-angiogenic factors bind to their corresponding transmembrane receptors in ECs, leading to a series of signaling pathways cascades that will modify certain characteristics of these cells, such as their capability to proliferate and migrate towards the stimulus[14].

The most known pro-angiogenic molecules and their receptors are included in **Table 1**.

Classically, the vascular endothelial growth factor (VEGF) family has been described to be comprised by five different growth factors: VEGF-A, commonly known as VEGF since it was the first to be discovered, VEGF-B, VEGF-C, VEGF-D and placental growth factor (PlGF)[15,16]. Additional minor VEGF growth factors have been described afterwards[17,18]. VEGF is the most important member of this family and can bind to receptors VEGFR1 (Flt-1) and VEGFR2 (KDR or Flk-1), although VEGFR1 is considered a negative regulator of VEGFR2 and the signal transductions exerted by VEGF are mediated by VEGFR2[19,20]. Additionally, the gene codifying for VEGF contains hypoxia response elements (HRE) in its sequence, and thus HIF-1α modulates VEGF expression[21]. VEGF-B is specific of the myocardium and binds to VEGFR1 but not to VEGFR2[22]. VEGF-C and D are involved in the formation of lymphatic blood

vessels, a process known as lymphangiogenesis, through their binding to VEGFR3, although they can also bind to VEGFR2[23]. Conversely, PlGF acts on cell lines different from ECs and seems to be involved in placental angiogenesis[24].

Table 1. Pro-angiogenic molecules and their receptors in endothelial cells.

Pro-angiogenic molecules	Receptor in ECs
Angiopoietins (especially Ang-1 and Ang-2)	Tie2/Tek
EGF (Epithelial Growth Factor)	EGFR
FGF-2 (basic Fibroblast Growth Factor)	FGFR1-4
HGF (Hepatocyte Growth Factor)	c-Met
IL-1	-
IL-8	CXCR1-2
IL-15	-
PD-ECGF (Platelet-Derived Endothelial Cell Growth Factor)	-
PlGF (Placental Growth Factor)	VEGFR1 (Flt-1)
SDF-1 (Stromal cell-Derived Factor 1)	CXCR4
TGFβ (Transforming Growth Factor beta)	TGFβR2
TNF-α (Tumor Necrosis Factor alpha)	-
VEGF-A (commonly known as VEGF)	VEGFR2 (KDR or Flk-1)

The VEGF/VEGFR2 signaling network is the major activator of angiogenesis[25]. VEGFR2 is a tyrosine-kinase (TK) receptor, which dimerizes once VEGF binds it, and gets activated through phosphorylation of tyrosine residues within its intracellular domain[26]. After its activation, VEGFR2 is able to phosphorylate different proteins containing SH2 (Src Homology 2) domains in their structure[27]. Two of the main signaling pathways activated through VEGF/VEGFR2 are the extracellular signal-regulated kinase/Mitogen-activated protein kinase (ERK/MAPK) and the phosphoinositide 3-kinase/Protein kinase B (PI3K/Akt) signaling pathways, among others[14].

The FGF-2/FGFR1 signaling network is also important during the angiogenic process. Similar to VEGFR2, FGFR1 is a TK receptor which phosphorylates a series of molecules after its activation, triggering different signaling pathways, also including ERK/MAPK and PI3K/Akt[14]. Interestingly, the signaling mediated by FGFR1 is not limited to ECs, but it also involves changes in signaling pathways of vascular smooth muscle cells (VSMC)[28].

1.1.1.3. Endogenous angiogenesis inhibitors

Once the new blood vessels are formed, the endothelium needs to become quiescent again, since a maintained angiogenesis would lead to a pathological condition. In order for this to occur, there are several natural angiogenesis inhibitors that regulate this process. The first to be discovered was trombospondin-1, but there are more than thirty proteins and molecules involved in the physiological inhibition of angiogenesis[29]. Many of them are contained inside the ECM, which get liberated via proteolysis, but others include hormones, coagulation factors and immune system proteins[30]. **Table 2** shows some of the most relevant endogenous angiogenesis inhibitors.

Table 2. Most relevant endogenous angiogenesis inhibitors.

ECM derived			
Anastellin (fibronectin fragment)	Arresten		Canstatin
Endorepellin	Endostatin		Fibulin
Targeting fibronectin-binding integrins	Thrombospondin-1 and -2 (TSP-1 and -2)		Tumstatin
Growth factors and cytokines			
Interferons	Interleukins	Pigment epithelium derived factor (PEDF)	
Fragments of blood coagulation factors			
Angiostatin	Antithrombin III	Prothrombin kringle 2	Platelet factor-4
Others			
2-methoxyestradiol	Chondromodulin		16 kDa prolactin fragment (16K-PRL)
PEX (noncatalytic domain of MMP-2)	Plasminogen activator inhibitor (PAI)		Soluble version of VEGFR-1 (sFlt-1)
TIMPs (tissue inhibitors of metalloproteinases)	Troponin I		Vasostatin

1.1.2. Extracellular matrix degradation

After the activation of ECs and for the formation of a new blood vessel to occur, these ECs need to degrade the surrounding ECM. The degradation of the ECM is finely regulated by multiple proteolytic enzymes and inhibitor factors. Although ECM degradation is important for allowing ECs to proliferate and migrate, ECs also need portions of intact ECM to adhere in order to migrate. Moreover, there are molecules imbibed within the ECM that will get active once they get free after the ECM is degraded. These molecules include both pro- and anti-angiogenic factors[31,32]. For those

reasons, a fine regulation of ECM degradation is essential for maintaining a controlled angiogenic process.

In the ECM degradation there are several levels of regulation. First, several angiogenic factors and hypoxia induce the expression of urokinase-type plasminogen activator (uPA), its receptor (uPAR) and matrix metalloproteases (MMPs). The regulation of the expression of these molecules is exerted at the transcriptional level, more specifically through the transcription factor Ets-1[33]. Ets-1 is a target of the ERK-MAPK1/2 signaling pathway, which gets activated by the binding of VEGF and FGF-2 to their receptors[14]. Those molecules are secreted as inactive proenzymes that will need to get activated. Additionally, a negative regulation is exerted by endogenous inhibitors including tissue inhibitors of MMPs (TIMPs), plasminogen activator inhibitors (PAIs) and α2-antiplasmin.

MMPs are zinc-containing proteolytic enzymes able to degrade some of the components of the ECM (collagen, fibronectin, laminin), depending of the type of MMP. There are more than twenty MMPs described up to now, and not all of them are present in ECs[34]. The two more common MMPs expressed by ECs are MMP-2, also known as gelatinase-A, and MMP-9, also known as gelatinase-B. However, MMP-9 expression in adults is induced by pro-inflammatory cytokines or the protein kinase C (PKC) activator phorbol 12-myristate 13-acetate (PMA)[35]. MMP-2 is considered essential for the acquisition of the activated phenotype of ECs[36]. However, MMP-2 is secreted as an inactive zymogen. Activation of MMPs is regulated by membrane-type MMPs (MT-MMPs) and plasmin. MT1-MMP (MMP-14) activates MMP-2, and its activity is regulated by perivascular cells[37]. Additionally, tissue plasminogen activator (tPA) and uPA convert plasminogen into plasmin, a serine-protease similar to trypsin. This plasmin is able to activate pro-MMPs along with MT-MMPs, and thus they altogether contribute to the degradation of the ECM.

A negative regulation is exerted both at the levels of MMPs, mediated mainly by TIMPs, and of uPA, mediated by PAI. There are four types of TIMPs described in vertebrates, TIMP-1, -2, -3 and -4, that inhibit all MMPs except for TIMP-1, which does not affect MT1-MMP[38]. Apart from TIMPs there are other less-known inhibitors of MMPs, such as RECK (Reversion-inducing cysteine-rich protein with Kazal motifs)[39]. Regarding PAIs, PAI-1 is the most studied. Its function is to block the conversion of plasminogen to plasmin, thus inhibiting the proteolytic cascade through the activation of MMPs.

1.1.3. Proliferation and migration of endothelial cells

Once the ECM is degraded, ECs need to proliferate and migrate towards the angiogenic stimulus in order to form a new blood vessel. After EC activation, these cells can acquire two different phenotypes. During this branch elongation, the leading cells are called tip cells, distinguished by long filopodial protrusions and a highly migratory capacity. Immediately after them, the highly proliferative stalk cells trail tip cells, stablish adherent unions and form the lumen of the new blood vessel[40,41]. These different types of ECs found during the branch elongation are determined by different signaling molecules. Tip cells are characterized by a high DLL4 (Delta like ligand 4) expression, whereas stalk cells present high levels of Notch. This expression pattern is regulated by the VEGF gradient. Tip cells have the leading position and thus receive more VEGF that binds to VEGFR2, which in turn increases DLL4 expression in these cells, and this DLL4 induces Notch signaling in stalk cells. Notch inhibits VEGFR2 expression and increases VEGFR1, which acts as a negative regulator of VEGF and thus the stalk phenotype is maintained in these cells[42]. Consequently, the phenotypic specialization of ECs as tip or stalk cells is a dynamic and reversible phenomenon.

The migration of ECs comprises the formation of focal adhesions and the loss of adhesion. Therefore, it is a dynamic process which involves cell-cell adhesion molecules, such as VE-cadherin, intercellular adhesion molecule-1 (ICAM-1) and vascular cell adhesion molecule-1 (VCAM-1), as well as cell-ECM adhesion molecules, mainly integrins[43,44]. Due to this loss of adhesion, survival mechanisms get activated in order to prevent cell death. The most common signaling pathway for promoting EC survival during branch elongation is the PI3K-Akt signaling pathway[14,45]. Stalk cells need to proliferate following the lead of migratory tip cells[46]. This proliferation is regulated by the ERK signaling pathway, which also promotes the degradation of the ECM that allows this proliferation[14].

1.1.4. Morphogenesis and stabilization of new blood vessels

EC sprouting continues until tip cells connect with an adjacent vessel and undergo anastomosis, leading to the fusion of the new vessel and the adjacent vessel[47]. Then, ECs start the transition back to a quiescent phenotype and become phalanx cells, another kind of ECs which are non-proliferating and stabilize the structure of the new blood vessel through the increase in cell adhesion[48]. Due to the previous degradation of the ECM, a new basal membrane and ECM need to be synthetized[49]. The recruitment of

perivascular cells (pericytes and VSMCs) through secretion of factors such as platelet-derived growth factor B (PDGFB) and TGFβ1 is also essential for the stabilization of the new blood vessel[50-52]. Additionally, once the vessel is formed, blood pressure and flow play a crucial role in regulating the diameter of the new capillary[53].

1.2. Pathological angiogenesis

As already mentioned, the angiogenic process is finely regulated by a balance of pro- and anti-angiogenic molecules. The deregulation of this angiogenic switch leads to several pathologies, characterized by an insufficient or an excessive angiogenesis (**Figure 2**)[8]. Therefore, there are two different therapeutic approximations for the treatment of these diseases. The therapeutic angiogenesis, which turns on the angiogenic switch, would be applied in those diseases in which there are malformations in blood vessels or vascular regression due to an insufficient angiogenesis[5,54,55]. These diseases include diabetes, stroke, neurodegenerative disorders, osteoporosis, ischemia or alopecia. Conversely, several diseases are characterized by an excessive and abnormal angiogenesis. This group includes diseases such as arthritis, diabetic retinopathies, endometriosis, atherosclerosis, age-related macular degeneration (AMD), psoriasis, cancer and several metabolic, inflammatory and infectious disorders. In order to prevent and/or treat this kind of diseases the angiogenic switch should be turned off through anti-angiogenic therapy[56,57]. In our group, more than twenty synthetic and natural compounds have been described up to now to present anti-angiogenic activity through inhibition of different steps of this process[58-78].

1.2.1. Cancer and angiogenesis

In 1971, Judah Folkman stablished that angiogenesis was essential during tumor development[79]. Thirty years later, angiogenesis was considered as one of the hallmarks of cancer[80]. Tumors are formed from a unique cell that starts dividing without control. At some point, the cells within the tumor run into a lack of oxygen and nutrients due to the large distance between them and the blood vessels, and stop growing after the tumor reaches approximately 2 mm of diameter[79]. Then, mainly two factors contribute to the turning on of the angiogenic switch in order to allow maintenance of the tumor growth: hypoxia and pro-angiogenic factors secreted by tumor and surrounding cells. It is clear that the high growth rate of tumor cells would create an hypoxic area in the center of the tumor, which in turn would induce the angiogenic switch[81]. Additionally, tumor cells are known to secrete several pro-angiogenic factors, such as VEGF and FGF-2, partly

due to the upregulation of their expression mediated by oncogenes[82]. There are also some microRNAs expressed in tumors that modulate the expression of several pro- and anti-angiogenic factors[83]. Moreover, there are many other cells composing the tumor and/or the angiogenic microenvironment. These cells, such as immune cells and fibroblasts, also secrete pro-angiogenic factors that contribute to the turning on of the angiogenic switch[84].

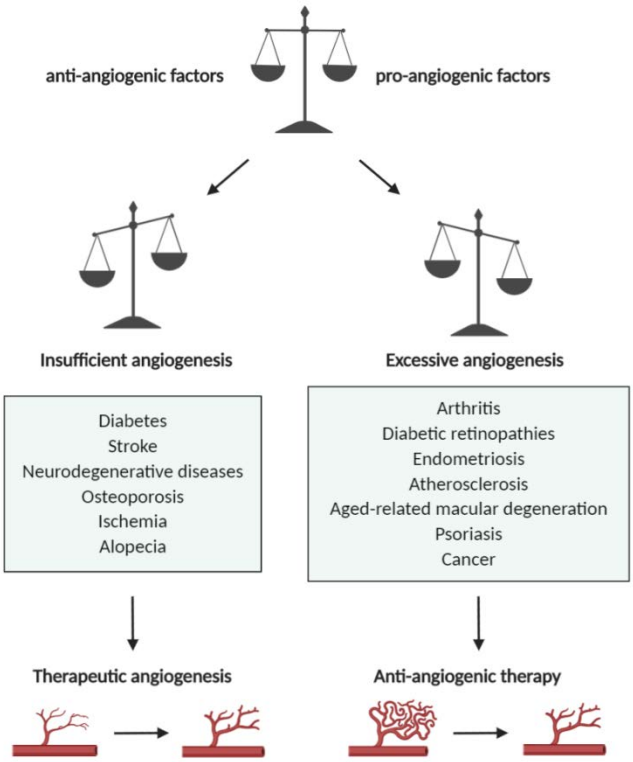

Figure 2. Pathological angiogenesis. The unbalance of anti- or pro-angiogenic factors leads to an insufficient or an excessive angiogenesis, characteristic of several diseases. Different therapeutic approximations are designed for the treatment of these diseases: therapeutic angiogenesis and anti-angiogenic therapy, respectively. This figure was created with BioRender.com.

However, the new vessels formed during tumorigenesis, in contrast with vessels formed in healthy situations, are disorganized, immature and permeable[85,86]. This is partly due to the lack of functional pericytes and the increase in their permeability[87,88]. Tumor cells would enter into the lumina of the blood vessels in a process called intravasation. Then, these cells would reach the tissue parenchyma of distant tissues, a process known as extravasation[89]. Therefore, the activation of angiogenesis would also lead to a metastatic phenotype.

The first described anti-angiogenic compounds date from the 1980s[90,91]. Angiogenesis has been considered an organizing principle for drug discovery for the treatment of several angiogenesis-dependent diseases[9]. Due to the high prevalence on cancer nowadays, many anti-angiogenic therapies have been developed in order to treat this disease. Targeting angiogenesis in a tumor context has a series of advantages: (1) Tumor cells are genetically unstable, whereas ECs are homogenous, genetically stable targets, reducing the possibilities of acquiring resistance to the drug; (2) activated ECs present specific markers not expressed in quiescent ECs and thus healthy ECs would not be affected by these treatments; (3) systemically administered drugs would reach ECs easily as these cells are in intimate contact with the blood circulation; (4) these anti-angiogenic therapies could be applied to different kinds of tumors[56].

Many synthetic and natural compounds present pre-clinical or clinical evidence for anti-angiogenic effects, and some of them have been approved by the FDA (Food and Drug Administration of the United States) for the treatment of cancer[92-94]. Interestingly, the Mediterranean diet is comprised by foods and seasonings that contain natural compounds with a proven anti-angiogenic and/or angiopreventive capacity in cancer. This was the main focus of a review article published in the journal *Nutrients* and forming part of this PhD Thesis (**Appendix 1**).

However, it should be taken into account that the anti-angiogenic therapy is often not enough for the treatment of cancer[95]. Anti-angiogenic therapies should be focused on the normalization of the vasculature in tumors rather than its total depletion[85,86]. Sometimes, the use of this therapeutic approximation could not lead to a recovery of the normal perfusion in tissue, but to an excess pruning or no change at all[96]. Therefore, additional strategies, such as classical radiotherapy or chemotherapy and the most recent immunotherapy, are being considered in the last years for the treatment of cancer alone or in combination with anti-angiogenic therapies[95,97-99]. Moreover, targeting ECs metabolism has emerged as a promising strategy for the treatment of angiogenesis-dependent diseases[100-103]. This last point will be further revised in a later section.

Additionally, there are tumors that are able to escape the anti-angiogenic therapy due to their capability to survive without inducing angiogenesis. Vascular mimicry and vessel co-option are two poorly-known non-angiogenic mechanisms given in those angiogenesis-independent tumors[104]. Vascular mimicry consists in the capability of cancer cells to form vascular channels in the absence of ECs[104,105]. Alternatively, some tumor cells are able to utilize pre-existing blood vessels to support tumor growth and

metastasis, in a poorly studied mechanism known as vessel co-option that was observed for the first time in the 19th century[106]. Therefore, anti-angiogenic therapies are useful in the treatment of cancer, but non-angiogenic mechanisms should also be considered as a therapeutic target for the recruitment of blood vessels (new or pre-existing) in cancer.

2. Metabolism within the angiogenic microenvironment

The metabolism of tumor cells has been widely studied since the last century. The studies performed by Otto Warburg, especially in his publications from 1925 and 1956, opened a new vision of metabolism. The so-called Warburg effect refers to the capacity of tumor cells to do glycolysis even in the presence of oxygen, a process known as aerobic glycolysis[107,108]. The role of glutamine in cancer has also been extensively studied[109-112]. Noticeably, the metabolic reprogramming of tumor cells was considered a new hallmark of cancer in 2011 along with immunosuppression[113].

However, the metabolism of ECs went almost unnoticed for many years, with some contradictory results[114-118]. In the last years, a considerable number of studies have been performed clarifying the metabolic features of these cells and its relation with the angiogenic process[119-123]. For instance, ECs need to produce ATP in order to migrate, since migration requires active remodeling of the cytoskeleton[124]. Additionally, several diseases, including cancer, have been associated to an EC metabolic deregulation[125]. Since then, the relation between EC metabolism and angiogenesis has gained great importance, and now novel therapies targeting different features of EC metabolism are being developed[101-103]. However, it is important to take into account that ECs may remain quiescent or start to proliferate after the angiogenic switch. The transcription factor forkhead box O1 (FOXO1) is considered a gatekeeper of endothelial quiescence, mediated by the downregulation of EC metabolism[126]. Another transcription factor, Krüppel-like factor 2 (KLF2), has a similar effect[127]. Therefore, metabolism of quiescent ECs is quite different from the one that present proliferating ECs[128]. After EC activation, tip, stalk and phalanx cells will acquire different metabolic features[129,130]. Nevertheless, contradictory results have been found[131].

For this PhD Thesis two review articles were written focusing on the metabolism within the tumor microenvironment (TME): a short review published in *Clinical Immunology, Endocrine & Metabolic Drugs* (**Appendix 2**), and an extensive review published later in *Medicinal Research Reviews* (**Appendix 3**). These reviews were focused on the TME, but most of the information contained in them also applies for the

angiogenic microenvironment, especially in a tumor context. Most of the main available information about metabolism within this microenvironment, as well as the interactions between the different cells of the microenvironment, is collected in the second review. A broad vision of the metabolism within the tumor and angiogenic microenvironment, as well as additional studies available after the publication of this review, will be exposed in a later section.

In this PhD Thesis, the attention was focused on the metabolism of two of the cell types present in an angiogenic microenvironment (in this case, a TME): tumor cells and ECs. **Chapter 1** on the Results and Discussion section shows the importance of glucose for lipid synthesis in the highly invasive breast tumor cells MDA-MB-231, whereas **Chapter 2** collects some aspects of glucose metabolism in immortalized microvascular ECs.

2.1. Glycolysis

Glucose is one of the main metabolic fuels in animal cells. Glucose from the diet enters the cell through glucose transporters from the solute carrier (SLC) superfamily. Glucose transporters divide into two families: the secondary sodium-glucose linked transporter (SGLT, family name SLC5A) and the facilitative glucose transporter (GLUT, family name SLC2A). Another transporter named SWEET (SLC50A1) has been reported in plants, but its presence in human cells has not been identified so far[132]. GLUTs constitute the most studied glucose transporters family. To date, fourteen members of the GLUT family have been identified, namely GLUT1-14[133]. These transporters are tissue specific, except for the ubiquitous GLUT1. Most tumor cells increase their glucose uptake, helped by an overexpression of glucose transporters, especially GLUT1 and GLUT3 in the corresponding tissues[132]. ECs predominantly express GLUT1, although vessels from the placenta and the brain are dependent on GLUT3[134]. Additionally, SGLT transporters are being considered a novel therapeutic target in diseases such as cancer or type 2 diabetes[135,136].

Glucose within the cell is rapidly converted into glucose 6-phosphate through hexokinase activity. Through several additional reactions represented in **Figure 3**, this glucose is converted into two molecules of pyruvate. This pyruvate will be later oxidized into acetyl-coenzyme A (acetyl-CoA) and incorporated into the tricarboxylic acid (TCA) cycle for glucose oxidation (see section 2.2.1 of Introduction) or converted into lactate in a reaction catalyzed by lactate dehydrogenase (LDH). There are two

isoforms of LDH: LDH-A converts pyruvate into lactate, whereas LDH-B catalyzes the reverse reaction.

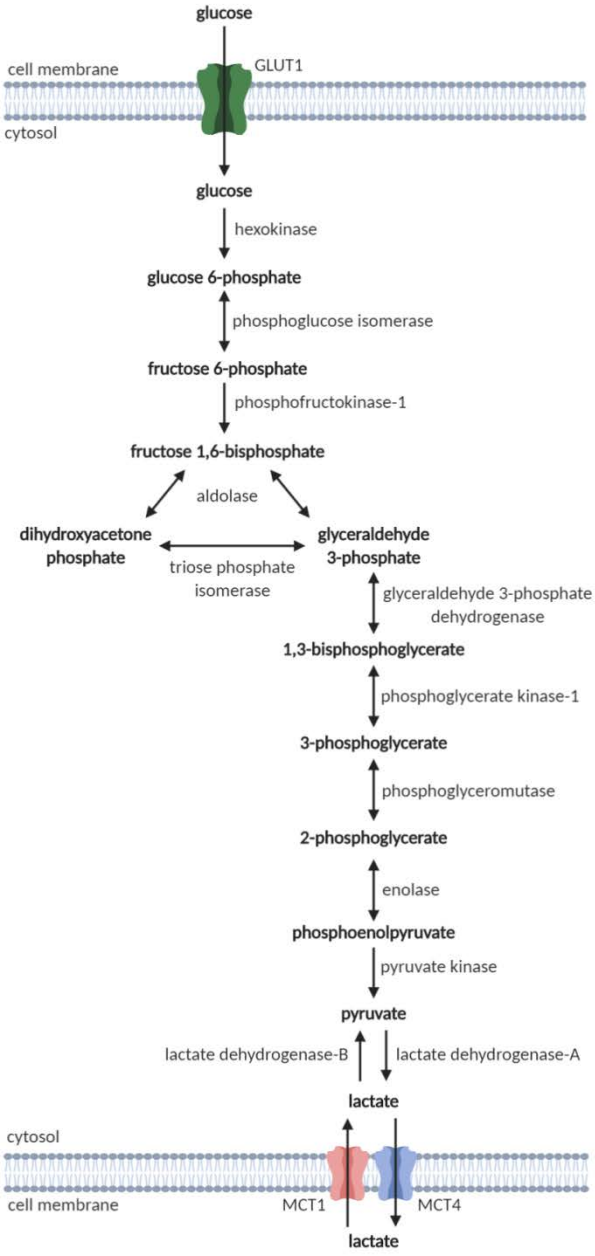

Figure 3. Glycolysis and lactate production from glucose.

Originally, production of lactate from glucose via glycolysis was defined as a metabolic process given only in the absence of oxygen (i.e. hypoxia) due to the Pasteur effect[137]. However, Otto Warburg observed in the first half of the 20th century that cancer cells were able to convert glucose into lactate even in the presence of oxygen, a process that was called aerobic glycolysis[107,108]. Nowadays it is known that not only cancer cells can rely on aerobic glycolysis, but also other cells of their

microenvironment, including immune cells and ECs[121,138,139]. For instance, inhibition of adenosine A2a receptor (ADORA2A), a regulator of several glycolytic enzymes through activation of HIF-1α, impairs EC migration[140]. Moreover, pro-angiogenic factors such as VEGF and FGF-2 increase the expression of glycolytic enzymes[121,141].

2.2. Tricarboxylic acid cycle

2.2.1. Glucose oxidation

As already mentioned glucose-derived pyruvate can be oxidized to acetyl-CoA and enter the TCA cycle in the mitochondria (**Figure 4**). This cycle is considered the central metabolic hub of the cell under aerobic conditions and it constitutes a major anaplerotic pathway. Some intermediates can leave the cycle and convert into other molecules involved in the synthesis of amino acids, lipids, nucleotides and heme.

Some of the reactions of this cycle are catalyzed by NAD(P)- or FAD-dehydrogenases, i.e. enzymes that oxidize a substrate while reducing $NAD(P)^+$ or FAD into their reducing equivalents NAD(P)H or $FADH_2$. In the presence of oxygen, the electrons that have been transferred to these reducing equivalents flow through an electron transport chain (ETC) in the inner mitochondrial membrane. Then a proton gradient is created, allowing the generation of adenosine triphosphate (ATP) linked to the presence of an ATP synthase at the end of the ETC. This process was first described by Peter Mitchell with his chemiosmotic theory in 1961[142]. The whole process is known as oxidative phosphorylation (OXPHOS).

The amount of ATP generated in a metabolic pathway will depend not only on the ATP produced during the reactions of the route *per se*, but also on the amount and type of reducing equivalents generated in the dehydrogenase reactions. The total oxidation of one mole of glucose can produce up to 30 or 32 moles of ATP. In contrast, only 2 moles of ATP are generated through glycolysis. Thus, it would seem that glycolysis is energetically more inefficient than OXPHOS. Surprisingly, observations made by Otto Warburg showed that cancer cells were able to produce more ATP from aerobic glycolysis than from respiration[107]. Indeed, it has been shown that glycolysis allows a faster generation of ATP[143]. This fact, along with the biosynthetic pathways diverging from glycolysis (see sections below), explains why a high glycolytic rate is efficient not only in cancer cells, but also in other non-tumorigenic cells that rely on glycolysis.

2.2.2. Glutamine oxidation

Glucose is not the only metabolic substrate that can enter the TCA cycle. Glutamine is the most abundant free amino acid in the blood and the most efficient vehicle for the transport of nitrogen between tissues, along with alanine[109,111]. There are fourteen glutamine transporters described in mammalian cells[144]. Additionally, glutamine can be synthetized from glutamate in a reaction catalyzed by the enzyme glutamine synthetase (GS). Once glutamine is available inside the cell, it can be used as a respiratory substrate, but it is also involved in other metabolic pathways[145].

First, glutamine needs to be converted into glutamate through glutaminase (GLS) activity. Four isoforms of GLS has been described so far: two encoded by the human *GLS* gene and two by the *GLS2* gene. GLS, especially the isoforms from the *GLS* group, has been shown to be upregulated in tumor cells compared to non-malignant cells[146,147]. Additionally, inhibition of GLS impairs tube formation by ECs, pointing out to the importance of glutamine metabolism in angiogenesis[122]. Interestingly, GS inhibition in ECs leads to EC migration impairment in a way that is independent of glutamine synthesis[148].

Glutamine can feed the TCA cycle through conversion of glutamate to α-ketoglutarate in a reaction catalyzed by the enzyme glutamate dehydrogenase (GDH). This α-ketoglutarate can also be synthetized from glutamate through transaminases. In the direction of α-ketoglutarate synthesis, alanine transaminase (ALT/GPT) converts pyruvate into alanine, and aspartate aminotransferase (AST/GOT) converts oxaloacetate into aspartate[149]. Once inside the TCA cycle, glutamine carbons can be oxidized for energy production and the TCA intermediates can follow different anaplerotic routes (**Figure 4**).

Besides the relevance of the Warburg effect in tumor metabolism, some tumors are not glycolytic and they rely on glutamine oxidation[150]. Additionally, most proliferative tumor cells are glutamine addictive, leading to consider glutamine metabolism as a therapeutic target in cancer[151,152].

2.2.3. Fatty acid oxidation

Fatty acids can also be oxidized in order to generate energy and/or intermediates in the TCA (**Figure 4**). Although the transport of external fatty acids across the cell membrane had been long thought to occur by passive diffusion, nowadays it is known

that a number of different membrane-associated transporters are involved in this process[153]. CD36 seems to be the major fatty acid transporter in ECs[154].

Fatty acids cannot be directly incorporated into the TCA. For that reason, they need to be first converted into acetyl-CoA in a process known as β-oxidation (also fatty acid oxidation, FAO). This pathway takes place in the mitochondrial matrix. However, long fatty acid chains cannot go through the mitochondrial membrane and need to be converted into fatty acyl-CoAs in a reaction that consumes ATP. Then, these fatty acyl-CoAs will stay in the cytosol for lipid synthesis (see section 2.9 of Introduction) or enter the mitochondria for β-oxidation. In order to enter the mitochondria, fatty acyl-CoAs are transferred to carnitine through carnitine palmitoyltransferase 1 (CPT1) activity, shuttled inside the mitochondria by a translocase, and liberated as free fatty acyl-CoAs mediated by the carnitine palmitoyltransferase 2 (CPT2) reaction. Once inside the mitochondria, fatty acyl-CoAs suffer a complex process in order to generate acetyl-CoA.

In highly proliferative cancer cells, fatty acids are often used for lipid synthesis rather than for oxidation[155]. However, different tumors or even cells within a particular tumor can present different metabolic features. Therefore, FAO is also considered a therapeutic target in this disease[156]. Furthermore, FAO has been shown to be essential for EC proliferation and vessel formation due to its role in nucleotide synthesis. Interestingly, the effects of FAO blockade could not be compensated by glucose or glutamine oxidation[123]. Moreover, pro-angiogenic factors such as VEGF and FGF-2 induce the expression of fatty acid transporters in ECs, and inhibition of these transporters diminishes EC proliferation and angiogenesis[157,158].

2.2.4. Lactate oxidation

Apart from these three main metabolic fuels, some cells are also able to oxidize extracellular lactate. Lactate can be taken up from the media through monocarboxylate transporter 1 (MCT1), whereas its secretion is mediated mainly by MCT4. Once incorporated into the cell, lactate can be converted into pyruvate through LDH-B activity. This pyruvate will be later converted into acetyl-CoA and incorporated into the TCA cycle (**Figure 4**).

In some tumors, both glycolytic and oxidative tumor cells coexist, and a metabolic symbiosis is stablished between them. One of the metabolites shared between these two kinds of tumors cells is lactate[159,160]. ECs do not oxidize lactate when glucose is present

in the media[115]. However, uptake of extracellular lactate has been shown to trigger angiogenesis[161-163]. Therefore, whereas lactate can fuel tumor cells, its role in ECs is independent of its oxidation.

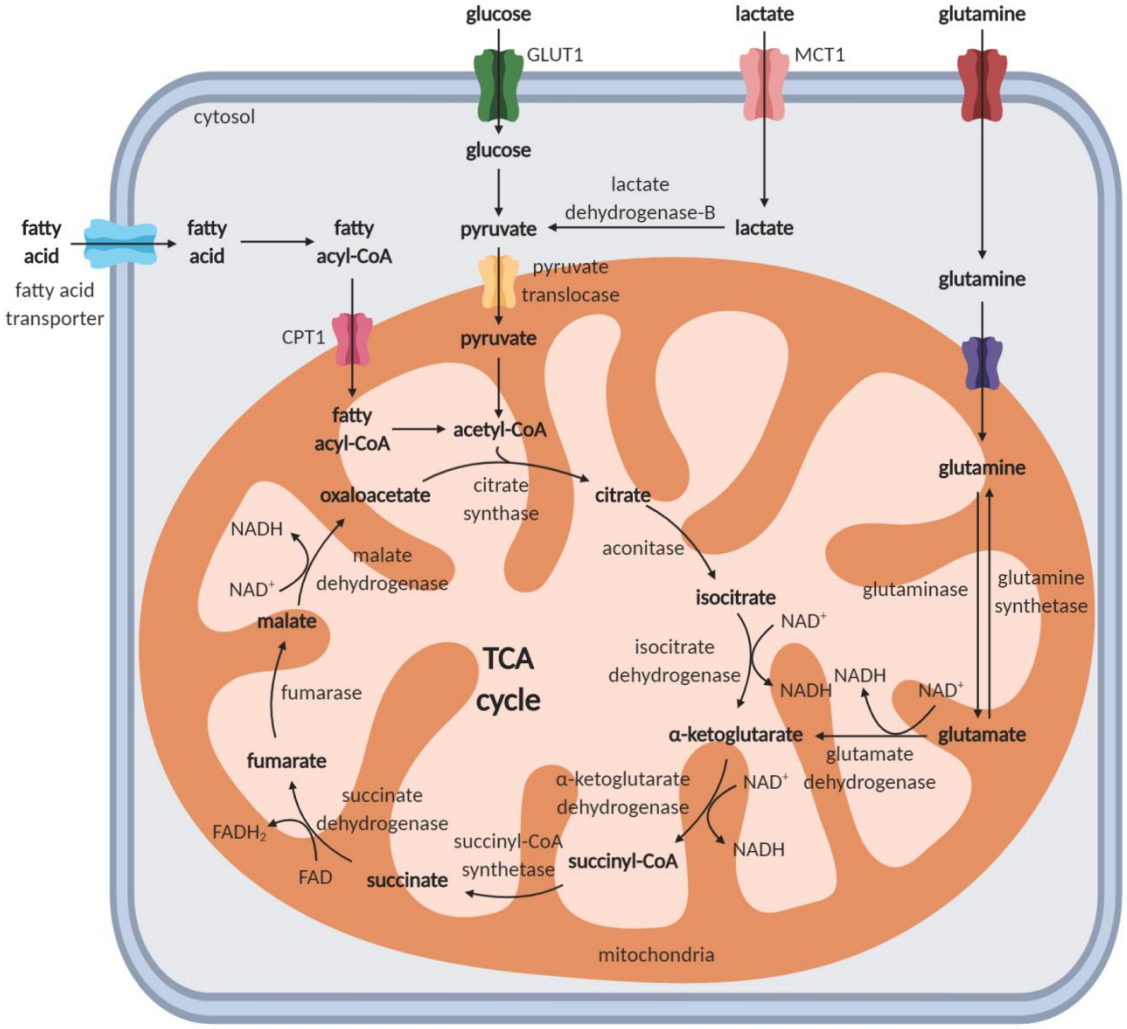

Figure 4. Oxidation of glucose, glutamine, fatty acids and lactate through the tricarboxylic acid (TCA) cycle. This figure was created with BioRender.com.

2.3. Pentose phosphate pathway

The aim of glycolysis is not only to produce pyruvate in order to generate energy, but some of the intermediates generated in the glycolytic pathway are the connection to biosynthetic pathways. Glucose 6-phosphate can be converted into ribose 5-phosphate through a series of reactions in the oxidative pentose phosphate pathway (oxPPP) (**Figure 5**). In this pathway, two molecules of NADPH are produced from each molecule of glucose 6-phosphate. Many reactions in biosynthetic pathways, especially lipid synthesis, require NADPH. Moreover, this NADPH helps in the defense against oxidative damage caused by the production of reactive oxygen species (ROS).

Additionally, the ribose 5-phosphate is the main scaffold for the synthesis of nucleotides and CoA. Therefore, the oxPPP has great relevance in cells with a high proliferation rate, such as tumor cells. Some authors found that inhibition of glucose 6-phosphate dehydrogenase (G6PDH), the first and rate-limiting enzyme of the route, diminished EC proliferation and migration, and impaired angiogenesis, but others failed to see an effect on EC migration[164,165].

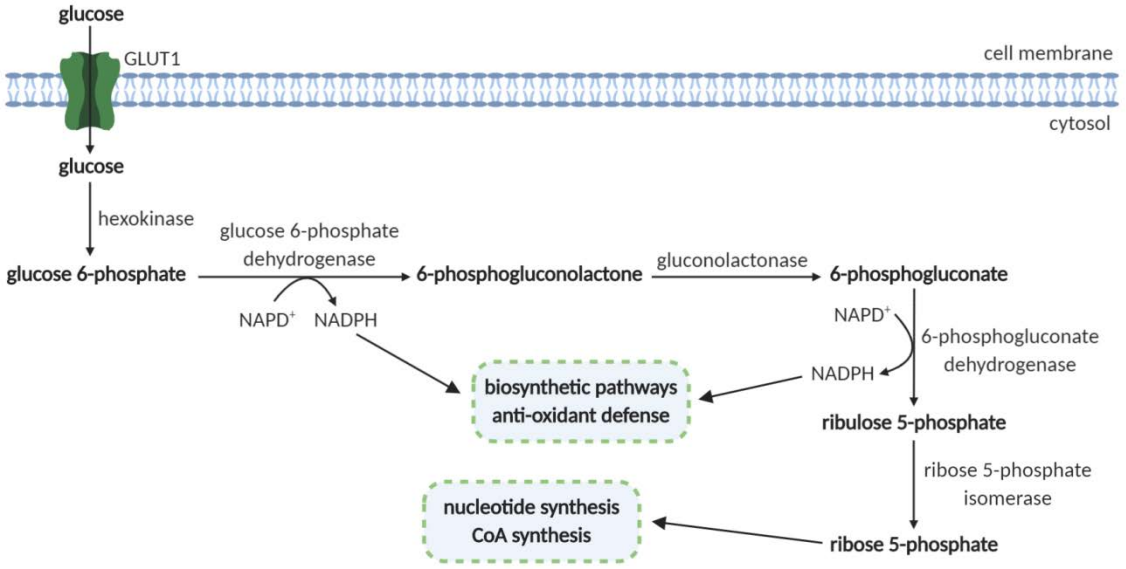

Figure 5. Oxidative pentose phosphate pathway (oxPPP). This figure was created with BioRender.com.

2.4. Hexosamine biosynthetic pathway

Another intermediate from the glycolysis, fructose 6-phosphate, is the substrate of the enzyme glutamine-fructose-6-phosphate aminotransferase (GFAT), which catalyzes the conversion of fructose 6-phosphate into glucosamine 6-phosphate through deamination of glutamine. Additional reactions would lead to the production of uridine diphosphate-N-acetylglucosamine (UDP-GlnAc) (**Figure 6**). Apart from glucose, amino acid, fatty acid and nucleotide metabolism are also necessary to provide nitrogen, acetyl-CoA and UTP to the reactions of the pathway.

This UDP-GlnAc is involved in intercellular signaling due to its role in N-linked and O-linked glycosylation. The hexosamine biosynthetic pathway (HBP) is upregulated in cancer, and inhibition of this pathway leads to an impairment of cancer cell migration and induces apoptosis in tumor cells[166-169]. N-glycosylation of GLUT1 is important for its transport activity[170]. Noticeably, O-linked glycosylation has been shown to be essential for angiogenesis[171,172]. Additionally, N-linked glycosylation regulates the

activation of VEGFR2[173]. The anti-angiogenic activity of the glucose analog 2-deoxyglucose (2-DG) has been associated to an inhibition of N-glycosylation[174]. For those reasons and additional O- and N-glycosylation targets, glycosylation is now considered a new pharmacological strategy for angiogenesis-dependent diseases[175]. Nonetheless, inhibition of GFAT has been shown to induce vessel sprouting[176].

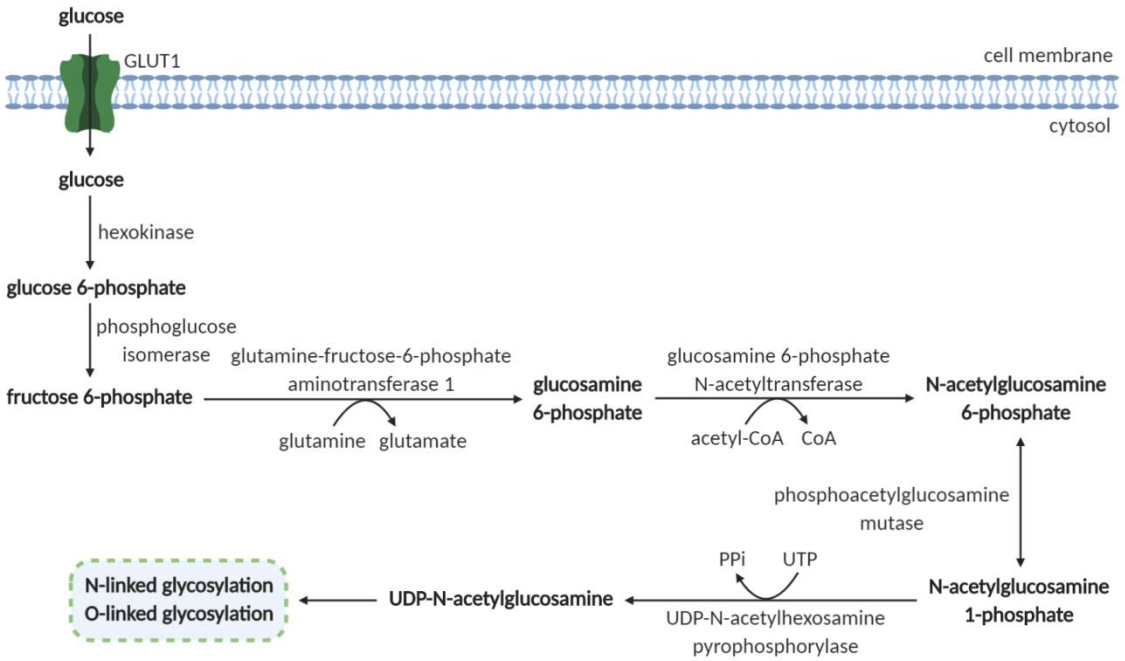

Figure 6. Hexosamine biosynthetic pathway (HBP). This figure was created with BioRender.com.

2.5. Glycogen metabolism

A different metabolic fate of glucose 6-phosphate is the synthesis of glycogen (**Figure 7**). Glycogen is the main storage of glucose in vertebrates. Breakdown of the accumulated glycogen (glycogenolysis) allows the recovery of glucose 6-phosphate which will be headed to glycolysis, oxidation or the PPP (**Figure 7**).

Although poorly studied in the cancer field, glycogen metabolism has been shown to be important for tumor cells[177,178]. Besides, inhibition of the glycogenolysis enzyme glycogen phosphorylase through direct or indirect inhibition via blockade of the activator phosphorylase kinase (PhK) results in a decrease in EC viability and migration and an impairment of angiogenesis[164,179].

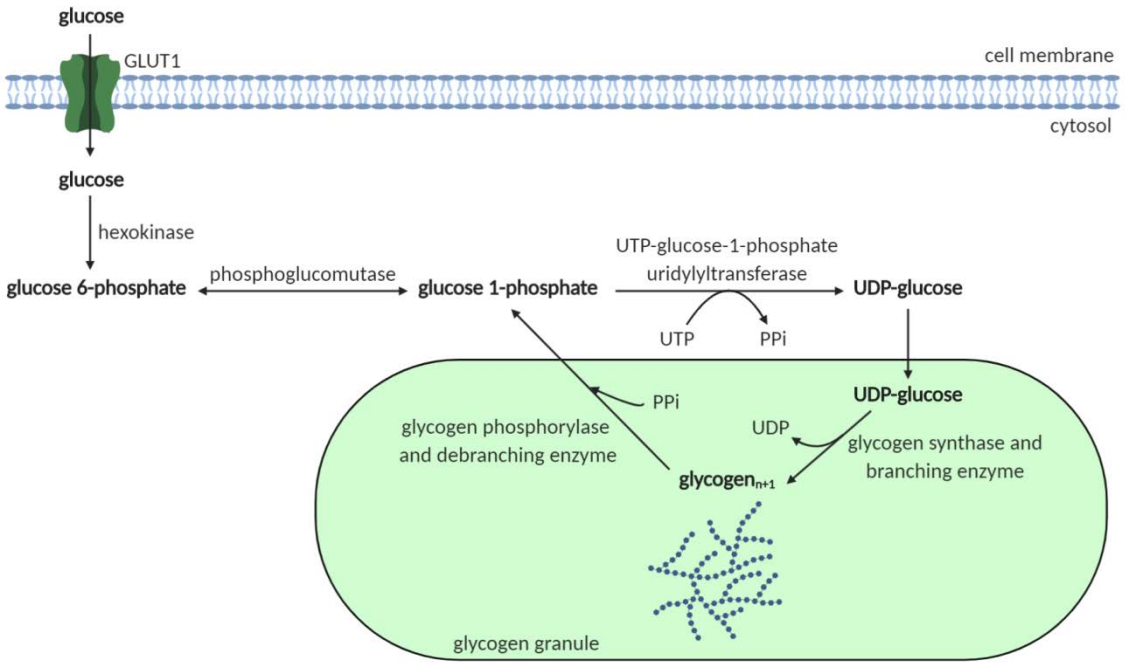

Figure 7. Glycogen synthesis and glycogenolysis. This figure was created with BioRender.com.

2.6. Synthesis of amino acids

There are nine essential amino acids in humans that cannot be synthetized *de novo* and must be supplied in the diet. The other eleven amino acids can be synthetized from different metabolic precursors, including essential amino acids. Alanine comes from pyruvate, whereas the serine synthesis pathway, which includes the synthesis of glycine and cysteine, starts with 3-phosphoglycerate (3-PG), being both substrates intermediates from the glycolysis. Glutamate, glutamine, proline and arginine are synthetized from α-ketoglutarate, and aspartate and asparagine come from oxaloacetate, both intermediates of the TCA cycle (**Figure 8**). As already mentioned (see section 2.2.2 of Introduction), alanine and aspartate can also be synthetized from transaminase reactions.

The importance of several of these amino acids, such as asparagine, serine and glycine, and the toxicity of others, such as proline, in cancer cells has been reviewed (**Appendix 3**). Also the role of glutamine and asparagine in angiogenesis was included in that review article[122,180]. Additionally, arginine can be converted into citrulline and nitric oxide (NO) through nitric oxide synthase (NOS). There are three isoforms of NOS in mammals: endothelial NOS (eNOS), neuronal NOS (nNOS) and inducible NOS (iNOS). Endothelial NO synthesis through eNOS activity is important for vessel formation[181].

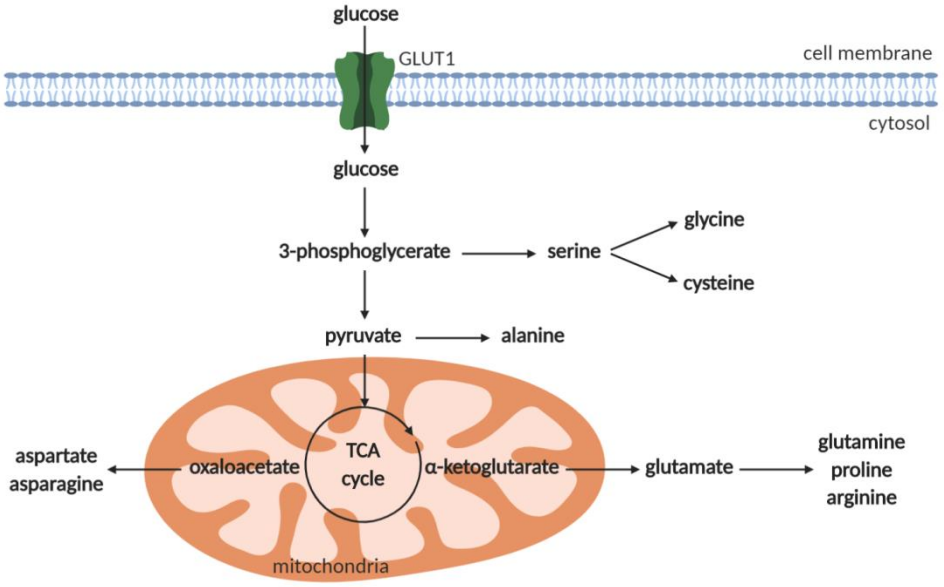

Figure 8. Synthesis of amino acids. This figure was created with BioRender.com.

A most recent work determined the importance of serine and glycine metabolism for proper EC function. 3-PG is the substrate of the enzyme phosphoglycerate dehydrogenase (PHGDH), a rate-limiting enzyme under cell culture conditions and the committed step in the serine synthesis[182]. The resultant 3-phosphohydroxypyruvate (PHP) is then converted into 3-phosphoserine (P-Ser) through phosphoserine aminotransferase (PSAT), and this P-Ser is finally the substrate of the enzyme phosphoserine phosphatase (PSPH), resulting in the synthesis of serine. Glycine is the product of the enzyme serine hydroxymethyltransferase (SHMT) from serine (**Figure 9**). Additionally, glycine is a precursor of the heme group, along with succinyl-CoA and glutamate. PHGDH has been demonstrated to be essential for EC function and angiogenesis due to the role of glycine in heme synthesis[119]. Moreover, glycine was seen to be required for VEGF-mediated angiogenesis[183]. Nevertheless, there are controversial results indicating an anti-angiogenic activity of glycine[184,185]. Taken together, these works suggest that the role of serine and glycine in angiogenesis is greatly complex.

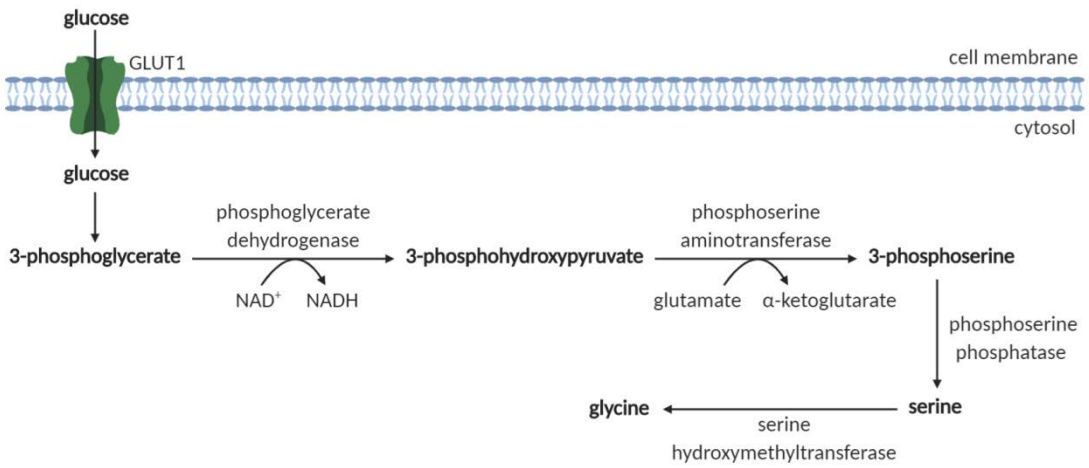

Figure 9. Serine and glycine synthesis pathway. This figure was created with BioRender.com.

2.7. Nucleotide biosynthesis

Several metabolites, such as glucose and amino acids, take part in *de novo* nucleotide biosynthesis (**Figure 10**). These nucleotides constitute the structural components of DNA and RNA, being closely involved in cell proliferation. Both purines (AMP and GMP) and pyrimidines (CMP, TMP and UMP) use phosphoribosyl pyrophosphate (PRPP) as scaffold. This PRPP is synthetized from ribose 5-phosphate from the PPP in a reaction catalyzed by the enzyme ribose-phosphate diphosphokinase (PRPS1). Glutamine is the main donor of nitrogen molecules in the nucleotide biosynthesis, and aspartate is essential for the synthesis of orotate, which will later combine with PRPP in the pyrimidine synthesis. Serine and glycine donate carbons in the purine synthesis, directly from glycine skeleton or through previous conversion into 10-formyl tetrahydrofolate (10-formil THF) in the one-carbon metabolism pathway[186].

Deprivation of glutamine leads to a drop on nucleotide levels in ECs, indicating its importance in nucleotide biosynthesis[122]. As already mentioned, FAO was shown to be relevant for aspartate synthesis, thus affecting pyrimidine synthesis, EC proliferation and vessel sprouting[123]. Moreover, serine and glycine metabolism is essential for both purine and pyrimidine metabolism in ECs. Neither serine nor glycine are directly involved in pyrimidine synthesis, but inhibition of PHGDH leads to a dysfunctional ETC and a consequent compromised dihydroorotate dehydrogenase (DHODH) activity, the enzyme that synthetizes orotate[119]. One-carbon metabolism has been a target for cancer therapy. Methotrexate, an inhibitor of dihydrofolate reductase (DHFR), has been

widely used as a chemotherapy agent[187]. Not surprisingly, methotrexate has been shown to inhibit angiogenesis in different models[188,189].

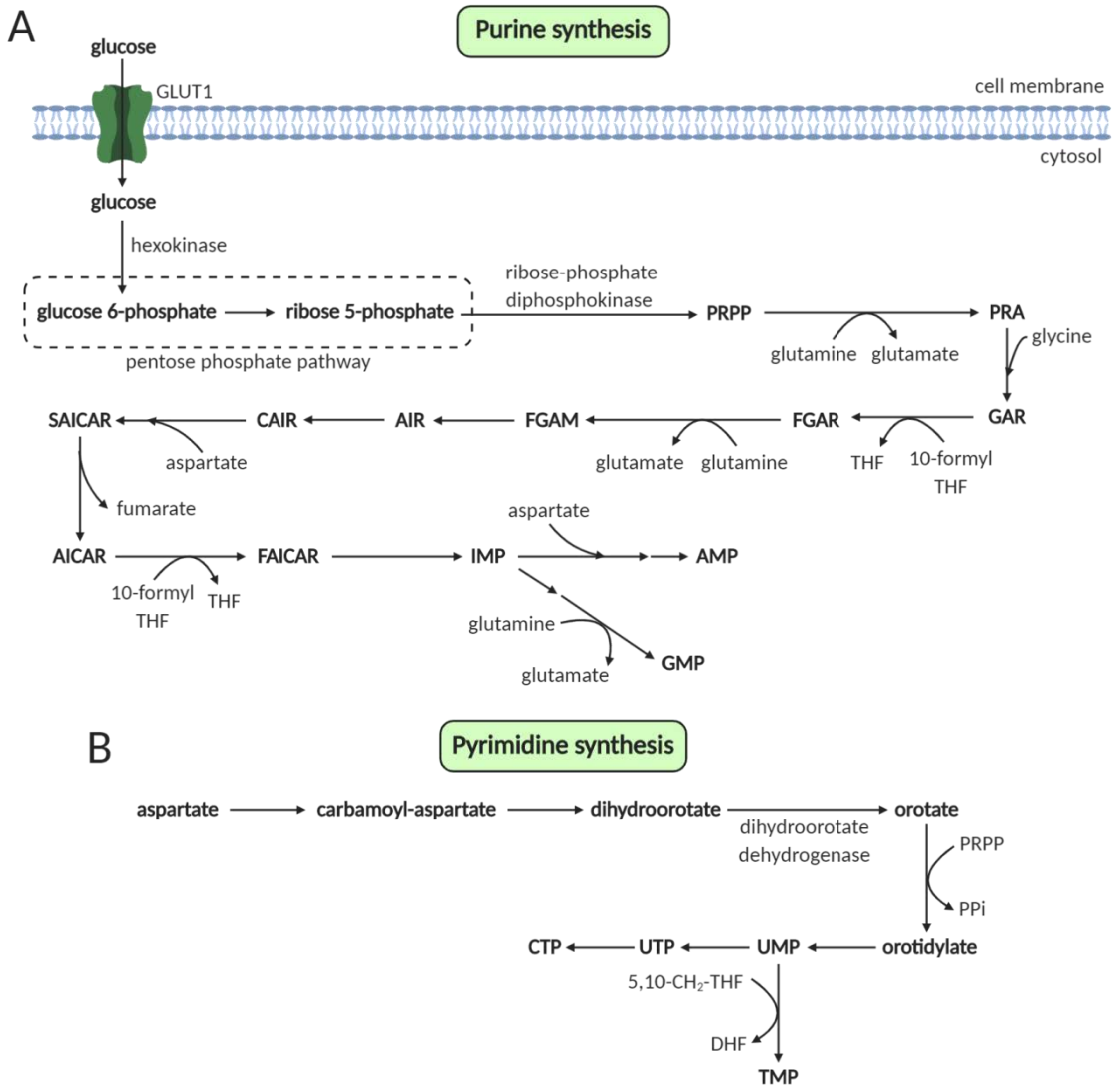

Figure 10. (A) *De novo* purine and (B) pyrimidine synthesis pathway. This figure was created with BioRender.com.

2.8. Synthesis of glutathione

Glutathione (GSH) is the most important antioxidant molecule in the cell, which prevents damage to cellular components caused by ROS. GSH can be synthetized *de novo* or it can be recycled from its oxidized form, GSSG, through glutathione reductase (GSR) activity, a reaction that requires NADPH (**Figure 11**). Alternatively, *de novo* synthesis involves intermediates of both glucose and glutamine metabolism, mainly glutamate, cysteine (synthetized from serine and homocysteine) and glycine (**Figure 11**).

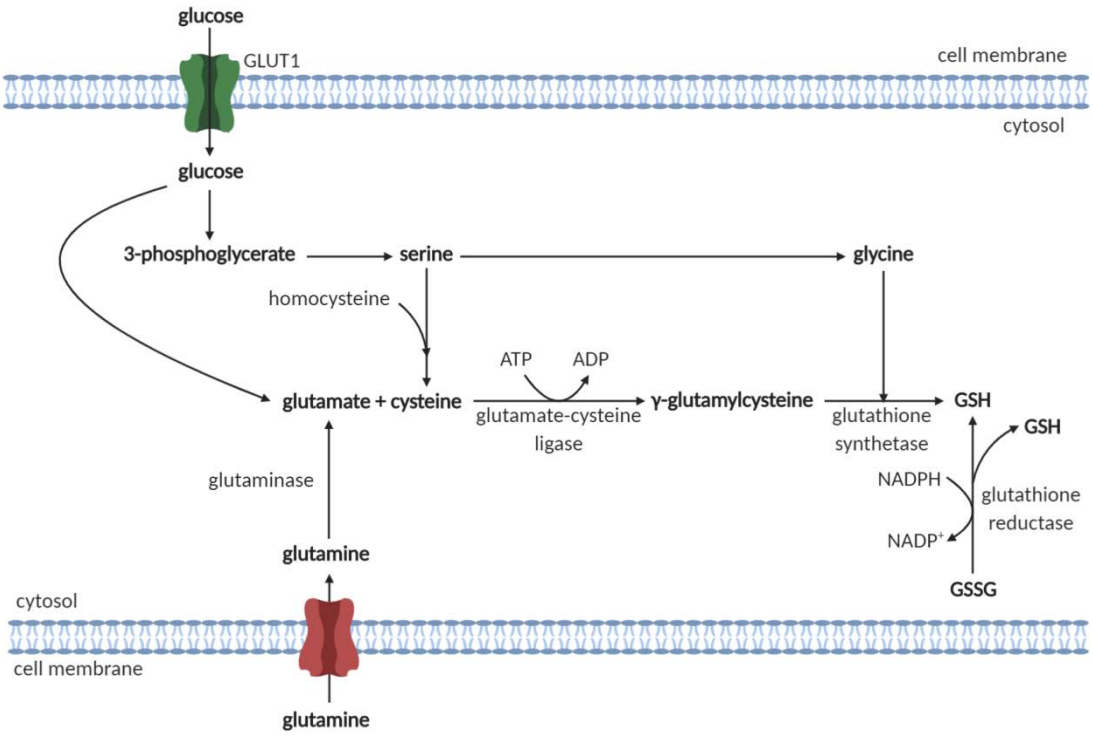

Figure 11. Glutathione synthesis. This figure was created with BioRender.com.

Cancer cells exhibit high levels of oxidative stress due to their high metabolic rate. However, HIF-1α induces GSH synthesis, leading to increase the oxidative defense of highly glycolytic cancer cells[190]. There are other signaling pathways, such as the nuclear factor erythroid 2 (NF-E2)–related factor 2 (Nrf2) anti-oxidant pathway, that are involved in GSH metabolism in cancer cells[191]. Moreover, tumor cells usually activate the PPP in order to generate NAPDH for the reduction of GSSG into GSH, and overexpression of G6PDH reduces oxidative stress in ECs[192,193]. Inhibition of $NADP^+$-dependent isocitrate dehydrogenase 2 (IDH2), an enzyme that convers isocitrate into 2-oxoglutarate outside the TCA cycle, induces oxidative stress in ECs, further emphasizing the importance of NADPH in redox homeostasis[194]. Interestingly, supplemental glycine increases GSH synthesis and can improve EC function[195]. Not surprisingly, glutamine starvation increases ROS levels and impairs GSH synthesis in ECs[122]. GSH has been shown to be essential for tumor angiogenesis, but activation of GSH metabolism inhibited angiogenesis in a non-tumorigenic model[196,197]. Additionally, targeting GSH metabolism in ECs does not always result in an improvement of cancer prognostic[198]. Furthermore, there are other non-metabolic factors involved in the redox control of angiogenesis[199]. Therefore, cancer and angiopreventive therapies based on GSH metabolism have to be carefully considered.

2.9. Lipid synthesis

The classification of lipids includes storage lipids, membrane lipids, cofactors, pigments and lipids involved in cell signaling[200]. Therefore, lipid synthesis is complex and different for different types of lipids. Fatty acids are the first scaffold for lipid synthesis. These fatty acids can be provided in the diet and incorporated into the cell, or they can be synthetized from citrate. The main enzyme involved in the synthesis of palmitate, a long-chain fatty acid with sixteen carbons, is fatty acid synthase (FAS). This enzyme has been shown to be upregulated in many proliferating tumor cells[201-203]. Interestingly, FAS inhibition in ECs impairs EC proliferation and tumor angiogenesis without affecting intracellular levels of palmitate, since it can be taken up from the extracellular milieu[204,205]. Another important enzyme involved in lipid synthesis is acetyl-CoA carboxylase (ACC). This enzyme is relevant for filopodia formation and migration of ECs[206].

Triglycerides (TAG) are the main storage molecule in cells. Its synthesis requires the generation of glycerol 3-phosphate from glucose, in a reaction catalyzed by the enzyme glycerol 3-phosphate dehydrogenase (GPDH), or from glycerol through glycerol kinase (GK). Then, two acyl-CoAs bind to this glycerol 3-phosphate, leading to the formation of phosphatidic acid. This phosphatidic acid will be later the substrate for TAG synthesis (**Figure 12**).

Phosphatidic acid can also lead to the synthesis of glycerophospholipids, one of the two main groups of membrane phospholipids (**Figure 12**), whereas sphingolipid synthesis requires the binding of serine to palmitoyl-CoA. The complex synthesis of phospholipids in mammals has been extensively reviewed elsewhere[207].

Cholesterol is an important component of cell membranes and a precursor of steroid hormones. This molecule is synthetized from acetyl-CoA in a series of reactions that include the one catalyzed by the enzyme β-hydroxy β-methylglutaryl-CoA reductase (HMG-CoA reductase), the rate-controlling enzyme of the mevalonate pathway (**Figure 13**). Statins are HMG-CoA reductase inhibitors that have been classically used in the prevention of cardiovascular diseases (CVD)[208]. Interestingly, cholesterol metabolism is now considered an emerging therapeutic target for angiogenesis and cancer[209].

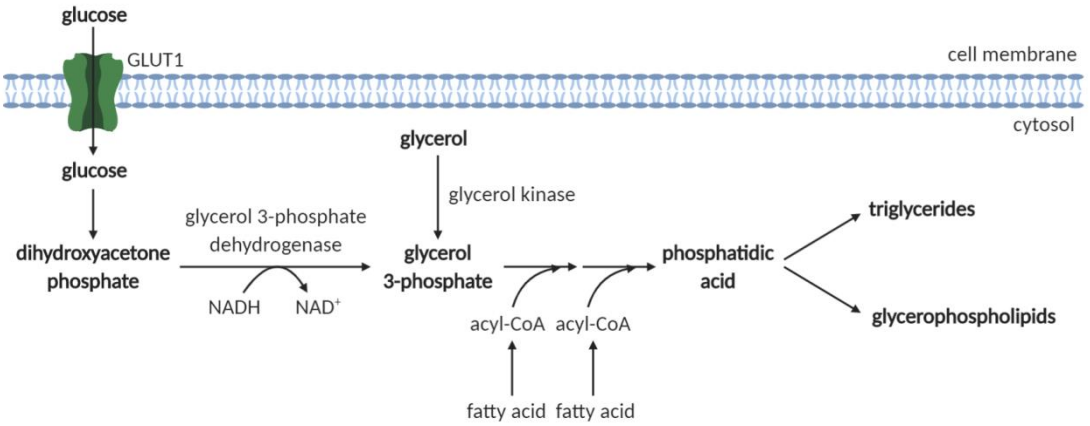

Figure 12. Synthesis of triglycerides and glycerophospholipids. This figure was created with BioRender.com.

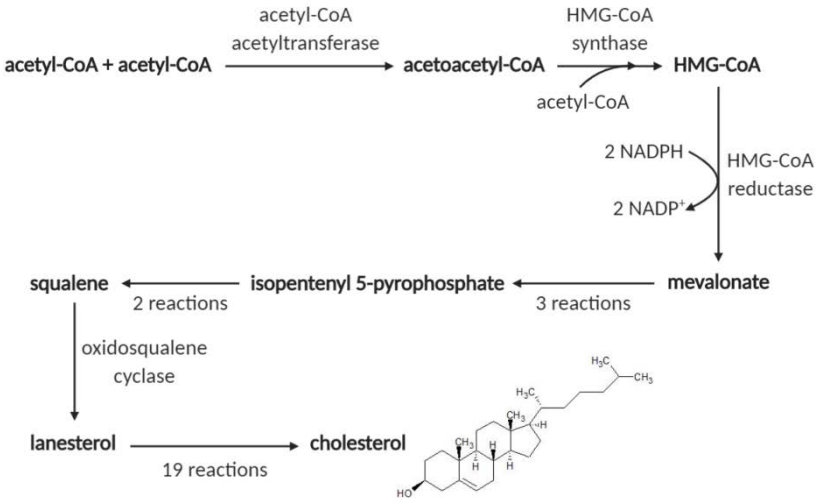

Figure 13. Cholesterol synthesis. Cholesterol chemical structure was drawn using ChemSketch software. This figure was created with BioRender.com.

All in all, lipid synthesis requires different metabolic substrates, including glucose, serine and citrate (from glucose, glutamine or fatty acid oxidation). Additionally, all the reactions involved in lipid synthesis consume high amounts of NAPDH. Therefore, the PPP is important for sustaining a high phospholipid synthesis which will allow the maintenance of a high proliferative rate.

3. **Targeting metabolism as a treatment for angiogenesis-dependent diseases**

For many years, different features of tumor metabolism have been considered as therapeutic targets for the treatment of cancer[210]. Dozens of metabolic modulators have been proven to present anti-tumor activity (Table 1 in **Appendix 3**). However, there is ample metabolic heterogeneity in cancer, mainly due to genetic alternations, tissue

origin, epigenetics and nutrient limitation[211]. Moreover, as already mentioned, tumor cells are not alone in their microenvironment. These cells interact with other cells of the TME and with the components of the ECM[212]. These interactions sometimes lead to chemoresistance in cancer patients[213]. For those reasons, targeting of other components of the TME rather than tumor cells is being considered as a good alternative for cancer treatment. This is partly supported by the fact that non-tumorigenic cells are genetically more stable than tumor cells, as previously emphasized[56,214].

Tumor angiogenesis has been targeted for many years. For that aim, several VEGF-targeted anti-angiogenic therapies have been developed. However, the benefits are sometimes less than expected, due to toxicity or resistance to the therapy[215,216]. One of the emerging targets in cancer treatment is EC metabolism[100-103]. Several metabolic enzymes and transporters have been inhibited in ECs causing a disruption in angiogenesis[119,121,122,180,217,218]. Interestingly, some of these therapeutic approximations have helped to improve chemotherapy[219]. Inhibition of cancer cells metabolism can also lead to an inhibition of angiogenesis[220]. Some compounds are also able to potentiate the effect of others. For example, chloroquine, a GDH inhibitor, enhances the anti-angiogenic effect of sunitinib[221]. There are also known anti-inflammatory drugs that inhibit both angiogenesis and metabolic features of ECs. For instance, aspirin diminishes GLUT1 expression in ECs[222]. **Table 3** summarizes some metabolic modulators that exhibited anti-angiogenic activity.

In this PhD Thesis, the effect on angiogenesis of a metabolic modulator, fasentin, was tested (**Chapter 3**), whereas the possible metabolic modulation of dimethyl fumarate (DMF), a previously described anti-angiogenic compound, was studied (**Chapter 4**).

Table 3. Metabolic modulators with proven anti-angiogenic capacity.

Compound	Target	References
	Glucose metabolism	
3-bromopyruvate	Hexokinase	223
3-PO	6-Phosphofructo-2-kinase/fructose-2,6-biphosphatase 3 (PFKFB3)	219
α-cyano-4-hydroxycinnamate (CHC)	MCT1	162
2-deoxyglucose (2-DG) (glucose analog)	Hexokinase	174,224,225
Dichloroacetate (DCA)	Pyruvate dehydrogenase kinase (PDK)	226
Gossypol	Glyceraldehyde 3-phosphate dehydrogenase (GAPDH) Lactate dehydrogenase (LDH)	227
Lonidamine	Hexokinase-II (HK2) MCT transporters	228,229
Shikonin	Pyruvate kinase M2 (PKM2)	230,231
Silibinin	GLUT transporters	232-235
	Glutamine metabolism	
Acivicin (glutamine analog)	Glutamine transport	236
Methionine sulfoximine (MSO)	Glutamine synthetase (GS)	148
	Fatty acid metabolism	
Etomoxir	Carnitine palmitoyl-transferase 1a (CPT1a)	123
Orlistat	Fatty acid synthase (FAS)	204
	Mevalonate pathway	
Atorvastatin (CI-981)	HMG-CoA reductase	237
Cerivastatin	HMG-CoA reductase	238
Fluvastatin	HMG-CoA reductase	239
Lovastatin	HMG-CoA reductase	240
	Polyamine metabolism	
Difluoromethylornithine (DFMO)	Ornithine decarboxylase (ODC)	241-243
	Nucleic acid synthesis	
Methotrexate	Dihydrofolate reductase (DHFR)	188,189

HYPOTHESES AND AIMS

Based on the information contained in the Introduction, two general working hypotheses were established:

Hypothesis 1: The presence of different metabolic fuels may affect the uptake and utilization of other metabolic substrates.

Hypothesis 2: Inhibitors of angiogenesis and modulators of metabolism can constitute interesting pharmacological therapies against cancer and other angiogenesis-dependent diseases.

Based on these hypotheses, the experimental work of the present PhD Thesis aims to fulfill the following objectives:

Objective 1: To study in depth different features of glucose, glutamine and palmitate metabolism in cells from the angiogenic microenvironment, such as tumor cells and endothelial cells.

Objective 2: To test whether compounds described as metabolic modulators are able to inhibit angiogenesis *in vitro* and *in vivo*.

Objective 3: To test whether compounds previously described as anti-angiogenic are able to modulate endothelial cell metabolism.

MATERIAL AND METHODS

1. Materials and reagents

1.1. Materials

MCDB-131 and glucose, glutamine and pyruvate free Dulbecco's Modified Eagle Medium (DMEM) cell culture media were obtained from Gibco (Paisley, Scotland, UK). Glucose, glutamine, serine and glycine free media were from Teknova (Hollister, CA, USA) and from US Biological Life Sciences (Salem, MA, USA). Other cell culture media, penicillin and streptomycin and trypsin were purchased from BioWhittaker (Verviers, Belgium). Fetal bovine serum (FBS) was purchased from Biowest (Kansas, USA). Dialyzed FBS (dFBS) was from Gemini Bioproducts (West Sacramento, CA, USA) and from Capricorn (Ebsdorfergrund, Germany). Plastic material for cell culture was from Nunc (Roskilde, Denmark) and Daslab (Barcelona, Spain). Transwells, 24-well plates and white 96-well plates were from Falcon (Corning, NY, USA).

Matrigel was purchased from Corning (Corning, NY, USA). Material for Seahorse experiments were from Agilent Technologies (Santa Clara, CA, USA). 2-NBDG and BODIPY FL C_{16} were supplied by Molecular Probes (Eugene, OR, USA). L-[U-^{14}C]-glutamine was acquired from Perkin Elmer (Waltham, MA, USA). D-[U-^{13}C]-glucose, L-[U-^{13}C]-glutamine, L-[U-^{13}C]-serine and L-[U-^{13}C]-glycine were purchased from Cambridge Isotope Laboratories (Tewksbury, MA, USA). Adipostatin-A and PD98059 were obtained from Cayman Chemical (Ann Arbor, MI, USA).

All other reagents not listed in this or later sections were provided by Sigma-Aldrich (St. Louis, MO, USA).

1.2. Compounds

Fasentin was acquired from Calbiochem (San Diego, CA, USA) and dimethyl fumarate (DMF) was from Sigma Aldrich (St. Louis, MO, USA). Both compounds were acquired as powder and dissolved in dimethyl sulfoxide (DMSO). A highly concentrated stock was prepared in order to reduce the percentage of DMSO in contact with the treated cells.

1.3. Metabolic substrates

Different metabolic substrates were used in this PhD Thesis. Their elaboration and storage is specified below.

- Glucose: glucose was dissolved in PBS (1x, pH 7.4) at a concentration of 1 M, sterile filtered and kept at 4 ºC.

- Glutamine: glutamine was dissolved in PBS (1x, pH 7.4) at a concentration of 100 mM and sterile filtered. Single-use aliquots were maintained at -20 ºC.

- Lactate: lactic acid was dissolved in cell media supplemented with 50 mM HEPES to a final concentration of 10 mM. Then pH was corrected to 7.4. Lactate solution was sterile filtered and kept at 4ºC and used within a week.

- Palmitate: palmitate was used as a conjugate with bovine albumin serum (BSA) essentially fatty acid free at 5:1 proportion prepared according to a published protocol (see section 1.3.1)[244].

1.3.1. Conjugate palmitate-BSA preparation

The protocol for the preparation of a conjugate palmitate-BSA at 5:1 proportion (7% BSA-5 mM palmitate) was as follows:

1. Dissolve BSA (essentially fatty acid free) in bidistilled water at 42 ºC with agitation in order to obtain a 7.5% solution.
2. Dissolve sodium palmitate in 1.3 mL of bidistilled water in a 50 mL centrifuge tube in order to obtain a 77 mM solution. For that aim, loose the cap and place the tube in a boiling water bath until total dissolution.
3. Cool the palmitate solution and add 18.7 mL of the 7.5% BSA solution. Immediately place the tube in a 42 ºC water bath with agitation.
4. Adjust pH to 7.4.
5. Sterile filter the solution.
6. Keep the aliquots at -20 ºC in glass tubes and use within six months. The same aliquot may be used within the same 2-3 days while keeping it at 4 ºC.

1.4. Primers

Primers used in this PhD Thesis for the determination of gene expression by real-time quantitative polymerase chain reaction (qPCR) were acquired from Sigma Aldrich. Primer sequences are collected in **Table 1**.

Table 1. List of primers used in this PhD Thesis.

Gene (protein)	Primer sequences	Optimal Tm (ºC)	Amplicon size (bp)
ACTB (β-actin)	Fw: GACGACATGGAGAAAATCTG Rv: ATGATCTGGGTCATCTTCTC	54	131
CD36 (CD36)	Fw: AGCTTTCCAATGATTAGACG Rv: GTTTCTACAAGCTCTGGTTC	54	111
FABP5 (FABP5)	Fw: AAGATGGGAAATTAGTGGTG Rv: AACAGTATGGAGATTTGCTC	53	153
LDHA (LDH-A)	Fw: CACCATGATTAAGGGTCTTTAC Rv: AGGTCTGAGATTCCATTCTG	54	87
LDHB (LDH-B)	Fw: CAACAATGGTAAAGGGGATG Rv: TCACTAGTCACAGGTCTTTTAG	54	189
MMP2 (MMP-2)	Fw: GACATACATCTTTGCTGGAGAC Rv: ACGCTCTTCAGACTTTGGTTCT	58	207
PLAU (uPA)	Fw: CGCCACACACTGCTTCATG Rv: CCCCTTGCGTGTTGGAGTT	60	89
PLAUR (uPAR)	Fw: GCCCAATCCTGGAGCTTGA Rv: TCCCCTTGCAGCTGTAACACT	60	63
SLC2A1 (GLUT1)	Fw: ACCTCAAATTTCATTGTGGG Rv: GAAGATGAAGAACAGAACCAG	54	105
SLC16A1 (MCT-1)	Fw: GAGGTCCTATCAGCAGTATC Rv: CAATGACTCCAATACAGACG	54	144
SLC16A3 (MCT-4)	Fw: CAGTTCGAGGTGCTCATGG Rv: ATGTAGACGTGGGTCGCAT	58	140
TIMP1 (TIMP-1)	Fw: CACCTTATACCAGCGTTATG Rv: TTTCCAGCAATGAGAAACTC	54	168
TIMP2 (TIMP-2)	Fw: GGCCTGAGAAGGATATAGAG Rv: CTTTCCTGCAATGAGATATTCC	54	104
TIMP3 (TIMP-3)	Fw: CTGACAGGTCGCGTCTATGATG Rv: AGCAAGGCAGGTAGTAGCAG	60	157
TIMP4 (TIMP-4)	Fw: AAATCTCCAGTGAGAAGGTAG Rv: TCTCAAACCCTTTGAACATC	54	105

Fw: Forward; Rv: Reverse; Tm: Annealing temperature.

1.5. Antibodies

All the antibodies used for Western blots in this PhD Thesis are collected in **Table 2**.

The secondary antibodies used were the ECL anti-rabbit IgG, horseradish peroxidase-linked species-specific whole antibody (from donkey) from GE Healthcare (used at 1:5000 dilution) and the anti-mouse IgG (whole molecule)-peroxidase antibody (from goat) from Sigma-Aldrich (used at 1:10000 dilution).

Table 2. List of antibodies used in this PhD Thesis.

Antibody	Source	Company	Dilution
Anti-Akt	Rabbit	Cell Signaling	1:1500
Anti-α-tubulin	Mouse	Cell Signaling	1:10000
Anti-calnexin	Mouse	Enzo Life Sciences	1:1000
Anti-HIF1α	Mouse	BD Biosciences	1:500
Anti-LC3B	Rabbit	Cell Signaling	1:1000
Anti-MCT1	Mouse	Santa Cruz Biotechnology	1:100
Anti-MCT4	Mouse	Santa Cruz Biotechnology	1:100
Anti-p44/42 MAPK (ERK1/2)	Rabbit	Cell Signaling	1:2000
Anti-PHGDH	Mouse	GeneTex	1:1000
Anti-phospho-Akt (Ser473)	Rabbit	Cell Signaling	1:250
Anti-phospho-p44/42 MAPK (ERK1/2) (Thr202/Tyr204)	Rabbit	Cell Signaling	1:1000
Anti-vinculin	Rabbit	Cell Signaling	1:5000

2. Cell culture

Growth media used for the maintenance of cells were supplemented with 2 mM L-glutamine, 50 U/mL penicillin, 50 µg/mL streptomycin and 10% FBS, unless specified otherwise. Cells were maintained at 37 ºC and 5% CO_2 under a humidified atmosphere for their routine growth. Adherent cell lines were cultured in 10 cm cell culture dishes.

For inducing anoxia, 200 µM $CoCl_2$ was added to the cells for 24 h. For hypoxic conditions, cells were maintained in an incubator with 1% O_2 (37 ºC and 5% CO_2). In these conditions, 5 mM HEPES was added to the cells.

In this PhD Thesis, cell treatments consisted in the presence of different compounds or presence/absence of different metabolic substrates (mentioned in section 1.3 of Material and Methods). Unless otherwise specified, compounds were added in growth media and controls contained the equivalent amount of DMSO. Regarding metabolic substrates, different media were used. For short-term incubations (<1 h), cells were cultured with different metabolic substrates in PBS supplemented with calcium and magnesium (DPBS). For long-term incubations (> 1 h), DMEM not containing glucose, glutamine or pyruvate was supplemented with different metabolic substrates and 10% FBS. For long-term serine/glycine starvation, DMEM not containing glucose, glutamine, pyruvate, serine or glycine was used along with 10% dFBS.

All cell lines were kept in liquid nitrogen in the presence of 10% DMSO, except for HL-60, which were maintained with 5% DMSO. After thawed, fresh media was immediately added in order to reduce DMSO concentration. HL-60 cells were centrifuged after thawed for complete elimination of DMSO.

Cell lines used in this PhD Thesis are collected in **Table 3**.

2.1. Endothelial cells

2.1.1. Human microvascular endothelial cells (HMEC)

Human microvascular endothelial cells (HMEC) were kindly supplied by Dr. Arjan W. Griffioen (Maastricht University, Netherlands). The establishment of this human immortalized dermal microvascular EC line was performed as previously described[245]. These cells were maintained in MCDB-131 medium supplemented with 1 µg/mL hydrocortisone and 10 ng/mL epithelial growth factor (EGF).

2.1.2. Bovine aortic endothelial cells (BAEC)

Bovine aortic endothelial cells (BAEC) were isolated from bovine aortic arches provided by Famadesa (Campanillas, Málaga, Spain) as previously described[246]. Cells were maintained in DMEM with 1 g/L glucose and used before passage 20.

2.1.3. Human umbilical vein endothelial cells (HUVEC)

Human vein endothelial cells (HUVEC) were isolated by a modified collagenase treatment as previously reported[247]. Cells were maintained in medium 199 supplemented with 20% FBS, 30 µg/mL endothelial cell growth supplement (ECGS) and 100 µg/mL heparin. Pre-coated cell culture dishes with 0.5% gelatin were required for improving cell adherence. Alternatively, these cells were purchased from Lonza (Basel, Switzerland) and maintained in Endothelial Cell Growth Basal Medium-2 (EBM-2 medium) supplemented with Endothelial Growth Media-2 (EGM-2) SingleQuots, containing hydrocortisone, FGF-B, VEGF, recombinant analog of insulin-like growth factor-1 (R3-IGF-1), ascorbic acid, EGF, GA-1000 (gentamicin, amphotericin B) and heparin. Cells were used between passages 2-9.

2.2. Tumor cells

All the tumor cell lines used in this PhD Thesis were acquired by the American Type Culture Collection (ATCC). Specifications for these tumor cells (HCC1937, HeLa, HL-60, Kelly, MCF7, MDA-MB-231 and MDA-MB-436) are collected in **Table 3**.

2.3. Other cell types

Human gingival fibroblasts (HGF) were maintained in DMEM with 4.5 g/L glucose and used before passage 25.

Table 3. Cell lines used in this PhD Thesis.

	Cell line	Description	Growth medium
Endothelial cells	**BAEC**	Bovine aortic endothelial cells	DMEM (1 g/L glucose)
	HMEC	Human microvascular endothelial cells	MCDB-131 (1 µg/mL hydrocortisone, 10 ng/mL EGF)
	HUVEC	Human umbilical vein endothelial cells	Medium 199 (20% FBS, 30 µg/mL ECGS, 100 µg/mL heparin) or EBM-2 supplemented with EGM-2 SingleQuots
Tumor cells	**HCC1937**	Human breast carcinoma	RPMI-1640
	HeLa	Human cervix adenocarcinoma	EMEM
	HL-60	Human leukemia	RPMI-1640 (20% FBS)
	Kelly	Human neuroblastoma	RPMI-1640
	MCF7	Human breast carcinoma	DMEM (4.5 g/L glucose)
	MDA-MB-231	Human breast carcinoma	RPMI-1640
	MDA-MB-436	Human breast carcinoma	RPMI-1640
Other cell types	**HGF**	Primary human gingival fibroblast	DMEM (4.5 g/L glucose)

DMEM: Dulbecco's Modified Eagle Medium; EBM-2: Endothelial Cell Growth Basal Medium-2; EGM-2: Endothelial Growth Media-2; EMEM: Eagle's Minimum Essential Medium.

3. Animal models

Fertilized chick eggs (*Gallus gallus domesticus*) used for the chorioallantoic membrane (CAM) assay (see section 5.1 of Material and Methods) were obtained from Granja Santa Isabel (Córdoba, Spain).

Zebrafish (*Dario rerio*) models included the wild-type AB strain and the transgenic model Tg(kdrl:ras-mCherry), which expresses the red fluorescent protein mCherry under the *Kdrl*-endothelial promoter (VEGFR2)[248]. The wild-type AB strain was from

Dr. Manuel Marí Beffa from the University of Málaga. The transgenic strain was shared by Dr. Berta Alsina from the Pompeu Fabra University (Barcelona, Spain).

All experimental procedures with animals were conducted in accordance with the Spanish Legislation (Real Decreto 53/2013, BOE, 34/-11421, 2013) in compliance with the European Community Directive 2010/63/EU regulating the use and care of laboratory animals. The protocols were approved by the Ethics Committee for Animal Experiments of the University of Málaga.

4. *In vitro* assays

4.1. Proliferation and survival assays

4.1.1. MTT cell viability assay

MTT (3-(4,5-dimethylthiazol-2-yl)-2,5-diphenyltetrazolium bromide) assay is a colorimetric assay for determining cell metabolic activity, which is often used for testing whether a compound is able to inhibit cell proliferation or induce cell death[249]. The assay is based on the capacity of the yellow MTT dye to react with mitochondrial NAD(P)H-dependent oxidoreductase enzymes, leading to the formation of its insoluble form, formazan, which acquires blue color. Therefore, living cells with active mitochondria would turn the MTT to formazan (blue), whereas cells with inactive mitochondria (most often dead cells) will not change the MTT yellow color. This change of color can be spectrophotometrically monitored at 550 nm (**Figure 1**).

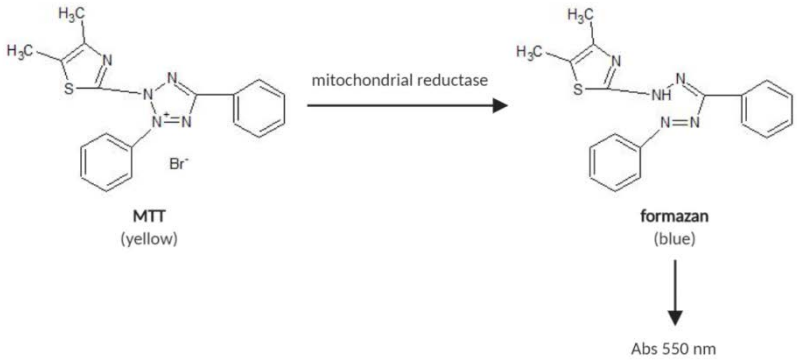

Figure 1. MTT reduction to formazan through mitochondrial reductases. Chemical structures were drawn using ChemSketch software.

The half maximal inhibitory concentration (IC_{50}) of a compound indicates the concentration of a certain compound which inhibits cell proliferation and/or induces cell death in a 50%. IC_{50} may be calculated using the MTT assay as follows.

Preparation of reagents

- MTT (5 mg/mL): dissolve 25 mg MTT in 5 mL PBS (1x pH 7.4). Sterile filter and keep at 4 ºC protected from light. The solution may be used within a couple of weeks.

- Acidified isopropanol: add 353 µL HCl to 500 mL 2-propanol to obtain a concentration of 0.04 N HCl.

Protocol

1. Considering quadruplicates for each condition fill a 96-well cell culture plate as follows:

   a. Add 100 µL cell media to blank wells or 50 µL cell media to the rest of the wells, except for those with the maximum concentration of the compound.

   b. Add 50 µL DMSO corresponding to the maximum concentration of the compound to the control wells.

   c. Add 100 µL of the compound dissolved in cell media at double the maximum concentration desired.

   d. Starting with the maximum concentration, make serial dilutions taking 50 µL of those wells to the following wells. Discard the last 50 µL. Each column of the plate will have half the concentration of compound present in the column on its left.

   e. Add cell suspension to all wells except for blanks.

      - Tumor cells: 2 x 10^3 cells/well.

      - ECs: 2.5 x 10^3 cells/well for HMEC and BAEC and 4 x 10^3 cells/well for HUVEC.

      - Fibroblasts: 2 x 10^3 cells/well.

2. Incubate the cells at 37 ºC and 5% CO_2 in humidified atmosphere for 72 h.
3. Add 10 µL MTT (5 mg/mL) to each well.
4. Incubate at 37 ºC and 5% CO_2 in humidified atmosphere for 4 h in the dark.
5. Add 150 µL acidified isopropanol to each well to dissolve the formazan crystals.
6. Read absorbance at 550 nm.

In this PhD Thesis, absorbance was read using an Eon Microplate Spectrophotometer from Bio-Tek Instruments (Winooski, VT, USA). Data were collected by Gen5 software from the same manufacturers.

Cell number was represented as the percentage of live cells, taking as 100% the absorbance of control cells. Dose-response curves were depicted and IC_{50} was calculated for each compound.

Independently, MTT assay can also be used for determining the toxicity of a compound. For that aim, a modified assay is performed: cells are initially seeded at a cell density of 2 x 10^4 cells/well and after 24 h adherence the desired concentrations of the tested substance are added for a certain time.

4.1.2. Cell growth curves

The classical way to determine cell proliferation is the counting of cells. For this aim, cells are seeded at low density in 24- or 6-well plates and after cell adherence different culture conditions are assayed (for example, to test compounds or change nutritional conditions). Cell number can be monitored each day either using a manual Neubauer chamber or an automatized Coulter counter from Beckman Coulter (Brea, CA, USA).

4.1.3. EdU proliferation assay

Cell proliferation can also be measured by the addition of nucleoside analogs during cell replication, whose incorporation into DNA can be detected by several techniques. Classically, [^{3}H]-thymidine or 5-bromo-2'-deoxyuridine (BrdU) have been used, using autoradiography or anti-BrdU antibodies for their detection. However, these analogs present several disadvantages, such as radioactivity and the requirement of DNA denaturation for the access of the anti-BrdU antibody.

5-ethynyl-2'-deoxyuridine (EdU) is another nucleoside analog. In this PhD Thesis the baseclick EdU flow cytometry kit (Baseclick GmbH) has been used in order to detect cell proliferation by means of a flow cytometry technique with the use of dye fluorescent reagents. EdU positive cells will represent active proliferating cells (S phase).

Cell proliferation was measured according to the instructions provided by the manufactures as follows.

Preparation of reagents

- EdU stock (10 mM): dissolve 1 mg EdU in 0.4 mL DMSO. Make aliquots and keep them at -20 ºC.

- PBS + 1% FBS: mix 0.5 mL FBS with 49.5 mL PBS (1x pH 7.4). Keep at 4 ºC.

- PBS + 1% BSA: dissolve 0.5 g BSA in 50 mL PBS (1x pH 7.4). Keep at 4 ºC

- Buffer additive 10x: dissolve 400 mg compound G in 5.5 mL bidistilled water. Make aliquots and keep them at -20 ºC.

- Saponin buffer: mix 3 mL component E with 27 mL PBS + 1% BSA. Keep at 4 ºC.

Protocol

1. Seed the cells at 1.5 x 10^5 cells/mL in 6-well plates.
2. After 24 h, treat the cells (compounds or metabolic conditions) for the desire time.
3. 2 hours before the end of the treatment, add 10 µM EdU to each well (except for the blank). Incubate for 2 h.
4. Collect the cells in PBS + 1% FBS.
5. Centrifuge the cells at 600 g for 5 min.
6. Wash the pellets with PBS + 1% BSA.
7. Centrifuge again.
8. Resuspend the pellet in 100 µL fixative solution (compound D).
9. Incubate 15 min at room temperature (RT) in the dark.
10. Centrifuge and wash with PBS + 1% BSA.
11. Centrifuge.
12. Resuspend the pellet in 100 µL saponin buffer 1x.
13. Add 0.5 mL of the following cocktail to each tube. Use within 15 min after preparation. For one sample:
    - PBS: 438 µL
    - Catalyst solution (compound F): 10 µL
    - Dye azide (10 mM) (compound B): 2.5 µL
    - Buffer additive 10x: 50 µL
14. Incubate 30 min at RT in the dark.
15. Centrifuge and wash with saponin buffer 1x.
16. Centrifuge.
17. Resuspend the pellet in 0.5 mL saponin buffer 1x.
18. Detect fluorescence in a flow cytometer (Ex 496/Em 516 nm).

In this PhD Thesis, a FACS VERSE™ cytometer from BD Biosciences (San Jose, CA, USA) was used. Data were analyzed with its software BD FACSuite.

4.2. Cell cycle analysis

Cell proliferation involves several cellular stages in a process known as cell cycle. There are four stages during cell cycle:

- SubG1: haplodiploid cells (DNA < 2n), corresponding to apoptotic cells with fragmented DNA.

- G0/G1: diploid cells (DNA = 2n), corresponding to quiescent cells (G0) or cells starting their cell cycle (G1).

- S: cells that are duplicating their DNA (DNA = 2n or 4n).

- G2/M: tetraploid cells (DNA = 4n), corresponding to cells that have already duplicated their DNA.

The percentage of cells in each of these phases can be determined by flow cytometry when labeled with propidium iodide after the removal of RNA by ribonuclease (RNase) treatment. Propidium iodide is a fluorescent intercalant agent able to bind DNA. Therefore, depending on the amount of DNA within each cell (< 2n, 2n or 4n), different amounts of fluorescence will be detected, distinguishing between different cell cycle stages.

Preparation of reagents

- PBS + 1% FBS + 10 mM HEPES (flow cytometry PBS): add 0.5 mL FBS and 0.5 mL 1 M HEPES to 49 mL PBS (1x pH 7.4). Keep at 4 ºC.

- RNase buffer solution: add 300 µL 15 mM NaCl and 133 µL 10 mM Tris/HCl to 20 mL bidistilled water. Adjust pH to 7.4. Keep at 4 ºC.

- RNase solution (10 mg/mL): dissolve 10 mg RNase in 1 mL RNase buffer solution. Heat at 100 ºC for 15 min. Make aliquots and keep them at -20 ºC.

Protocol

1. Seed the cells at 1.5 x 10^5 cells/mL in 6-well plates.
2. After 24 h, treat the cells (compounds or metabolic conditions) for the desire time. Use 10 µM 2-methoxystradiol as positive control[250].
3. Collect media and cells with flow cytometry PBS.
4. Centrifuge at 600 g for 5 min.
5. Wash the pellets with flow cytometry PBS.
6. Centrifuge.
7. Resuspend the pellets with 100 µL flow cytometry PBS.
8. Add 1 mL cold 70% ethanol drop by drop with slow agitation.
9. Incubate 1 h at 4 ºC. Alternatively, tubes can be stored at -20 ºC for several days.
10. Centrifuge.
11. Wash the pellets with flow cytometry PBS twice.
12. Centrifuge.
13. Resuspend the pellet in 0.5 mL of the following cocktail. For one sample:

- Flow cytometry PBS: 0.5 mL
- RNase solution (10 mg/mL): 5 µL (final concentration 100 µg/mL)
- Propidium iodide solution (1 mg/mL): 20 µL (final concentration 40 µg/mL)

14. Add 100 µL 50 mM EDTA to each tube.
15. Incubate in a water bath at 37 ºC for 30 min in the dark.
16. Detect fluorescence in a flow cytometer (Ex 493/Em 636 nm).

In this PhD Thesis, a FACS VERSE^{TM} cytometer from BD Biosciences (San Jose, CA, USA) was used. Data were analyzed with its software BD FACSuite.

4.3. Experimental approaches for the study of angiogenesis

The study of angiogenesis has gained great importance in the last decades. Many techniques have been developed in order to study several characteristics of this process. However, there are always technical limitations. For that reason, some consensus guidelines have been stablished regarding the study of angiogenesis *in vitro*, *ex vivo* and *in vivo*[251].

Several of these techniques have been performed in this PhD Thesis, but these limitations have to be taken into account.

4.3.1. Endothelial cell morphogenesis assay on Matrigel

In the last step of the angiogenic process, ECs form a new blood vessel. This can be simulated *in vitro* seeding the cells on top of a synthetic "ECM". Matrigel is a commercialized protein mixture secreted by Engelbreth-Holm-Swarm (EHS) mouse sarcoma cells which simulates acellular microenvironment of tissues[252]. Therefore, Matrigel has been widely used in many *in vitro* and *in vivo* experiments not only using ECs, but also for testing the invasiveness of tumor cells[253].

The EC morphogenesis assay on Matrigel was performed in order to test the capacity of a compound to inhibit tube formation *in vitro*.

Preparation of reagents

- Matrigel aliquots: defrost Matrigel in ice inside the refrigerator overnight. Then, make several aliquots in a cell culture hood for the maintenance of sterility keeping them on ice. Store aliquots at -20 ºC.

Protocol

1. Defrost a Matrigel aliquot in ice.

2. Add 50 µL Matrigel to each well of a 96-well plate on ice. Do not let any bubble to form.

3. Incubate the plate at 37 ºC for 30 min for the polymerization of Matrigel.

4. Prepare a cell solution with a cell density of 3 x 10^5 cells/mL for HMEC in cell culture media without FBS.

5. Once Matrigel is polymerized, seed 200 µL of the cell solution to each well.

6. Prepare the compounds to test at the desired concentrations in the corresponding cell culture media without FBS. Use 2 µM staurosporine as positive control[254].

7. Add 5 µL of the compound to the corresponding wells.

8. Incubate the plate at 37 ºC and 5% CO_2 for 3-5 h.

9. Take photographs of the wells.

In this PhD Thesis, the camera used for taking the photographs was a Nikon DS-Ri2 connected to a Nikon Eclipse Ti microscope (Nikon, Tokyo, Japan).

The number of "tubule-like" structures formed by ECs was counted in each condition, considering the control condition as 100%.

4.3.2. Tube disruption assay on Matrigel

A modified morphogenesis assay on Matrigel was also performed. In this assay, it is not the capacity of a compound to inhibit tube formation what is tested, but its capacity to disrupt pre-existing tubes. Therefore, the main experimental differences are:

- Cells are seeded on Matrigel in the absence of the compound.

- Once the "tubule-like" structures are formed, the compound is added to the wells for 90 min.

- 0.2 µM combretastatine 4-phosphate (CA4P) is used as positive control[255].

4.3.3. Wound healing assay

ECs need to migrate as part of the angiogenic process. The migratory capacity of cells under different circumstances can be determined by means of a very simple experiment such as the wound healing assay. In this assay, some cells are mechanically removed from the plate, leaving a free space for other cells to migrate towards it. This experiment was performed for 4 and 7h incubations. For longer incubations in which cells could proliferate, mitomycin B (10 ng/mL) needs to be added in order to inhibit DNA synthesis and proliferation[256].

Protocol

1. Seed the cells in 6-well plates and wait until they reach confluence.
2. Make a crosswise scratch in the confluent monolayer using a sterile 200 µL pipette tip.
3. Wash cells with PBS.
4. Add fresh media containing the desired compounds/metabolic substrates to test.
5. Take photographs of the same branch of the "wound" at 0, 4 and 7 h.

In this PhD Thesis, the camera used for taking the photographs was a Nikon DS-Ri2 connected to a Nikon Eclipse Ti microscope (Nikon, Tokyo, Japan).

Cell-free areas were measured using Image J software. Wound closure was calculated as the percentage of the initial wounded area (time 0) that had been recovered by migrating ECs after 4 or 7 h.

4.3.4. Transwell cell migration assay

Additional experiments for assessing the migratory capacity of cells are established. The transwell cell migration assay, also known as Boyden chamber assay, determines the capacity of cells to migrate towards a stimulus, such as FBS after a serum-fasted incubation. Migrating cells will be trapped in an 8 µm diameter membrane at the bottom of the transwell (**Figure 2A**). One advantage of this assay respect to the wound healing assay is that proliferation cannot influence the results.

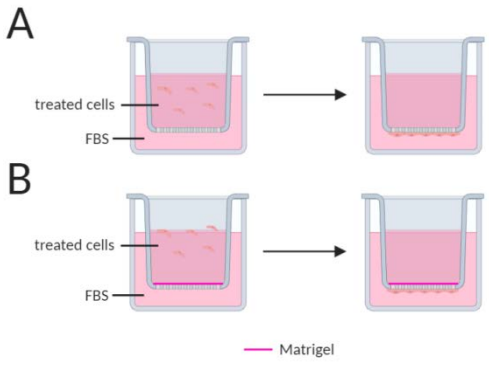

Figure 2. Transwell assays. (A) Treated cells are seeded in a transwell put inside a well containing medium with FBS. Cells will migrate towards FBS and they will be trapped at the bottom of the transwell. (B) Addition of Matrigel to the transwell allows assaying cell invasive capacity. This figure was created with BioRender.com.

Preparation of reagents

- 0.5% gelatin: add 0.5 g gelatin to 100 mL bidistilled water. Sterilize using an autoclave. Gelatin solution will be dissolved.

- 1% violet crystal: dissolve 0.1 g violet crystal in 10 mL 2% ethanol.

Protocol

1. Add 0.5 mL 0.5% gelatin to the wells of a 24-well plate.

2. Put a transparent-bottom transwell insert in each of the wells without forming bubbles and add 100 µL 0.5% gelatin on top.

3. Keep the plate at 4 ºC overnight.

4. Fast cells in fresh medium without FBS supplemented with 0.1% BSA for 24 h.

5. Prepare cell suspensions of 1.5 x 10^5 cells/mL for HMEC in medium without FBS supplemented with 0.1% BSA containing the desired concentrations of the compounds to test.

6. Aspirate the gelatin from the wells and from the top of the inserts.

7. Add 200 µL of the cell suspensions to the top of the inserts.

8. Add 0.7 mL medium without FBS for the negative control or with FBS for the rest of the conditions to the bottom of the wells.

9. Incubate at 37 ºC and 5% CO_2 for the desired time (for example, 16 h).

10. After the incubation, discard the media on the top of the transwells.

11. Put the transwells in clean wells containing 0.5 mL 4% paraformaldehyde (PFA).

12. Incubate 15 min at RT.

13. Wash the transwells in clean wells containing 1 mL PBS.

14. Put the transwells in clean wells containing 0.7 mL 1% violet crystal. The same violet crystal solution can be used several times.

15. Incubate 20 min at RT.

16. Extensively wash the transwells with distilled water.

17. Eliminate the remaining violet crystal on the top of the transwell using softly a cotton swab.

18. Let the transwells get dried at RT.

19. Take photographs of several random fields.

In this PhD Thesis, the camera used for taking the photographs was a Nikon DS-Ri2 connected to a Nikon Eclipse Ti microscope (Nikon, Tokyo, Japan).

The number of migrating cells was counted in each photograph and the mean was calculated for each condition. Cell number in control condition with FBS in the bottom well was considered as 100%.

4.3.5. Transwell cell invasion assay

A modified Boyden chamber assay can be performed in order to test the invasive capacity of cells. The same protocol as for the transwell cell migration assay was performed, but with differences (**Figure 2B**):

- 100 µL of a 0.12 mg/mL solution of Matrigel in medium without FBS are added to the top of the transwells instead of gelatin.

- The plate containing the transwells with Matrigel is left without the lid overnight inside the laminar flow hood.

4.3.6. Gelatin zymography

In order to migrate, ECs need to degrade the ECM. For that aim, ECs are able to secrete to the media MMPs, especially MMP-2 under normal conditions *in vitro*. The proteolytic activity of this 72 kDa MMP can be determined by means of a gelatin zymography. In this assay, proteins extracted from the extracellular media or from cell extracts are loaded on gelatin-containing gels and separated by electrophoresis (SDS-PAGE, sodium dodecyl sulfate-polyacrylamide gel electrophoresis) under non-reducing conditions, so that the activity of the proteins remains unaltered. Then, proteins are renaturalized by elimination of sodium dodecyl sulfate (SDS), a denaturing agent, and gels are stained with Coomassie Brilliant Blue. Active gelatinase proteins will degrade the gelatin, leaving an undyed band on the gels (**Figure 3A**). The effect of a compound on the synthesis, secretion and activity of MMPs can be detected by means of this zymographic assay.

Preparation of reagents

- Lysis buffer: prepare a 0.1 M Tris-HCl solution pH 7.4. Add 0.2% (w/v) Triton X-100 using a micropipette. Add water to the desired volume. Keep at 4 ºC. Add 200 KIU/mL aprotinin (a protease inhibitor) right before its use.

- 10% SDS: add 10 mg SDS to 100 mL bidistilled water. SDS is toxic and volatile. Put a mask lab while weighting it! Keep at RT.

- 0.5% gelatin: add 10 mg gelatin to 2 mL bidistilled water. Dissolve in a water bath at 40 ºC. Prepare right before its use.

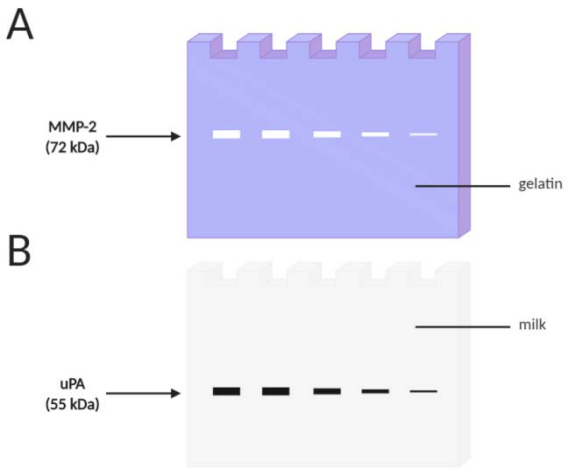

Figure 3. Zymographic assays. (A) Gelatin zymography showing MMP-2 bands and (B) plasminogen zymograpghy showing uPA bands of different samples. This figure was created with BioRender.com.

- 10% APS: add 100 mg ammonium persulfate to 1 mL bidistilled water. Keep at -20 ºC.

- Separating (resolving) buffer: prepare a 1.5 M Tris-HCl solution pH 8.8. Keep at 4 ºC.

- Stacking buffer: prepare a 0.5 M Tris-HCl solution pH 6.8. Keep at 4 ºC.

- Running buffer (10x): add 30 g Tris base (25 mM), 144 g glycine (192 mM) and 10 g SDS (0.1% w/v) to bidistilled water to make 1 L buffer. SDS is toxic and volatile. Put a mask lab while weighting it! Do not adjust pH. Keep at RT. 1x running buffer may be used twice.

- Loading buffer (4x): add 2.5 mL stacking buffer (12.5% v/v), 8 mL glycerol (40% v/v), 1.6 g SDS (8% w/v) and 10 mg bromophenol blue (0.05% w/v) to 9.5 mL bidistilled water. SDS is toxic and volatile. Put a mask lab while weighting it! Make 1 mL aliquots and keep them at -20 ºC.

- Wash buffer 1: prepare a 0.05 M Tris-HCl solution pH 7.4. Add 2% (w/v) Triton X-100. Keep at 4 ºC.

- Wash buffer 2: prepare a 0.05 M Tris-HCl solution pH 7.4. Keep at 4 ºC.

- Substrate buffer: prepare a 0.05 M Tris-HCl solution pH 7.4. Add 5 mM $CaCl_2$, 0.02% sodium azide and 1% (w/v) Triton X-100. Keep at 4 ºC.

- Coomassie Brilliant Blue solution: add 0.1% (w/v) Coomassie R-250 to a bidistilled water/methanol/acetic acid (5:5:2) solution. For 500 mL, add 0.5 g Coomassie R-250 to

210 mL bidistilled water, 210 mL methanol and 80 mL acetic acid. Keep at RT. This solution can be used more than once.

- Destaining buffer: prepare a bidistilled water/methanol/acetic acid (6:3:1) solution. For 500 mL, add 300 mL bidistilled water, 150 mL methanol and 50 mL acetic acid. Keep at RT.

Protocol

Sample collection

1. Seed the cells on 6-well plates. Seed two wells for each experimental condition in separated plates.
2. When cell cultures have reached sub-confluence, wash each well twice and add fresh media without FBS supplemented with 0.1% BSA and 200 KIU/mL aprotinin with the corresponding treatments.
3. After incubation with the treatments, put one set of plates on ice.
4. Collect conditioned media in microcentrifuge tubes on ice.
5. Wash each well twice with cold PBS (1x pH 7.4).
6. Add 0.3 mL lysis buffer to each well and collect the cell extracts by mechanical shearing on ice.
7. Centrifuge the samples at 1000 g and 4 ºC for 10 min.
8. Collect the supernatants and make single-use aliquots. Keep them at -20 ºC.
9. Use the additional set of places for cell counting using an automatized Coulter counter from Beckman Coulter (Brea, CA, USA). Cell number will be used for norrmalization of the samples, so that the same amount of protein is loaded into each lane of the gels.

Gel preparation

- Resolving (lower) gel (10%) (amounts for 2 gels -1 mm-)

Bidistilled water	2.925 mL
Acrylamide/Bis-acrylamide 40%	2.475 mL
Separating (resolving) buffer	2.5 mL
10% SDS	100 µL
0.5% gelatin	2 mL
Polymerization agents	
10% APS	50 µL
TEMED	5 µL

- Stacking (upper) gel (10%) (amounts for 2 gels -1 mm-)

Bidistilled water	3.062 mL
Acrylamide/Bis-acrylamide 40%	0.638 mL
Separating (resolving) buffer	1.25 mL
10% SDS	50 µL
Polymerization agents	
10% APS	50 µL
TEMED	10 µL

Gels can be used immediately or stored at 4 ºC for a couple of days.

Zymography

1. Put the casting frame with the gels inside an electrophoresis chamber and fill it with 1x running buffer.

2. Mix 21 µL of each sample diluted with bidistilled water with 7 µL loading buffer 4x.

3. Load samples into the gels. Additionally, load 5 µL of a prestained protein ladder.

4. Run the gels at 30 mA per gel and 4 ºC for approximately 1 h.

5. Put the separating gels in a 150 mm Petri dish filled with wash buffer 1. Mark one corner of the gel.

6. Incubate for 10 min with continuous agitation. Change the wash buffer and incubate again.

7. Wash the gels twice for 10 min with continuous agitation with wash buffer 2.

8. Add substrate buffer and incubate for 16 h at 37 ºC to activate the gelatinase activity.

9. After the incubation, wash the gels with distilled water.

10. Incubate the gels with Coomassie solution in continuous agitation until the gels get stained.

11. Replace the Coomassie solution with destaining solution and incubate with continuous agitation until the bands can be seen.

12. Replace the destaining solution with distilled water.

13. Take images of the gels.

In this PhD Thesis, photographs of the gels were taken using a Chemidoc XRS System (BioRad) with its software Image Lab.

Band areas were quantified using Image J software. Band area of the control condition was considered as 100%.

A modified version of this assay can be performed in order to detect changes specifically in MMP activity by means of an *in situ* gelatin zymography. The following modifications are made:

- Only extracts from the control condition are subjected to SDS-PAGE.

- Treatments are added along with the substrate buffer to different fragments of the gel containing individual lanes. This way the direct effect on MMP activity exerted by a compound can be determined.

4.3.7. Plasminogen zymography

For ECM degradation not only MMPs are produce, but also uPA, whose activity can be detected by means of a plasminogen zymography. The substrate of this zymography is milk. Therefore, active uPA will activate plasmin, which will degrade milk casein. As a result, transparent bands will appear after uPA activity. A black background is often used so that the bands corresponding to uPA activity will be black (**Figure 3B**).

Preparation of reagents

- Plasminogen buffer: prepare a 0.1 M sodium phosphate buffer pH 7.5 by mixing 16 mL 0.2 M $NaH_2PO_4 \cdot H_2O$ and 84 mL 0.2 M $Na_2HPO_4 \cdot 7H_2O$. Mix this buffer with NaCl and bidistilled water in order to obtain a 20 mM sodium phosphate buffer pH 7.5 + 100 mM NaCl. Sterile filter and keep it at 4 ºC.

- Plasminogen (44 U/mL): add 455 µL of plasminogen buffer to 20 U plasminogen. Make aliquots and keep them at -20 ºC.

The following reagents are common with gelatin zymographies:

- Lysis buffer
- 10% SDS
- 10% APS
- Separating (resolving) buffer
- Stacking buffer
- Running buffer (10x)
- Loading buffer (4x)
- Wash buffer 1
- Wash buffer 2

Protocol

Sample collection

Proceed as for gelatin zymographies.

Gel preparation

- Resolving (lower) gel (10%) (amounts for 2 gels -1 mm-)

Bidistilled water	4.925 mL
Acrylamide/Bis-acrylamide 40%	2.475 mL
Separating (resolving) buffer	2.5 mL
10% SDS	100 µL
Polymerization agents	
10% APS	50 µL
TEMED	5 µL

- Stacking (upper) gel (10%) (amounts for 2 gels -1 mm-)

Bidistilled water	3.062 mL
Acrylamide/Bis-acrylamide 40%	0.638 mL
Separating (resolving) buffer	1.25 mL
10% SDS	50 µL
Polymerization agents	
10% APS	50 µL
TEMED	10 µL

Gels can be used immediately or stored at 4 ºC for a couple of days.

Zymography

Steps 1-7 are identical to the ones for gelatin zymography. Starting from that point:

1. In a laminar flow hood, heat a thermoblock at 45 ºC with an electrophoresis short glass plate on top.

2. Dissolve 0.16 g skimmed milk powder in 1 mL PBS (1x pH 7.4) at 45 ºC in a water bath.

3. Add 37.5 mg agar to 3.75 mL PBS (1x pH 7.4) in a 15 mL centrifuge tube with a loosen cap. Put the tube inside a glass beaker with water. Melt agar in a microwave and put the tube at 45 ºC in a water bath.

4. Add 0.75 mL of milk dissolved in PBS to the tube containing agar.

5. Add 40 µL plasminogen (44 U/mL) and 9 µL sodium azide (0.2%).

6. Mix well and expand on the glass plate using a micropipette tip.

7. Move the glass plate off the thermoblock for solidification of the substrate gel.

8. Put the gels on top of the substrate gel and incubate them for 12 h at 4 ºC inside a humidified closed recipient. Under these conditions proteins will transfer to the substrate gel.

9. Incubate at 37 ºC until the appearance of casein-degraded bands, which indicates uPA activity.

10. Take images of the gels.

In this PhD Thesis, photographs of the gels were taken using a Chemidoc XRS System (BioRad) with its software Image Lab.

Band areas were quantified using Image J software. Band area of the control condition was considered as 100%.

4.3.8. In vitro VEGFR2 tyrosine kinase activity assay

VEGFR2 is of great importance during the angiogenesis process. This receptor gets activated through phosphorylation of tyrosine residues within its intracellular domain[26]. The anti-angiogenic capacity of a compound could be exerted by inhibition of VEGFR2 phosphorylation. The VEGFR2 (KDR) Kinase Assay Kit (BPS Bioscience) is designed to measure VEGFR2 kinase activity *in vitro* by luminiscence in the presence of different compounds. The assay is based on its combination with Kinase-Glo max reagent (Promega). Luminiscence signal obtained is inversely proportional to the amount of kinase activity due to a major amount of ATP that has not been used for luciferase activity. VEGFR2 kinase activity was measured according to the instructions provided by the manufactures as follows.

Protocol

1. Add 25 µL of the following master mix to each well of a white 96-well plate. For one sample:

- 5x kinase buffer: 6 µL
- ATP (500 µM): 1 µL
- PTK substrate (10 mg/mL): 1 µL
- Water: 17 µL

2. Add 5 µL of compound at 10x the desired final concentration to each well. Use 1 µM sunitinib as positive control[257,258].

3. Add 20 µL 1x kinase buffer to blanks.

4. Add 20 µL 1x kinase buffer containing VEGFR2 (1 ng/µL) (previously diluted with 1x kinase buffer to that concentration).

5. Incubate for 45 min at 30 ºC.

6. Thaw Kinase-Glo Max reagent.

7. Add 50 µL Kinase-Glo Max reagent to each well.

8. Incubate for 15 min at RT in the dark.

9. Measure chemiluminiscence using a microplate reader.

In this PhD Thesis, a GloMax-96 microplate luminometer from Promega was used.

Measurements were subtracted from blank signal. Control condition was considered as a 100% of VEGFR2 activity.

4.4. Experimental approaches for the study of metabolism

The study of metabolism can be addressed from high-throughput analysis to specific metabolites uptake/production, as well as through the study of enzymatic activity. In this PhD Thesis, several methodological approximations were used for the study of tumor and EC basal metabolism or in order to check the possible effect of a compound on the metabolic features of ECs. Some of the most used approaches to monitor metabolic activities of ECs have been collected in the bibliography[251].

4.4.1. Extracellular flux analyzer experiments

The Seahorse XF extracellular flux analyzers were commercialized for the first time in 2006. These instruments revolutionized the field for the study of metabolism, since in a short-time and easy-to-use experiment OXPHOS and glycolysis could be estimated in intact cells in the presence of different compounds that could be mechanically injected in real-time[259]. Two parameters are measured by this instrument: the oxygen consumption rate (OCR), which corresponds to the OXPHOS rate, and the extracellular acidification rate (ECAR), estimating glycolysis. In this PhD Thesis, a Seahorse XF^{e}24 extracellular flux analyzer and its software Wave were used. Different metabolic substrates, metabolic modulators or compounds to test have been used for the study of general metabolism of cultured cells (**Figure 4**) and different parameters have been determined accordingly (**Box 1**).

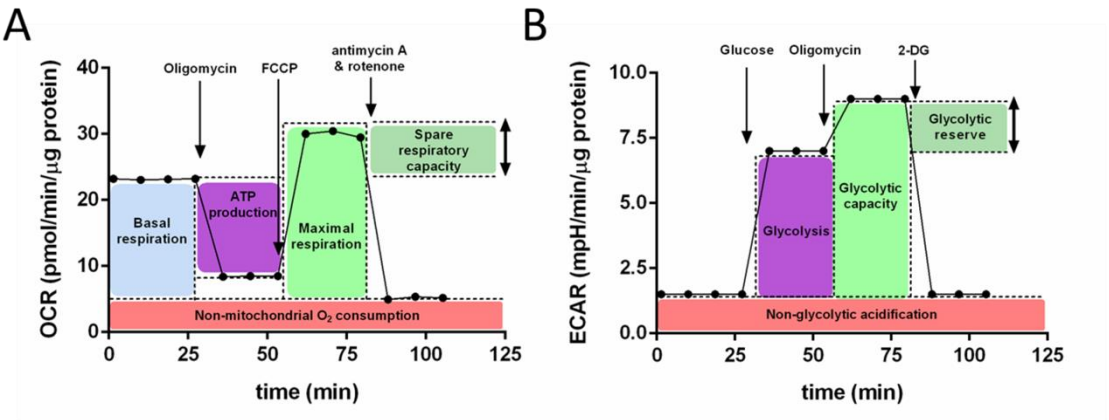

Figure 4. (A) Oxygen consumption rate (OCR) along time. Oligomycin is an inhibitor of the ATP synthase (complex V). FCCP is an uncoupling agent that collapses the proton gradient and disrupts the mitochondrial membrane potential, stimulating the ETC activity. Antimycin A is an inhibitor of complex III and rotenone inhibits complex I, shutting down mitochondrial respiration. (B) Extracellular acidification rate (ECAR) along time. Glucose boosts glycolysis. Oligomycin drives glycolysis. 2-DG is a glucose analog that inhibits glycolysis.

Box 1. Parameters determined using the Seahorse XF^{e}24 extracellular flux analyzer.

Basal respiration: oxygen consumption used to meet the endogenous energetic demand of the cell.
ATP production: ATP produced by the mitochondria to meet the endogenous energetic demand of the cell.
Maximal respiration: maximal oxygen consumption reached under a high energetic demand.
Spare respiratory capacity: capacity of a cell to respond to an energetic demand through OXPHOS, indicating the cell fitness or flexibility.
Non-mitochondrial respiration: oxygen consumption exerted by non-mitochondrial enzymes.
Glycolysis: glycolytic rate after the addition of glucose.
Glycolytic capacity: maximum glycolytic rate reached after disruption of oxidative metabolism.
Glycolytic reserve: capacity of a cell to respond to an energetic demand through glycolysis.
Non-glycolytic acidification: increase in ECAR not due to glycolysis.

Protocol

Cell preparation

1. Seed the cells in a Seahorse XF24 cell culture microplate (Agilent). Seed MDA-MB-231 cells at a cell density of 5 x 10^4 cells/well and HMECs at 3 x 10^4 cells/well in a volume of 100 µL. It is essential to seed the cells so they form a perfect monolayer. Include 3-4 blank wells without cells.
2. Incubate the plate at 37 ºC and 5% CO_2 for 4-5 hours to allow cell adherence.
3. Add 150 µL media to each well, containing or not the compound to test (if any).
4. Incubate the plate at 37 ºC and 5% CO_2 overnight.

Instrument calibration

On the same day the cells are seeded, the instrument needs to be calibrated. If the experiment cannot be performed the next day, the calibrated plate can be stored at 4 ºC for 72 h avoiding evaporation.

1. Add 1 mL Seahorse XF calibrant solution to each well of a Seahorse XF24 sensor cartridge.

2. Incubate the plate at 37 ºC without CO_2 overnight.

Data acquisition

In this PhD Thesis, three different methodological approximations have been applied:

a. The study of the metabolic preference for different metabolic substrates.

b. The study of the capacity of DMF to modulate OXPHOS (OCR).

c. The study of the capacity of DMF to modulate glycolysis (ECAR).

For each of them, different media and injections have been added to the wells.

1. After overnight incubation, wash each well twice with Seahorse XF base medium (not containing sodium bicarbonate or serum) pH 7.4.

2. Add 525 µL of the corresponding Seahorse XF base medium to each well: (a) Seahorse XF base medium pH 7.4; (b) Seahorse XF base medium pH 7.4 containing 10 mM glucose and 4 mM glutamine and DMSO/DMF; (c) Seahorse XF base medium pH 7.4 containing 4 mM glutamine and DMSO/DMF.

3. Incubate the plate at 37 ºC without CO_2 for 1 h.

4. Prepare the injections for the sensor cartridge plate to obtain the following final concentrations in the wells using the corresponding media from step 2:

a. 5 mM glucose, 0.5 mM glutamine and/or 0.5 mM palmitate.

b. 1 µM oligomycin, 0.6 µM carbonyl cyanide-4-(trifluoromethoxy)phenylhydrazone (FCCP) and 1 µM antimycin A and 1 µM rotenone.

c. 10 mM glucose, 1 µM oligomycin and 25 mM 2-DG.

5. Load 75 µL of the injections into the corresponding injection channel. Load 75 µL Seahorse XF base medium pH 7.4 for blank wells. All wells have to have the same number of loaded injection channels.

6. Introduce the sensor cartridge plate with the loaded injections and the calibrant solution but without the hydro booster in the instrument for calibration.

7. Introduce the cell culture plate in the instrument for data acquisition with the following measurement protocol: 3 initial measurement cycles and 3 measurement cycles after each injection. In this PhD Thesis, each measurement cycle consisted on 3 min mix, 2 min wait and 3 min measure. 3-5 wells corresponded to each experimental condition.

For the study of the metabolic preference for different metabolic substrates, data were normalized to the last basal measurement before the metabolic substrate injection.

For the study of the effect of DMF on metabolism, data were normalized to protein amount. After data acquisition, extract proteins were extracted by adding 75 µL RIPA buffer (50 mM Tris-HCl pH 7.4, 150 nM NaCl, 1% Triton X-100, 0.25% sodium deoxycholate and 1 mM EDTA) to each well on ice for 20 min, centrifuged at 10000 g at 4 ºC for 5 min, supernatants were collected and protein quantification was performed using the DC Protein Assay from BioRad, based on the Lowry assay, following the manufacturer's instructions. Make a standard curve with 0, 0.05, 0.075, 0.1, 0.2, 0.3, 0.4 and 0.5 µg/µL BSA. Mix 20 µL reagent S with 1 mL reagent A. Add 5 µL sample, 25 µL reagent mix and 200 µL reagent B to a 96-well plate and incubate at RT for 15 min in the dark. Measure absorbance at 750 nm.

In this PhD Thesis, an Eon Microplate Spectrophotometer from Bio-Tek Instruments (Winooski, VT, USA) was used. Samples were run in triplicates.

4.4.2. Glucose uptake

Glucose uptake can be determined by several methodological approaches. For glucose uptake after 16/24 h, cell media were run in an automated electrochemical analyzer (BioProfile Basic-4 analyzer; NOVA) and compared to the initial glucose concentration in an aliquot of the used media. This was performed during a three month fellowship in the Ralph DeBerardinis laboratory in Dallas. However, for short-time experiments, such as 30 min incubation, this approximation is not sensitive enough in order to detect differences in extracellular glucose concentration after the incubation. In this PhD Thesis, cells were incubated with the glucose fluorescent analog 2-(N-(7-nitrobenz-2-oxa-1,3-diazol-4-yl)amino)-2-deoxyglucose (2-NBDG) and glucose (2-NBDG) uptake was monitored by flow cytometry as previously described[260]. In order to do not alter the activity of glucose transporters, physiological concentrations of glucose were added along with 2-NBDG.

Preparation of reagents

- DPBS: prepare 1x PBS pH 7.4 and add $CaCl_2 \cdot 2\ H_2O$ and $MgCl_2 \cdot 6\ H_2O$ to a final concentration of 1 mM. Sterilize by filtration using a 0.22 µm filter. Keep at RT. Do not heat.

- 2-NBDG (15 mM): add 974 µL absolute ethanol to 5 mg 2-NBDG. Make aliquots and let them to dry inside a laminar flow hood. Once the ethanol is evaporated, keep the tubes at -20 ºC. Before its use, add the equivalent volume of DMSO to each tube, corresponding to the initial aliquot volume.

- PBS + 1% FBS + propidium iodide: add 0.5 mL FBS to 49.5 mL 1x PBS. Keep it at 4 ºC. Immediately before its use, add propidium iodide to a final concentration of 1 µg/mL.

Protocol

1. Seed cells in 96-well plates. Seed MDA-MB-231 cells at a cell density of 1 x 10^4 cells/well and any other cell line at 2 x 10^4 cells/well in a volume of 100 µL.

2. After cell adherence, add the compounds to test and incubate for the corresponding incubation time. If no compound is to be added, proceed immediately to the next step.

3. Wash the cells with DPBS twice.

4. Add 100 µL DBPS to each well containing or not the compound to test (if any).

5. Incubate the cells at 37 ºC and 5% CO_2 for 30 min.

6. Remove DBPS and add 100 µL fresh DBPS containing 5 mM glucose and 0.5 mM glutamine and/or 0.5 mM palmitate along with 100 µM 2-NBDG and the compound to test (if any). Include a well containing no 2-NBDG as blank.

7. Incubate the cells at 37 ºC and 5% CO_2 for 30 min.

8. Put the plates on ice and remove the media.

9. Wash the cells twice with cold 1x PBS.

10. Collect the cells in 200 µL 1x PBS containing 1% FBS and propidium iodide. Keep the samples on ice.

11. Detect fluorescence in a flow cytometer (Ex 467/Em 542 nm).

In this PhD Thesis, a FACS VERSE^{TM} cytometer from BD Biosciences (San Jose, CA, USA) was used. Data were analyzed with its software BD FACSuite. Data were normalized to the control condition (media with only glucose or without the compound to test).

4.4.3. Glutamine uptake

For glutamine uptake after 16/24 h, cell media were run in an automated electrochemical analyzer (BioProfile Basic-4 analyzer; NOVA) and compared to the initial glutamine concentration in an aliquot of the used media. Due to degradation of glutamine, it is important to add media to a plate without cells and obtain the media from that plate instead of getting it from the bottle after the incubation time. This was performed during a three month fellowship in the Ralph DeBerardinis laboratory in Dallas. However, as happens with glucose uptake for short-time experiments, such as 30 min incubation, this approximation is not sensitive enough in order to detect differences in extracellular glutamine concentration after the incubation. In this PhD Thesis, glutamine uptake was determined by using the radioactive tracer L-[^{14}C(U)]-glutamine. All these assays were carried out at the Radioactive Facilities of the University of Málaga, authorized with reference IR/MA-13/80 (IRA-0940) for the use of non-encapsulated radionuclides.

Preparation of reagents

- $HClO_4$ (10%): dissolve $HClO_4$ (70%) with bidistilled water to a final concentration of 10%. Use glass material.

The following reagents are common with glucose uptake:

- DPBS

Protocol

1. Seed cells in 96-well plates. Seed MDA-MB-231 cells at a cell density of 1 x 10^4 cells/well and any other cell line at 2 x 10^4 cells/well in a volume of 100 µL.

2. After cell adherence, add the compounds to test and incubate for the corresponding incubation time. If no compound is to be added, proceed immediately to the next step.

3. Wash the cells with DPBS twice.

4. Add 100 µL DBPS to each well containing or not the compound to test (if any).

5. Incubate the cells at 37 ºC and 5% CO_2 for 30 min.

6. Remove DBPS and add 100 µL fresh DPBS containing 0.5 mM glutamine and 5 mM glucose and/or 0.5 mM palmitate along with 0.5 µCi/mL L-[^{14}C(U)]-glutamine and the compound to test (if any). Include a well containing no L-[^{14}C(U)]-glutamine as blank.

7. Incubate the cells at 37 ºC and 5% CO_2 for 30 min.

8. Put the plates on ice and remove the media.

9. Wash the cells twice with cold 1x PBS.

10. Collect the cells in 100 µL $HClO_4$ (10%).

11. Mix the cells with 4 mL scintillation liquid.

12. Measure the disintegrations per minute (dpm) of ^{14}C.

In this PhD Thesis, a Beckman Coulter LS6500 liquid scintillation counter (Fullerton, CA, USA) was used for the measurements.

Dpm data were converted to nmol of glutamine using the specific activity of the radiotracer and the $^{12}C/^{14}C$ proportion. Data were normalized to protein amount of parallel wells and the control condition (media with only glutamine or without the compound to test) was considered as 100%. For protein quantification, proteins were collected with lysis buffer (see section 4.3.6. of Material and Methods), centrifuged at 10000 g at 4 ºC for 5 min and supernatants were collected. Protein quantification was performed using the Bio-Rad Protein Assay, based on the Bradford assay, according to the purchaser's instructions. Briefly, make a standard curve with 0, 0.05, 0.075, 0.1, 0.2, 0.3, 0.4 and 0.5 µg/µL BSA. Add 10 µL diluted sample and 200 µL dye reagent (previously diluted 5 times with bidistilled water) to a 96-well plate and incubate at RT for 5 min in the dark. Measure absorbance at 595 nm within an hour.

In this PhD Thesis, an Eon Microplate Spectrophotometer from Bio-Tek Instruments (Winooski, VT, USA) was used. Data were collected by Gen5 software from the same manufacturers.

4.4.4. Palmitate uptake

Cells were incubated with palmitate linked to the fluorescent molecule BODIPY and palmitate (BODIPY FL C_{16} or 4,4-difluoro-5,7-dimethyl-4-bora-3a,4a-diaza-s-indacene-3-hexadecanoic acid) uptake was monitored by flow cytometry as previously described with modifications[261]. In order to do not alter the activity of lipid transporters, physiological concentrations of palmitate were added along with BODIPY FL C_{16}.

Preparation of reagents

- Cell buffer: add BSA to a final concentration of 0.1% (w/v) to DPBS. Dissolve at 37 ºC.

- BODIPY FL C_{16} (2 mM): add 1054 µL absolute ethanol to 1 mg BODIPY FL C_{16}. Make aliquots and let them to dry inside a laminar flow hood. Once the ethanol is evaporated, keep the tubes at -20 ºC. Before its use, add the equivalent volume of DMSO to each tube, corresponding to the initial aliquot volume.

The following reagents are common with glucose uptake:

- DPBS

- PBS + 1% FBS + propidium iodide (except that a final concentration of 25 μg/mL propidium iodide was used).

Protocol

1. Seed cells in 24-well plates until they reach sub-confluence.

2. Add the compounds to test and incubate for the corresponding incubation time. If no compound is to be added, proceed immediately to the next step.

3. Wash the cells with DPBS twice.

4. Add 0.5 mL DBPS to each well containing or not the compound to test (if any).

5. Incubate the cells at 37 ºC and 5% CO_2 for 30 min.

6. Remove DBPS and add 0.5 mL cell buffer containing 0.5 mM palmitate and 5 mM glucose and/or 0.5 mM glutamine along with 2 μM BODIPY FL C_{16} and the compound to test (if any). Include a well containing no BODIPY FL C_{16} as blank.

7. Incubate the cells at 37 ºC and 5% CO_2 for 30 min.

8. Put the plates on ice and remove the media.

9. Wash the cells twice with cold 1x PBS.

10. Collect the cells in 0.5 mL 1x PBS containing 1% FBS and propidium iodide. Keep the samples on ice.

11. Detect fluorescence in a flow cytometer (Ex 485/Em 528 nm).

In this PhD Thesis, a FACS VERSE™ cytometer from BD Biosciences (San Jose, CA, USA) was used. Data were analyzed with its software BD FACSuite. Data were normalized to the control condition (media with only palmitate or without the compound to test).

4.4.5. Lactate production

For lactate production after 16/24 h, cell media were run in an automated electrochemical analyzer (BioProfile Basic-4 analyzer; NOVA). This was performed during a three month fellowship in the Ralph DeBerardinis laboratory in Dallas. However, as happens with glucose and glutamine uptake for short-time experiments, such as 30 min incubation, this approximation is not sensitive enough in order to detect lactate production after such a short time. In this PhD Thesis, lactate production was measured using a lactate assay kit (Abnova). Sample collection was performed as previously described with modifications[262].

Preparation of reagents

- KOH (20%): dissolve 7.06 g KOH (85%) to 30 mL bidistilled water.

The following reagents are common with glucose/glutamine uptake:

- DPBS
- $HClO_4$ (10%)

Protocol

Sample collection

1. Seed cells in 6-well plates until they reach sub-confluence.
2. Add the compounds to test and incubate for the corresponding incubation time. If no compound is to be added, proceed immediately to the next step.
3. Wash the cells with DPBS twice.
4. Add 1.5 mL DBPS to each well containing or not the compound to test (if any).
5. Incubate the cells at 37 ºC and 5% CO_2 for 30 min.
6. Remove DBPS and add 1.5 mL fresh DBPS containing 5 mM glucose and/or 0.5 mM glutamine and/or 0.5 mM palmitate along with the compound to test (if any). Include a well containing no metabolic substrate as blank.
7. Incubate the cells at 37 ºC and 5% CO_2 for 30 min.
8. Put the plates on ice.
9. Collect 0.5 mL of the media on ice and add 100 µL $HClO_4$ (10%). Collect cells for protein quantification as in section 4.4.3 of Materials and Methods.
10. Centrifuge at 10000 g for 5 min.
11. Collect 0.5 mL of the supernatants.
12. Add 10 µL pH indicator solution to each tube.
13. Add 20% KOH until pH reaches approximately 7.4. Correct with 10% $HClO_4$ if necessary. Annotate the volume added to each tube for data correction.
14. Keep the tubes on ice for 10 min.
15. Centrifuge at 10000 g for 5 min.
16. Collect 0.5 mL of the supernatants.
17. Make aliquots and use them immediately or keep them at -80 ºC.

Lactate measurement

Lactate measurement was performed following the manufacturer's instructions.

1. Prepare a lactate standard curve with lactate concentrations of 0, 20, 40, 60, 80 and 100 pmol/well.

2. Add 2-50 µL standard or samples to each well of a 96-well plate.
3. Adjust volume to 50 µL using lactate assay buffer.
4. Add 50 µL reaction mix consisting on:
   - 47.6 µL lactate assay buffer
   - 2 µL lactate enzyme mix
   - 0.4 µL lactate probe
5. Incubate the plate at RT for 30 min in the dark.
6. Measure fluorescence in a fluorescence microplate reader (Ex 535/Em 590 nm).

In this PhD Thesis, a FL600FA fluorescence microplate reader from Bio-Tek Instruments (Winooski, VT, USA) was used. Data were collected using KC4 software.

Data were normalized to protein amount as in section 4.4.3 of Materials and Methods.

4.4.6. Glutamine oxidation

Glutamine oxidation through the TCA cycle can be determined by the measurement of the CO_2 liberated in the conversion of α-ketoglutarate to succinyl-CoA. The use of the radioactive tracer L-[^{14}C(U)]-glutamine allows the specific detection of CO_2 coming from glutamine carbons using a simple system (**Figure 5**). This assay was carried out at the Radioactive Facilities of the University of Málaga, authorized with reference IR/MA-13/80 (IRA-0940) for the use of non-encapsulated radionuclides.

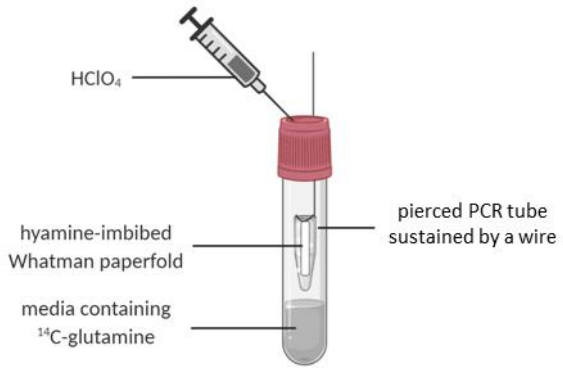

Figure 5. System for the detection of CO_2 coming from glutamine carbons. Media containing ^{14}C-glutamine is collected in a round-bottom glass tube with screw-cap. Each glass tube contains a Whatman™ paperfold imbibed with hyamine inside a pierced PCR tube sustained by a wire. $HClO_4$ is added through the cap using an insulin syringe. This $HClO_4$ will free CO_2, which will get captured by hyamine. This figure was created with BioRender.com.

Preparation of reagents

The following reagents are common with glutamine uptake:

- DPBS
- $HClO_4$

Protocol

1. Seed cells in 24-well plates until they reach sub-confluence.

2. Add the compounds to test and incubate for the corresponding incubation time. If no compound is to be added, proceed immediately to the next step.

3. Wash the cells with DPBS twice.

4. Add 0.5 mL DBPS to each well containing or not the compound to test (if any).

5. Incubate the cells at 37 ºC and 5% CO_2 for 30 min.

6. Remove DBPS and add 0.5 mL fresh DPBS containing 0.5 mM glutamine and 5 mM glucose and/or 0.5 mM palmitate along with 0.5 µCi/mL L-[^{14}C(U)]-glutamine, 25 mM HEPES and the compound to test (if any). The high concentration of HEPES will keep CO_2 inside the cell in the form of HCO_3^-. Include a well containing no L-[^{14}C(U)]-glutamine as blank.

7. Incubate the cells at 37 ºC and 5% CO_2 for 30 min.

8. Put the plates on ice.

9. Collect the media in a round-bottom glass tube with screw-cap. Each glass tube must contain a Whatman™ paperfold imbibed with benzethonium hydroxide (hyamine). Additionally, collect the cells and add them to additional tubes. In each case, keep 10 µL to mix with scintillation liquid to measure the amount of ^{14}C-glutamine in each sample.

10. Add 0.4 mL $HClO_4$ (10%) to each tube through the cap using an insulin syringe in order to free CO_2, which will get captured by hyamine.

11. Incubate in a water bath at 37 ºC with continuous shaking for 30 min.

12. Put each hyamine-imbibed Whatman™ paperfolds inside a vial containing scintillation liquid.

13. Measure the disintegrations per minute (dpm) of ^{14}C.

In this PhD Thesis, a Beckman Coulter LS6500 liquid scintillation counter (Fullerton, CA, USA) was used for the measurements.

Dpm data were converted to nmol of glutamine using the specific activity of the radiotracer and the ^{12}C/^{14}C proportion, and data from cell media and cell extracts for

each condition were combined. Data were normalized to protein amount of parallel wells and the control condition (media with only glutamine or without the compound to test) was considered as 100%. Protein quantification was performed as in section 4.4.3 of Materials and Methods.

4.4.7. Ammonia production

In the GLS reaction, ammonia is released from glutamine along with glutamate. Ammonia production can be thus measured in cell media using a commercial kit such as the L-glutamine/ammonia assay kit (Megazyme) following the purchaser's instructions. This experiment was performed during a three month fellowship in the Ralph DeBerardinis laboratory in Dallas.

Protocol

1. Add 10 µL sample to each well of a 96-well plate.
2. Add the following reaction mix to each well:
   - 172 µL bidistilled water
   - 30 µL solution 2 (buffer)
   - 20 µL solution 3 (NADPH)
3. Mix, incubate for 4 min and read absorbance at 340 nm.
4. Add 2 µL of suspension 5 (GDH) to each well.
5. Mix, incubate for 10 min and read absorbance at 340 nm.

In this PhD Thesis, a FLUOstar Omega microplate reader from BMG LABTECH (Ortenberg, Germany) was used. Data were normalized to cell number.

4.4.8. Measurement of intracellular metabolites with the AbsoluteIDQ p180 kit

The AbsoluteIDQ p180 kit (Biocrates) allows the high-throughput analysis of up to 188 intracellular metabolites from cells in culture, including 21 amino acids, 21 biogenic amides, hexoses as a whole, 39 acylcarnitines, 90 glycerophospholipids and 15 sphingolipids (**Tables 4-8**). This experiment was performed during a 5 days fellowship in the Marta Cascante laboratory in Barcelona.

Table 4. Amino acids detected by the AbsoluteIDQ p180 kit (Biocrates).

Alanine	Arginine	Asparagine
Aspartate	Citrulline	Glutamine
Glutamate	Glycine	Histidine
Isoleucine	Leucine	Lysine
Methionine	Ornithine	Phenylalanine
Proline	Serine	Threonine
Tryptophan	Tyrosine	Valine

Table 5. Biogenic amides detected by the AbsoluteIDQ p180 kit (Biocrates).

Acetylornithine	Asymmetric dimethylarginine (ADMA)	α-aminoadipic acid (alpha-AAA)
Carnosine	Creatine	Dihydroxyphenylalanine (DOPA)
Dopamine	Histamine	Kynurenine
Methionine sulfoxide (Met-SO)	Nitrotyrosine	Phenylethylamine
Cis-4-hydroxyproline (c4-OH-Pro)	Trans-4-hydroxyproline (t4-OH-Pro)	Putrescine
Sarcosine	Symmetric dimethylarginine (SDMA)	Serotonin
Spermidine	Spermine	Taurine

Table 6. Acylcarnitines detected by the AbsoluteIDQ p180 kit (Biocrates).

C0 (Carnitine)	C2 (Acetylcarnitine)
C3 (Propionylcarnitine)	C3:1 (Propenoylcarnitine)
C3-OH (Hydroxypropionylcarnitine)	C4 (Butyrylcarnitine)
C4:1 (Butenoylcarnitine)	C4-OH (Hydroxybutyrylcarnitine)
C5 (Valerylcarnitine)	C5:1 (Tiglylcarnitine)
C5:1-DC (Glutaconylcarnitine)	C5-DC (Glutarylcarnitine)
C5-M-DC (Methylglutarylcarnitine)	C5-OH (Hydroxyvalerylcarnitine)
C6 (Hexanoylcarnitine)	C6:1 (Hexenoylcarnitine)
C7-DC (Pimelylcarnitine)	C8 (Octanoylcarnitine)
C9 (Nonanoylcarnitine)	C10 (Decanoylcarnitine)
C10:1 (Decenoylcarnitine)	C10:2 (Decadienylcarnitine)
C12 (Dodecanoylcarnitine)	C12:1 (Dodecenoylcarnitine)
C12-DC (Dodecanedioylcarnitine)	C14 (Tetradecanoylcarnitine)
C14:1 (Tetradecenoylcarnitine)	C14:1-OH (Hydroxytetradecenoylcarnitine)
C14:2 (Tetradecadienylcarnitine)	C14:2-OH (Hydroxytetradecadienylcarnitine)

Table 6 (continued)

C16 (Hexadecanoylcarnitine)	C16:1 (Hexadecenoylcarnitine)
C16:1-OH (Hydroxyhexadecenoylcarnitine)	C16:2 (Hexadecadienylcarnitine)
C16:2-OH (Hydroxyhexadecadienylcarnitine)	C16-OH (Hydroxyhexadecanoylcarnitine)
C18 (Octadecanoylcarnitine)	C18:1 (Octadecenoylcarnitine)
C18:1-OH (Hydroxyoctadecenoylcarnitine)	C18:2 (Octadecadienylcarnitine)

The number of carbon atoms and double bonds, as well as the presence or not of a hydroxyl group (OH) or a dicarboxylic acid (DC) are indicated.

Table 7. Glycerophospholipids detected by the AbsoluteIDQ p180 kit (Biocrates).

lysoPC a C14:0	lysoPC a C16:0	lysoPC a C16:1	lysoPC a C17:0	lysoPC a C18:0
lysoPC a C18:1	lysoPC a C18:2	lysoPC a C20:3	lysoPC a C20:4	lysoPC a C24:0
lysoPC a C26:0	lysoPC a C26:1	lysoPC a C28:0	lysoPC a C28:1	PC aa C24:0
PC aa C26:0	PC aa C28:1	PC aa C30:0	PC aa C30:2	PC aa C32:0
PC aa C32:1	PC aa C32:2	PC aa C32:3	PC aa C34:1	PC aa C34:2
PC aa C34:3	PC aa C34:4	PC aa C36:0	PC aa C36:1	PC aa C36:2
PC aa C36:3	PC aa C36:4	PC aa C36:5	PC aa C36:6	PC aa C38:0
PC aa C38:1	PC aa C38:3	PC aa C38:4	PC aa C38:5	PC aa C38:6
PC aa C40:1	PC aa C40:2	PC aa C40:3	PC aa C40:4	PC aa C40:5
PC aa C40:6	PC aa C42:0	PC aa C42:1	PC aa C42:2	PC aa C42:4
PC aa C42:5	PC aa C42:6	PC ae C30:0	PC ae C30:1	PC ae C30:2
PC ae C32:1	PC ae C32:2	PC ae C34:0	PC ae C34:1	PC ae C34:2
PC ae C34:3	PC ae C36:0	PC ae C36:1	PC ae C36:2	PC ae C36:3
PC ae C36:4	PC ae C36:5	PC ae C38:0	PC ae C38:1	PC ae C38:2
PC ae C38:3	PC ae C38:4	PC ae C38:5	PC ae C38:6	PC ae C40:1
PC ae C40:2	PC ae C40:3	PC ae C40:4	PC ae C40:5	PC ae C40:6
PC ae C42:0	PC ae C42:1	PC ae C42:2	PC ae C42:3	PC ae C42:4
PC ae C42:5	PC ae C44:3	PC ae C44:4	PC ae C44:5	PC ae C44:6

lysoPC: lysophosphatidylcholine; PC: phosphatidylcholine; aa indicates that both moieties at the sn-1 and sn-2 position are fatty acids bound to the glycerol backbone via ester bonds; ae indicates that either the sn-1 or the sn-2 position is a fatty acid alcohol bound via an ether bond. The number of carbon atoms and the number of double bonds are indicated.

Table 8. Sphingolipids detected by the AbsoluteIDQ p180 kit (Biocrates).

SM (OH) C14:1	SM C16:0	SM C16:1	SM (OH) C16:1	SM C18:0
SM C18:1	SM C20:2	SM C22:3	SM (OH) C22:1	SM (OH) C22:2
SM C24:0	SM C24:1	SM (OH) C24:1	SM C26:0	SM C26:1

SM: Sphingomyelin. The number of carbon atoms and double bonds, as well as the presence or not of a hydroxyl group (OH) are indicated.

Protocol

Sample preparation

1. Seed the cells in 10 cm cell culture dishes until they reach subconfluence.

2. Treat the cells with the desired metabolic fuels or compounds to test for the desired time.

3. Put the plates on ice and remove the media.

4. Wash the cells with ice-cold 1x PBS.

5. Collect the cells and centrifuge them at 600 g at 4 ºC for 5 min.

6. Wash the pellets twice with 10 mL ice-cold 1x PBS.

7. Resuspend the pellets in 1 mL ice-cold 1x PBS and transfer the cell solutions to microcentrifuge tubes.

8. Centrifuge at 600 g at 4 ºC for 5 min.

9. Discard the supernatants and freeze the pellets with liquid nitrogen.

10. Store at -80 ºC or use immediately.

11. Resuspend the pellets in 70 µL 85% ethanol in PBS.

12. Sonicate the suspension three times using a titanium probe (15 s with 5 s pause between sonications) and keeping the tube in ice (sonication conditions: output 25, tune 50).

13. Submerge the tubes in liquid nitrogen for 30 s and thaw at 95 ºC in a heat block.

14. Repeat steps 12 and 13.

15. Centrifuge at 20000 g at 4 ºC for 5 min.

16. Collect the supernatants and transfer them immediately into the Biocrates plate wells (annotate volume for each sample) or store them at -80 ºC.

17. Use the pellets for protein quantification. Resuspend the pellets in 150 µL KOH (30%) and heat them at 100 ºC for 15 min. Centrifuge at 10000 g for 5 min and collect the supernatants. For protein quantification, the Bio-Rad Protein Assay, based on the Bradford assay, was performed according to the purchaser's instructions (see section 4.4.3 of Material and Methods).

Samples and calibration standards were added to the Biocrates plate (10 µL for standards, internal standards and quality controls, and up to 50 µL for samples). The experiment was run by a specialized technician according to the purchaser's instructions.

In this PhD Thesis, a Vibra-Cell sonicator from Sonics & Materials Inc. (Newtown, CT, USA) was used. Metabolites were determined by LC/MS or flow injection analysis

(FIA)-tandem mass spectrometry using a Sciex 4000 QTRAP mass spectrometer, which was coupled to an Agilent 1200 HPLC for the LC/MS analysis. Data were analyzed with Analyst and MetIDQ software and normalized to protein amount.

4.4.9. Metabolomics and labeling experiments using stable isotopes

The use of stable isotopes, such as ^{13}C, allows the tracing of carbons from the labeled molecule through the synthesis of different metabolites in different metabolic pathways. In this PhD Thesis, [U-^{13}C]-glucose, [U-^{13}C]-glutamine, [U-^{13}C]-serine and [U-^{13}C]-glycine have been used in order to trace their metabolic fates in the presence of DMF by means of gas chromatography/mass spectrometry (GC/MS) and liquid chromatography/mass spectrometry (LC/MS). Combination of both techniques allows the detection for hundreds of intracellular metabolites. Additionally, the total amount of intracellular metabolites was determined using these techniques, although in this case the use of stable isotopes is not necessary. These experiments were performed during a three month fellowship in the Ralph DeBerardinis laboratory in Dallas.

Preparation of reagents

- Methoxyamine (10 mg/mL): add 10 mg methoxyamine to 1 mL pyridine. Keep at 4 ºC and use within 2 weeks.

Protocol

Sample preparation

1. Seed the cells in 60 mm cell culture dishes at a cell density of 5 x 10^5 cells/dish and let them grow for 48 h or 1 x 10^6 cells/dish and let them grow for 24 h.
2. Wash the cells with 1x PBS.
3. Add 2 mL labeling media containing 10 mM glucose or [U-^{13}C]-glucose and 4 mM glutamine or [U-^{13}C]-glutamine in DMEM supplemented with 10% dFBS in the presence or absence of the compound to test. For experiments of serine and glycine withdrawal or labeling, add 10 mM glucose, 4 mM glutamine, 0.4 mM serine or [U-^{13}C]-serine and/or 0.4 mM glycine or [U-^{13}C]-glycine for 24 h in serine and glycine free RPMI-1640 or DMEM supplemented with 10% dFBS containing or not the compound to test.
4. Incubate at 37 ºC and 5% CO_2 for the desired time.
5. Put the dishes on ice and wash the cells with 0.9% NaCl.
6. Collect the cells in 1 mL cold 80% methanol.

7. Lyse the cells with three freeze-thaw cycles placing the tubes in liquid nitrogen and in a 37 ºC water bath.

8. Centrifuge at 17000 g at 4 ºC for 15 min to eliminate cell debris.

9. Collect supernatants.

10. For LC/MS experiments, dry supernatants in a SpeedVac vaccum concentrator and keep the dried samples at -80 ºC until analysis.

11. For GC/MS experiments, add 50 nmol sodium 2-oxobutyrate as internal standard to each sample. Evaporate the samples and continue with the protocol or store them at -80 ºC. Add 40 µL methoxyamine (10 mg/mL in pyridine), incubate at 70 ºC for 15 min, add 75 µL N-(tert-butyldimethylsilyl)-N-methyltrifluoroacetamide (MTBSTFA) to each tube and incubate at 70 ºC for 1 h. Transfer the samples to GC/MS autoinjector vials.

GC/MS

In this PhD Thesis, samples were injected in either an Agilent 6890 or 7890 gas chromatograph coupled to an Agilent 5973N or 5975C Mass Selective Detector, respectively. Data were acquired using MSD ChemStation software (Agilent). The observed distributions of mass isotopologues were corrected for natural abundance. Intracellular relative abundance of metabolites was normalized to cell number.

LC/MS

For LC/MS analysis, a specialized technician reconstituted the samples in 0.1% formic acid in water. 5 µL were injected into a 1290 UHPLC liquid chromatography system interfaced to a high-resolution mass spectrometry (HRMS) 6550 iFunnel Q-TOF MS (Agilent). The MS was operated in both positive and negative (ESI+ and ESI-) modes. Analytes were separated on an Acquity UPLC® HSS T3 column (1.8 µm, 2.1 x 150 mm, Waters, MA). The column was kept at RT. Mobile phase A composition was 0.1% formic acid in water and mobile phase B composition was 0.1% formic acid in 100% acetonitrile. The LC gradient was 0 min: 1% B; 5 min: 5% B; 15 min: 99%; 23 min: 99%; 24 min: 1%; 25 min: 1%. The flow rate was 250 µL/min. Data were acquired using Profinder B.08.00 SP3 software (Agilent). Intracellular relative abundance of metabolites was normalized by total ion current (TIC) normalization.

4.4.10. PHGDH activity assay

PHGDH activity in cells was measured using the Phosphoglycerate Dehydrogenase (PHGDH) Activity Assay Kit (BioVision). This assay is based on the reduction of a

probe in the presence of NADH, generated in the PHGDH reaction, which generates a strong absorbance signal at 450 nm. This experiment was performed during a three month fellowship in the Ralph DeBerardinis laboratory in Dallas.

Protocol

Sample preparation

1. Seed the cells in 10 cm cell culture dishes until they reach sub-confluence.
2. Treat the cells with the compound to test for the desired time.
3. Put the dishes on ice.
4. Remove the media and add 0.4 mL ice-cold PHGDH Assay Buffer.
5. Incubate on ice for 10 min.
6. Centrifuge at 10000 g at 4 ºC for 5 min.
7. Collect the supernatants.
8. Precipitate proteins using saturated 4.32 M ammonium sulfate to 65% (1:2).
9. Put on ice for 30 min.
10. Centrifuge at 10000 g at 4 ºC for 10 min.
11. Resuspend the pellet with PHGDH Assay Buffer.

PHGDH activity assay

1. Prepare a NADH standard curve with 0, 2, 4, 6, 8, 10 and 12.5 nmol/well of NADH in a 96-well plate.
2. Add 2-50 µL samples, so that final concentration is 100 µg protein/well.
3. Adjust volume to 50 µL with PHGDH Assay Buffer.
4. Add 50 µL reaction mix to each well containing:
   - 46 µL PHGDH assay buffer
   - 2 µL PHGDH developer
   - 2 µL PHGDH substrate
5. Incubate for 10 min at 37 ºC in the dark.
6. Measure absorbance at 450 nm at 37 ºC.

In this PhD Thesis, a FLUOstar Omega microplate reader from BMG LABTECH (Ortenberg, Germany) was used. Data were normalized to protein amount.

4.4.11. Measurement of ROS levels

Oxidative metabolism can lead to an excessive production of ROS. Additionally, some compounds can favor the production or elimination of ROS through different

mechanisms. Intracellular ROS levels can be easily measured by the use of 2′,7′-dichlorofluorescin diacetate (DCFH-DA). This compound enters the cell and different esterases cut the diacetate, leaving DCFH trapped inside the cell, which is oxidized in the presence of ROS, converting into the fluorescent compound DCF. Therefore, higher intracellular ROS levels would lead to higher fluorescence (**Figure 6**).

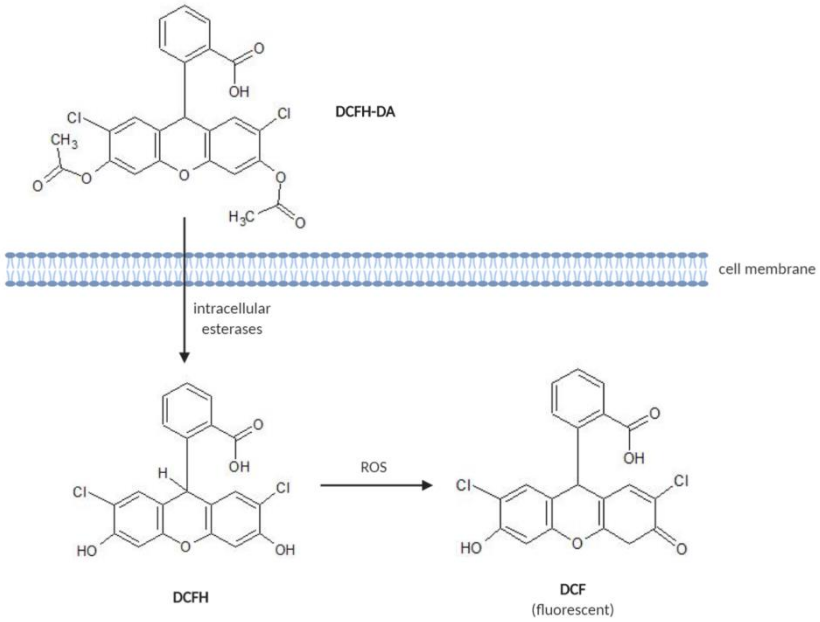

Figure 6. Measurement of ROS levels using DCFH-DA. DCFH-DA enters the cell and intracellular esterases cut the diacetate (DA) motif, leaving DCFH trapped inside the cell, which is oxidized in the presence of reactive oxygen species (ROS), converting into the fluorescent compound DCF. Chemical structures were drawn using ChemSketch software. This figure was created with BioRender.com.

Protocol

1. Seed the cells in a 24-well plate until they reach sub-confluence.
2. Wash the cells with 1x PBS.
3. Incubate cells with 40 µM DCFH-DA in media without serum at 37 ºC and 5% CO_2 for 30 min. Leave at least one well without DCFH-DA as blank.
4. Wash the cells with 1x PBS.
5. Add media with serum containing the compound to test in the presence or absence of 300 µM H_2O_2 and incubate at 37 ºC and 5% CO_2 for the desired time. Use 200 µM antimycin A as positive control. Optimal concentrations should be empirically determined for each cell line.

6. Measure fluorescence using a fluorescence microplate reader (Ex 485/Em 530 nm).

In this PhD Thesis, a FL600FA fluorescence microplate reader from Bio-Tek Instruments (Winooski, VT, USA) was used. Data were collected using KC4 software.

4.5. Gene and protein expression assays

4.5.1. Gene expression studies by quantitative PCR (qPCR)

The most common technique for the study of gene expression is qPCR. In this PhD Thesis, both basal gene expression and its modification by different environmental conditions or treatment with different compounds were tested. The details for the primers used in this PhD Thesis are collected in section 1.4 of the Materials and Methods section.

Protocol

RNA extraction

The first step for the study of gene expression is the extraction of mRNA. In this PhD Thesis, the Direct-zol™ RNA MiniPrep (Zymo Research) was used according to manufacturer's instructions.

1. Seed cells in 6-well plates and add the corresponding treatment.

2. Put the plates on ice, remove the media and immediately freeze the plates at -80ºC or proceed to RNA extraction. For cells in suspension, collect the pellets, freeze them in liquid nitrogen and keep them at -80 ºC.

3. Add 0.3 mL Tri-reagent to each well or 0.6 mL to pellets from cells in suspension.

4. For adherent cells, collect the samples in microcentrifuge tubes and incubate for 3-5 min at RT.

5. Add an equal volume of 100% ethanol to each tube and mix by tube inversion.

6. Transfer the mixture into a Zymo-Spin™ IIC Column in a Collection Tube and centrifuge at 13000 g for 1 min.

7. Discard the flow-through and the collection tube, and then transfer the column into a new collection tube.

8. Add 0.4 mL RNA Wash Buffer and centrifuge at 13000 g for 1 min.

9. Add 80 µL DNase I mix (5 µL DNase (6 U/µL) + 75 µL DNA Digestion Buffer) to each tube and incubate at RT for 15 min.

10. Add 0.4 mL Direct-zol™ RNA PreWash and centrifuge at 13000 g for 1 min. Repeat this step.

11. Add 0.7 mL RNA Wash Buffer and centrifuge at 13000 g for 2 min.

12. Transfer the columns to a new microcentrifuge tube.

13. Add ≥ 25 µL DNase/RNase-free water to elute RNA and centrifuge at 13000 g for 1 min.

14. Check RNA amount and quality (260/280 ratio). A 260/280 ratio similar to 2 indicates a good RNA quality.

In this PhD Thesis, a NanoDrop ND-1000 (Thermo Scientific) was used for the measurement of RNA amount and quality.

cDNA synthesis

In order to detect gene expression, the extracted mRNA has to be converted into its complementary DNA (cDNA). In this PhD Thesis, two different kits have been used for this step: the High-Capacity cDNA Reverse Transcription Kit (Applied Biosystems) or the PrimeScript™ RT reagent Kit (Takara) following the purchaser's instructions. In the first case, 1 µg cDNA was synthetized, whereas up to 500 ng cDNA were synthetized using the second kit. This had to be taken into account for the dilution of the cDNA in the qPCR experiment. In this PhD Thesis, a 2720 Thermal Cycler from Applied Biosystems was used.

qPCR

In order to amplify and detect the cDNA corresponding to the gene of interest, the KAPA SYBR Fast Master Mix (2x) Universal (KAPA Biosystems) was used according to the manufacturer's instructions. The PCR reactions were carried out in an Eco Real-Time PCR System (Illumina).

1. Prepare the SYBR Green + primers mix. 10.8 µL of this mix will be added to each well of the PCR plate.

2. Prepare the corresponding dilution of the cDNA (1/10 for 1 µg cDNA or 1/5 for 500 ng cDNA).

3. Prepare the sample + DNase/RNase-free water mix. 9.2 µL of this mix will be added to each well of the PCR plate. Use 9.2 µL DNase/RNase-free water as blanks. Use the same dilutions for RNA samples as negative controls.

4. Load the PCR plate (first the SYBR Green + primers mix and then the diluted samples).

5. Briefly spin the PCR plate in order to eliminate bubbles.

6. Perform the qPCR using the following thermal cycling profile:

- 95 ºC 3 min.
- 40 cycles of: 95 ºC 5 s, Tm 30 s.
- 95 ºC 15 s.
- 55 ºC 15 s.
- 95 ºC 15 s.

β-actin was used as housekeeping gene. Gene expression was calculated by double delta quantification cycle (Cq) analysis. In the cases a control condition was added, gene expression was normalized to that control condition (this does not apply for basal gene expression).

4.5.2. Protein expression studies by Western blot

The most widely used experimental approach for the quantitative study of protein expression is the use of monoclonal or polyclonal antibodies in Western blot. Many different versions have been designed, depending on the sample procedure, the protein of interest or the detection method, among others. The antibodies used in this PhD Thesis are collected in section 1.5 of the Material and Methods section.

Preparation of reagents

- RIPA buffer: prepare a solution containing 50 mM Tris-HCl pH 7.4, 150 nM NaCl, 1% Triton X-100, 0.25% sodium deoxycholate and 1 mM EDTA. Keep at 4 ºC. Immediately before use, add protease inhibitors according to the manufacturer's instructions (cOmplete™, Mini Protease Inhibitor Cocktail Tablets from Roche -Mannheim, Germany-). Additionally, for the study of phosphorylated proteins add 1 mM sodium orthovanadate, 3 mM β-glycerophosphate and 3 mM sodium fluoride to RIPA buffer immediately before use.

- Laemli buffer (6x): for 10 mL, prepare a solution containing 3.5 mL 0.5 M Tris-HCl pH 6.8, 1.2 mg bromophenol blue, 1.28 g SDS, 3.6 mL glycerol and 0.5 mL βME. Dissolve in a water bath at 37 ºC. Make aliquots and keep them at -20 ºC.

- Transfer buffer (10x): add 15.15 g Tris (25 mM) and 72.05 g glycine (192 mM) to 1 L bidistilled water. Do not adjust pH. Immediately before use, add methanol to transfer buffer 1x at a final concentration of 20%. 1x transfer buffer may be used twice.

- Ponceau S stain: add 0.1 g Ponceau S and 5 mL acetic acid to 95 mL bidistilled water. Keep at RT. This solution can be used more than once.

- TBS (10x): add 24.2 g Tris (20 mM) and 80 g NaCl (137 mM) to 1 L bidistilled water. Adjust pH to 7.6. Immediately before use, add 0.1% Tween 20 to 1x TBS to make TBS-T.

- Stripping buffer: make a solution containing 62.5 mM Tris-HCl pH 6.8, 2% SDS and 0.77% βME.

The following reagents are common with gelatin zymographies:

- 10% SDS
- 10% APS
- Separating (resolving) buffer
- Stacking buffer
- Running buffer (10x)

Protocol

Protein extraction

In this PhD Thesis, in all the cases samples were from cells cultured in 6-well plates. Three different methods were applied for protein extraction depending on several factors:

- *Samples from control cells or cells treated for a short period of time:* in these cases, the protein amount between samples should be similar, so that protein quantification is not strictly necessary. Place cells on ice and wash once with cold 1x PBS. Collect proteins in 150 µL 2x Laemli buffer, maintain them at RT for 5 min, then heat at 95 ºC for 5 min and immediately use or store them at -20 ºC.

- *Samples from cells treated for several hours:* some treatments can affect cell viability and/or proliferation, so that different conditions could present different protein amounts. In these cases, place cells on ice and wash once with cold 1x PBS. Then, add 200 µL RIPA buffer to each well for 20 min on ice. Collect proteins, centrifuge at 13000 g and 4 ºC for 5 min for the removal of cell debris and use supernatants immediately or store them at -80 ºC. For protein quantification, the Bio-Rad Protein Assay, based on the Bradford assay, was performed according to the purchaser's instructions (see section 4.4.3 of Material and Methods). Alternatively, for protein quantification performed during the fellowship in Dallas the Pierce™ BCA Protein Assay Kit from Thermo Scientific was used following the purchaser's instructions. Make a standard curve with 0, 0.125, 0.25, 0.5, 1 and 2 µg/µL BSA. Mix 50 µL reagent A with 200 µL reagent B. Add 5 µL sample and 200 µL reagent mix to a 96-well plate

and incubate at 37 ºC for 30 min in the dark. Measure absorbance at 562 nm within an hour. In this PhD Thesis, a FLUOstar Omega microplate reader from BMG LABTECH (Ortenberg, Germany) was used. Samples were run in triplicates for both methods.

- *Samples for HIF-1α detection:* since HIF-1α degrades in the presence of oxygen, proteins need to be quickly extracted using 2x Laemli buffer in order to avoid this degradation. However, Laemli buffer contains β-mercaptoethanol (βME) and bromophenol blue, which do not allow protein quantification using colorimetric methods. For that reason, collect proteins quickly using 1x Laemli buffer without these two components. Due to the large amount of SDS contained in this buffer, the DC Protein Assay from BioRad, based on the Lowry assay, was used for protein quantification following the manufacturer's instructions (see section 4.4.1 on Material and Methods). Once quantified, add βME and bromophenol blue to each sample at the desired final concentration and store samples at -20 ºC.

Gel preparation

- Resolving (lower) gel (amounts for 2 gels -1 mm-)

Gel percentage was chosen depending on the size of the proteins of interest (15% was used for smaller proteins, such as LC3B).

	10%	**15%**
Bidistilled water	5.286 mL	3.446 mL
Acrylamide/Bis-acrylamide 40%	2.476 mL	3.75 mL
Separating (resolving) buffer	2.5 mL	2.6 mL
10% SDS	100 µL	100 µL
Polymerization agents		
10% APS	100 µL	100 µL
TEMED	6 µL	4 µL

- Stacking (upper) gel (amounts for 2 gels -1 mm-)

Bidistilled water	3.06 mL
Acrylamide/Bis-acrylamide 40%	0.638 mL
Separating (resolving) buffer	1.25 mL
10% SDS	50 µL
Polymerization agents	
10% APS	50 µL
TEMED	10 µL

When preparing 1.5 mm gels, prepare more volume for each gel.

Electrophoresis

1. In the case of samples collected in RIPA buffer, add the corresponding amount sample and 6x Laemli buffer in order to load the desired amount of protein and get a final concentration of 1x Laemli buffer.

2. Heat samples at 95 ºC for 5 min to denaturalize proteins.

3. Load the corresponding amount of sample depending on gel size.

4. Run gels in the electrophoresis chamber containing 1x running buffer at 60 V until samples enter the resolving gel. Then, increase voltage to 120 V and run the gels until the desired protein sizes are clearly separated. Different voltages were used during the fellowship in Dallas due to the different electric power in USA.

Transfer

In this PhD Thesis, the traditional wet or tank transfer was used, but other methods (such as the semi-dry or the dry transfer) could have been used instead. Additionally, nitrocellulose blotting membranes were used in the Western blots performed in Málaga, but polyvinylidene difluoride (PVDF) membranes were used during the fellowship in Dallas.

1. Inside a container with 1x transfer buffer put the cathode core of the transfer system, a sponge pad, two Whatman™ filter papers, the gel containing the proteins, the blotting membrane, two Whatman™ filter papers, a sponge pad and the anode core. For PVDF membranes, wet them in methanol or ethanol before putting them in the transfer buffer.

2. Put this “transfer sandwich” vertically in the transfer tank containing 1x transfer buffer.

3. Perform the transfer at 4 ºC at 100 V for 1 h for 1 mm gels or 1.5 h for 1.5 mm gels. 3 h transfer was performed for HIF-1α detection. Different voltage was used during the fellowship in Dallas due to the different electric power in USA.

4. In order to check that proteins have been transferred to the blotting membrane, membranes can be stained with Ponceau S Stain. Wash the membranes with distilled water and with TBS-T.

5. Cut the membranes depending on the proteins of interest and mark the gel to stablish its orientation.

Blocking

In order to avoid unspecific unions between the antibodies and the membrane, membranes are blocked before incubation with the primary antibody.

1. Prepare a solution containing 10% skimmed milk powder in TBS-T.

2. Incubate the membranes in the blocking solution at RT for 1 h with continuous gentle shaking.

3. After the incubation, briefly wash the membranes with TBS-T to eliminate the milk.

Antibody incubation

For each antibody, manufacturer's instructions should be followed. Usually antibodies are diluted in TBS-T containing 5% BSA and 0.02% sodium azide. Dilutions of the antibodies used in this PhD Thesis are collected in section 1.4 of Material and Methods.

1. Incubate the membranes with the desired primary antibody for 1 h at RT or overnight at 4 ºC with continuous shaking. Primary antibodies were later kept at 4 ºC or -20 ºC for additional uses.

2. Wash the membranes three times with TBS-T for 10 min with continuous shaking.

3. Incubate the membranes with the corresponding secondary antibody diluted in TBS-T containing 10% skimmed milk powder for 1 h at RT with continuous shaking.

4. Wash the membranes three times with TBS-T for 10 min with continuous shaking.

Detection and visualization

Two methods for detection of protein bands were used during this PhD Thesis. In Málaga, a ChemiDoc™ XRS+ System (Bio-Rad) and its software Image Lab were used, whereas in Dallas proteins were transferred to films that were revealed using a Medical film processor from Konica Minolta (Tokyo, Japan). In both cases, membranes were incubated with the Supersignal® West Pico chemiluminescent substrate system (Thermo Scientific) at 1:1 for 5 min with continuous shaking. Densitometry analyses were made with Image J software.

Detection of phosphorylated proteins

For the detection of phosphorylated proteins two methods were applied:

a. Samples were run in duplicate in different gels; one gel was incubated for the detection of the phosphorylated form of the protein, and the other for the detection of the total protein. For both gels, a housekeeping protein was detected independently.

b. Membranes were incubated for the detection of the phosphorylated protein, and then membranes were stripped for 30 min at 50 ºC and incubated again for the detection of the total protein. This method has the advantage of using the exact sample for the detection of both forms of the protein, but it extends the duration of the protocol and the stripping buffer may damage the membranes.

4.5.3. Massive protein expression analysis by proteomics

The large-scale protein expression of cells was determined by means of a high-throughput approach such as the proteomics protein expression analysis.

Sample collection

1. Seed cells in 10 cm dishes and once they reach sub-confluence treat the cells with the desired compound.
2. Put the plates on ice and extensively wash the cells with cold 1x PBS five times.
3. Freeze the plates at -80 ºC.

Proteomics analysis

Samples were handed to a specialized technician and the proteomics analysis was performed in the Proteomics Core Facility of the Research Support Central Services (SCAI) of the University of Málaga. Mass spectrometry (MS) analysis was performed using an Easy nLC 1200 UHPLC system coupled to a hybrid linear trap quadrupole Orbitrap Q-Exactive HF-X mass spectrometer (Thermo Scientific). Software versions used for the data acquisition and operation were Tune 2.9 and Xcalibur 4.1.31.9. The acquired raw data were analyzed using Proteome Discoverer^{TM} 2.2 (Thermo Scientific). Normalization was performed based on specific abundance of human β-actin protein and samples were scaled to controls average.

5. *In vivo* assays

5.1. Angiogenesis CAM assay

The chorioallantoic membrane (CAM) of the chick embryo is formed during embryonic development from the partial fusion of the allantois and the chorion. An active angiogenesis can be detected on the CAM during days 8 to 10 of the embryonic

development. For that reason, the addition of potential anti-angiogenic drugs to the CAM is a valid experiment for the discovery of compounds with anti-angiogenic capacity[263].

Preparation of reagents

- 2% methylcellulose solution: add 2 g methylcellulose to 100 mL bidistilled water. Keep at 4 ºC. Mix well before use it.

Methylcellulose discs preparation

1. Prepare 100 µL of the compound in microcentrifuge tubes to prepare 10 discs of each condition as follows:
    - Sterile bidistilled water.
    - Compound to the desired concentration or DMSO (negative control).
    - 2% methylcellulose solution: 50 µL (final concentration 1%).
2. Add 10 µL of each tube to an UV sterilized Teflon-coated surface to form a disc.
3. Leave the discs inside the laminar flow hood overnight to allow the discs to dry.

Protocol

1. Clean the eggshell of fertilized eggs with 70% ethanol.
2. Horizontally incubate the fertilized eggs at 38 ºC and humidified atmosphere with agitation for three days. In this PhD Thesis, a Mesalles 25 L-HS incubator (Barcelona, Spain) was used.
3. Extract albumin (3-4 mL) from one side of the egg using a 5 mL syringe with a needle. Cover the gap with adhesive tape. An air chamber will be formed inside the egg.
4. Open a window in the eggshell using dissecting scissors and cover with adhesive tape. This allows the identification of fertilized eggs and live chicks.
5. Horizontally incubate the fertilized eggs at 38 ºC and humidified atmosphere without agitation for five additional days.
6. One day before the end of the incubation, prepare the methylcellulose discs containing the compounds as detailed above. Use aeroplysinin-1 (3 nmol/CAM) as positive control[76].
7. Put one disc in a vessel-free area inside each egg. Cover the egg again with adhesive tape.
8. Horizontally incubate the fertilized eggs at 38 ºC and humidified atmosphere without agitation for two additional days.

9. Take photographs of the area surrounding the disc inside the eggs examined under a stereomicroscope.

10. Sacrifice the chick embryos by decapitation.

In this PhD Thesis, the camera used for taking the photographs was a Nikon DS-Ri2 connected to a Nikon SMZ 745T stereomicroscope (Nikon, Tokyo, Japan).

The evaluation was a double-blind, qualitative evaluation made by two different observers. A lower vascular density in the disc area, vasculature disorganization, rebounds of vessels and/or a centrifugal growth of peripheral vessels were considered as a positive (anti-angiogenic) result. The number of positive eggs was then divided by the total of evaluated eggs in order to obtain the fraction of positive eggs.

5.2. Intersegmental vessels formation assay

During the embryo development of the zebrafish the vasculature is completed through angiogenesis. For example, there is an active angiogenesis in the dorsal aorta for the formation of the intersegmental vessels (ISVs). The use of transgenic models of zebrafish with fluorescent ECs allows the characterization of potential anti-angiogenic compounds able to inhibit the formation of these ISVs[264].

Preparation of reagents

- E3 medium: prepare a solution with 5 mM NaCl, 0.17 mM KCl, 0.33 mM $CaCl_2 \cdot 2 H_2O$ and 0.33 mM $MgSO_4 \cdot 7 H_2O$. Add 10 µL 1% methylene blue to 500 mL E3 medium in order to avoid fungi and other microorganisms' growth.

- Bleach solution (0.002%): dissolve 100 µL molecular bleach in 50 mL E3 medium.

- Pronase solution (2 mg/mL): dissolve 20 mg pronase in 10 mL E3 medium.

- Tricaine solution (0.2 mg/mL): dissolve 10 mg tricaine (ethyl 3-aminobenzoate methanesulfonate salt) in 50 mL E3 medium.

Protocol

1. Mate adult zebrafish in a special fish tank where eggs will be inaccessible for the adults, separating males and females with a removable plastic wall.

2. In the early morning, remove the plastic walls and wait until the fertilized eggs are deposited at the bottom of the tank.

3. Collect the fertilized eggs in E3 medium.

4. Wash the fertilized eggs with E3 medium containing 0.002% (v/v) molecular bleach for 1 min.

5. Wash the fertilized eggs 3-5 times with E3 medium.

6. Discard non-fertilized eggs under a stereomicroscope.

7. Incubate the fertilized eggs at 28 ºC until they reach 24 hpf (hours post fertilization).

8. Prepare a 96-well plate with the compounds to test. Add to each well 50 µL of E3 medium containing double the concentration of the compound. Include negative controls with and without DMSO. Use 20 µM GR-24 as positive control[59].

9. Discard deceased 24 hpf embryos under a stereomicroscope.

10. Incubate the 24 hpf embryos in a 2 mg/mL pronase solution for approximately 5 min to remove the chorions.

11. Quickly wash the dechorionated embryos 5 times with E3 medium in order to dilute the pronase.

12. Place the dechorionated embryos in a Petri dish containing E3 medium.

13. Put one dechorionated embryo in each well of the 96-well plate taking 50 µL E3 medium and the embryo with a cut 200 µL pipette tip.

14. Incubate at 28 ºC for 24 h.

15. Anesthetize the embryos in a freshly prepared tricaine solution (0.2 mg/mL).

16. Take photographs of the ISVs in the caudal region of the 48 hpf embryos.

17. Euthanize embryos by rapid freezing at -80 ºC.

In this PhD Thesis, the camera used for taking the photographs was a Nikon DS-Ri2 connected to a Nikon Eclipse Ti fluorescence microscope (Nikon, Tokyo, Japan). The stereomicroscope used for discarding deceased embryos was a Nikon SMZ 745T (Nikon, Tokyo, Japan).

Angiogenesis inhibition in this model can be appreciated by the lack or incomplete formation of ISVs, as well as abnormal ISVs. Embryos presenting lordosis, pericardial edema or loss of heartbeat were considered as non-valuable samples.

5.3. Caudal fin regeneration assay

Zebrafish present a high tissue regeneration capacity[265]. After amputation of the caudal fin, a mass of undifferentiated cells known as blastema is formed. These cells rapidly proliferate and differentiate in order to regenerate all the damaged tissues. Therefore, an active angiogenesis is necessary to form new blood vessels in this process. For that reason, this assay is considered a model to evaluate anti-angiogenic drugs *in vivo*[264].

Preparation of reagents

- Tricaine solution (0.2 mg/mL): dissolve 10 mg tricaine (ethyl 3-aminobenzoate methanesulfonate salt) in 50 mL fish water.

Protocol

1. Anesthetize an adult zebrafish in a freshly prepared tricaine solution (0.2 mg/mL) and put it on a microscope slide.

2. Cut the more distal part of the caudal fin using a scalpel.

3. Take photographs of the caudal fin under a stereomicroscope (0 dpa –days post amputation-).

4. Let the animal recover from the anesthesia in fish water for at least 15-30 min.

5. Incubate the animal in fish water containing the compound to test (minimum 100 mL) at 28 ºC for 3 days.

6. Anesthetize the animals and take photographs of the caudal fin at 3 dpa. Videos from caudal fin circulation can also be recorded.

7. Sacrifice the animals by decapitation while anesthetized.

In this PhD Thesis, the camera used for taking the photographs was a Nikon DS-Ri2 connected to a Nikon SMZ 745T stereomicroscope or a Nikon Eclipse Ti microscope (Nikon, Tokyo, Japan).

A lower area regenerated or abnormal blood circulation were considered as positive results for angiogenesis inhibition.

RESULTS AND DISCUSSION

CHAPTER 1

Metabolic preferences studies on tumor cells

1. Considerations for the study of breast tumor metabolism

Breast cancer is the second leading cause of cancer death among women[266]. Nevertheless, mortality from breast cancer in North America and the European Union has decreased due to early detection and the development of efficient therapies, thanks to the increasing knowledge on the processes occurring inside tumor cells. Due to the importance of the metabolic reprogramming in cancer, metabolism of breast cancer cells has been exhaustively studied in the last years in order to know more about this disease and design more effective therapies.

However, there is a high diversity in breast tumors. Classification of breast tumors is made based on their genetic expression profile[267]. Three main markers have been described for the classification of breast tumors: the estrogen receptor (ER), the progesterone receptor (PR) and the human epidermal growth factor receptor type 2 (HER2). Triple negative breast cancers (TNBC) are defined as tumors that lack expression of these three receptors[268]. Most of these TNBC are highly invasive ductal carcinomas with high proliferative activity, higher risk of developing distant metastasis and a poorer prognosis[269]. Interestingly, different metabolic features have been found for different breast cancer subtypes, including TNBC[270]. Therefore, studying the metabolism of a specific type of breast cancer must include the study of a different breast cancer subtype in order to get to conclusions.

MDA-MB-231 is one of the most studied TNBC cell lines. This cell line is known to be highly metastatic, invasive and glycolytic[271]. Most of the metabolic studies performed in these cells are carried out after incubations no shorter than 24 h, often because those studies are focused on the effects on the proliferation rate and invasive capacity of these cells. Moreover, palmitate is one of the most abundant fatty acids, but it has been shown to induce apoptosis in MDA-MB-231 and other breast tumor cell lines[272]. Nevertheless, lipid metabolism is important for MDA-MB-231 tumorigenesis[273].

In this chapter, two features of TNBC metabolism, in particular metabolism of MDA-MB-231 cells, were studied: 1) the effect of glucose and/or glutamine starvation on proliferation and 2) the possible alterations in metabolism after short-time incubation with different combinations of glucose, glutamine and/or palmitate. Combining long and short-term experiments covers different possible scenarios, such as the short-term response of the cells to a drastic nutritional change (their immediate fuel preference) and the long-term consequence of that change (their ability to adapt to a different

nutritional condition). Moreover, non-physiological concentrations are often used in many metabolomics works. In this PhD Thesis physiological concentrations of different metabolic substrates were used in controlled conditions: 5 mM glucose, 0.5 mM glutamine and 0.5 mM palmitate[274].

Increasing knowledge in the metabolic flexibility of breast cancer cells could allow the design of specific therapies in order to inhibit tumor progression. Therefore, this study may lead to further research in the metabolomics of breast cancer cells and the inhibition of breast cancer progression.

Most of the results presented herein are already published in an original research article (**Appendix 4**).

2. Long-term metabolic dependence of breast tumor cells

2.1. Long-term palmitate exposure is toxic for MDA-MB-231 cells

Palmitate is known to induce apoptosis in MDA-MB-231 cells after exposures longer than 6-8 hours[272]. Accordingly, 0.5 mM palmitate decreased cell number in MDA-MB-231 cells after 16 h (**Figure 1**).

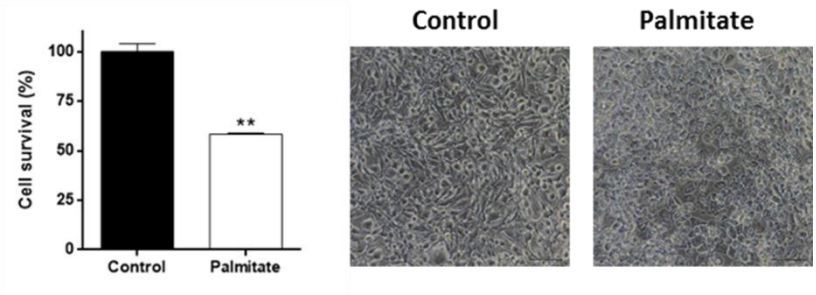

Figure 1. Representative photographs and quantification of 0.5 mM palmitate effect on MDA-MB-231 cells viability in media containing glucose and glutamine after an overnight incubation. Bar scale = 91.75 μm. Data are expressed as means ± SD of a unique experiment with duplicates. **$p < 0.01$.

The apoptotic effect of palmitate in these cells was found to be most likely due to a decrease in cardiolipin synthesis, which triggers Bcl-2 mediated apoptosis[272,275]. Furthermore, it is known that other fatty acids, such as oleate, rescue this pro-apoptotic effect[272]. In an individual, not only palmitate would be present in the blood and extracellular media, but also other fatty acids, so that this pro-apoptotic effect is not likely exerted.

2.2. Glucose and glutamine are essential for MDA-MB-231 cells proliferation

Due to the lethal effect of long-term exposure to palmitate found in these cells, the dependence of MDA-MB-231 cells to glucose and glutamine, but not palmitate, for proliferation was tested.

It has been already reported that MDA-MB-231 cells cannot grow in the absence of glucose and glutamine, getting into G2/M block after 2-4 hours and inducing apoptosis[276]. Glutamine is essential for MDA-MB-231 cell growth even in the presence of glucose[277]. Nevertheless, proliferation of MDA-MB-231 cells had not been tested under glucose starvation in the presence of glutamine. The results herein show a total dependence on both glucose and glutamine for sustaining cell growth in MDA-MB-231 cells (**Figure 2**). Interestingly, these cells were able to survive, without growing, in the presence of only glutamine in hypoxia (**Figure 2B**).

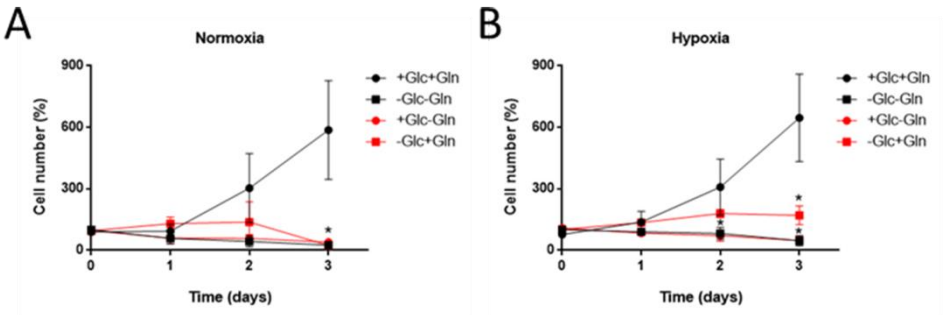

Figure 2. (A) Cell growth in the presence or absence of 5 mM glucose and/or 0.5 mM glutamine in MDA-MB-231 cells in normoxia or (B) hypoxia (1% O_2). Data are expressed as means ± SD of three independent experiments. *p < 0.05 versus glucose and glutamine condition.

Growth of the non-invasive, ER positive breast cancer cell line MCF7 was also tested under glucose and/or glutamine deprivation. Both fuels were important for proliferation of these cells, but they seemed to be more sensitive to glucose deprivation (**Figure 3**). These data reinforce the fact that a distinction between different types of breast cancer cells has to be considered for the study of breast cancer progression.

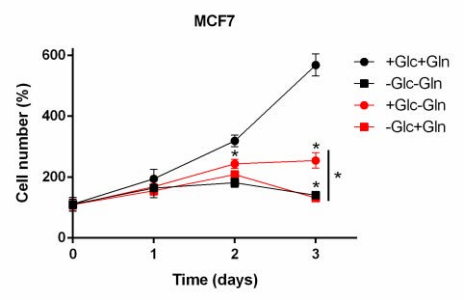

Figure 3. Cell growth in the presence or absence of 5 mM glucose and/or 0.5 mM glutamine in MCF7 cells in normoxia. Data are expressed as means ± SD of three independent experiments. *$p < 0.05$ versus glucose and glutamine condition.

Furthermore, glutamine, but not glucose, withdrawal changed MDA-MB-231 cells morphology, making them longer and with a fusiform shape (**Figure 4**).

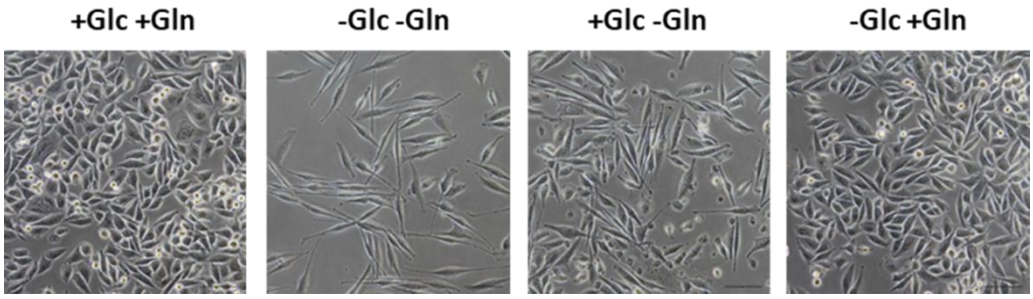

Figure 4. Representative photographs of MDA-MD-231 cells morphology in the presence or absence of 5 mM glucose and/or 0.5 mM glutamine for 24 h. Bar scale = 200 µm.

This fact may indicate changes in cytoskeleton structure due to inhibition of proliferation in the absence of glutamine, suggesting a more critical role of this amino acid in sustaining cell growth in these cells. Remarkably, glutamine deprivation has been shown to affect cell invasion of melanoma cells through decreasing α5 integrin expression, focal adhesion kinase (FAK) phosphorylation and inhibition of actin cytoskeleton remodeling[278]. However, in this PhD Thesis the role of glutamine in cytoskeletal structure was not studied.

3. Short-term preference for different metabolic fuels in breast cancer cells

Once performed the long-term preference for metabolic substrate in order to elucidate the importance of glucose and glutamine for MDA-MB-231 cells proliferation, the short-term response of these cells to a drastic nutritional change was studied. In order to avoid possible interferences with other metabolites from culture media and serum, the short-time experiments were carried out in very restrictive

conditions, although it should be taken into account that other metabolites may also be present in an individual.

3.1. Effect of different metabolic fuels on general metabolism

The effect of glucose, glutamine and/or palmitate on OCR and ECAR was tested. Glutamine was the major oxidative substrate in MDA-MB-231 cells as shown by the higher OCR increase after glutamine addition. Glucose was also used as an oxidative substrate, but to a lesser extent. Interestingly, OCR was not increased in the presence of palmitate in MDA-MB-231 cells. Combination of different metabolic substrates slightly increased the maximum OCR values (**Figure 5A**). Accordingly, highly proliferative and glycolytic cell lines are described to have a great avidity for FAs, using them for lipid biosynthesis instead of oxidation[279-282].

Additionally, the MDA-MB-231 cell line was corroborated to be highly glycolytic in the presence of glucose (**Figure 5B**), as previously described[271,283]. Glutamine also increased ECAR values (**Figure 5B**), but this is most likely due to deprotonation of HCO_3^- resulting from oxidation[284].

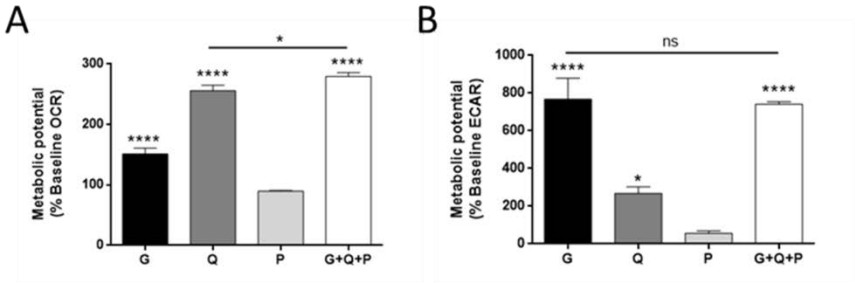

Figure 5. Flux analysis in MDA-MB-231 cells. (A) Oxygen consumption rate (OCR) and (B) extracellular acidification rate (ECAR) in the presence of 5 mM glucose, 0.5 mM glutamine or 0.5 mM palmitate. Data are expressed as means ± SD of three independent experiments with triplicate samples each. *p < 0.05, ****p < 0.0001 versus control without any metabolic substrate. ns: non-significant. G: glucose; Q: glutamine; P: palmitate.

3.2. Effect of different metabolic fuels on glucose and glutamine metabolism

Next, the effect of glucose, glutamine and palmitate on glucose and glutamine uptake and utilization was tested. Neither glutamine nor palmitate alone had any significant effect on glucose uptake or lactate production after 30 minutes, although combination of glucose with both glutamine and palmitate increased lactate production in these cells (**Figure 6**). Moreover, no lactate production was detected in the absence of glucose

(**Figure 6B**). This is in contrast with data from other tumor cell lines, such as glioblastoma cells, which are able to produce lactate from glutamine[285,286].

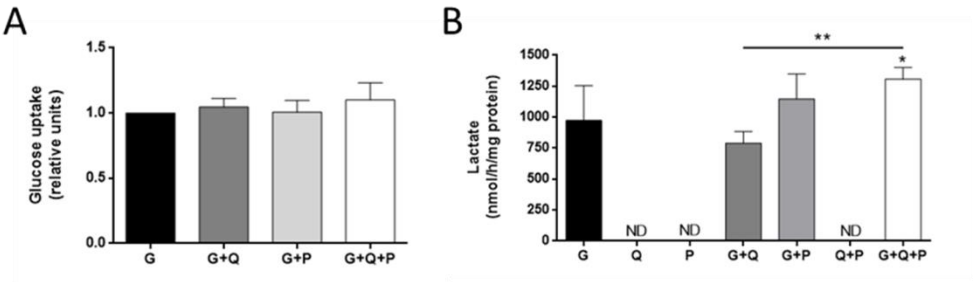

Figure 6. (A) Glucose uptake and (B) lactate production in MDA-MB-231 cells in the presence or absence of 5 mM glucose, 0.5 mM glutamine and/or 0.5 mM palmitate. Data are expressed as means ± SD of three independent experiments. *p < 0.05 versus glucose condition, **p < 0.01. ND: non-detected. G: glucose; P: palmitate; Q: glutamine.

Regarding glutamine metabolism, two different features were analyzed: glutamine uptake from the media and glutamine oxidation. Glucose did not statistically affect glutamine uptake in MDA-MB-231 cells, but it decreased glutamine oxidation (**Figure 7**), indicating a preference for glycolysis versus OXPHOS from glutamine. Surprisingly, combination of glucose and palmitate increased glutamine uptake, whereas this combination decreased glutamine oxidation (**Figure 7**).

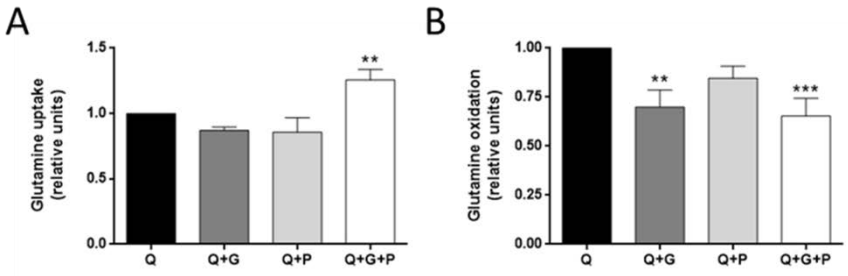

Figure 7. (A) Glutamine uptake and (B) oxidation in MDA-MB-231 cells in the presence or absence of 0.5 mM glutamine, 5 mM glucose and/or 0.5 mM palmitate. Data are expressed as means ± SD of three independent experiments. **p < 0.01, ***p < 0.001 versus glutamine condition. G: glucose; P: palmitate; Q: glutamine.

Besides the role of glutamine in feeding the TCA cycle, there are other non-oxidative metabolic fates for this amino acid, such as providing nitrogen skeletons for nucleotides and glycosylation reactions, amino acid synthesis or signal transduction, mostly involving cell proliferation[145]. Glucose metabolism is also important for anaplerosis[287]. Moreover, free fatty acids such as palmitate can be used for lipid synthesis, such as TAGs and phospholipids. The increase in glutamine uptake in the presence of glucose

and palmitate, which are both involved in biosynthetic pathways, along with a decrease on its oxidation rate could be related to an elicitation of anaplerotic metabolism.

3.3. Glucose increases palmitate uptake in MDA-MB-231 and other invasive tumor cell lines

The effect of glucose and glutamine on palmitate uptake was also analyzed. Glutamine did not affect palmitate uptake in MDA-MB-231 cells. However, 5 mM glucose significantly increased palmitate uptake after 30 minutes (**Figure 8A**). Surprisingly, this effect on palmitate uptake was independent of glucose concentration (**Figure 8B**).

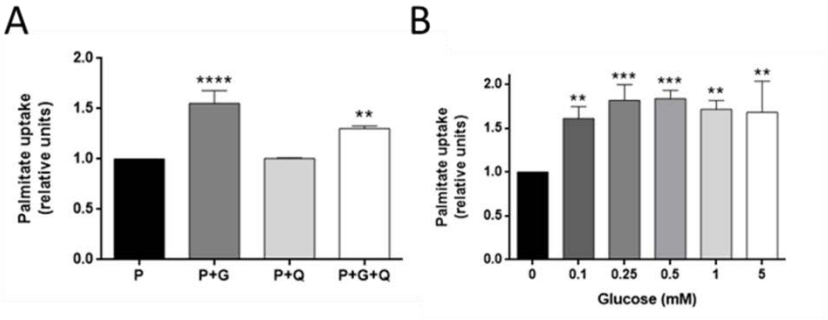

Figure 8. (A) Palmitate uptake in MDA-MB-231 cells in the presence or absence of 0.5 mM palmitate, 5 mM glucose and/or 0.5 mM glutamine or (B) in the presence of 0.5 mM palmitate and different concentrations of glucose. Data are expressed as means ± SD of three independent experiments. **p < 0.01, ***p < 0.001, ****p < 0.0001 versus palmitate condition. G: glucose; P: palmitate; Q: glutamine.

This is the first time that this effect of glucose is documented in this cell line, although the same happens in Ehrlich ascetic tumor cells. In the last model, glucose also diminished FAO and favored the biosynthetic fate of palmitate[288]. However, the mechanism by which glucose stimulates palmitate uptake was not determined in Ehrlich ascetic tumor cells.

Palmitate uptake has been shown to promote invasiveness in hepatocellular carcinoma and pancreatic cancer[289,290]. For that reason, it was also tested whether this effect of glucose on palmitate uptake was found in other breast cancer cell lines, especially comparing invasive and non-invasive cell lines. For this purpose, other TNBC cell lines, such as MDA-MB-436 and HCC1937 cells, and a non-invasive, ER positive breast cancer cell line, MCF7, were used. Additionally, this experiment was also performed using a mild invasive cervix adenocarcinoma cell line, HeLa, and a

highly invasive neuroblastoma cell line, Kelly, along with a non-tumor cell line, such as the EC line HUVEC. Glucose increased palmitate uptake in the two TNBC cell lines, but no effect was found for MCF7 cells. Moreover, glucose slightly increased palmitate uptake in HeLa cells and, to a major extent, in Kelly cells, whereas no effect was found in HUVECs (**Figure 9**).

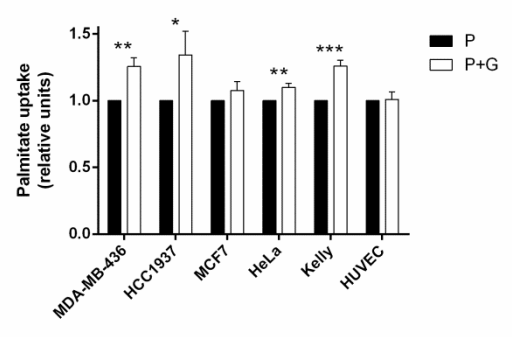

Figure 9. Palmitate uptake in MDA-MB-436, HCC1937, MCF7, HeLa, Kelly and HUVE cells in the presence or not of 5 mM glucose. Data are expressed as means ± SD of three independent experiments. *p < 0.05, **p < 0.01, ***p < 0.001 versus palmitate condition. G: glucose; P: palmitate.

Hence, the effect of glucose on palmitate uptake seems to be related to the invasive capacity of the tumor cell line, independently of the type of cancer.

3.4. The effect of glucose on palmitate uptake is independent of the ERK signaling pathway

Importantly, lipid transporters are regulated by the ERK signaling pathway. ERK phosphorylation has been found to increase CD36 expression in the membrane of muscle cells during muscle contraction[291]. However, MDA-MB-231 barely express CD36 transporters, also known as fatty acid translocase (FAT), whereas they express fatty acid binding protein 5 (FABP5) (**Figure 10**). Therefore, it seems unlikely that CD36 helps fatty acid uptake in these cells in a significant manner.

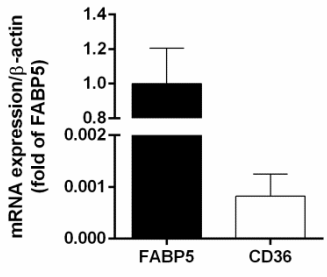

Figure 10. mRNA expression of FABP5 and CD36 transporters in MDA-MB-231 cells. Data are expressed as means ± SD of three independent experiments.

Interestingly, CD36 expression has been reported to be inversely correlated with the metastatic potential of breast cancer cell lines[292]. This fact may support the relationship between palmitate uptake, fatty acid transporters expression and cancer invasiveness.

Nevertheless, inhibition of ERK phosphorylation has been shown to also diminish FABP5 expression in MCF7 cells, thus pointing to a regulation of this lipid transporter by the ERK signaling pathway[293]. Therefore, this pathway could also have a role in the effect of glucose on palmitate uptake. Nevertheless, after 30 minutes incubation with 5 mM glucose, no effect was observed on ERK phosphorylation compared to glucose withdrawal (**Figure 11A**). Furthermore, 30 μM PD98059 was added to the cells for 30 minutes in order to inhibit ERK phosphorylation (**Figure 11A**). However, the strong inhibition caused by PD98059 did not affect the upregulation of palmitate uptake in the presence of glucose (**Figure 11B**).

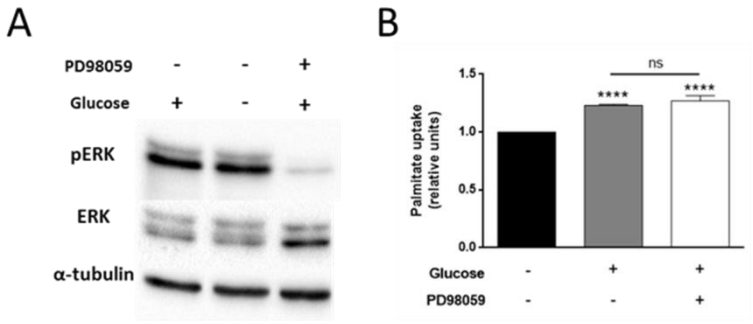

Figure 11. (A) ERK phosphorylation and (B) palmitate uptake in MDA-MB-231 cells in the presence or not of 5 mM glucose alone or along 30 μM PD98059. Data are expressed as means ± SD of three independent experiments. ****$p < 0.0001$ versus condition without glucose and PD98059.

These data indicate that glucose acts on palmitate uptake in a way that is independent of the ERK signaling pathway. Additional experiments should be carried out in order to elucidate the exact molecular mechanism by which glucose affects palmitate uptake in these cells.

3.5. Glucose is needed for palmitate metabolism in MDA-MB-231 cells

In order to test whether glucose needs to be metabolized to exert its effect on palmitate uptake, different metabolic inhibitors were used.

The presence of the glucose analog 2-DG, which cannot be metabolized through glycolysis, at a concentration of 5 mM not only failed to increase palmitate uptake, but it decreased it. Increasing glucose concentration along with 5 mM 2-DG reestablished

the increase on palmitate uptake beyond the effect of 2-DG, completely restoring this effect when glucose and 2-DG were present at the same concentration (**Figure 12**). These results suggest that indeed glucose needs to be metabolized in order to increase palmitate uptake in these cells.

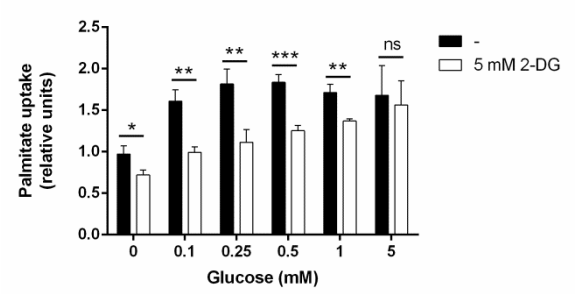

Figure 12. Palmitate uptake in MDA-MB-231 cells in the presence of different concentrations of glucose along with 5 mM 2-DG. Data are expressed as means ± SD of three independent experiments. *p < 0.05, **p < 0.01, ***p < 0.001, ****p < 0.0001 versus condition without 2-DG. ns: non-significant.

Glucose is a precursor of lipid synthesis through conversion to glycerol 3-phosphate, which will incorporate two acyl-CoAs in a reaction mediated by mitochondrial glycerol-3 phosphate acyltransferase (GPAT2), generating phosphatidic acid. This phosphatidic acid will be diverted to phospholipid or to diglyceride (DAG) and TAG synthesis[294]. GPDH, the enzyme that converts dihydroxyacetone phosphate (DHAP) into glycerol 3-phosphate, is important for reoxidation of cytosolic NADH in glycolytic cells, as well as regulation of cytosolic glycerol 3-phosphate, thus regulating glycolysis, lipogenesis and OXPHOS[295]. Treatment of MDA-MB-231 cells with adipostatin A, an inhibitor of GPDH, diminished the effect of glucose on palmitate uptake in a dose-dependent manner (**Figure 13**).

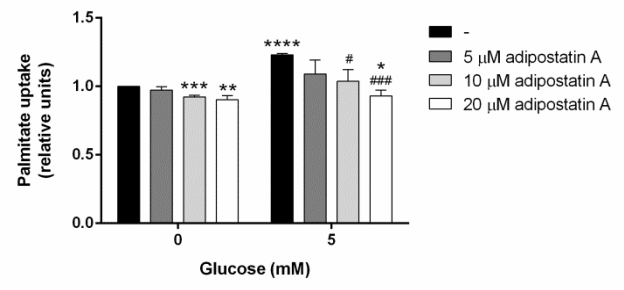

Figure 13. Palmitate uptake in MDA-MB-231 cells in the presence or not of glucose along with different concentrations of adipostatin A. Data are expressed as means ± SD of three independent experiments. *p < 0.05, **p < 0.01, ***p < 0.001, ****p < 0.0001 versus condition without glucose; #p < 0.05, ###p < 0.001 versus condition with glucose.

This inhibition of GPDH by adipostatin A would most likely lead to lower glycerol 3-phosphate synthesis and availability, decreasing the backbone amount to which palmitoyl-CoA could bind to in order to synthetize phosphatidic acid in the reaction catalyzed by GPAT2. Therefore, due to the uselessness of glucose in generating glycerol 3-phosphate it could be logic that less palmitate uptake would be necessary. This fact suggests the possible role of glucose in tumor cell proliferation and invasiveness through modulation of lipid synthesis.

Noticeably, GPAT2 is associated with higher rates of cell proliferation and migration in cancer cells and higher tumorigenicity[294,296]. In accordance with the results presented herein, GPAT2 expression was found to be much higher in MDA-MB-231 than in HeLa and MCF7 cells lines, which present a low GPAT2 expression[294]. Moreover, glucose was seen to be incorporated into glycerol and fatty acyl chains in breast epithelial cells and in the ER positive breast tumor cell lines MCF7 and ZR75-1, but only to glycerol in MDA-MB-231 cells. However, in that article the effect of glucose on fatty acids uptake was not studied[297].

Furthermore, palmitate in MCF7 cells is set aside for mitochondrial oxidation. Whereas palmitate uptake has been found to be similar in MCF7 and MDA-MB-231 cell lines, only MDA-MB-231 cells, in which palmitate has a different metabolic fate, underwent apoptosis after palmitate exposure[298]. Whether glucose is involved in the pro-apoptotic effect of palmitate in MDA-MB-231 cells or if palmitate also triggers an apoptotic response in other invasive tumor cell lines in comparison to non-invasive ones needs to be further researched.

Palmitate is known to be mainly led to phospholipid and TAG synthesis in MDA-MB-231 cells[299]. In this PhD Thesis, MDA-MB-231 cells labeled with the fluorescent analog of palmitate BODIPY FL C_{16} were observed under a confocal microscope. Interestingly, no fluorescence was found in the plasma membrane of MDA-MB-231 cells (**Figure 14**), pointing out to a possible accumulation of TAG instead of phospholipid synthesis.

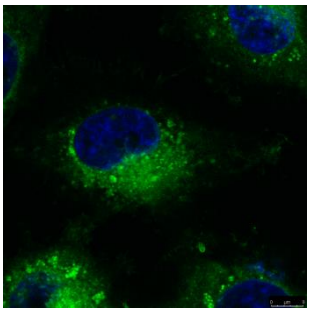

Figure 14. Representative photograph of BODIPY FL C_{16} intracellular location in MDA-MB-231 cells. Bar scale = 8 μm.

Other authors found out that MDA-MB-231 cells with an active glucose oxidative metabolism and incubated with oleate accumulated TAG inside lipid droplets. In that work, the authors speculated that glucose was being converted to glycerol 3-phosphate in order to sustain TAG synthesis[300]. However, this statement was not supported by any experimental data beyond the glucose oxidation rate. The results of this chapter of this PhD Thesis demonstrate that glucose metabolism, through conversion of glucose to glycerol 3-phosphate, supports palmitate uptake in the MDA-MB-231 cell line, most likely followed by incorporation into glycerol 3-phosphate to form phosphatidic acid, the precursor of TAG.

4. Conclusions

The data obtained point out to an essential role of glucose in the breast cancer cell line MDA-MB-231 for proliferation, glycolysis and lipid synthesis, thus adding interesting information for the metabolic profiling of these highly proliferative and invasive, estrogen insensitive breast cancer cells. However, MDA-MB-231 cells can survive up to two days in the absence of glucose but not in the absence of glutamine. Despite the pro-apoptotic effect of palmitate after long incubations, glucose induced in a dose-independent and ERK-independent manner an increase in palmitate uptake after 30 minutes, probably for the synthesis of TAGs. This effect of glucose was also exerted in other TNBC cell lines such as MDA-MB-436 and HCC1937, and in other invasive tumor cell lines such as HeLa and Kelly, whereas no effect was found in the non-invasive breast cancer cell line MCF7. These results point out to a regulation between glucose and lipid metabolism in invasive cancer cells not given in the non-invasive tumor cells studied, and open new horizons for the targeting of glucose and lipid metabolism for the inhibition of cancer progression.

CHAPTER 2

Metabolic preferences studies on endothelial cells

1. Considerations for the study of endothelial cell metabolism

Study of EC metabolism and its relationship with angiogenesis has been an emerging topic in the last decade. Most of these studies have focused the attention on gene silencing or long-time incubations with inhibitors of different key steps of the main metabolic pathways in order to see their effect on the angiogenic process[121-123,126,301]. These publications highlighted the importance of glucose, glutamine and fatty acid metabolism on angiogenesis.

However, often non-physiological concentrations are used in many works. It is important to take into account that the concentration of the metabolic fuels that are present in the extracellular media can greatly affect EC metabolism differentially[251,302]. For instance, hyperglycemia has been shown to impair vascular function[303]. Moreover, due to the well-known degradation of glutamine to ammonia in aqueous solutions, this amino acid is usually added to cell culture media at concentrations higher than the physiological one[304]. Therefore, in this PhD Thesis physiological concentrations of different metabolic substrates were used in controlled conditions: 5 mM glucose, 0.5 mM glutamine and 0.5 mM palmitate[274].

HUVECs have been extensively used for angiogenic and EC metabolic studies since these cells are easy to culture and commercially available. Nevertheless, most pathological events take place at the microvasculature level, which constitutes the vast majority of the human vascular compartment[245]. The isolation and culture of primary microvascular ECs is tedious. Fortunately, the immortalization of this kind of ECs surpasses the disadvantages of the use of primary cultures. For example, these cells would grow faster and have less strict nutritional requirements than primary microvascular ECs (i.e. they do not need as much serum concentration in the media in order to grow)[245]. For this chapter, a human dermal microvascular EC line, HMEC, has been mainly used. Nonetheless, due to their peculiar features compared to a primary culture, the results from proliferation or apoptosis assays using these immortalized cell lines should be carefully interpreted[305].

Most of the results presented herein are already published in an original research article (**Appendix 5**).

2. Long-term metabolic dependence of endothelial cells

2.1. Long-term palmitate exposure is toxic for endothelial cells

The dependence of several EC lines for different metabolic substrates was tested. Not only glucose and glutamine, the two main metabolic fuels in cell culture media, have been shown to be essential for EC proliferation, but also fatty acids, such as the 16-carbon saturated fatty acid palmitate[123]. Nevertheless, an anti-angiogenic role of palmitate through inhibition of EC invasion has also been observed[306]. Moreover, palmitate is known to induce apoptosis in several cell lines in culture, such as tumor cells, macrophages, pericytes, both macrovascular and microvascular ECs and many others[272,307-311]. Accordingly, palmitate was also found to decrease cell viability in HMECs after only 6 hours incubation (**Figure 1**). For that reason, this fatty acid was not included for the long-term preference studies in these cells.

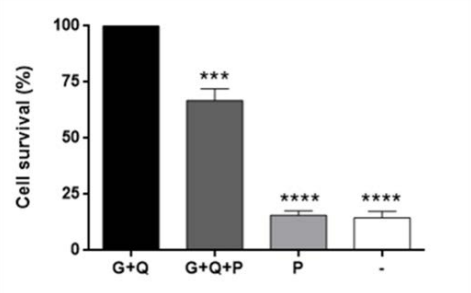

Figure 1. Cell survival in HMECs after 6 h incubation in DMEM supplemented with 5 mM glucose, 0.5 mM glutamine and/or 0.5 mM palmitate. Data are normalized to the condition with glucose and glutamine and expressed as means ± SD of three independent experiments. ***$p < 0.001$, ****$p < 0.0001$ versus glucose and glutamine condition. G: glucose; P: palmitate; Q: glutamine.

Several mechanisms have been described explaining the pro-apoptotic role of palmitate in cultured cells. Results presented in Du *et al.* demonstrated that concentrations as low as 100 µM palmitate for 4h induced microvascular EC apoptosis through increase in ROS intracellular levels, which also diminished DNA synthesis in these cells. Treating cells with the antioxidant N-acetylcysteine (NAC) decreased the number of apoptotic cells and recovered the rate of DNA synthesis in these ECs[309].

Nevertheless, several studies performed in adult populations showed a wide range of palmitic acid concentrations in plasma and serum, as high as 4.1 mM[312,313]. Therefore, it is not easy to determine why palmitate would kill cultured cells whilst similar or even higher concentrations are found in healthy individuals. It seems likely that a systemic regulation could regulate palmitate metabolism in individuals. It has been shown that

oleate rescues the apoptotic phenotype induced by palmitate[272]. Thus, a regulation by other fatty acids that could be present in an individual but not added to cell culture may be exerted.

2.2. Glucose and glutamine dependence for endothelial cell proliferation

The dependence of ECs on glucose and glutamine for sustaining cell growth was tested. Cells were seeded at low cell density and exposed to physiological concentrations of glucose and/or glutamine for five days. The results for HMECs show a total dependence for glutamine to grow, whereas these cells were able to proliferate in the absence of glucose for three days at the same rate as cells grown with both glucose and glutamine as long as glutamine was available in the media (**Figure 2A**). This did not happen in a macrovascular EC line such as BAEC (**Figure 2B**) or in the cervix adenocarcinoma tumor cell line HeLa (**Figure 2C**). Due to the strict nutritional requirements of cultured HUVECs, this experiment could not be performed in these cells, since they died after day 1 in these conditions (**Figure 2D**). The interesting data about glucose independence in HMEC led to the further research of glucose and glutamine long-term dependence in this cell line.

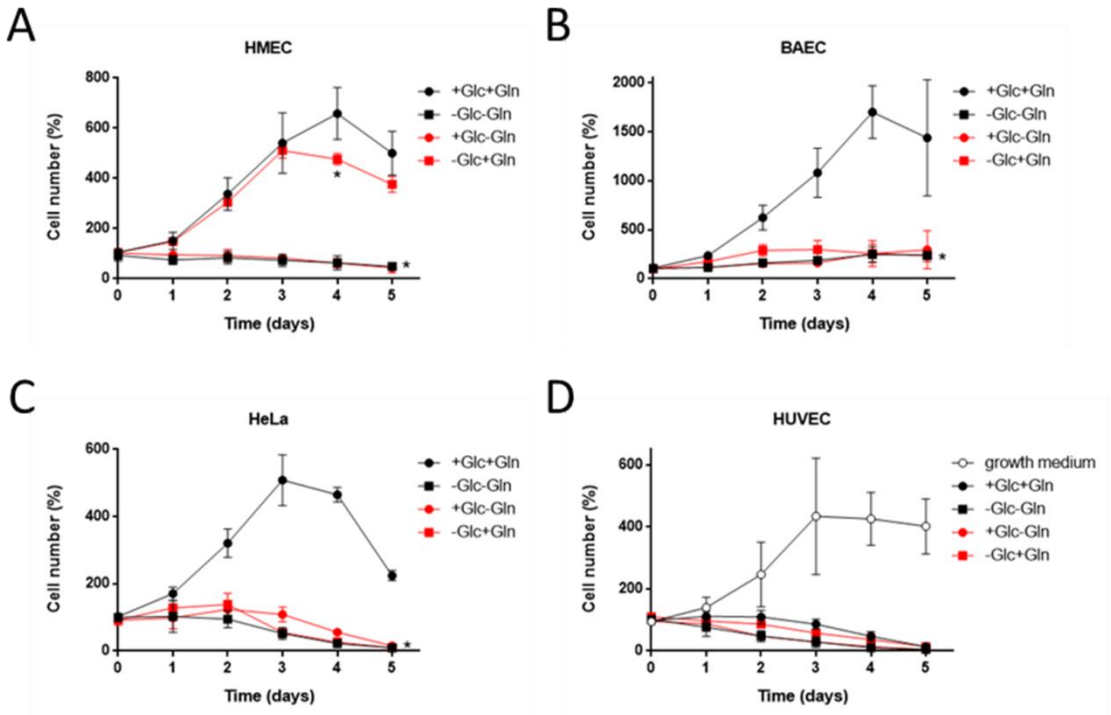

Figure 2. Cell growth in the presence or absence of 5 mM glucose and/or 0.5 mM glutamine in (A) HMEC, (B) BAEC, (C) HeLa and (D) HUVEC cell lines. Data are expressed as means ± SD of three independent experiments. *p < 0.05 versus glucose and glutamine condition.

Importantly, these cell growth curves were performed using a different medium (DMEM) than the growth medium that HMECs are cultured with (MCDB-131). Growth rate was lower in DMEM as compared to growth medium (**Figure 3A**). One major difference between these media is the presence or not of sodium pyruvate. Thus, an additional experiment was performed in the presence or absence of pyruvate along with glucose and/or glutamine. 1 mM sodium pyruvate was added to the media, instead of its physiological concentration in blood, since this is the concentration found in commercial MCDB-131. Pyruvate slightly increased growth rate in all conditions, although it was statistically significant only in the condition without glutamine (**Figure 3A**).

Another important difference is glutamine concentration. Glutamine in MDCB-131 growth medium is added at 2 mM, whereas physiological 0.5 mM glutamine was added to DMEM used for the elaboration of these growth curves. Nevertheless, increasing glutamine up to 2 mM in DMEM did not improve growth rate in HMECs (**Figure 3B**), whereas an increase in proliferation was found in these conditions in HUVECs[180].

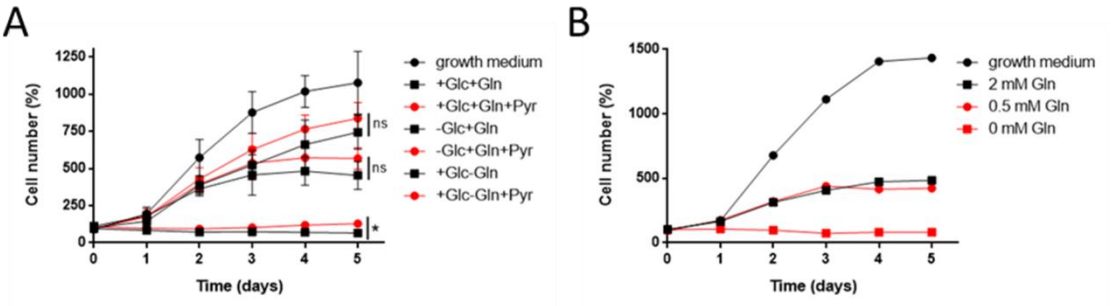

Figure 3. (A) Cell growth in HMECs in the presence or absence of 5 mM glucose and/or 0.5 mM glutamine supplemented with 1 mM pyruvate. Data are expressed as means ± SD of three independent experiments. *p < 0.05 versus condition without pyruvate. ns: non-significant. (B) Cell growth in HMECs in the presence of 5 mM glucose and 0.5 mM or 2 mM glutamine. Data are expressed as the results of a unique experiment.

It should be taken into account though that MCDB-131 medium contains additional metabolites not present in DMEM that could improve cell growth of HMECs. These metabolites are alanine, asparagine, aspartate, proline, biotin, vitamin B12, adenine, lipoic acid, putrescine and thymidine.

Moreover, ECs often confront hypoxia. For that reason, HMECs were also grown in the presence or absence of glucose and/or glutamine under hypoxia. Glucose starvation still allowed cells to grow in the presence of glutamine as compared to the ones grown

in the presence of glucose and glutamine, but to a lesser extent than in normoxic conditions (**Figure 4**). Interestingly, it has been shown that under hypoxic conditions glutamine can still be oxidized by tumor cells in order to sustain cell metabolism[314,315].

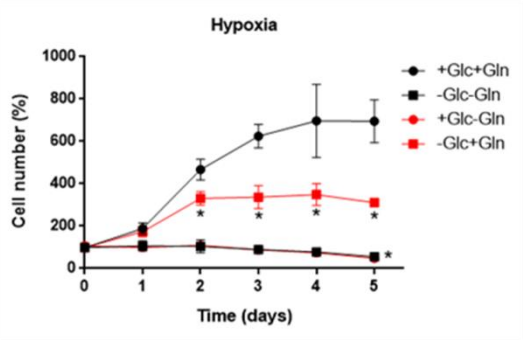

Figure 4. Cell growth in HMECs in the presence or absence of 5 mM glucose and/or 0.5 mM glutamine in hypoxia. Data are expressed as means ± SD of three independent experiments. *p < 0.05 versus condition with glucose and glutamine.

Additionally, cell proliferation was also determined by means of an EdU proliferation assay. In the absence of glutamine, the number of proliferating cells was quite low, whereas glucose starvation did not affect proliferation after 24 h incubation (**Figure 5**).

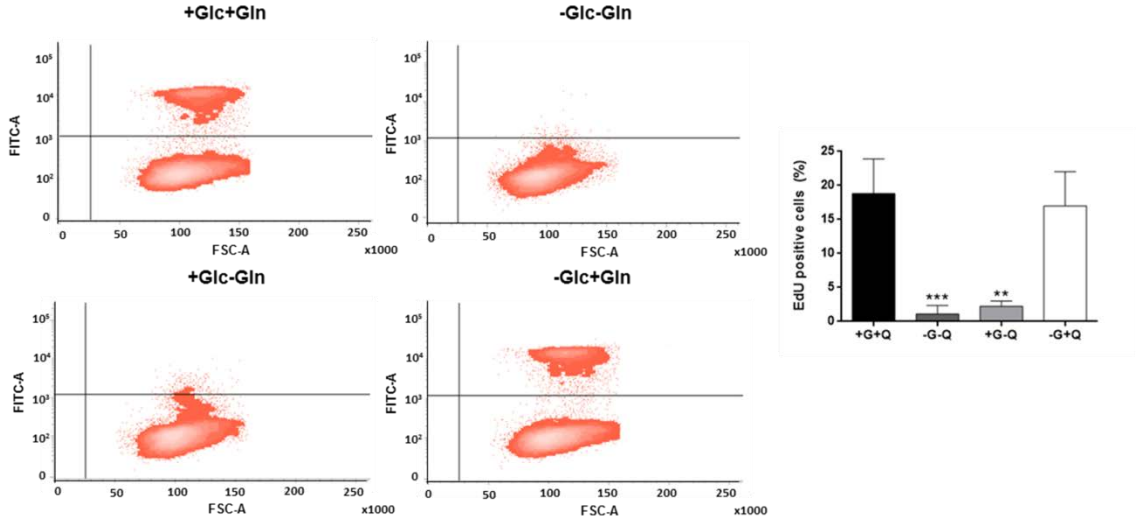

Figure 5. HMECs proliferation after 24 h in the presence or absence of 5 mM glucose and/or 0.5 mM glutamine. EdU incorporation to proliferating cells was detected using a FACS VERSE™ cytometer. Data are expressed as means ± SD of three independent experiments. **p < 0.01, ***p < 0.001 versus condition with glucose and glutamine. G: glucose; Q: glutamine.

Noticeably, HMECs incubated for 6 h in the absence of glutamine were found to have lower levels of aspartate compared to the condition in which both glucose and glutamine were present, whereas an accumulation of aspartate was found when only

glutamine was present in the media under normoxic conditions (**Figure 6**). Aspartate synthesis is essential for supporting cell growth[316,317]. Therefore, the inhibition of cell proliferation and cell survival in the absence of glutamine could be partly due to a decrease in intracellular aspartate levels. The differential levels of aspartate in normoxia and hypoxia could also explain the different cell growth under glucose starvation in both conditions. Moreover, aspartate is present in MCDB-131 growth medium. It would be interesting to test whether aspartate supplementation to the media rescues, even partially, cell proliferation in the absence of glutamine. Unfortunately, these experiments were not carried out during the course of this PhD Thesis.

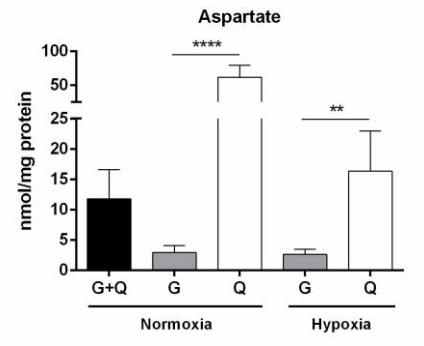

Figure 6. Intracellular aspartate levels in HMECs in the presence or absence of 5 mM glucose and/or 0.5 mM glutamine in normoxia and hypoxia. Data are expressed as means ± SD of three independent experiments with triplicates. **p < 0.01, ****p < 0.0001. G: glucose; Q: glutamine.

2.3. Glucose and glutamine dependence for endothelial cell migration

EC migration is another essential feature involved in angiogenesis. Different results have been obtained for migration of HUVECs in the absence of glucose or glutamine[122,180]. The results presented herein show that glucose is not essential for migration of HMECs, whereas cell migration was drastically reduced in the absence of glutamine (**Figure 7**). Nonetheless, it is important to take into account that after 7 h incubation under glutamine starvation cells began to detach. Thus, most likely glutamine withdrawal does not affect specifically cell migration in these cells but cell function in general.

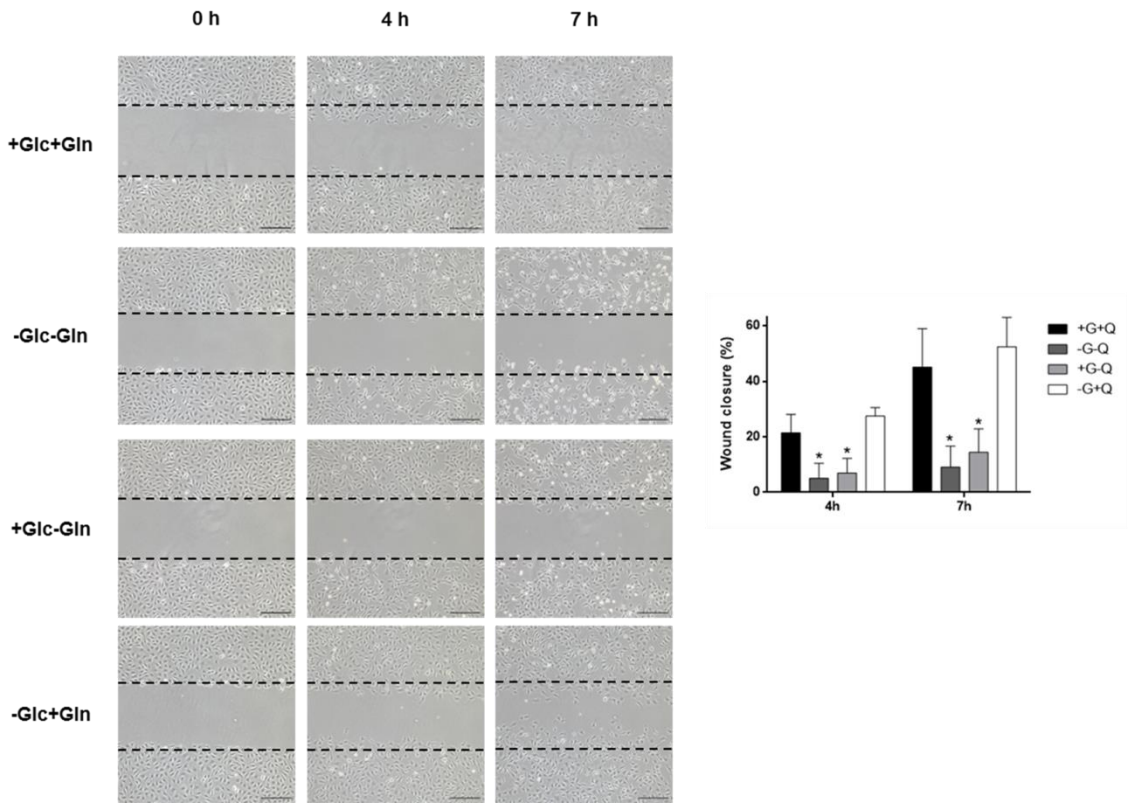

Figure 7. Representative images and quantification of wound closure of HMECs incubated in the presence or absence of 5 mM glucose and/or 0.5 mM glutamine for 0, 4, and 7 h. Bar scale = 200 μm. Data are expressed as means ± SD of three independent experiments. *p < 0.05 versus condition with glucose and glutamine. G: glucose; Q: glutamine.

2.4. Glucose starvation does not affect cell cycle distribution in HMECs

A cell cycle analysis by flow cytometry was performed in the presence or absence of glucose for 48 h. According to the results from cell proliferation, glucose starvation did not altered cell cycle distribution in HMECs (**Figure 8**). Moreover, glucose withdrawal did not induced cell accumulation in subG1 phase, an indicator of apoptotic cells (**Figure 8**). These results differ from the observed increase in caspase 3 levels in retinal capillary ECs after 24 h glucose withdrawal[318].

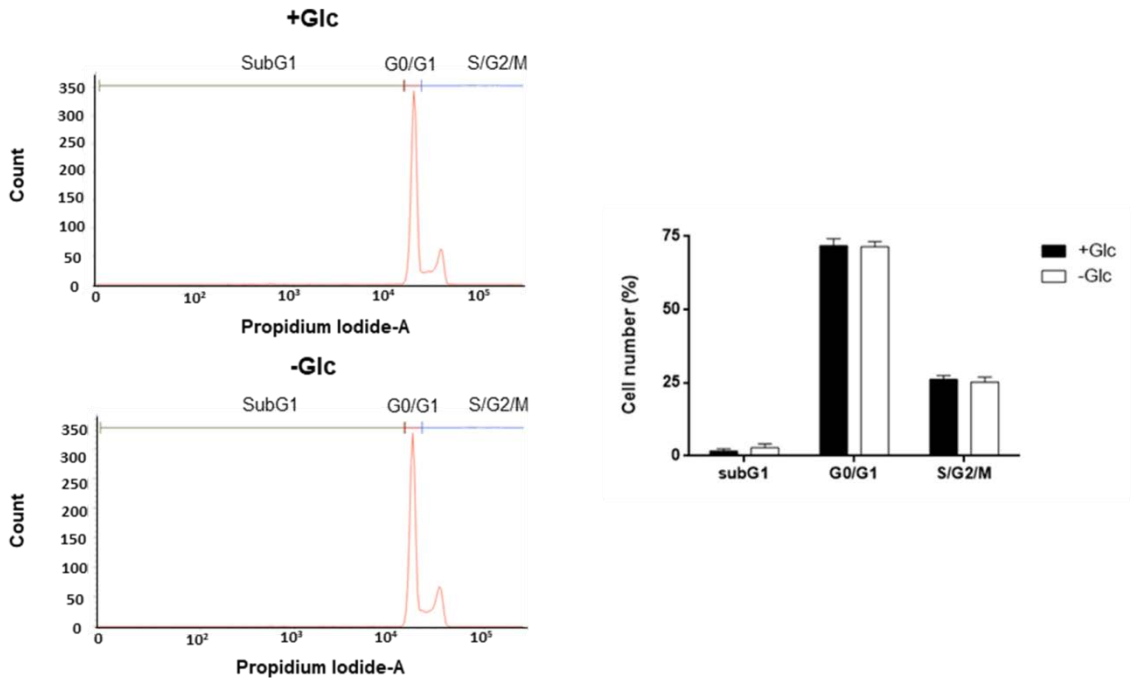

Figure 8. Cell cycle distribution of subpopulations of HMECs grown in the presence or absence of 5 mM glucose for 48 h. 0.5 mM glutamine was present in the media. Percentage of cells in subG1, G1 and S/G2/M phases were determined using a FACS VERSE^{TM} cytometer. Data are expressed as means ± SD of three independent experiments.

2.5. Glucose starvation does not induce autophagy in HMECs

Autophagy is a physiological process that occurs within cells in order to degrade or recycle cellular components. It is known that under nutrient depletion conditions autophagy may be induced in order to protect cells from starvation and assure cell survival[319]. For instance, glucose starvation in mouse microvascular ECs, as well as inhibition of glucose metabolism with 2-DG in HUVECs, have been shown to induce autophagy[320]. In order to corroborate whether the survival of HMECs in the absence of glucose was supported by an activation of autophagy, a Western blot of LC3B was performed. The LC3B-II/LC3B-I ratio is an indicator of autophagy[321]. However, glucose starvation did not increase the LC3B-II/LC3B-I ratio (**Figure 9**).

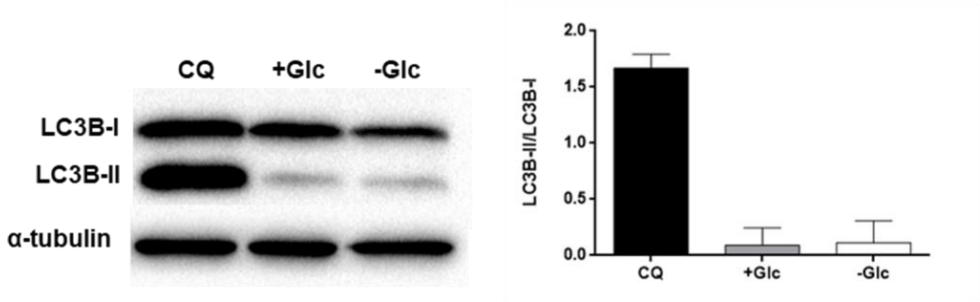

Figure 9. LC3B-I and LC3B-II protein expression were measured by Western blot in HMECs grown in the presence or absence of 5 mM glucose for 48 h. 0.5 mM glutamine was present in the media. A positive control incubating cells with 5 mM glucose and 50 μM chloroquine for 16 h was included. Data from Western blot are normalized against α-tubulin expression and expressed as means ± SD of three independent experiments. CQ: chloroquine.

These results suggest that a mechanism different from autophagy may regulate the capacity of these cells to grow and survive under glucose withdrawal. Other authors found that ECs are able to alter their metabolism in order to survive in the absence of glucose. These mechanisms include a reduced protein synthesis, the use of endogenous TAGs as an alternative energy fuel, stimulation of *de novo* synthesis of adenine nucleotides and activation of glycogenolysis and glycogen synthesis[164,322,323].

3. Short-term preference for different metabolic fuels in endothelial cells

During the last century, uptake and utilization of different metabolic substrates were tested in the presence of these different metabolic fuels alone or in combination, using tumor cell lines or healthy cell lines[288,324-326]. Nevertheless, few studies were carried out under these conditions in ECs[115,117,327,328]. In this chapter, the direct influence of different metabolic substrates on the uptake and utilization of others after a short period of time was tested. For that aim, supplementation of additional metabolites, such as amino acids, was avoided whenever possible.

3.1. Influence of glucose, glutamine and palmitate to oxygen consumption and extracellular acidification rates in HMECs

OCR and ECAR are indicators of OXPHOS and glycolysis, respectively. These parameters were measured in HMECs in the presence or absence of 5 mM glucose, 0.5 mM glutamine and/or 0.5 mM palmitate using an XF^{e}24 Seahorse Flux Analyzer. The results presented herein show that HMECs slightly oxidize glucose, glutamine and palmitate, as indicated by a low increase in OCR after substrate addition to the media

(**Figure 10A**). Conversely, ECAR greatly increased after glucose injection, pointing out to a high glycolytic capacity of these cells (**Figure 10B**). Therefore, it seems that HMECs preferably converts glucose into lactate instead of oxidizing glucose or glutamine. Glutamine addition also increased ECAR, but to a lesser extent (**Figure 10B**). However, this is most likely explained by deprotonation of HCO_3^- resulting from oxidation[284].

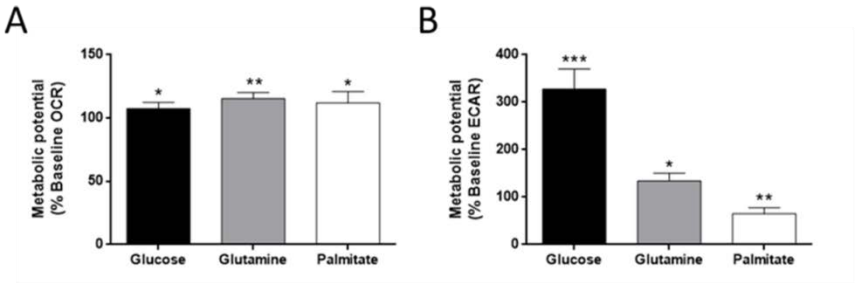

Figure 10. Flux analysis in HMECs. (A) Oxygen consumption rate (OCR) and (B) extracellular acidification rate (ECAR) in the presence of 5 mM glucose, 0.5 mM glutamine or 0.5 mM palmitate. Data are expressed as means ± SD of three independent experiments with triplicate samples each. *p < 0.05, **p < 0.01, ***p < 0.001 versus control without any metabolic substrate.

3.2. Effect of glutamine and palmitate on glucose uptake and lactate production in HMECs

The effect of 0.5 mM glutamine and 0.5 mM palmitate on glucose uptake and lactate production was studied in HMECs. The results show that neither glutamine nor palmitate affect glucose uptake in these cells in the conditions used (**Figure 11A**). Furthermore, glutamine did not affect lactate production from glucose, whereas palmitate increased it (**Figure 11B**). No lactate was detected in the absence of glucose, which reinforces the theory about the increase in ECAR in the presence of glutamine (**Figure 11B**)[284].

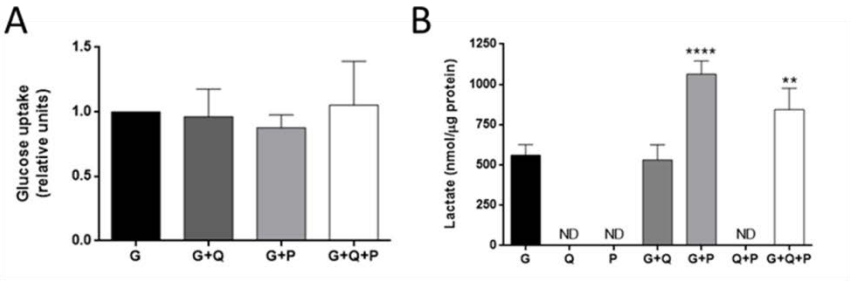

Figure 11. (A) Glucose uptake and (B) lactate production in HMECs in the presence or absence of 5 mM glucose, 0.5 mM glutamine and/or 0.5 mM palmitate. Data are expressed as means ± SD of three independent experiments. **p < 0.01, ****p < 0.0001 versus glucose condition. ND: non-detected. G: glucose; P: palmitate; Q: glutamine.

Moreover, glutamine did not affect glucose uptake or lactate production in the macrovascular EC model HUVEC (**Figure 12**).

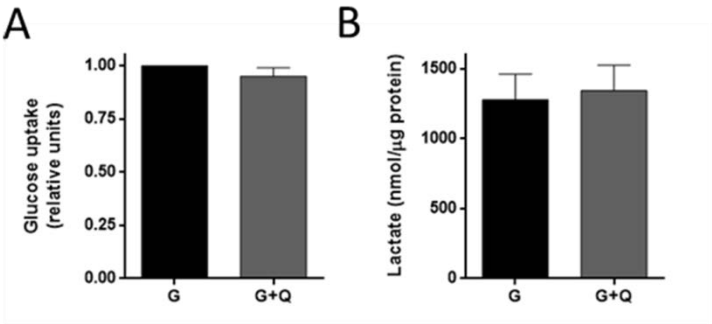

Figure 12. (A) Glucose uptake and (B) lactate production in HUVECs in the presence or absence of 5 mM glucose and 0.5 mM glutamine. Data are expressed as means ± SD of three independent experiments. G: glucose; Q: glutamine.

3.3. Effect of glucose and palmitate on glutamine uptake and oxidation in HMECs

Addition of 5 mM glucose and/or 0.5 mM palmitate did not significantly affect glutamine uptake in HMECs (**Figure 13A**). However, glucose and, to a lesser extent, palmitate decreased glutamine oxidation in these cells (**Figure 13B**). These data reinforce the high increase in ECAR in the presence of glucose in comparison with the slight increase in OCR when only glutamine was available.

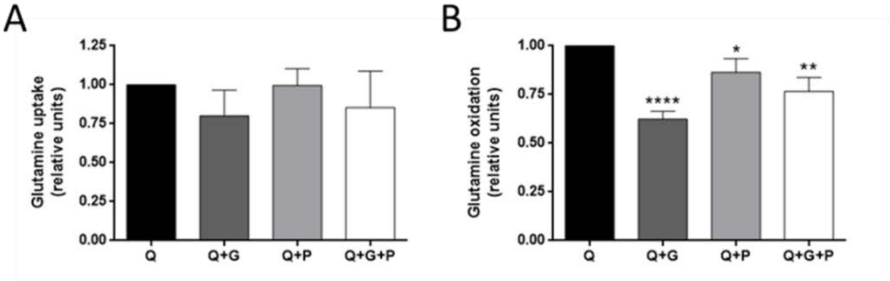

Figure 13. (A) Glutamine uptake and (B) glutamine oxidation in HMECs in the presence or absence of 0.5 mM glutamine, 5 mM glucose and/or 0.5 mM palmitate. Data are expressed as means ± SD of three independent experiments. *p < 0.05, **p < 0.01, ****p < 0.0001 versus glutamine condition. G: glucose; P: palmitate; Q: glutamine.

Similar results were obtained with HUVECs (**Figure 14**).

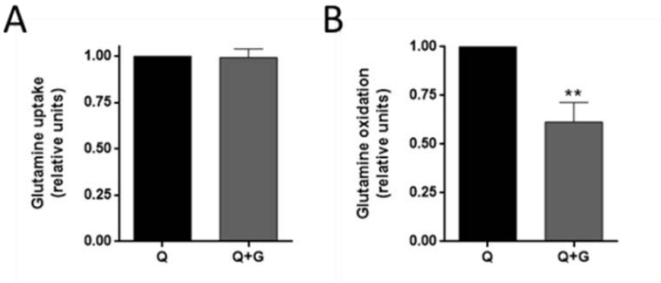

Figure 14. (A) Glutamine uptake and (B) glutamine oxidation in HUVECs in the presence or absence of 0.5 mM glutamine and 5 mM glucose. Data are expressed as means ± SD of three independent experiments. **p < 0.01 versus glutamine condition. G: glucose; Q: glutamine.

As a conclusion, this model of microvascular ECs is highly glycolytic and glucose seems to repress glutamine metabolism. This fact corroborates how cells can rely on different metabolites depending on their necessities. HMECs probably obtain more energy from glucose via glycolysis, like many tumor cells do, whereas they need glutamine most likely in order to synthesize acetyl-CoA for lipid synthesis to sustain cell growth. Moreover, the fact that HMECs behave in a similar way than HUVECs coincide with the high glycolytic profile of ECs described in most of the data available in the bibliography[114,115,118,121]. Nevertheless, it should be taken into account that the use of different models can lead to different metabolic responses[117].

3.4. Effect of glucose and glutamine on palmitate uptake in HMECs

The effect of 5 mM glucose and/or 0.5 mM glutamine on palmitate uptake was tested in HMECs. No statistically significant effect of these two metabolic fuels was found in the conditions used (**Figure 15**).

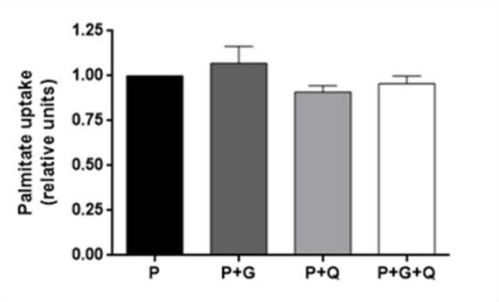

Figure 15. Palmitate uptake in the presence or absence of 5 mM glucose and/or 0.5 mM glutamine in HMECs. Data are expressed as means ± SD of three independent experiments. G: glucose; P: palmitate; Q: glutamine.

4. Lactate metabolism in endothelial cells

It is well-known that in the TME cancer cells secrete large amounts of lactate[107]. This extracellular lactate can be taken up by stromal cells. For example, cancer-associated fibroblasts (CAFs) use this lactate to obtain energy via oxidation[329]. Moreover, this extracellular lactate can exert different effects in the surrounding cells of the microenvironment, such as promoting immunosuppression, invasion and angiogenesis[330]. Regarding the induction of angiogenesis, lactate activates this process through different mechanisms: (1) inducing IL-8 expression in a nuclear factor kappa B (NF-κB)-dependent manner, (2) increasing VEGF, its receptor VEGFR2 and FGF-2 expression through HIF-1α stabilization and (3) promoting Akt phosphorylation, all these effects given after its incorporation via MCT1 transporters[161-163]. Indeed, targeting the MCT1 transporter or LDH-B enzyme reverses the effect to the one observed in the control without lactate[161,162]. However, most of these experiments have been performed using macrovascular ECs, and no evidence of MCT1 expression in microvascular ECs existed in models different from brain and eye tissues[331,332]. For that reason, lactate metabolism was studied in this model of dermal microvascular ECs.

First, the capacity of HMECs to oxidize lactate was tested. It is known that ECs do not oxidize lactate at a major extent when glucose is present[115]. Even that physiological lactate concentration in blood is 0.5-2 mM, concentrations as high as 40 mM have been found in tumors[333]. Therefore, the same lactate concentration of each lactate-carbon derived from 5 mM glucose, i.e. 10 mM lactate, seems appropriate to be added to the media. Nonetheless, lactate failed to increase OCR in HMECs even in the absence of glucose (**Figure 16A**). Not surprisingly, ECAR was reduced when lactate was present

in the media (**Figure 16B**), exerting a negative feedback in glycolysis by end product inhibition.

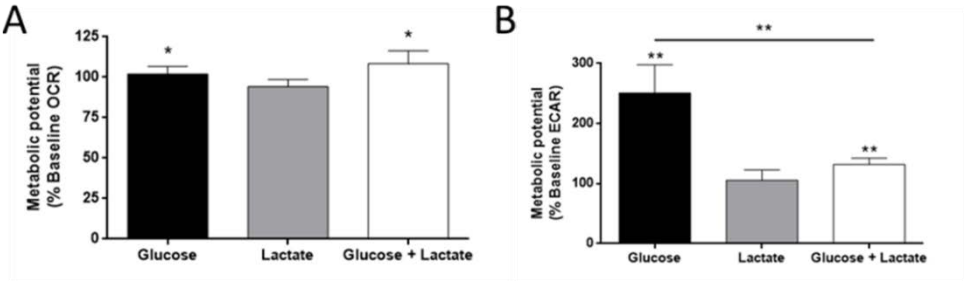

Figure 16. (A) Oxygen consumption rate (OCR) and (B) extracellular acidification rate (ECAR) in the presence of 5 mM glucose and/or 10 mM lactate in HMECs. Data are expressed as means ± SD of three independent experiments. *p < 0.05, **p < 0.01 versus condition without glucose or lactate.

Lactate oxidation requires both the uptake from the extracellular media and later conversion to pyruvate. In order to look into the reason why lactate could not be oxidized in these cells, gene expression of proteins involved in lactate metabolism was measured. Whereas HMECs expressed LDH-A and MCT4, no expression for either LDH-B or MCT1 was found (**Figure 17**).

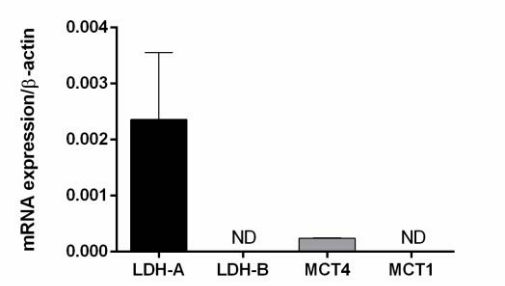

Figure 17. mRNA expression of LDH-A, LDH-B, MCT4 and MCT1 in HMECs. Data are normalized against β-actin expression and expressed as means ± SD of three independent experiments. ND: non-detected.

Hypoxic conditions are usually given in the angiogenic microenvironment. It is known that MCT1 does not have HREs at its promoter[334]. However, MCT1 gene expression was found to be higher in mesenchymal stem cells, but not in HUVECs, under hypoxia[335]. Therefore, lactate transporters expression was also tested under oxygen restrictive conditions in HMECs. First, the induction of HIF-1α was measured under both hypoxic and anoxic conditions by Western blot. HIF-1α was induced in cells cultured both in anoxia and hypoxia (**Figure 18**).

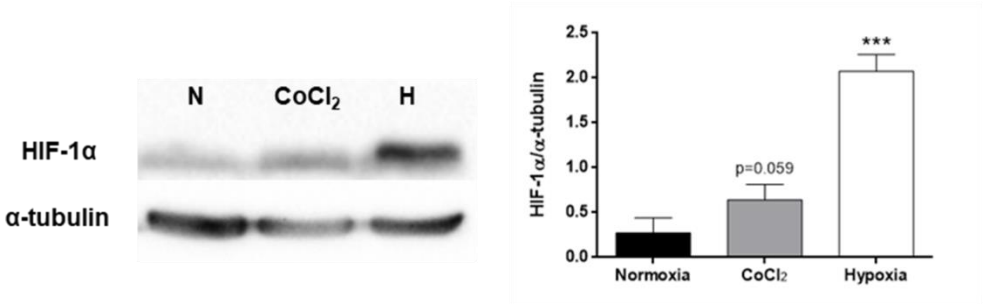

Figure 18. HIF-1α protein expression was determined by Western blot in HMECs under normoxia, anoxia (200 μM $CoCl_2$) or 1% hypoxia. Data are normalized against α-tubulin expression and expressed as means ± SD of three independent experiments. *p < 0.05, ***p < 0.001 versus normoxia condition. N: normoxia; H: hypoxia.

Then, MCT1 and MCT4 expression were tested under these conditions. Both anoxia and hypoxia increased MCT4 gene expression, whereas no MCT1 mRNA was detected in any condition (**Figure 19A**). In order to check whether MCT1 expression is regulated at the protein level with a low gene expression, MCT1 protein levels were determined by Western blot under these conditions. Still, no MCT1 protein expression was detected in HMECs (**Figure 19B**).

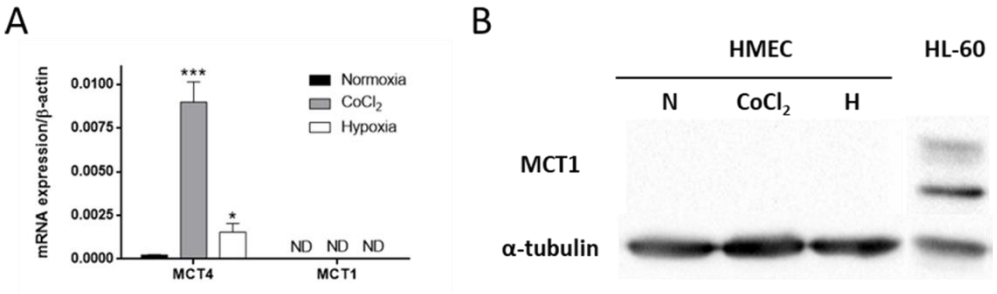

Figure 19. (A) MCT4 and MCT1 mRNA expression and (B) MCT1 protein expression in HMECs under normoxia, anoxia (200 μM $CoCl_2$) or 1% hypoxia. Extracts from HL-60 under normoxia were used as positive control in Western blots. Data from qPCR are normalized against β-actin expression, and data from Western blot are normalized against α-tubulin expression. Data are expressed as means ± SD of three independent experiments. *p < 0.05, ***p < 0.001 versus normoxia condition. ND: non-detected. N: normoxia; H: hypoxia.

Finally, it was tested whether extracellular lactate could induce MCT1 expression in these cells. Nevertheless, no MCT1 protein expression was detected even in the presence of 10 mM lactate (**Figure 20**).

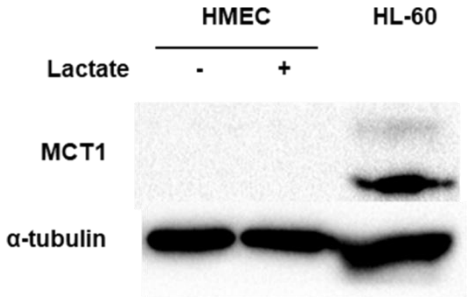

Figure 20. MCT1 protein expression was determined by Western blot in HMECs in the presence or absence of 10 μM lactate. Extracts from HL-60 under normoxia were used as positive control. Data are normalized against α-tubulin expression and expressed as means ± SD of three independent experiments.

HUVECs are known to express MCT1[161,162]. Nevertheless, extracts from HL-60 leukemia cells were used as a positive control for MCT1 expression due to its availability in the laboratory at the moment when these Western blots were performed[336].

MCT1 is the main and most characterized transporter described for lactate uptake. Other less characterized and minority lactate transporters, such as MCT2, have been reported in certain tissues[337]. However, the presence of these transporters in ECs has not been described yet.

5. Conclusions

Microvascular ECs have been less studied compared to macrovascular ECs. Their laborious isolation, as well as their usual dependence on human serum makes them non-friendly cells for reproducible results. In this work, the use of an immortalized microvascular EC line allowed to consistently demonstrate their short and long-time dependency on glucose and glutamine metabolism, respectively. The results obtained point out to (1) a total dependency for glutamine to grow, whereas glucose was unnecessary for cell proliferation for several days specifically in HMECs and (2) a similar short-time glucose and glutamine dependence of HMECs compared to other ECs such as the well-studied HUVEC model.

Besides, whereas MCT1 is highly expressed in HUVECs and ECs from the brain and retina, this lactate-H^+ transporter is not present in this model of dermal microvascular ECs. Although the short-time preferences were similar between HMECs and HUVECs, results from MCT1 expression suggest that different ECs can behave in a different way, most likely depending on the kind of capillary they were isolated from, as well as the

tissue origin. Therefore, a model of ECs is not representative of all kinds of ECs[338,339]. It has been demonstrated that targeting MCT1 can inhibit tumor angiogenesis *in vivo*[162]. However, the results presented herein suggest the limitations of this target. Thus, it seems likely that targeting glycolytic enzymes may offer a better strategy for the treatment of angiogenesis-dependent diseases, which could certainly be improved with additional MCT1 targeting in some tissues such as those in the brain and retina[331].

CHAPTER 3

Studies on the potential anti-angiogenic activity of fasentin, a GLUT1 and GLUT4 inhibitor

1. Fasentin is a GLUT1 and GLUT4 inhibitor

Fasentin (N-[4-chloro-3-(trifluoromethyl)phenyl]-3-oxobutanamide) (**Figure 1**) has been described as a chemical sensitizer to the death receptor stimuli FAS, due to its effect on glucose uptake in tumor cells. A microarray analysis showed that *PCK2* gene expression was upregulated in the presence of fasentin[340]. This gene has been previously associated with glucose deprivation[341]. By means of an *in silico* study, fasentin was seen to bind to the intramembrane channel of the glucose transporter GLUT1. The binding site of fasentin was different from those of other GLUT1 inhibitors such as dipyridamole, phloretin and cytochalasin B. However, fasentin inhibited glucose uptake more potently in cell lines preferentially expressing GLUT4. Therefore, both GLUT1 and GLUT4 were considered as targets for the inhibitory activity of this compound[340]. The activity of fasentin on glucose uptake was previously described in leukemia and prostate cancer cells, but later other authors found that this compound is also able to inhibit glucose uptake in breast cancer, glioblastoma, oral squamous cell carcinoma, cervix adenocarcinoma, head neck cancer, colon carcinoma, osteosarcoma and corticotropinoma cell lines[340,342-344].

Silibinin, a GLUT4 transporter inhibitor, was seen to inhibit angiogenesis[232,233]. Due to the known role of EC metabolism, and especially glucose metabolism, in EC function and angiogenesis, in this PhD Thesis the possible anti-angiogenic activity of fasentin was tested.

Most of the results presented herein are part of a manuscript that is under revision in *Scientific Reports* (**Appendix 6**).

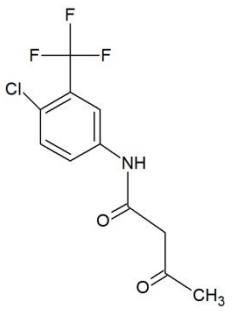

Figure 1. Chemical structure of fasentin. This chemical structure was drawn using ChemSketch software.

2. Fasentin inhibits endothelial cell proliferation

In order to stablish the IC_{50} of fasentin the MTT assay was performed in cells seeded at low density in the presence of increasing doses of fasentin for 72 h. Three EC lines, three tumor cell lines and a fibroblast cell line were used in this experiment. Results are collected in **Figure 2** and **Table 1**. These results show that fasentin diminishes cell number in all the cell lines tested, but that its effect on fibroblasts was lower compared to the effect on tumor and ECs.

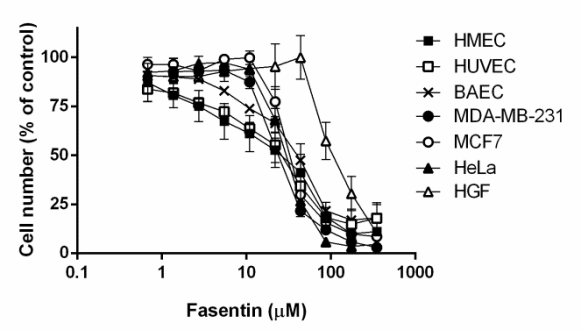

Figure 2. Dose-response curves showing the effect of fasentin on the *in vitro* growth of different cell lines after 72 hours treatment from low density seeding conditions. Cell number is represented as the percentage of cells compared to the condition containing no drug. Concentrations are represented in logarithmic scale. Data are expressed as means ± SD of three independent experiments with quadruplicates.

Table 1. Half-maximal inhibitory concentration (IC_{50}) values (μM) for fasentin treatment in different cell lines determined by the MTT assay. Data are expressed as means ± SD of three independent experiments with quadruplicate samples each.

	IC_{50} (μM)
HMEC	27.9 ± 14.5
HUVEC	27.6 ± 3.7
BAEC	42.7 ± 9.5
MDA-MB-231	26.3 ± 4.8
MCF7	34.7 ± 4.0
HeLa	31.9 ± 1.4
HGF	111.2 ± 27.0

However, the MTT assay performed under these conditions does not indicate whether the compound tested inhibits cell proliferation or if it induces cell death. For that reason, additional experiments were performed in the EC line HMEC.

A modified MTT assay was carried out by seeding cells at high density, allow them to attach and then the compound was added for 16 h in order to check whether it killed the cells. Doses of fasentin up to 100 μM did not significantly diminish cell number after this incubation time (**Figure 3**).

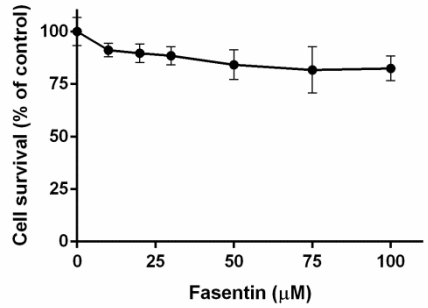

Figure 3. Dose-response curve showing the effect of fasentin on the *in vitro* cytotoxicity in HMECs after 16 h incubation. Data are expressed as means ± SD of three independent experiments with quadruplicate samples each.

In addition, HMECs were seeded to sub-confluence and different doses of fasentin were added. Cell number was monitored at 0, 4, 7, 16 and 24 h using a Neubauer chamber. Addition of trypan blue allowed the exclusion of dead cells from the cell counting. Fasentin decreased cell proliferation in a dose-dependent manner, totally inhibiting it at 100 μM (**Figure 4A**). Initial cell number did not decrease with fasentin, indicating that this compound did not compromise cell survival. Additionally, number of death cells was not statistically different between control and fasentin-treated cells (**Figure 4B**).

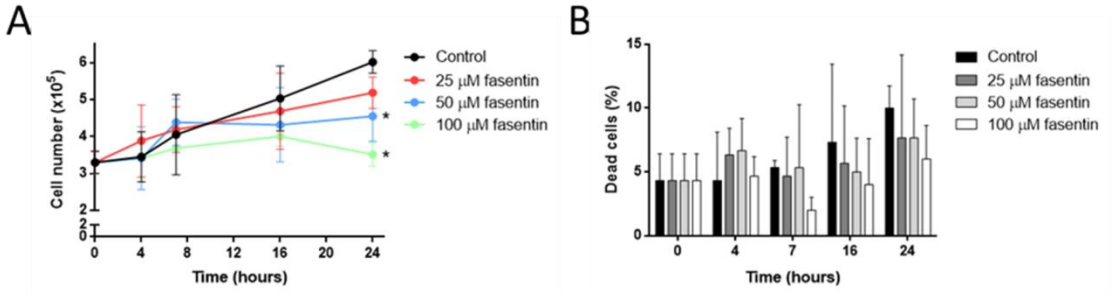

Figure 4. (A) Monitoring of cell number of HMECs treated with different doses of fasentin over 24 h. (B) Percentage of dead cells after fasentin treatment over 24 h. Data are expressed as means ± SD of three different experiments. *$p < 0.05$ versus untreated control.

A cell cycle analysis was also performed. Fasentin induced a cell cycle arrest in G0/G1 phase and reduced the cell number in S phase in a dose-dependent manner after

both 16 and 24 h incubation (**Figure 5**). Moreover, this compound did not increase the subG1 phase population, which comprises apoptotic cells (**Figure 5**). These results corroborate the anti-proliferative role of fasentin more than its effect on cell survival.

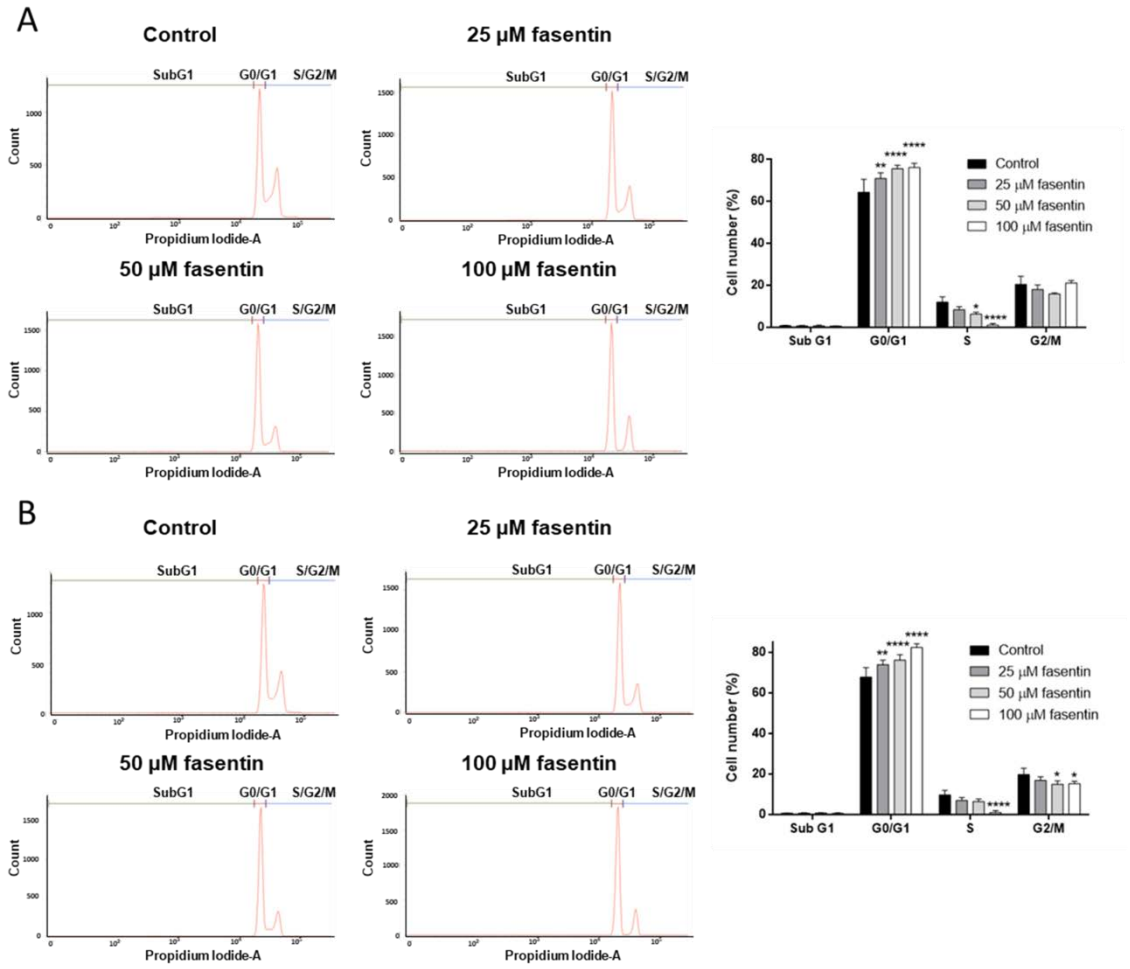

Figure 5. HMECs were exposed for (A) 16 h or (B) 24 h to fasentin at the indicated concentrations, stained with propidium iodide and percentages of cells in subG1, G1, S and G2/M phases were determined using a FACS VERSE^{TM} cytometer. A representative result and the calculated values for cell subpopulations, expressed as means ± SD of three independent experiments, are shown. *$p < 0.05$, **$p < 0.01$, ****$p < 0.0001$ versus untreated control.

Moreover, in order to confirm the anti-proliferative role of fasentin in HMECs, an EdU proliferation assay was carried out after 24 h incubation with this compound. Accordingly, the results obtained verified that fasentin diminishes HMECs proliferation in a dose-dependent manner (**Figure 6**).

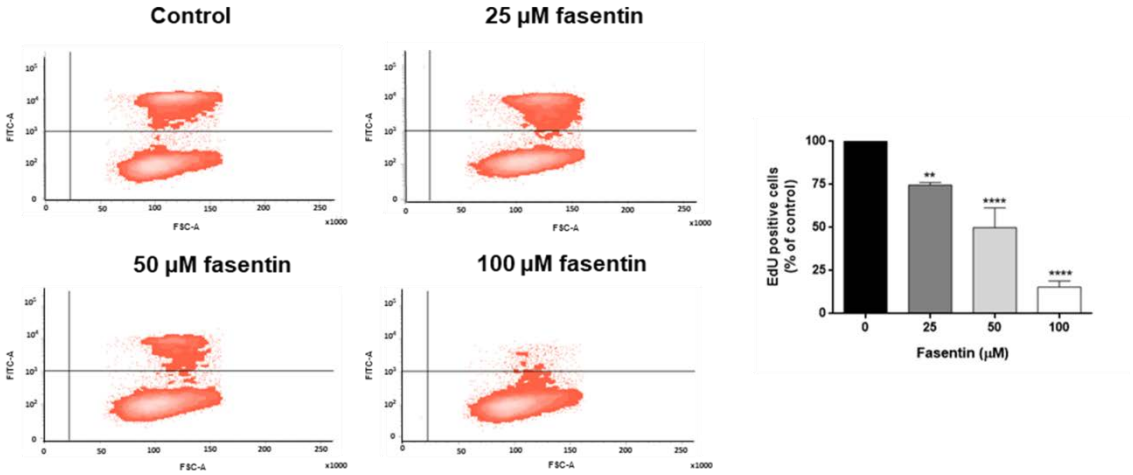

Figure 6. 10 µM EdU was added for 2 h to HMECs treated with fasentin for 22 h and EdU incorporation was determined using a FACS VERSE^{TM} cytometer. A representative result and the calculated values for EdU positive cells expressed as means ± SD of three independent experiments are shown. **p < 0.01, ****p < 0.0001 versus untreated control.

Therefore, fasentin does not induce cell death in HMECs, but it decreases EC proliferation. Nonetheless, in some cancer cells, but not all, fasentin was shown to induce apoptosis at some extent[340,343]. Thus, fasentin does not have a cytotoxic effect in HMECs at the concentrations tested, but it has a cytostatic effect in a dose-dependent manner, which could differ in other cell types.

3. Fasentin impairs *in vitro* and *in vivo* angiogenesis

Angiogenesis can be simulated *in vitro* by seeding ECs on Matrigel. In the absence of serum, ECs would form tube-like cords, similar to the three-dimensional network of new tubes that occurs *in vivo* when angiogenesis is active. By means of this assay, 25 and 50 µM fasentin was seen to partially inhibit tube formation in HMECs, whereas a concentration of 100 µM exerted a total inhibition of *in vitro* tube formation (**Figure 7**).

The lack of "tubular" structures on Matrigel could be due to both an inhibition of angiogenesis or to a disruption of tubes. In order to discern between these two possibilities, HMECs were seeded on Matrigel, let to form these cords and then fasentin was added. The results obtained show that this compound does not disrupt already formed tubes (**Figure 8**). Therefore, fasentin is able to inhibit tube formation *in vitro*.

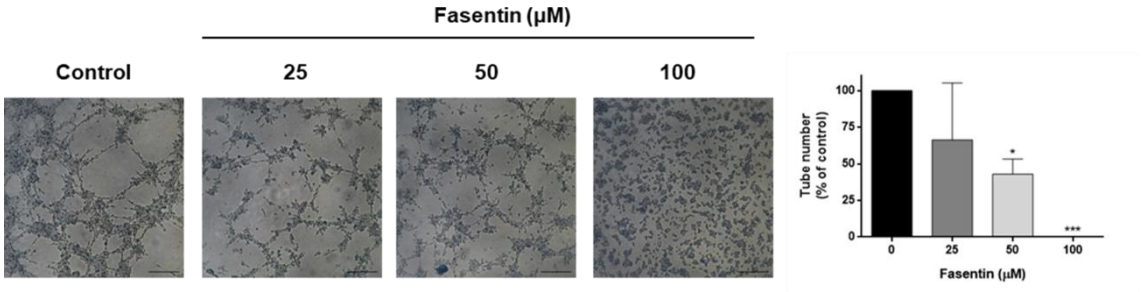

Figure 7. Representative photographs and quantitative analysis of "tubular" structures formed by control (untreated) and fasentin-treated HMECs on Matrigel. Control cells formed tubes (left panel). 100 μM fasentin completely inhibited HMECs alignment and cord formation, with partial inhibition observed at 25 and 50 μM. Cells were photographed 5 h after seeding and drug administration under an inverted microscope. Bar scale = 200 μm. Data are represented as means ± SD for three independent experiments with duplicate samples each. *$p < 0.05$; ***$p < 0.001$ versus untreated control.

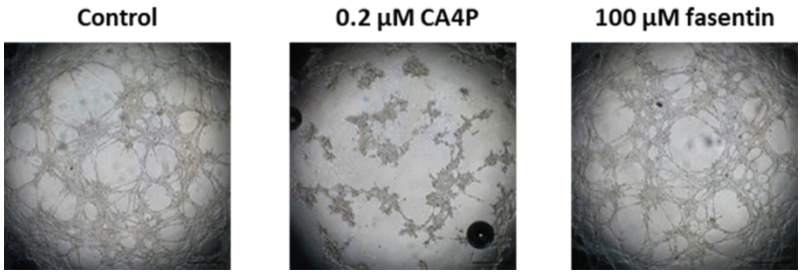

Figure 8. Representative photographs of control (untreated) and fasentin-treated HMECs in the "tubule-like" structure disruption assay. Bar scale = 500 μm. CA4P was used as a positive control.

Next, the possible anti-angiogenic activity of fasentin was tested *in vivo*. For that aim, the CAM assay was first performed. In control eggs blood vessels formed a dense and spatially oriented, branching network of vascular structures whose diameter decreases as they branch (**Figure 9**, left panel), whereas aeroplysinin-1, used as positive control, disrupted angiogenesis in this model (**Figure 9**, central panel). The main effect observed for fasentin was the apparent vessels rebounds close to the methylcellulose discs (that never occurs in the DMSO controls) at a dose of 50 nmol per disc. In addition, the general pattern of vascularization in the CAM was altered in the fasentin condition, compared to the regular and hierarchic network observed in the DMSO controls (**Figure 9**, right panel). **Table 2** summarizes the evaluation of the *in vivo* impairment of angiogenesis in the CAM assay by fasentin, understood as the number of eggs out of the total number of evaluated eggs in which some of these altered vascular

characteristics were detected. 50 nmol fasentin was the most effective amount of this compound for the modulation of angiogenesis in this model. The effects observed for fasentin in the CAM assay cannot be considered a canonical angiogenesis inhibition (reduction of the number of vessels in the treated area), but there is no doubt that this compound is impairing the normal vascularization of the membrane, somehow modulating the angiogenic process.

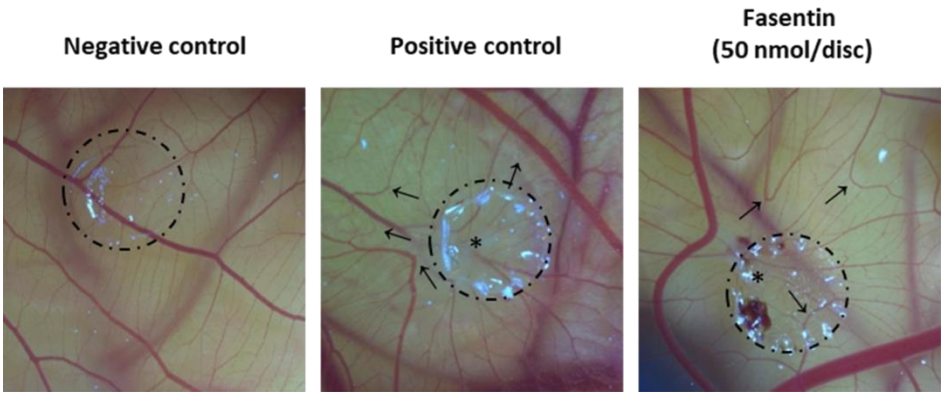

Figure 9. Chorioallantoic membrane (CAM) assay with fasentin. Methylcellulose discs containing the substance vehicle alone (DMSO) (left panel), 3 nmol aeroplysinin-1 as positive control (central panel) and 50 nmol fasentin (right panel) were added to the CAMs. Circles show the locations of the methylcellulose discs. Arrows point to rebound of vessels outward from the treated area. Asterisks indicate disrupted vessels.

Table 2. Impairment of *in vivo* angiogenesis by fasentin. Percentage of treated egg CAMs that showed some degree of impairment of angiogenesis after fasentin treatment.

Fasentin (nmol/disc)	Positives/total	Inhibition fraction
0	0/21	0
1.25	0/4	0
2.5	0/4	0
5	2/10	0.2
12.5	4/16	0.2
25	4/18	0.2
50	7/8	0.9

Additional *in vivo* angiogenesis assays were carried out in order to confirm the modulatory capacity of fasentin on *in vivo* angiogenesis. The ISV formation assay on zebrafish was performed. Low doses of fasentin (10 and 25 μM) had no effect on the development of the vasculature (**Figure 10**). However, increasing doses of the compound (similar to those used *in vitro*) caused a dramatic impairment of the general

development of the embryo, which presented lordosis, pericardial edema and loss of heartbeat. Others found that inhibition of GLUT1 in zebrafish embryos caused apoptosis during embryonic development and severe defects on the formation of the blood-brain barrier and the sinus venosus[345-347]. This lethality made impossible to evaluate the influence of fasentin on the vasculature development in this model.

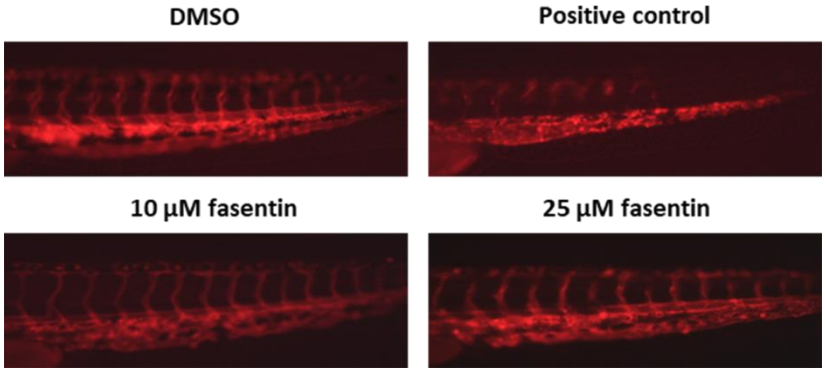

Figure 10. Representative photographs of the intersegmental vessel (ISV) formation in the Tg(kdrl:ras-mCherry) zebrafish in the presence of fasentin. 20 µM GR-24 was used as positive control.

Due to the limitations found for the ISV formation assay using this compound, the caudal fin regeneration assay in the adult zebrafish was also performed. The regenerated area was slightly smaller in animals treated with 30 µM at 3 dpa (**Figure 11**). However, it should be taken into account that only 2 animals could be used for each condition in this experiment. Therefore, no statistical analysis could be performed and these results present limited strength. Moreover, higher doses of fasentin caused animal death. Inhibition of angiogenesis usually does not imply a lethal effect in the zebrafish model. Therefore, it could be possible that inhibition of GLUT transporters in these animals sensitizes them to other complications that finally lead them to death.

Even though the modest effect of fasentin *in vivo*, its capacity for disorganizing the vasculature in the CAM assay and the slight effect on the caudal fin regeneration assay should not be ignored.

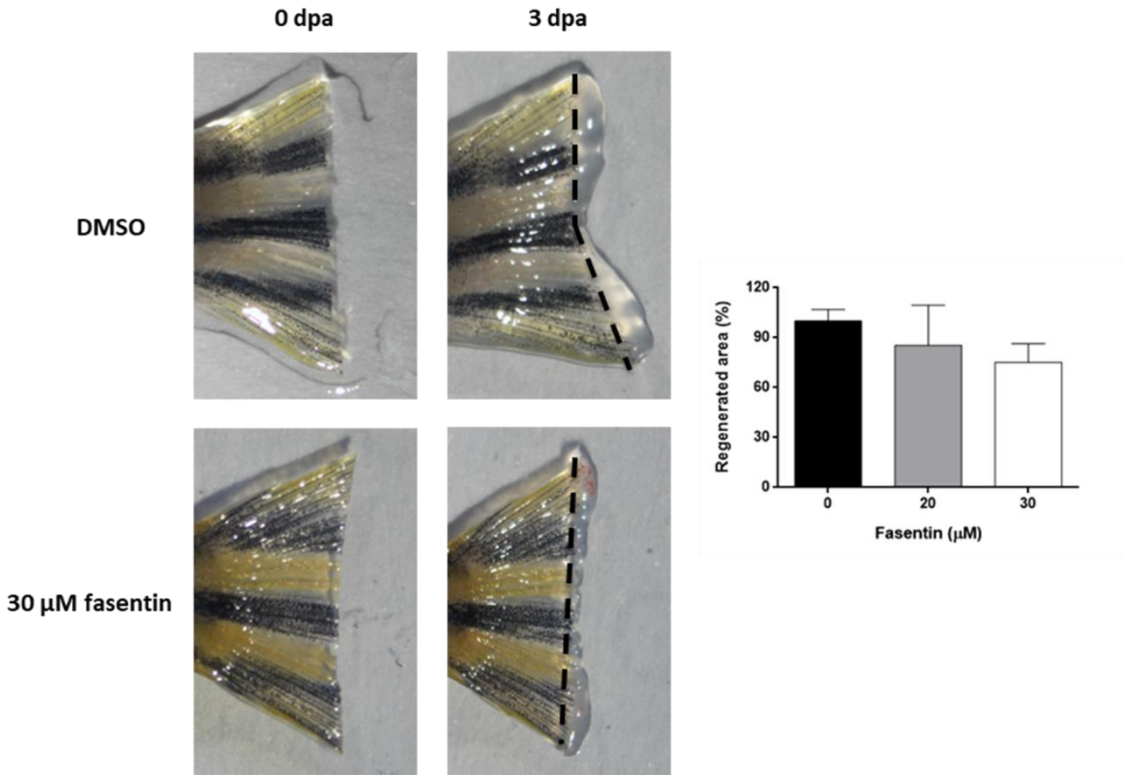

Figure 11. Representative photographs and quantification of caudal fin regeneration assay in WT adult zebrafish, in control condition (DMSO) or treated with 20 or 30 µM fasentin after 3 dpa. Data are means ± SD of n = 2 for each condition.

4. Effect of fasentin on the migratory and invasive capacity of endothelial cells

Apart from proliferation and differentiation of ECs, the angiogenic process comprises other important steps, such as migration and invasion.

In order to test the migratory capacity of ECs in the presence of fasentin, first the wound healing assay was performed. The results obtained show that fasentin does not have a significant effect on migration of HMECs (**Figure 12A**). However, this assay has several limitations, such as the interference of cell proliferation, which limits the experiment to shorter incubations. The addition of an agent that blocks proliferation, such as hydroxyurea or mitomycin, solves this problem[256]. This assay was performed at 4 and 7 h of treatment because cell doubling time is much higher than these times, and thus cell proliferation should not affect the results of this assay. In order to check the effect of fasentin for longer incubation times, a Boyden chamber assay was performed. Fasentin did not affect cell migration after 16 h incubation either (**Figure 12B**).

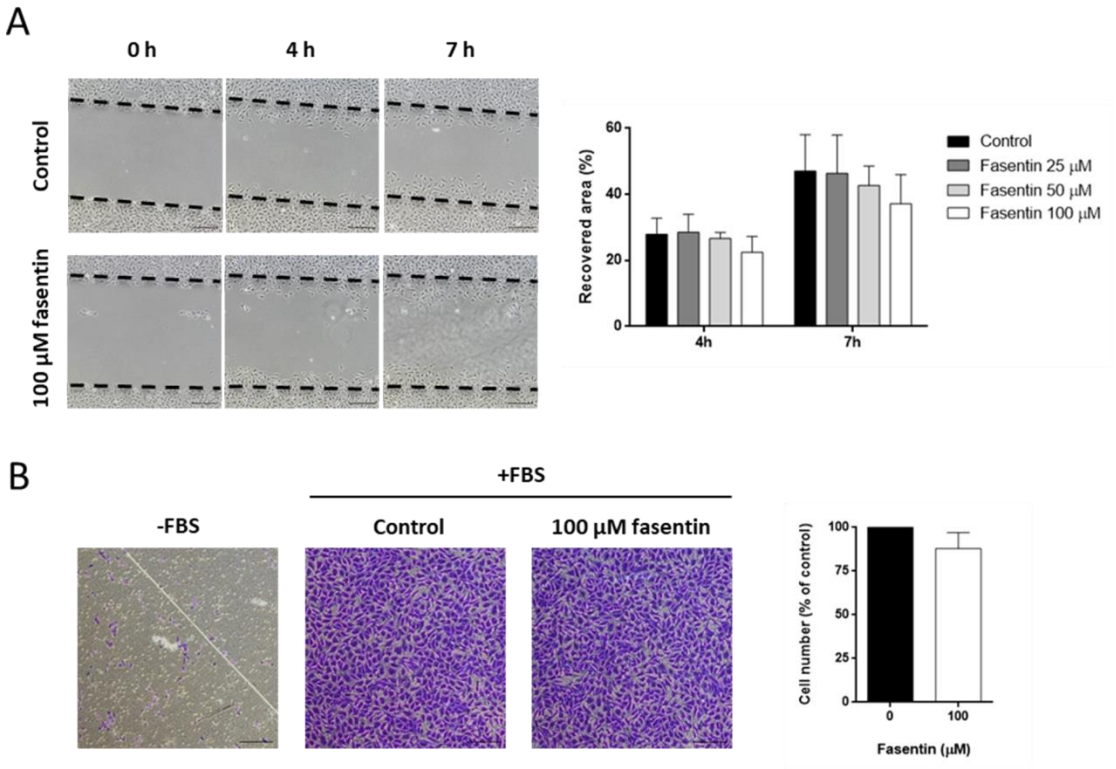

Figure 12. (A) Representative images and quantification of the recovered area in the wound healing assay of control and fasentin-treated HMECs. (B) Representative photographs and quantification of cell migration of control and fasentin-treated HMECs after 16 h incubation in a transwell insert coated with gelatin. FBS was added as chemoattractant to the lower wells. Bar scale = 200 µm. Data are expressed as means ± SD of three independent experiments.

ECs need to degrade their surrounding ECM in order to migrate. This remodeling of the ECM involves different proteases, such as MMP-2 and uPA. These proteases need to be secreted to the media to exert its activity. Secretion of MMP-2 was not affected by fasentin in HMECs (**Figure 13A**). However, 100 µM fasentin diminished the intracellular levels of MMP-2 (**Figure 13A**). Nevertheless, MMP-2 gene expression levels were unaffected by fasentin (**Figure 13B**). Moreover, this compound did not affect MMP-2 activity, as seen by an *in situ* gelatin zymographic assay (**Figure 13C**). Additionally, gene expression of the MMP-2 inhibitors TIMPs was not affected either by fasentin (**Figure 13D**). These results point out to a post-transcriptional regulation of MMP-2 exerted by fasentin rather than an effect on MMP-2 secretion or activity.

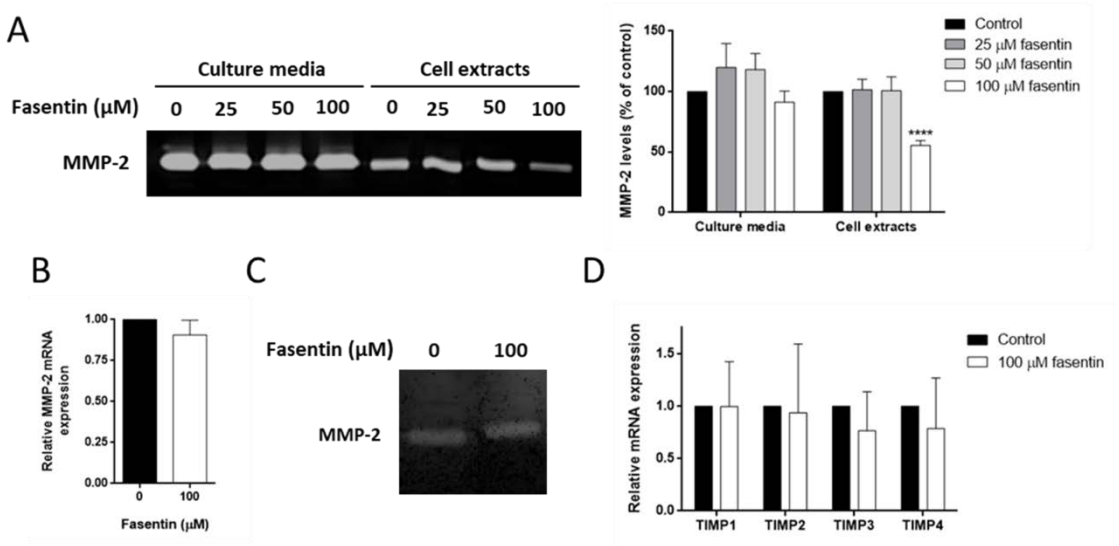

Figure 13. (A) Representative zymography and quantification of MMP-2 levels in culture media and cell extracts from HMECs treated or not with fasentin. (B) Relative MMP-2 gene expression in HMECs treated or not with 100 μM fasentin. (C) Representative zymography of MMP-2 activity in cell extracts from HMECs in the presence of fasentin. (D) Relative TIMPs gene expression in HMECs treated or not with 100 μM fasentin. Data from qPCR are normalized against β-actin expression. Data are expressed as means ± SD of three independent experiments. ****$p < 0.0001$ versus untreated control.

Furthermore, fasentin greatly diminished uPA levels in HMECs (**Figure 14**).

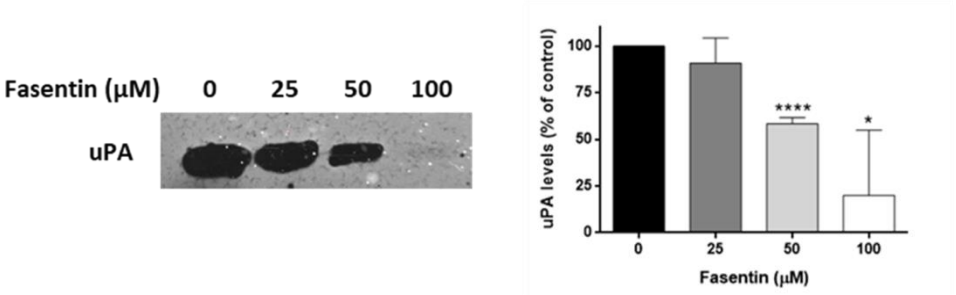

Figure 14. Representative zymography and quantification of uPA levels in cell extracts from HMECs treated or not with fasentin. Data are expressed as means ± SD of three independent experiments. *$p < 0.05$, ****$p < 0.0001$ versus untreated control.

According to these results, fasentin was seen to decrease cell invasion through Matrigel in a dose-dependent manner (**Figure 15**). However, the level of inhibition was greater than expected based on the decrease in MMP-2 and uPA levels. Therefore, these results suggest that additional molecules could be involved in the inhibition of EC invasion exerted by fasentin.

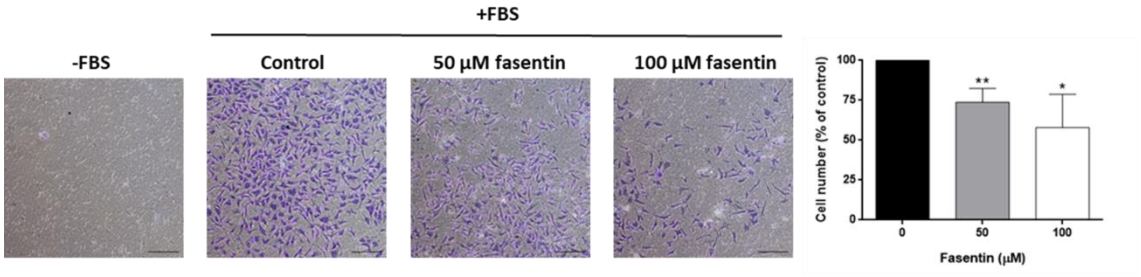

Figure 15. Representative photographs and quantification of cell invasion of control and fasentin-treated HMECs after 16 h incubation in a transwell insert coated with Matrigel. FBS was added as chemoattractant to the lower wells. Bar scale = 200 µm. Data are expressed as means ± SD of three independent experiments. *p < 0.05, **p < 0.01 versus untreated control.

5. Effect of fasentin on glucose uptake in endothelial cells

In this PhD Thesis, fasentin has been shown to present anti-angiogenic activity through inhibition of EC proliferation and invasion. This compound has been described as a GLUT1 and GLUT4 inhibitor in tumor cells[340]. However, fasentin just slightly diminished glucose uptake in HMECs at the maximum concentration used for the study of its anti-angiogenic activity, whereas no effect was found at 50 µM or lower doses (**Figure 16**).

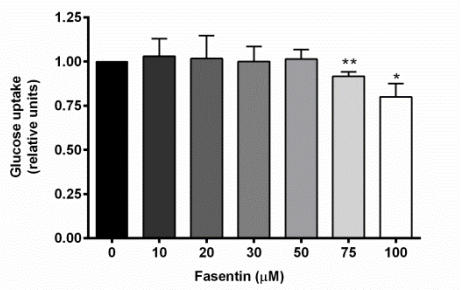

Figure 16. Relative glucose uptake in HMECs treated for 16 h with different doses of fasentin. Data are expressed as means ± SD of three independent experiments. *p < 0.05, **p < 0.01 versus untreated control.

This slight reduction in glucose uptake observed in HMECs was not expected due to the strong inhibitory activity reported for fasentin in bibliography. However, in HMECs GLUT1 is not the only glucose transporter expressed. GLUT14 was also found to be expressed in these cells (data from proteomic analysis of control cells), which could compensate for the partial inhibition of GLUT1 exerted by fasentin. Therefore, the anti-proliferative, anti-invasive and anti-angiogenic capacity of fasentin in ECs is most likely not related to an inhibition of glucose metabolism and no correlation between these apparently independent effects should be made.

6. Study of the mechanistic effect of fasentin on endothelial cells

The results found for glucose uptake in ECs treated with fasentin suggest that additional mechanisms are involved in the inhibition of EC proliferation, invasion and differentiation.

VEGFR2 is a tyrosine kinase receptor that plays a central role in angiogenesis. Upon ligand binding, VEGFR2 undergoes autophosphorylation and becomes activated. However, no significant effect was found for fasentin on the *in vitro* VEGFR2 tyrosine kinase activity (**Figure 17**). Therefore, the anti-angiogenic activity of fasentin is not related to an impairment of VEGFR2 activation.

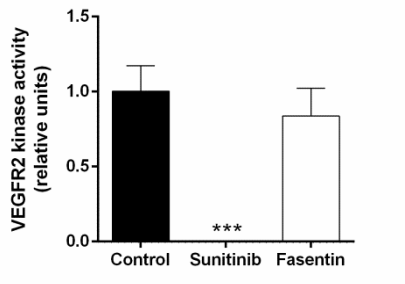

Figure 17. *In vitro* VEGFR2 kinase activity in the presence of 100 μM fasentin. 1 μM sunitinib was used as a positive control. Data are expressed as means ± SD of a unique experiment with triplicates.

Moreover, the angiogenesis triggering is regulated by a complex network of signaling pathways, which finally controls the response of ECs to pro-angiogenic stimulus. Two main pathways are closely related to angiogenesis: the ERK1/2 and the PI3K/Akt signaling pathways, which get active after phosphorylation of ERK and Akt proteins, respectively.

Fasentin slightly diminished ERK1/2 phosphorylation in HMECs at a concentration of 100 μM (**Figure 18**). However, since this decrease was rather small and lower doses of fasentin also affected cell proliferation and invasion, but did not inhibit the ERK1/2 signaling pathway, additional mechanisms are most likely involved in the modulatory activity of fasentin in ECs.

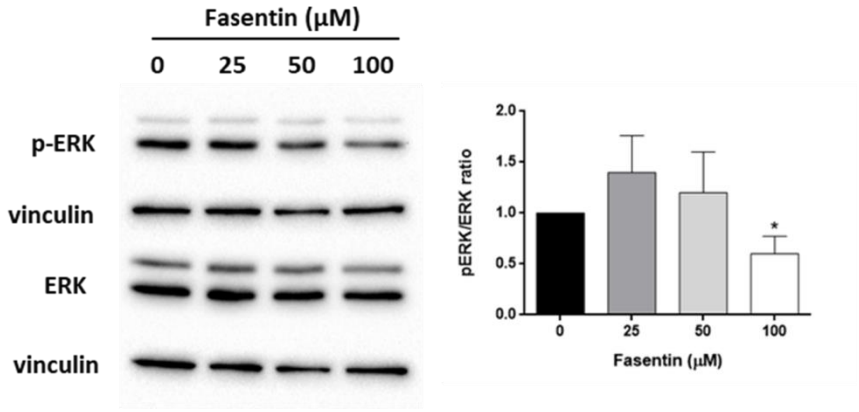

Figure 18. Representative blots and quantification of phosphorylated and total ERK1/2 in protein extracts from HMECs treated or not with fasentin for 16 h. Dara are normalized against vinculin expression and expressed as means ± SD of three independent experiments. *p < 0.05 versus untreated control.

The PI3K/Akt signaling pathway is also involved in the angiogenic function. Activation of Akt leads to EC proliferation and survival[348]. Unexpectedly, fasentin greatly increased the phosphorylated form of Akt in a dose-dependent way (**Figure 19**).

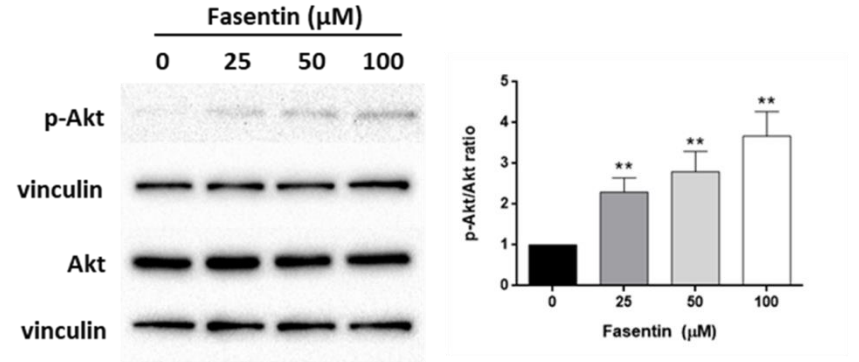

Figure 19. Representative blots and quantification of phosphorylated and total Akt in protein extracts from HMECs treated or not with fasentin for 16 h. Data are normalized against vinculin expression and expressed as means ± SD of three independent experiments. **p < 0.01 versus untreated control.

Several explanations for the upregulation of the Akt signaling pathway could be suggested. On the one hand, inhibition of cell proliferation usually leads to cell death, but fasentin decreases cell proliferation without compromising cell survival. The induction of Akt phosphorylation could protect cells from cell death in the presence of fasentin. Furthermore, this pathway is also known to be involved in the regulation of glucose metabolism. Among other effects, activation of Akt leads to an increase in GLUT1 expression[349,350]. Therefore, both the expression of GLUT14 in these cells and

the upregulation of the PI3K/Akt signaling pathway could explain the slight effect of fasentin on glucose uptake in HMECs. However, whether this activation of the PI3K/Akt signaling pathway compensates for the putative inhibition of GLUT1 activity in HMECs would require additional research.

7. Conclusions

The potential role of fasentin for the inhibition of angiogenesis was tested. The results obtained show a decrease in EC proliferation and invasion, as well as an inhibition of EC tube formation *in vitro*. In spite of several experimental impediments, most likely due to a systemic effect exerted by the compound, a slight yet consistent effect was found for the *in vivo* angiogenic modulation of fasentin. This anti-angiogenic activity was accompanied by a decrease in MMP-2 and uPA production and a slight decrease in activation of the ERK1/2 signaling pathway in ECs. However, this compound failed to diminish glucose uptake to a greater extent in ECs. This could be due to the upregulation of the PI3K/Akt signaling pathway and/or the expression of additional glucose transporters, such as GLUT14.

Two main conclusions could be drawn from the results shown herein: 1) Fasentin is a modest inhibitor of EC proliferation, invasion and tube formation; and 2) fasentin barely decreases glucose uptake in ECs and therefore the observed angiogenic modulatory capacity of fasentin is most likely independent of the inhibition of GLUT1.

CHAPTER 4

Studies on the potential capacity of dimethyl fumarate to modulate metabolism in endothelial cells

1. Dimethyl fumarate: a promising drug

Dimethyl fumarate (DMF) (**Figure 1**) is a methyl ester of fumaric acid. In 2013, this compound was approved by the FDA and the EMA for the treatment of relapsing forms of multiple sclerosis, marketed under the name Tecfidera (previously called BG-12). Its mechanism of action is considered to be the induction of the Nrf2 anti-oxidant pathway[351]. However, DMF has been shown to present anti-inflammatory and immunoregulatory effects in a Nrf2-independent way[352].

Additionally, a mixture of DMF (approximately 60% of the mixture) and different derivatives was officially registered in 1994 in Germany under the brand name Fumaderm and used as an anti-psoriatic drug for more than 50 years[353]. In 2017, the EMA approved a new oral formulation, under the name Skilarence, containing only DMF for the treatment of moderate-to-severe plaque psoriasis not only in Germany but in all Europe[354]. Psoriasis is an inflammatory disorder characterized by the permeation of lymphocytes in the skin, where they release several cytokines, inducing hyperplasia in keratinocytes and the consequent inflammation and skin lesion[355]. The usefulness of DMF in the treatment of psoriasis could be explained due to its anti-inflammatory activity through the inhibition of NF-κB activation[356,357]. However, psoriasis has been associated with an exacerbated angiogenesis[358]. Interestingly, DMF has been demonstrated to exert anti-angiogenic activity through inhibition of VEGFR2 without affecting its phosphorylation[69,359]. Nevertheless, several *in vitro*, *ex vivo* and *in vivo* studies have shown that inhibition of Nrf2 impairs several features of angiogenesis, but also that Nrf2 blocks VEGFR2 phosphorylation[360-362]. Therefore, a more complex regulation of the anti-angiogenic capacity of DMF, probably independent of its effects on the Nrf2 signaling pathway, cannot be discarded. Further studies on the DMF mechanisms of action should be carried out in order to elucidate the exact role of the angiogenesis inhibition in DMF activity[363].

DMF is a cell permeable fumaric acid ester that can be converted into fumarate inside the cell, thus feeding the TCA cycle. Additionally, besides its known role as an anti-oxidant transcriptional regulator, Nrf2 has also been shown to regulate metabolism related genes[364,365]. Moreover, EC energetic metabolism is essential for a proper EC function and hence for correct angiogenesis triggering. All these facts suggest that DMF could modulate energetic cell metabolism, especially in ECs. Interestingly, this compound has been found to inhibit glyceraldehyde 3-phosphate dehydrogenase (GAPDH) activity in macrophages[366]. Furthermore, diverse, cell- and dose-dependent

effects of DMF were found on global cell metabolism in different cell types, including T cells, retinal epithelial cells and fibroblasts[367-369]. However, the role of DMF in EC energetic metabolism has not been studied so far. Since glycolysis has been shown to be essential for proper EC function, these facts suggested that the anti-angiogenic activity of DMF could be partially exerted by modulation of EC metabolism, especially glycolysis[121]. Therefore, in this PhD Thesis the potential role of DMF in the energetic metabolism of human microvascular ECs has been studied.

Most of the results presented herein are part of a manuscript pending to be sent to publication in a scientific journal (**Appendix 7**).

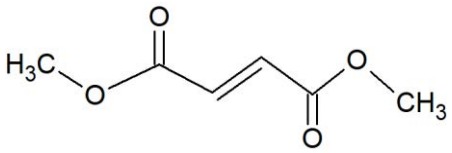

Figure 1. Chemical structure of dimethyl fumarate. This chemical structure was drawn using ChemSketch software.

2. Dimethyl fumarate inhibits tube formation in microvascular endothelial cells

The anti-angiogenic capacity of DMF has been tested *in vivo* and *in vitro* using macrovascular ECs[69,359]. However, its effect on microvascular ECs tube formation had not been demonstrated yet. In order to be able to establish a correlation between the possible effect of DMF on EC metabolism and angiogenesis, a tube formation assay on Matrigel was performed in HMECs. Consistent with the effect on macrovascular ECs, a total inhibition of morphogenesis on Matrigel by 50 and 100 μM DMF was found in microvascular ECs (**Figure 2**).

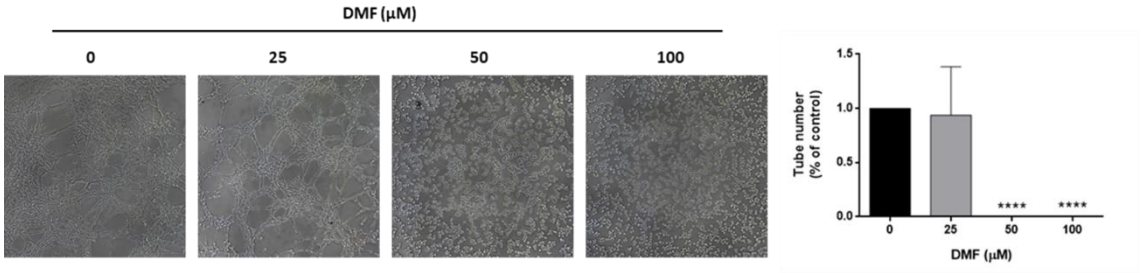

Figure 2. Representative photographs and quantitative analysis of "tubular" structures formed by control (untreated) and DMF-treated HMECs on Matrigel. Control cells formed tubes (left panel). 50 and 100 μM DMF completely inhibited HMECs alignment and cord formation. Cells were photographed 5 h after seeding and drug administration under an inverted microscope. Bar scale = 200 μm. Data are represented as means ± SD for three independent experiments with duplicates each. ****$p < 0.0001$ versus untreated control.

3. Effect of dimethyl fumarate on cell respiration and glycolysis

Next, the capacity of DMF to modulate global metabolism in HMECs was tested. For that purpose, OCR and ECAR, as estimators of OXPHOS and glycolysis, respectively, were measured using a Seahorse flux analyzer.

Cells incubated for 20 h with 50 µM DMF had lower maximal respiration and ATP production rates (**Figure 3A**), whereas their glycolytic rate was substantially increased (**Figure 3B**). This was surprising since DMF was found to inhibit glycolysis in macrophages through targeting of GAPDH activity[366]. However, this compound also increased the glycolytic rate while diminishing OCR in fibroblasts with intact Nrf2 expression[368]. Why DMF affects energetic metabolism differently in different cell types has yet to be answered.

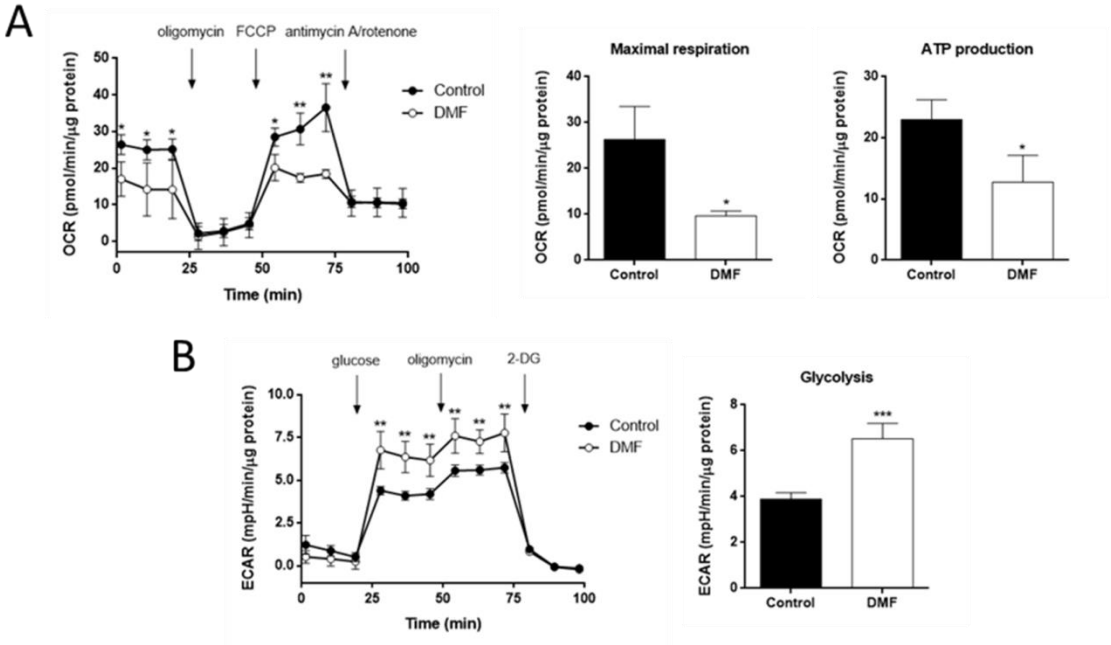

Figure 3. Flux analysis in HMECs. (A) Oxygen consumption rate (OCR), maximal respiration, ATP production, (B) extracellular acidification rate (ECAR) and glycolysis in HMECs in the presence or not of 50 µM DMF. Representative data of one experiment with triplicates are expressed as means ± SD, although three independent experiments were performed with similar results. *p < 0.05, **p < 0.01, ***p < 0.001 versus untreated control.

This increased glycolytic rate was correlated with an increased glucose uptake in HMECs. HMECs cultured overnight with several concentrations of DMF were then exposed to a 30 minutes fasting period in DPBS in the presence of DMF, followed by additional 30 minutes incubation in the presence of glucose and glutamine. Glucose taken up during those 30 minutes in the presence of DMF was measured. DMF

increased glucose uptake in HMECs in a dose-dependent manner (**Figure 4**). Since 100 μM DMF exerted a greater effect than 50 μM, 100 μM DMF were used for next experiments.

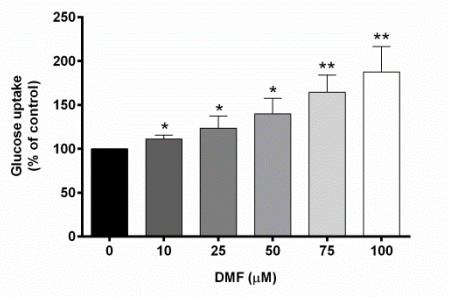

Figure 4. Glucose uptake after 30 min incubation with 5 mM glucose and 0.5 mM glutamine in HMECs treated or not with different concentrations of DMF for 16 h. Data are expressed as means ± SD of three independent experiments. *$p < 0.05$, **$p < 0.01$ versus untreated control.

In order to elucidate if a transcriptional regulation was necessary for DMF to exert this effect or whether its mere presence along with glucose was enough, glucose uptake in cells incubated with DMF overnight and in cells incubated with DMF only during the last 30 minutes incubation in the presence of glucose was studied. 100 μM DMF increased glucose uptake in HMECs after 30 minutes incubation to a lesser extent than after overnight incubation, yet the increase was statistically significant (**Table 1**). The effect of DMF on glucose uptake was also found in macrovascular ECs BAECs and HUVECs, although the increase after 30 minutes incubation was not statistically significant (**Table 1**). Moreover, the effect of DMF on glucose uptake was also tested on tumor cells and fibroblasts. 100 μM DMF, both after 30 minutes or after overnight incubation, increased glucose uptake in breast adenocarcinoma MDA-MB-231 and MCF7, cervix adenocarcinoma HeLa and HGF cell lines. In all these cells lines, except for HeLa, the effect after long time incubation was greater than when DMF was present only along glucose for 30 minutes (**Table 1**). These results suggest the need for a transcriptional regulation by DMF for boosting up glucose metabolism, although additional quicker mechanisms are most likely involved.

Interestingly, Nrf2 has been shown to modulate the glycolytic activity of ECs through transcriptional regulation of PFKFB3[370]. Whether the effect of DMF on glycolysis in HMECs is related to its known activation of the Nrf2 signaling pathway remains to be studied.

Table 1. Glucose uptake after 30 minutes incubation with 5 mM glucose and 0.5 mM glutamine in several cell lines treated with 100 µM DMF for 30 minutes or 16 h. Data are expressed as means ± SD of the percentage of glucose uptake of three different experiments. *p < 0.05 versus untreated control.

	30 min	16 h
HMEC	116.2 ± 4.2*	187.6 ± 29.1*
HUVEC	120.2 ± 13.6	159.5 ± 21.4*
BAEC	116.7 ± 12.7	166.6 ± 19.7*
MDA-MB-231	162.0 ± 28.2*	270.1 ± 52.8*
MCF7	140.3 ± 8.7*	198.1 ± 8.2*
HeLa	159.9 ± 11.2*	160.3 ± 3.3*
HGF	141.5 ± 20.5*	191.4 ± 12.7*

Since OCR was lower with DMF, and glutamine is mainly incorporated into the TCA and oxidized, the effect of 100 µM DMF on glutamine oxidation after overnight incubation was also studied. The same conditions as in glucose uptake experiments were used. 100 µM DMF halved glutamine oxidation in HMECs (**Figure 5**). A slight effect, yet not statistically significant, was found in HUVECs, whereas a significant effect was found in tumor MDA-MB-231 cells and no effect was found in HeLa cells (**Figure 5**). Since HeLa is a highly glutamine-dependent, oxidative cell line, it may be possible that DMF favors the glycolytic metabolism in highly glycolytic cell lines, while reduction in oxidative metabolism is not affected in cells with low glycolytic rates[150].

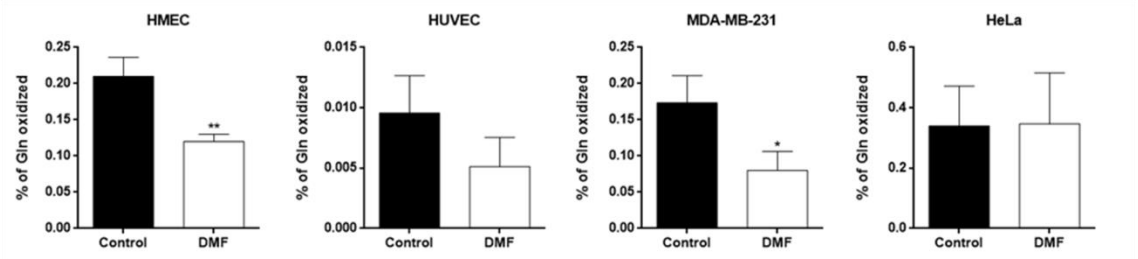

Figure 5. Glutamine oxidation after 30 minutes incubation with 5 mM glucose and 0.5 mM glutamine in HMECs, HUVECs, MDA-MB-231 and HeLa cells treated or not with 100 µM DMF for 16 h. Data are expressed as means ± SD of three independent experiments. *p < 0.05 versus untreated control.

All these experiments were performed in very restrictive conditions so that direct effects on the metabolic substrates of interest could be detected. In order to simulate a

condition more similar to the physiological one, glucose and glutamine uptake and lactate production, as well as glutamate and ammonia secretion derived from GLS activity, were measured in HMECs after overnight or 24 h incubation in the presence of 100 µM DMF in complete medium. Results were similar after 16 and 24 h, and hence 24 h incubation was preferred for next experiments. Either way, glucose uptake and lactate secretion were greater with DMF (**Figures 6A and 6B**). In contrast, glutamine uptake was lower in cells cultured with DMF, whereas glutamate secretion to the medium was slightly higher (**Figures 6C and 6D**). No differences in ammonia production were found (**Figures 6C and 6D**). Moreover, hexoses intracellular levels, including glucose, were higher in HMECs treated with DMF for 16 h, as shown by the results obtained with the AbsoluteIDQ p180 kit (Biocrates) (**Figure 7** and **Appendix 10**). These results reinforce the enhanced glycolytic induction exerted by DMF in ECs.

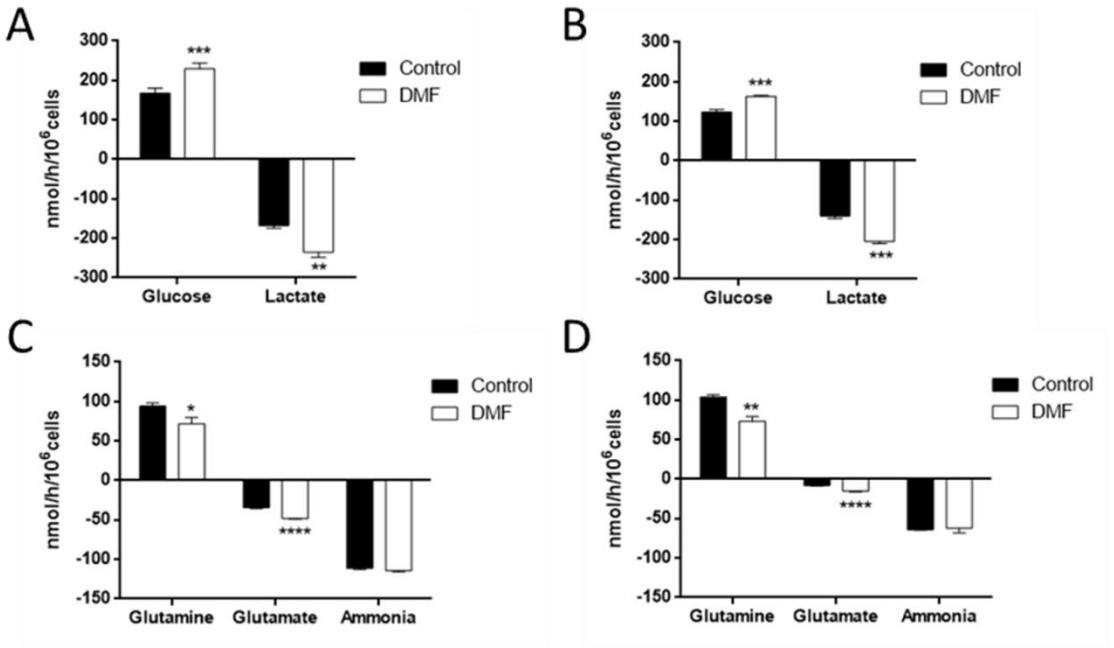

Figure 6. (A) Glucose uptake and lactate secretion in HMECs treated with 100 µM DMF for 16 h or (B) 24 h in medium with 10 mM glucose and 4 mM glutamine. (C) Glutamine uptake and glutamate and ammonia secretion in cells treated with 100 µM DMF for 16 h or (D) 24 h in medium with 10 mM glucose and 4 mM glutamine. Representative data of one experiment with triplicates are expressed as means ± SD, although at least three independent experiments were performed with similar results. *$p < 0.05$, **$p < 0.01$, ***$p < 0.001$, ****$p < 0.0001$ versus untreated control.

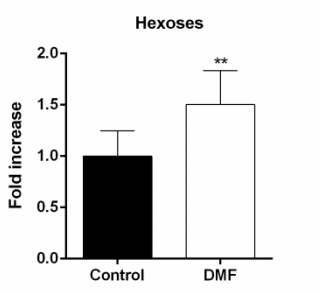

Figure 7. Intracellular hexoses levels in HMECs treated or not with 100 μM DMF for 16 h. Data are expressed as means ± SD of three independent experiments with triplicates. **p < 0.01 versus untreated control.

4. Dimethyl fumarate upregulates GLUT1 expression without affecting HIF-1α

Due to the greater effect of DMF on glucose uptake after longer incubation, this compound might modulate glucose and/or glutamine metabolism through modulation of gene and/or protein expression. To test this premise, a quantitative proteomics analysis was performed in samples from HMECs treated with 100 μM DMF for 24 h. An upregulation on protein expression was considered when at least a 1.5 fold increase in the abundance ratio (DMF/DMSO) was found and a downregulation on those proteins with a 0.75 fold or lower expression in the abundance ratio (DMF/DMSO). A total of 2302 proteins were identified with a high confidence level and at least two peptides detected. Of those, 465 presented a ≥1.5 fold increase and 77 a ≤0.75 fold expression. However, only those changes with a p-value lower than 0.01 were considered to be statistically significant, thus selecting 37 upregulated proteins and 31 downregulated with DMF (**Figure 8** and **Appendices 8 and 9**). Among the upregulated proteins, glucose transporters GLUT1 and GLUT14 expressions were found to be 3.72 fold and 4.06 fold compared to the control condition, respectively (see **Appendix 8**). The MS proteomics data were deposited to the ProteomeXchange Consortium via the PRIDE partner repository with the dataset identifier PXD014489[371].

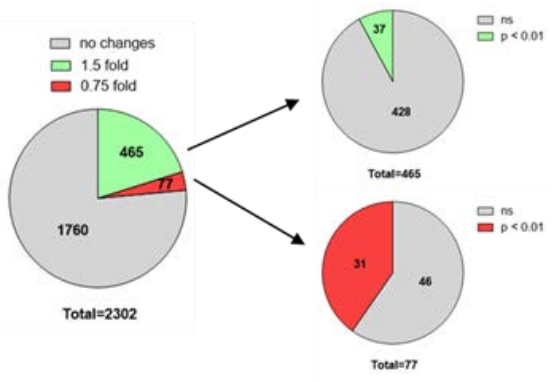

Figure 8. Results from a proteomics analysis of HMECs treated with 100 μM DMF for 24 h.

The upregulation of GLUT1 was also found at the transcriptional level. 100 μM DMF increased GLUT1 mRNA expression in HMECs (**Figure 9A**). Since GLUT1 is under the transcriptional control of HIF-1α, and DMF was shown to stabilize HIF-1α in human embryonic kidney cells, HIF-1α protein levels were checked in HMECs treated with DMF[372]. However, no HIF-1α was detected in normoxia with DMF (**Figure 9B**). Thus, this increase in GLUT1 expression is not likely the consequence of a stabilization of HIF-1α in normoxia in the presence of DMF.

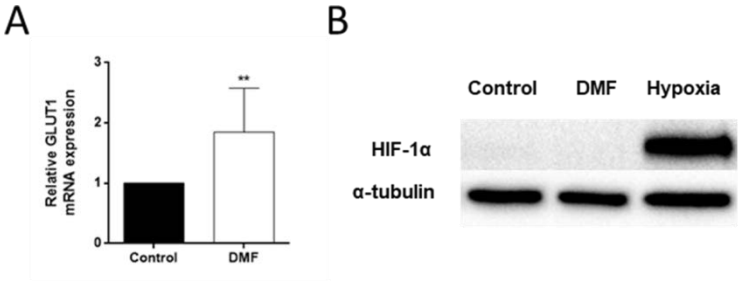

Figure 9. (A) GLUT1 mRNA expression in HMECs treated or not with 100 μM DMF for 24 h. (B) Representative Western blot for HIF-1α protein expression in HMECs treated or not with 100 μM DMF for 24 h. Hypoxia (1% O_2) was used as positive control. Data from qPCR are normalized against β-actin expression, whereas data from Western blot are normalized against α-tubulin expression. Data are expressed as means ± SD of at least three different experiments. **$p < 0.01$ versus untreated control.

5. Dimethyl fumarate affects aspartate and TCA cycle intermediates levels

In order to study the possible changes in the intracellular pool of several metabolites as a consequence of the deregulated glycolytic and oxidative metabolism in DMF treated cells, a steady-state metabolite experiment in complete medium was performed. The most consistent changes repeated in independent experiments are collected in a heatmap elaborated using Heatmapper (**Figure 10**)[373].

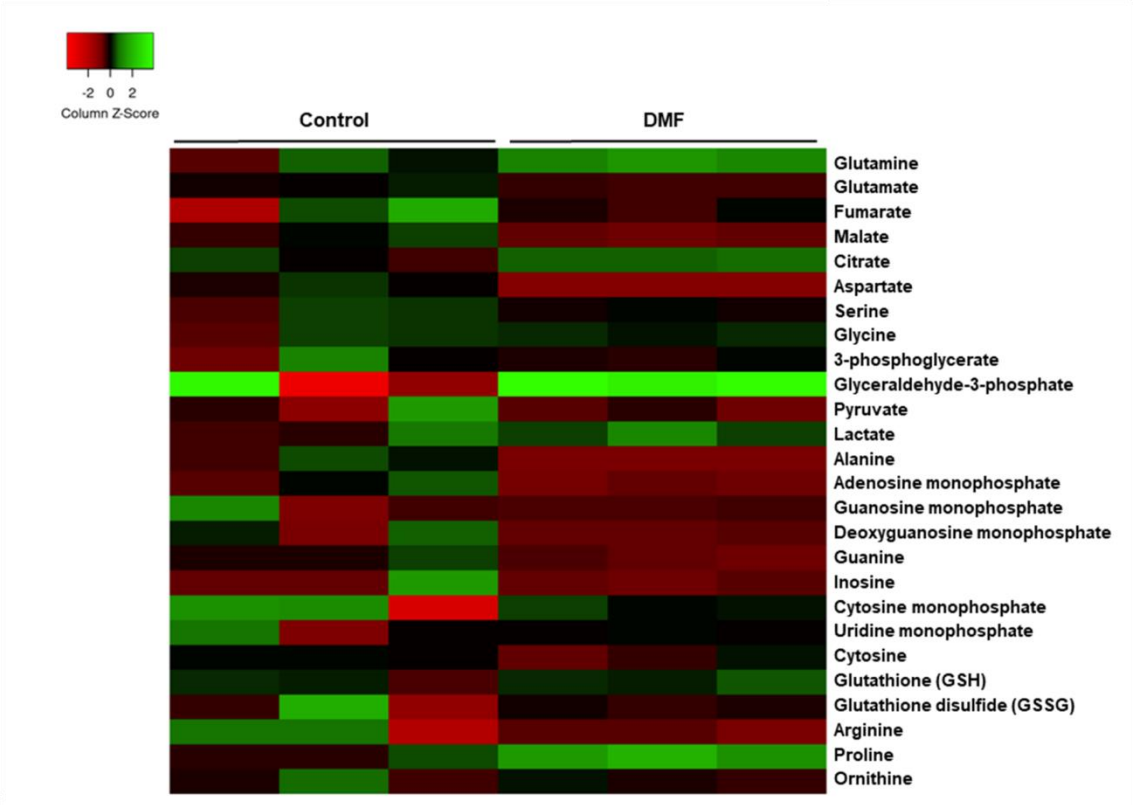

Figure 10. Heatmap of intracellular metabolite levels in HMECs treated or not with 100 µM DMF for 24 h. Representative data of one experiment are expressed as fold from the control condition, although at least three independent experiments were performed with similar results.

Among these changes, aspartate levels were drastically lower in DMF treated HMECs (**Figure 11A**). Of note, aspartate is absent in DMEM formulation, which was used for these experiments, and hence cells need to synthetize it. However, this experiment was also performed in RPMI-1640 medium, which contains aspartate. Aspartate levels in DMF treated cells in this aspartate-containing medium were also lower, but to a lesser extent (**Figure 11B**). Additionally, by means of the AbsoluteIDQ p180 kit (Biocrates) lower intracellular levels of aspartate were also found in HMECs treated with 100 µM DMF for 16 h in MCDB-131 medium, which also contains aspartate in its formulation (**Figure 11C** and **Appendix 10**).

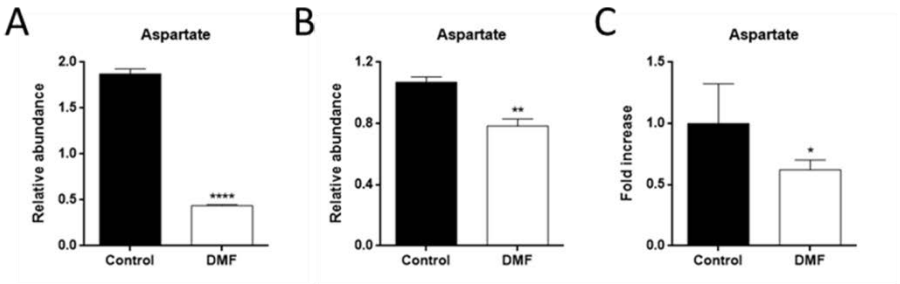

Figure 11. (A) Intracellular aspartate levels in HMECs treated with 100 μM DMF for 24 h in DMEM or in (B) RPMI-1640 medium, or (C) for 16 h in MCDB-131 medium. Data are expressed as means ± SD of a unique experiment with triplicates (A-B) or of three independent experiments with triplicates (C). *p < 0.05, **p < 0.01, **** p < 0.0001 versus untreated control.

Aspartate is essential for proliferating cells, and its synthesis is regulated by the ETC activity[316,317]. Accordingly, a lower respiration rate and a diminished glutamine oxidation were found in HMECs after DMF treatment. For that reason, stable isotope-labeling studies using glucose and glutamine labeled with carbon-13 in their six carbons ([U-^{13}C]-glucose and [U-^{13}C]-glutamine) were performed in order to follow the labeling of the TCA intermediates (**Figure 12**).

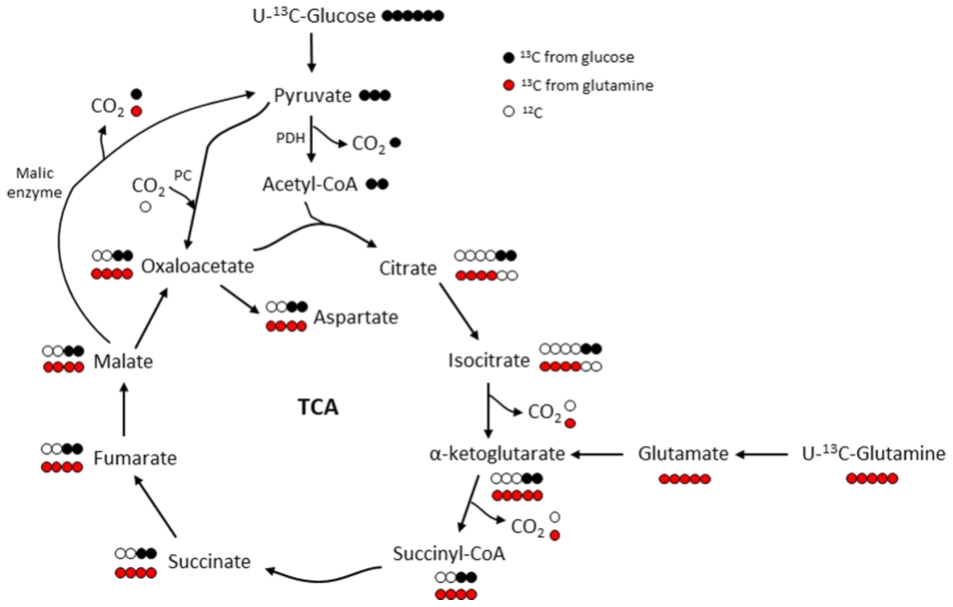

Figure 12. Scheme of the TCA cycle illustrating labeling from [U-^{13}C]-glucose or from [U-^{13}C]-glutamine. PC: pyruvate carboxylase; PDH: pyruvate dehydrogenase.

As expected, labeling of aspartate, glutamate, fumarate, malate and citrate from glutamine was lower in DMF treated cells (**Figure 13**), corroborating a lower incorporation into the TCA cycle.

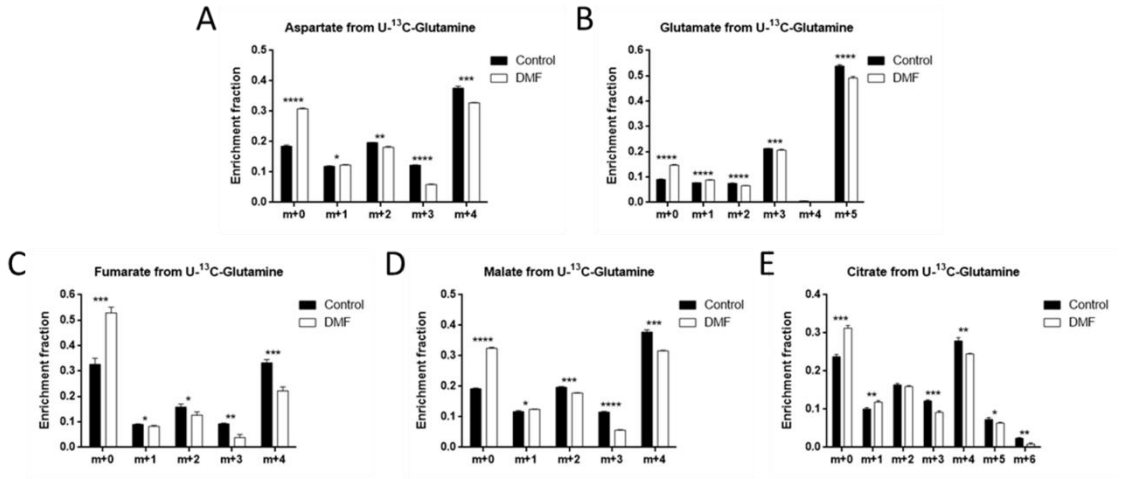

Figure 13. (A) Fractional labeling of aspartate, (B) glutamate, (C) fumarate, (D) malate and (E) citrate from [U-^{13}C]-glutamine in HMECs treated with 100 μM DMF for 24 h. Representative data of one experiment with triplicates are expressed as means ± SD, although at least two independent experiments were performed with similar results. *p < 0.05, **p < 0.01, ***p < 0.001, ****p < 0.0001 versus untreated control.

Nevertheless, labeling of aspartate, malate and citrate from glucose were higher in cells treated with DMF (**Figure 14**). These results suggest that DMF could induce an increase in the metabolism of glucose opposite to a reduction in glutamine metabolism.

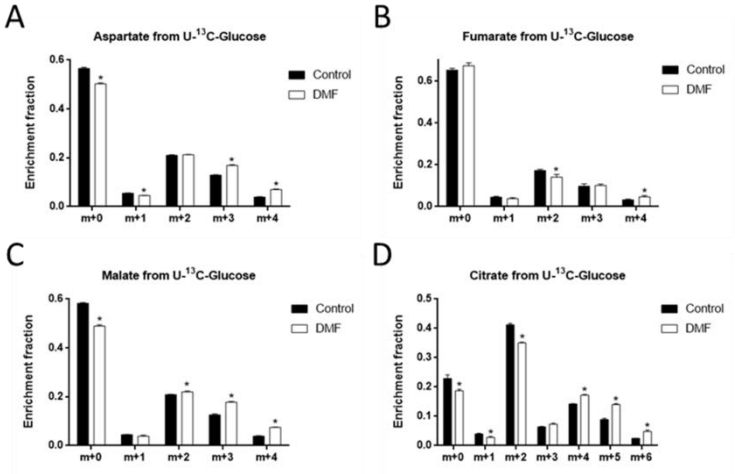

Figure 14. (A) Fractional labeling of aspartate, (B) fumarate, (C) malate and (D) citrate from [U-^{13}C]-glucose in HMECs treated with 100 μM DMF for 24 h. Representative data of one experiment with triplicates are expressed as means ± SD, although at least two independent experiments were performed with similar results. *p < 0.05 versus untreated control.

According to the labeling results, which pointed out to an inhibition of the flux of glutamine into the TCA cycle, lower intracellular levels of glutamate and malate were found in cells treated with DMF. The fumarate pool was not affected, probably due to the external addition of fumarate from DMF. However, citrate levels were increased after DMF treatment, which may contribute to the inhibition of the TCA cycle (**Figure 15**).

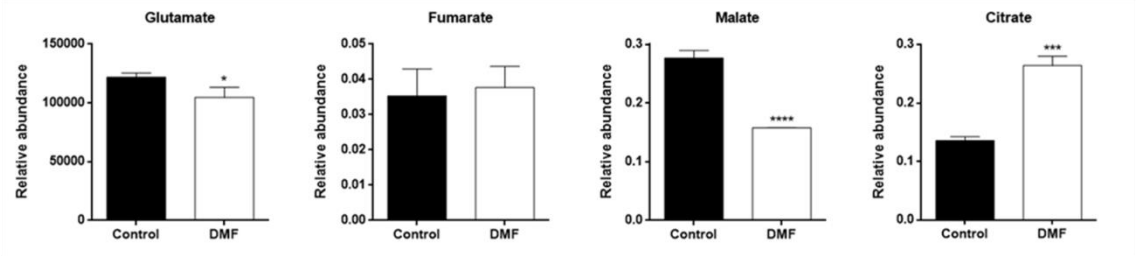

Figure 15. Intracellular levels of glutamate, fumarate, malate and citrate in HMECs treated with 100 µM DMF for 24 h Representative data of one experiment with triplicates are expressed as means ± SD, although at least three independent experiments were performed with similar results. *p < 0.05, ***p < 0.001, **** p < 0.0001 versus untreated control.

6. Dimethyl fumarate decreases serine and glycine synthesis in HMECs

Interestingly, by means of the steady-state metabolite experiment, higher levels of intracellular glycine were found in DMF treated cells, whereas serine levels were not significantly affected (**Figure 16**).

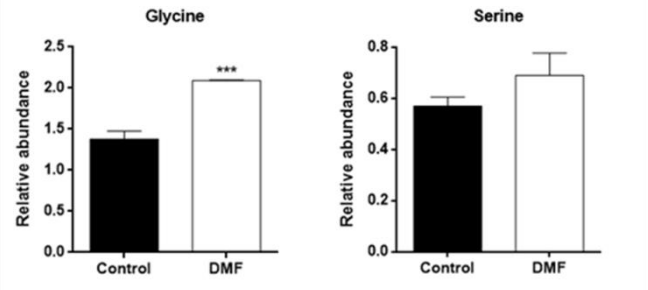

Figure 16. Intracellular levels of glycine and serine in HMECs treated with 100 µM DMF for 24 h. Representative data of one experiment with triplicates are expressed as means ± SD, although at least three independent experiments were performed with similar results. ***p < 0.001 versus untreated control.

Similar results were obtained from HMECs treated with 100 µM DMF overnight or with 50 µM DMF for 24 h (**Figure 17**).

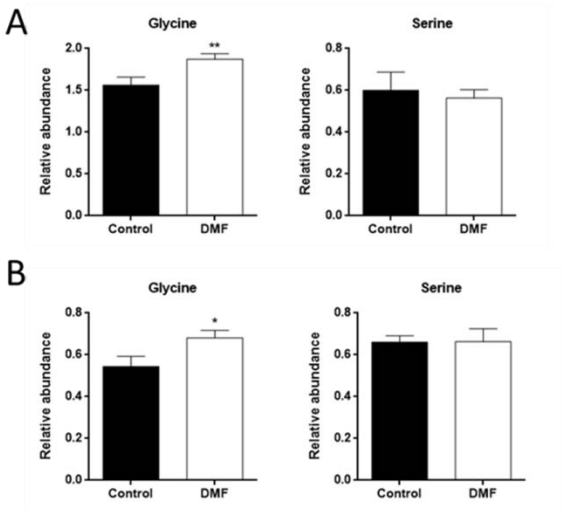

Figure 17. (A) Intracellular levels of glycine and serine in HMECs treated with 100 μM DMF for 16 h or (B) with 50 μM DMF for 24 h. Data are expressed as means ± SD of a unique experiment with triplicates. *p < 0.05, **p < 0.01 versus untreated control.

In addition, the proteomic analysis revealed a 4.5 fold expression of PSPH, the third and last enzyme in the serine synthesis pathway (see **Appendix 8**). A stable isotope-labeling study using glucose labeled with carbon-13 in its six carbons ([U-^{13}C]-glucose) was performed in order to check whether DMF boosted serine and glycine synthesis in HMECs (**Figure 18**).

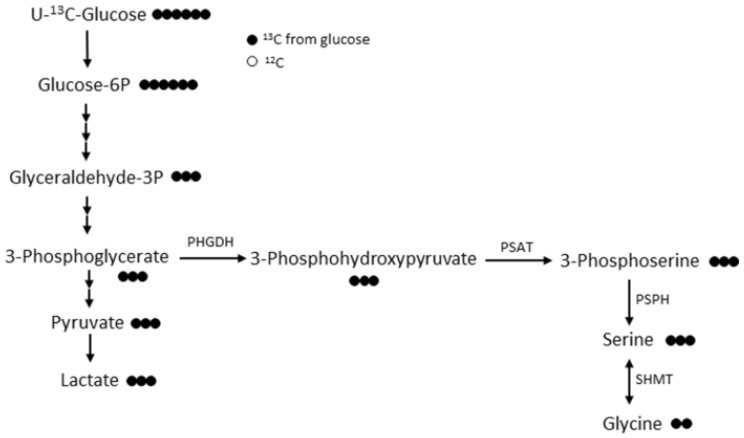

Figure 18. Scheme of glycolysis and the serine and glycine synthesis pathway illustrating labeling from [U-^{13}C]-glucose.

Surprisingly, not only serine m+3 from glucose was lower after 24 h incubation with 100 μM DMF (**Figure 19A**), but an even greater decrease in glycine m+2 was detected (**Figure 19B**). No changes in 3-PG m+3 labeling or intracellular levels were found (**Figures 19C and 19D**), which could have been expected due to the higher glycolytic

activity in DMF-treated cells. Similar effects were found in HMECs treated with 100 μM DMF overnight or with 50 μM DMF for 24 h (**Figures 20 and 21**, respectively).

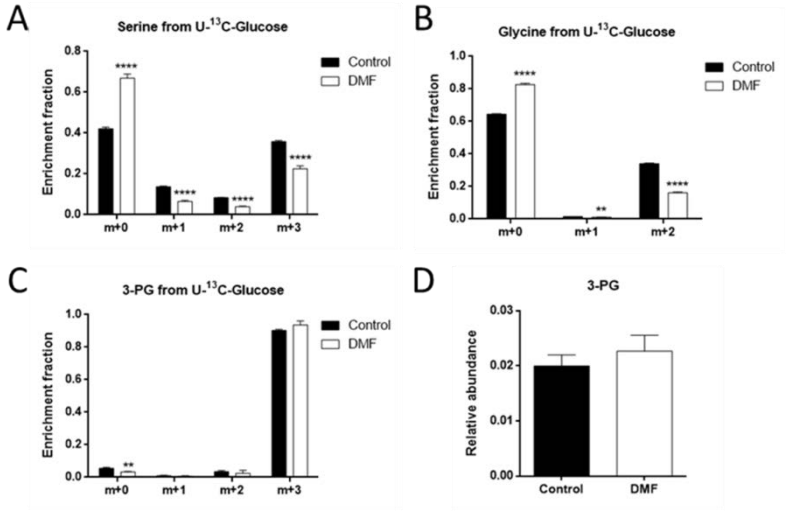

Figure 19. (A) Fractional labeling of serine, (B) glycine and (C) 3-PG from [U-^{13}C]-glucose in HMECs treated with 100 μM DMF for 24 h. (D) Intracellular levels of 3-PG in HMECs treated with 100 μM DMF for 24 h. Representative data of one experiment with triplicates are expressed as means ± SD, although at least two independent experiments were performed with similar results. **p < 0.01, ****p < 0.0001 versus untreated control.

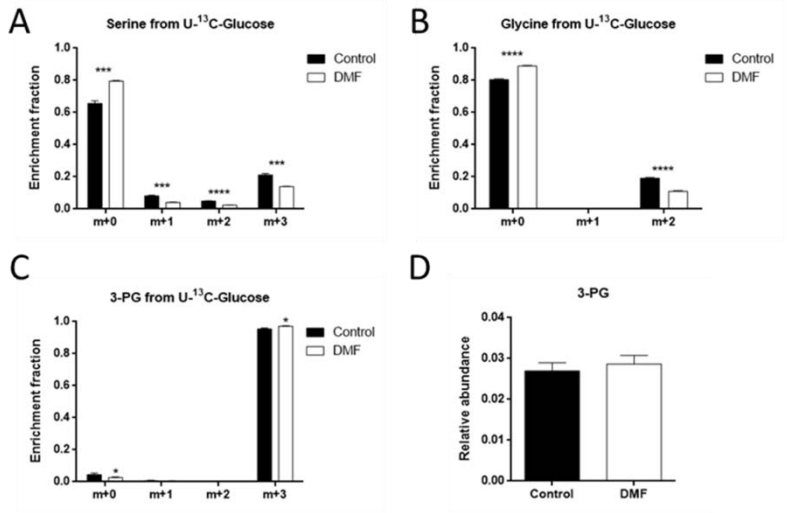

Figure 20. (A) Fractional labeling of serine, (B) glycine and (C) 3-PG from [U-^{13}C]-glucose in HMECs treated with 100 μM DMF for 16 h. (D) Intracellular levels of 3-PG in HMECs treated with 100 μM DMF for 16 h. Data are expressed as means ± SD of a unique experiment with triplicates. *p < 0.05, ***p < 0.001, ****p < 0.0001 versus untreated control.

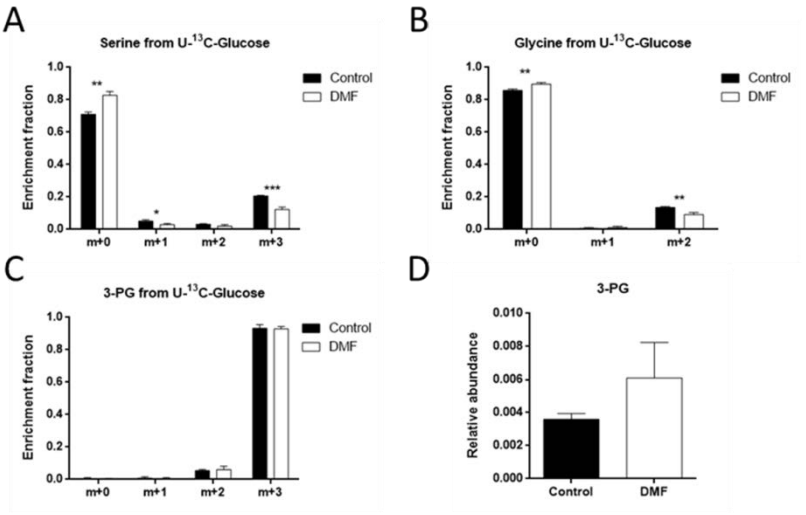

Figure 21. (A) Fractional labeling of serine, (B) glycine and (C) 3-PG from [U-^{13}C]-glucose in HMECs treated with 50 μM DMF for 24 h. (D) Intracellular levels of 3-PG in HMECs treated with 50 μM DMF for 24 h. Data are expressed as means ± SD of a unique experiment with triplicates. *p < 0.05, **p < 0.01, ***p < 0.001 versus untreated control.

6.1. Dimethyl fumarate diminishes PHGDH activity in HMECs

PHGDH is the rate-limiting step in the serine synthesis pathway in cell culture conditions. PHGDH protein levels were not significantly changed in the DMF treatment as seen by means of the proteomics analysis. Western blot corroborated that PHGDH protein levels were unaffected by DMF treatment in HMECs (**Figure 22**).

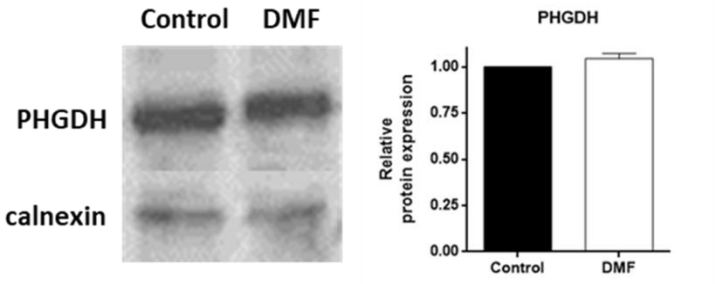

Figure 22. Representative Western blot and quantification of PHGDH protein expression in HMECs treated or not with 100 μM DMF for 24 h. Data are normalized against calnexin expression and expressed as means ± SD of three different experiments.

These results point out to the possible modulation of enzymatic activity exerted by DMF. Accordingly, 100 μM DMF diminished PHGDH activity in HMECs to similar levels to the decrease in serine m+3 labeling from glucose. Nevertheless, addition of DMF *in vitro* to control HMEC extracts did not have any effect on PHGDH activity (**Figure 23**). Some cellular mechanism seems thus to be involved in the regulation of

PHGDH activity. Therefore, even if PSPH protein levels are higher with DMF, a lower PHGDH activity is most likely limiting the serine and glycine synthesis rate in HMECs.

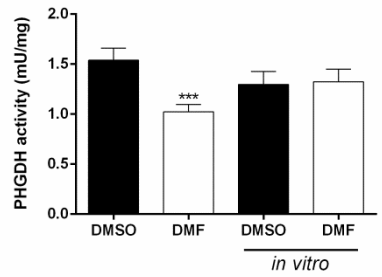

Figure 23. PHGDH activity in HMECs treated or not with 100 µM DMF for 24 h. The *in vitro* results show PHGDH activity in extracts from control HMECs after addition of DMSO or 100 µM DMF just before the assay. Data are expressed as means ± SD of four independent experiments. ***$p < 0.001$ versus untreated control.

The serine synthesis pathway has been described to be essential for the progression of several types of tumors, and the development of PHGDH inhibitors has emerged as a promising cancer therapy[374]. Interestingly, about the same time that these experimental results pointed out to the inhibition of serine synthesis by DMF, the role of PHGDH in EC metabolism and angiogenesis was published. In that work, PHGDH silencing impaired angiogenesis through inhibition of *de novo* purine, pyrimidine and heme synthesis, which also caused mitochondrial respiration defects[119]. This seems to reinforce the possibility that PHGDH inhibition by DMF triggers an increased glycolytic rate in an indirect manner. Nevertheless, an increased glucose uptake was found in several cell lines treated with DMF, including MDA-MB-231, a triple negative breast cancer cell line which lacks PHGDH[375]. Therefore, an additional mechanism must regulate the increase in the glycolytic rate exerted by DMF.

Nrf2 has been shown to induce protein expression of genes from the serine and glycine synthesis pathway, including PHGDH, through ATF4 in cancer cells[376]. Thus, the induction of Nrf2 activation mediated by DMF is not likely related to the modulation of PHGDH activity. Several studies regarding the transcriptional regulation of PHGDH by molecules affected by DMF, such as p53 and GAPDH, have been reported[377,378]. Nevertheless, DMF was able to diminish PHGDH activity without affecting its protein levels.

By extensive search in the available bibliography, two possibilities for the role of DMF in modulation of PHGDH activity arose. On the one hand, PHGDH is known to

be inhibited by phosphorylation mediated by protein kinase C zeta (PKCζ), and silencing this protein kinase decreases glucose uptake and lactate production in colorectal carcinoma, whereas it increases glutamine metabolism[379]. A possible scenario where DMF increases PKCζ expression, thus promoting PHGDH phosphorylation and inactivation should not be discarded. If changes in glucose and glutamine metabolism are an additional effect of PKCζ silencing and not a consequence of PHGDH inhibition, this could explain why DMF favors glycolysis against glutamine metabolism in cells not expressing PHGDH. Furthermore, DMF is known to be an electrophilic molecule able to bind to protein cysteine residues in a process called succination, hence modifying their activity[380]. Indeed, inhibition of Keap1 and GAPDH has been demonstrated to be due to cysteine succination[366,381]. Interestingly, a global analysis of cysteine ligandability performed in cancer cells revealed that Cys369 of PHGDH can react with electrophilic small molecules[382]. Whether DMF binds to and modifies Cys369 of PHGDH, thus decreasing its activity, remains unstudied. However, the results obtained in this PhD Thesis suggest that some cellular process is involved in the regulation of PHGDH activity mediated by DMF.

6.2. Effect of extracellular serine and glycine deprivation on serine and glycine metabolism in HMECs

All these experiments were carried out in media containing both serine and glycine in their formulation. For that reason, the experiments were repeated using media without serine and glycine.

Serine and glycine withdrawal did not affect glucose uptake or lactate production in either control or DMF treated cells compared to conditions with extracellular serine and glycine (**Figure 24**).

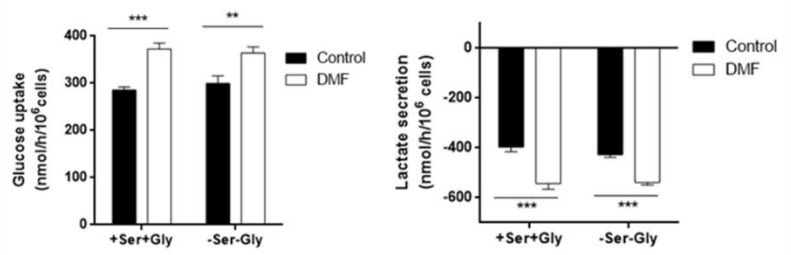

Figure 24. Glucose uptake and lactate secretion in HMECs treated with 100 μM DMF for 24 h in media with 10 mM glucose and 4 mM glutamine and containing or not serine and glycine. Data are expressed as means ± SD of a unique experiment with triplicates. **p < 0.01, ***p < 0.001.

Regarding serine and glycine synthesis from glucose, serine m+3 was higher in control and DMF treated cells incubated in the absence of both serine and glycine (**Figure 25A**), indicating the need for serine synthesis when no extracellular serine is available. Serine pools were higher in DMF treated cells when serine and glycine were present in the medium, whereas serine levels were low in serine and glycine depleted medium in both conditions (**Figure 25B**).

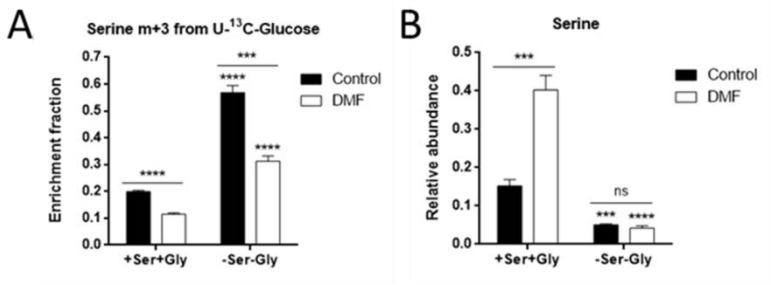

Figure 25. (A) Fractional labeling of serine from [U-^{13}C]-glucose and (B) intracellular serine levels in HMECs treated with 100 μM DMF for 24 h in the presence or absence of extracellular serine and glycine. Data are expressed as means ± SD of a unique experiment with triplicates. ***p < 0.001, ****p < 0.0001 versus condition with extracellular serine and glycine. ns: no significant.

Glycine m+2 was also higher in control cells when no extracellular serine and glycine was available (**Figure 26A**). However, DMF treated cells failed to increase glycine m+2 labeling from glucose in the absence of these two amino acids to the same extent as they did with serine (**Figure 26A**). Furthermore, intracellular glycine levels were increased in DMF treated cells when there was serine and glycine in the medium, but the glycine pool was almost totally depleted during serine and glycine withdrawal (**Figure 26B**).

No remarkable changes were found in either 3-PG labeling or intracellular pool between control and DMF treated cells in conditions with or without extracellular serine and glycine (**Figure 27**).

These data point out to a greater effect on glycine synthesis by DMF due to PHGDH inhibition. Additionally, it not only confirms the effect of DMF on serine and glycine synthesis, but it also indicates the need of extracellular serine and glycine to support the maintenance of intracellular levels of these two amino acids even when the serine synthesis pathway is intact.

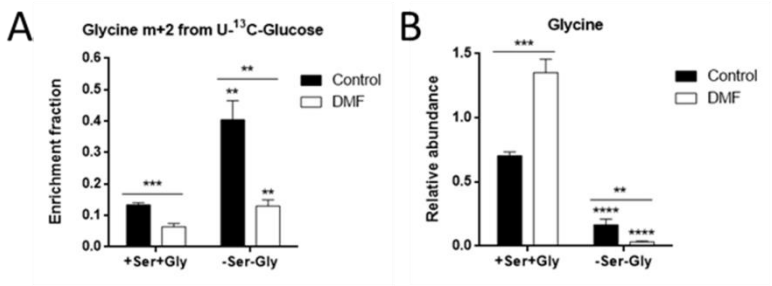

Figure 26. (A) Fractional labeling of glycine from [U-^{13}C]-glucose and (B) intracellular glycine levels in HMECs treated with 100 μM DMF for 24 h in the presence or absence of extracellular serine and glycine. Data are expressed as means ± SD of a unique experiment with triplicates. **p < 0.01, ***p < 0.001, ****p < 0.0001 versus condition with extracellular serine and glycine.

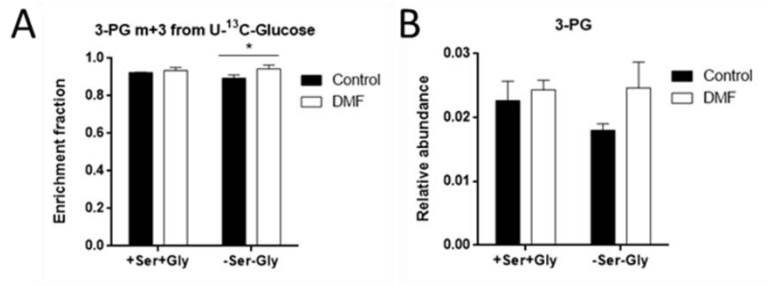

Figure 27. (A) Fractional labeling of 3-PG from [U-^{13}C]-glucose and (B) intracellular 3-PG levels in HMECs treated with 100 μM DMF for 24 h in the presence or absence of extracellular serine and glycine. Data are expressed as means ± SD of a unique experiment with triplicates. *p < 0.05.

In order to corroborate whether cells with a compromised serine and glycine synthesis pathway take up greater amounts of extracellular serine and glycine, stable isotope-labeling studies using serine or glycine labeled with carbon-13 in their six carbons ([U-^{13}C]-serine or [U-^{13}C]-glycine) were performed. Extracellular glycine was absent in medium supplemented with labeled serine, whereas serine was no added to the medium with labeled glycine in order to avoid interferences, since these two amino acids can be converted into each other through SHMT activity (**Figure 28**).

As expected, cells treated with 100 μM DMF incorporated more extracellular serine, as indicated by a higher serine m+3 labeling from labeled serine (**Figure 29**, left panel). Glycine m+2, which comes from this extracellular serine, was also higher with DMF, but to a lesser extent (**Figure 29**, right panel).

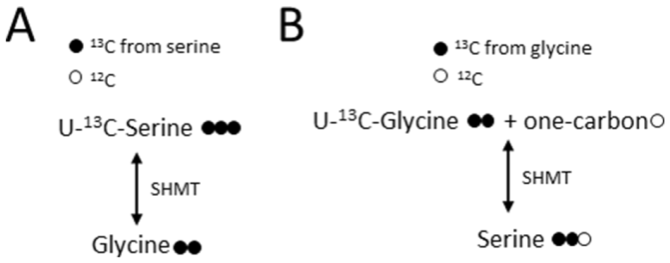

Figure 28. (A) Scheme of serine and glycine interconversion illustrating labeling from [U-^{13}C]-serine or (B) from [U-^{13}C]-glycine.

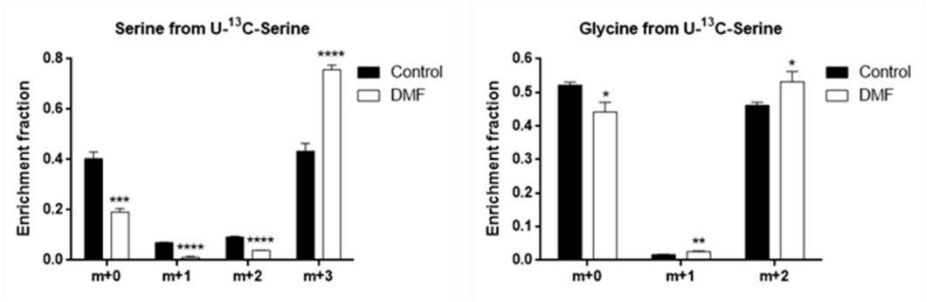

Figure 29. Fractional labeling of serine and glycine from [U-^{13}C]-serine in HMECs treated with 100 µM DMF for 24 h in the absence of extracellular glycine. Data are expressed as means ± SD of a unique experiment with triplicates. *p < 0.05, **p < 0.01, ***p < 0.001, ****p < 0.0001 versus untreated control.

However, labeled glycine uptake was not as high in DMF treated cells respect to the control condition compared to serine uptake (**Figure 30**, left panel). No significant differences were found in serine labeling from glycine (**Figure 30**, right panel).

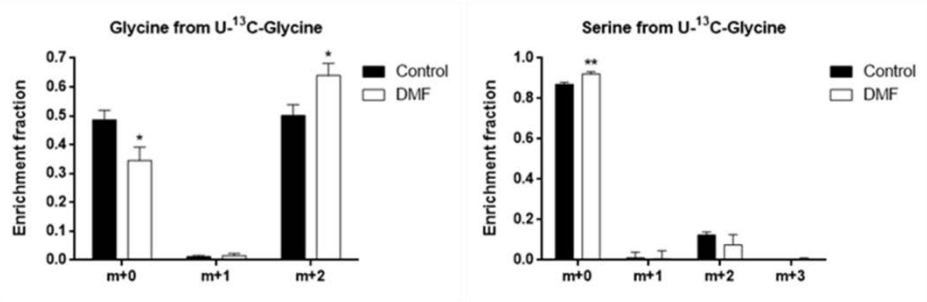

Figure 30. Fractional labeling of glycine and serine from [U-^{13}C]-glycine in HMECs treated with 100 µM DMF for 24 h in the absence of extracellular serine. Data are expressed as means ± SD of a unique experiment with triplicates. *p < 0.05, **p < 0.01 versus untreated control.

Regarding the intracellular serine and glycine pools, when serine, but not glycine, was present in the media, intracellular serine levels were higher in DMF treated cells but glycine levels were lower (**Figure 31A**). Nevertheless, depleting serine from the

media while extracellular glycine is available diminished, yet not significantly, serine levels in DMF treated cells, whereas glycine pool was unexpectedly decreased (**Figure 31B**).

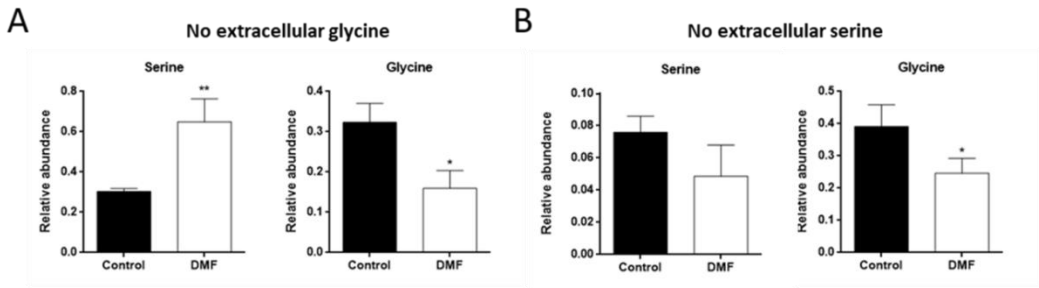

Figure 31. (A) Intracellular levels of serine and glycine in HMECs treated with 100 μM DMF for 24 h in the absence of extracellular glycine or (B) serine. Data are expressed as means ± SD of a unique experiment with triplicates. *p < 0.05, **p < 0.01 versus untreated control.

It was already reported that *de novo* mitochondrial glycine synthesis is highly active in ECs and more important than cellular uptake[383]. These results confirm the major effect on glycine metabolism through inhibition of serine synthesis by DMF, and reinforces the high dependence on both serine and glycine availability in order to sustain the intracellular glycine pool especially when serine synthesis is compromised.

7. Dimethyl fumarate inhibits endothelial cell proliferation

Since serine and glycine are important for cell proliferation, the effect of DMF on cell proliferation was studied. The number of cells treated with 100 μM DMF for three days did barely increase even in the presence of extracellular serine and glycine. Additionally, growth of control cells was independent of the presence of these two amino acids (**Figure 32**), indicating that serine and glycine synthesis can sustain cell growth even when there is no extracellular availability.

However, monitoring of cell number is not as sensitive as proper proliferation assays. For that reason, cell proliferation was tested in the presence of DMF using an EdU-based proliferation assay kit. By means of this experiment, it was observed that 50 and 100 μM DMF substantially diminished cell proliferation after 24 h (**Figure 33**). In all conditions, including control without DMF, cell proliferation was lower in the serine and glycine withdrawal condition, although it was not statistically significant compared to the condition where serine and glycine were present in the medium (**Figure 33**).

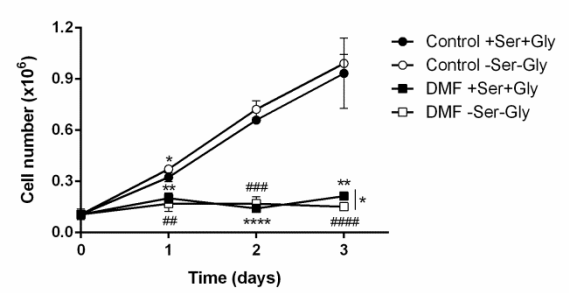

Figure 32. Cell growth curves of HMECs treated with 100 µM DMF for 72 h in the presence or absence of extracellular serine and glycine. Data are expressed as means ± SD of a unique experiment with triplicates. *p < 0.05, **p < 0.01, ****p < 0.0001 versus control with serine and glycine; ##p < 0.01, ###p < 0.001, ####p < 0.0001 versus control without serine and glycine.

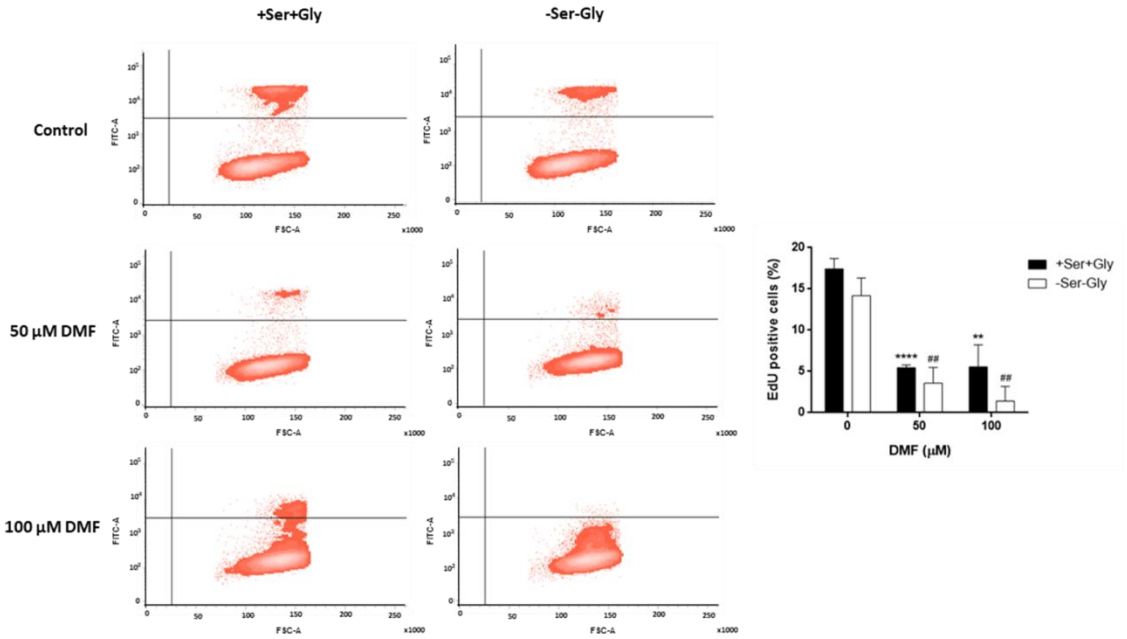

Figure 33. 10 µM EdU was added for 2 h to HMECs treated with DMF for 22 h in the presence or absence of extracellular serine and glycine and EdU incorporation was determined using a FACS VERSE™ cytometer. A representative result and the calculated values for EdU positive cells expressed as means ± SD of three independent experiments are shown. **p < 0.01, ****p < 0.0001 versus condition with extracellular serine and glycine; ##p < 0.01 versus condition without extracellular serine and glycine.

This decrease in cell proliferation after incubation with 100 µM DMF was accompanied by an accumulation of cells in S/G2/M phase in a way that was independent of serine and glycine availability (**Figure 34**). However, no major

differences in cell cycle distribution with 50 µM or between conditions with and without serine and glycine were found (**Figure 34**).

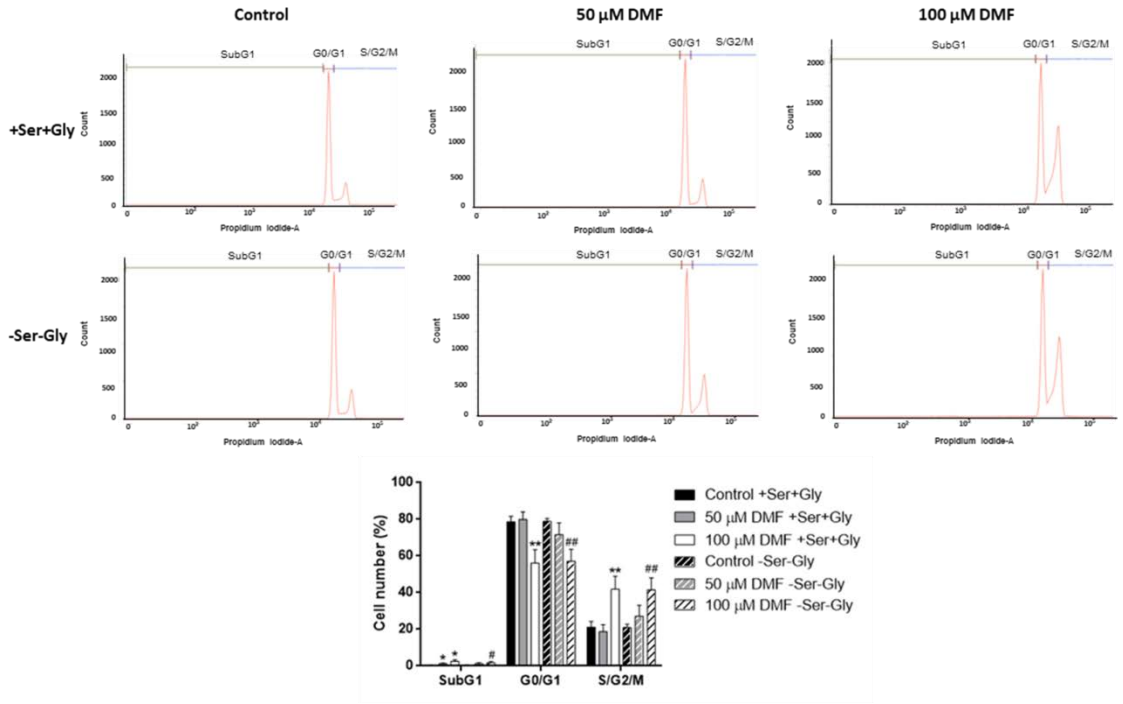

Figure 34. HMECs were exposed for 24 h to DMF at the indicated concentrations in the presence or absence of extracellular serine and glycine, stained with propidium iodide and percentages of cells in subG1, G1 and S/G2/M phases were determined using a FACS VERSE^{TM} cytometer. A representative result and the calculated values for cell subpopulations, expressed as means ± SD of three independent experiments, are shown. *p < 0.05, **p < 0.01 versus condition with extracellular serine and glycine; #p < 0.05, ##p < 0.01 versus condition without extracellular serine and glycine.

Therefore, it is most likely that DMF exerts an anti-proliferative effect that is independent of serine and glycine synthesis. Indeed, it was found out that DMF decreases proliferation in VSMCs through indirect inhibition of cyclin D and pRb[384].

7.1. Dimethyl fumarate affects *de novo* nucleotide synthesis in HMECs

Serine and glycine are involved in purine metabolism. PRPP, which serves as backbone for *de novo* purine synthesis, comes from glucose. To this PRPP, two carbons of glycine and two carbons of two molecules of 10-formil THF derived from one-carbon metabolism are incorporated, along with an additional carbon from CO_2 and three nitrogen molecules from glutamine and aspartate (**Figure 35**).

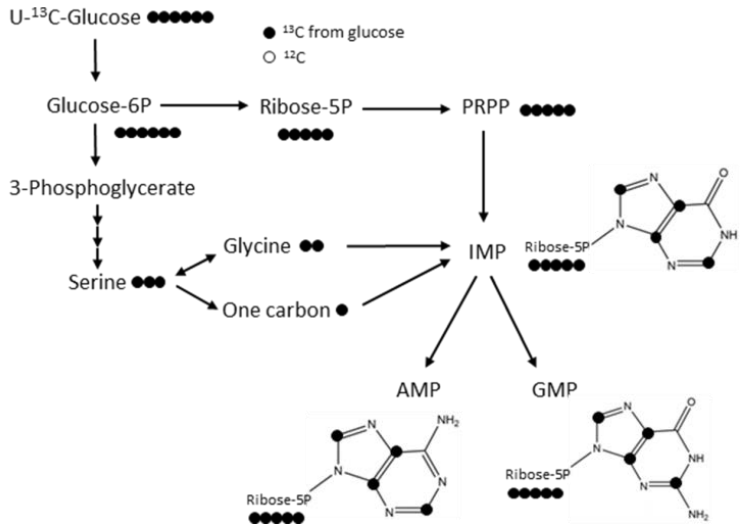

Figure 35. Scheme of *de novo* purine synthesis illustrating labeling from [U-^{13}C]-glucose.

Labeling of purines from glucose was studied in order to test whether the inhibition on the serine and glycine synthesis pathway affected *de novo* purine synthesis. DMF diminished purine m+6 to m+9 labeling from glucose, corresponding to carbons from serine and glycine metabolism, and increased m+5 labeling, which corresponds to PRPP (**Figure 36**).

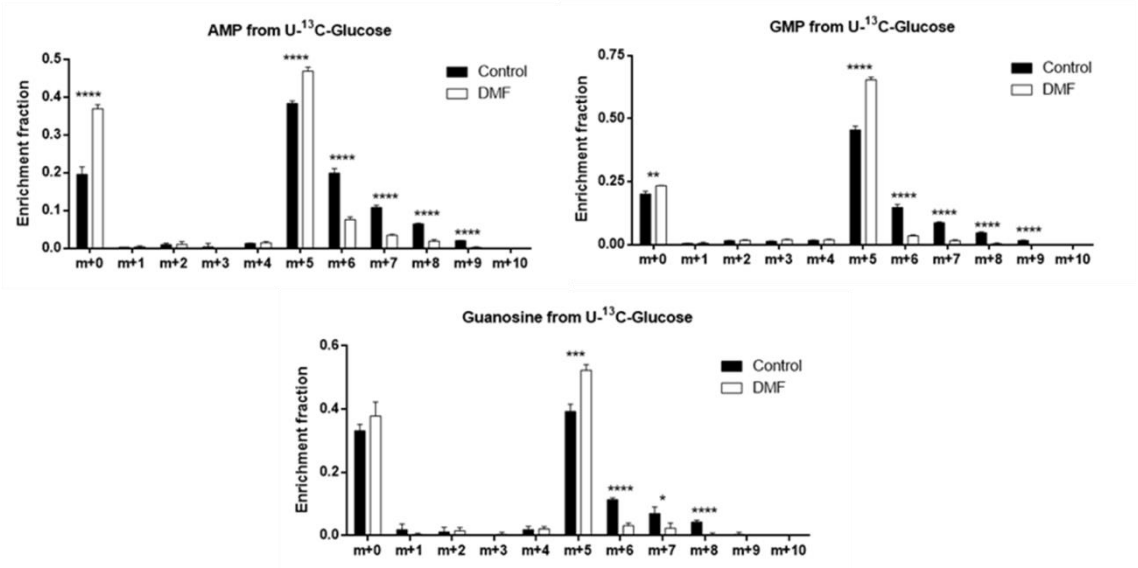

Figure 36. Fractional labeling of AMP, GMP and guanosine from [U-^{13}C]-glucose in HMECs treated with 100 μM DMF for 24 h. Data are expressed as means ± SD of a unique experiment with quadruplicates. *p < 0.05, **p < 0.01, ***p < 0.001, ****p < 0.0001 versus untreated control.

Moreover, intracellular levels of some of these purines, but not all of them, were reduced in cells treated with DMF (**Figure 37**).

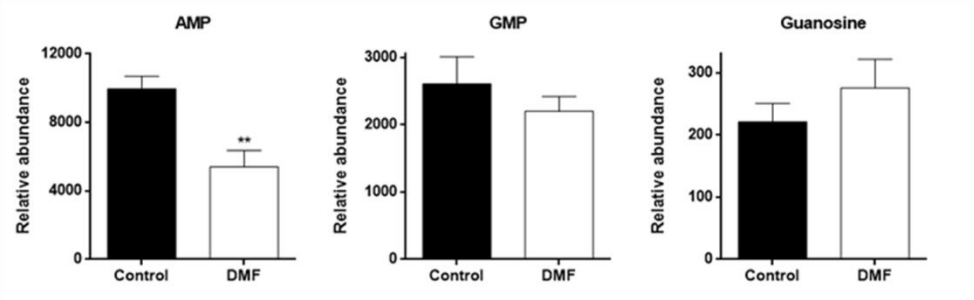

Figure 37. Intracellular levels of AMP, GMP and guanosine in HMECs treated with 100 μM DMF for 24 h. Data are expressed as means ± SD of a unique experiment with quadruplicates. **p < 0.01 versus untreated control.

Then, extracellular serine and glycine were depleted from the media. Similar effects were found in the labeling of purines from glucose in conditions either with or without serine and glycine. However, a greater m+7-9 labeling in the absence of serine and glycine in control cells compared to cells incubated with these amino acids suggest an increase in the contribution of glucose metabolism to *de novo* purine synthesis when extracellular serine and glycine are not available (**Figure 38**).

Similar results were obtained for the intracellular levels of several purines in the presence or absence of extracellular serine and glycine (**Figure 39**).

All these data indicate that exogenous serine and glycine are not enough to maintain serine homeostasis in cells with serine synthesis deficit[385].

The precipitous drop in m+6 labeling from glucose in the presence of extracellular serine and glycine suggests a possible malfunction of one-carbon metabolism in cells treated with DMF. The one-carbon donor formate is known to rescue cell growth after SHMT inhibition[386]. Nevertheless, formate failed to rescue cell growth of cells treated with DMF (**Figure 40)**, indicating that most likely the inhibition of cell proliferation exerted by DMF is not due to an inhibition of SHMT activity.

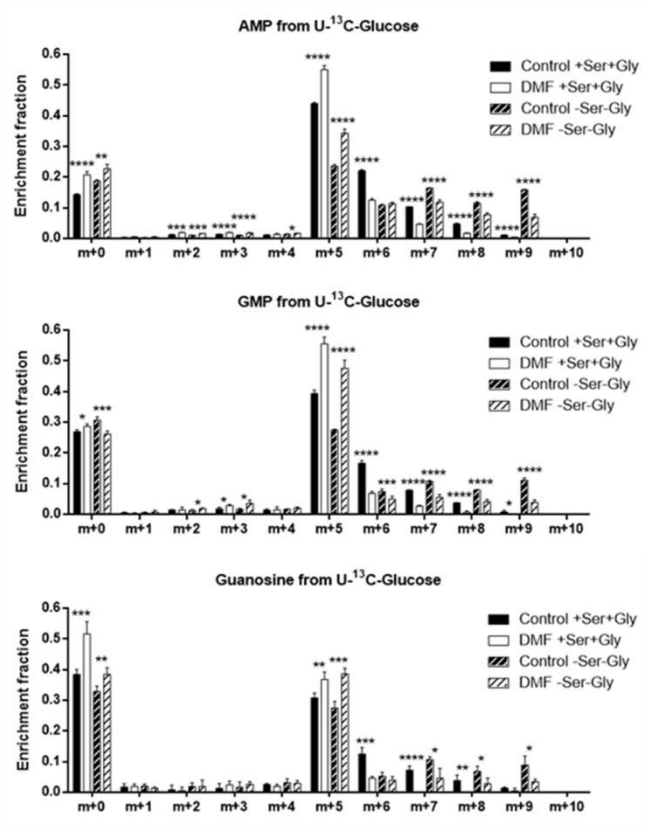

Figure 38. Fractional labeling of AMP, GMP and guanosine from [U-^{13}C]-glucose in HMECs treated with 100 µM DMF for 24 h in the presence or absence of extracellular serine and glycine. Data are expressed as means ± SD of a unique experiment with quadruplicates. *p < 0.05, **p < 0.01, ***p < 0.001, ****p < 0.0001 versus untreated control.

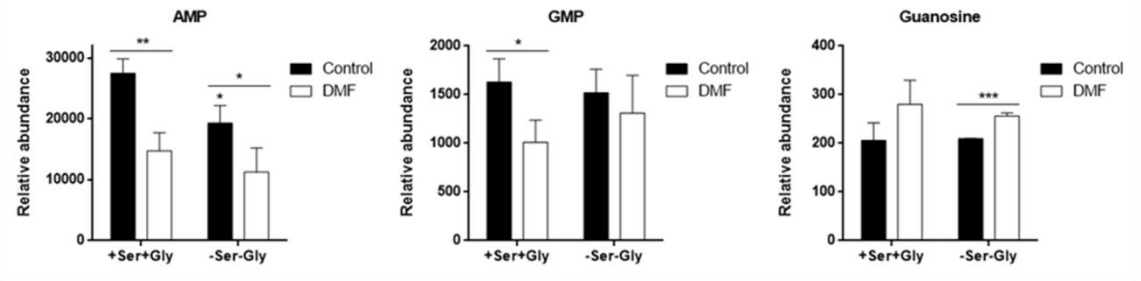

Figure 39. Intracellular levels of AMP, GMP and guanosine in HMECs treated with 100 µM DMF for 24 h in the presence or absence of extracellular serine and glycine. Data are expressed as means ± SD of a unique experiment with quadruplicates. *p < 0.05, **p < 0.01, ***p < 0.001 versus condition without extracellular serine and glycine.

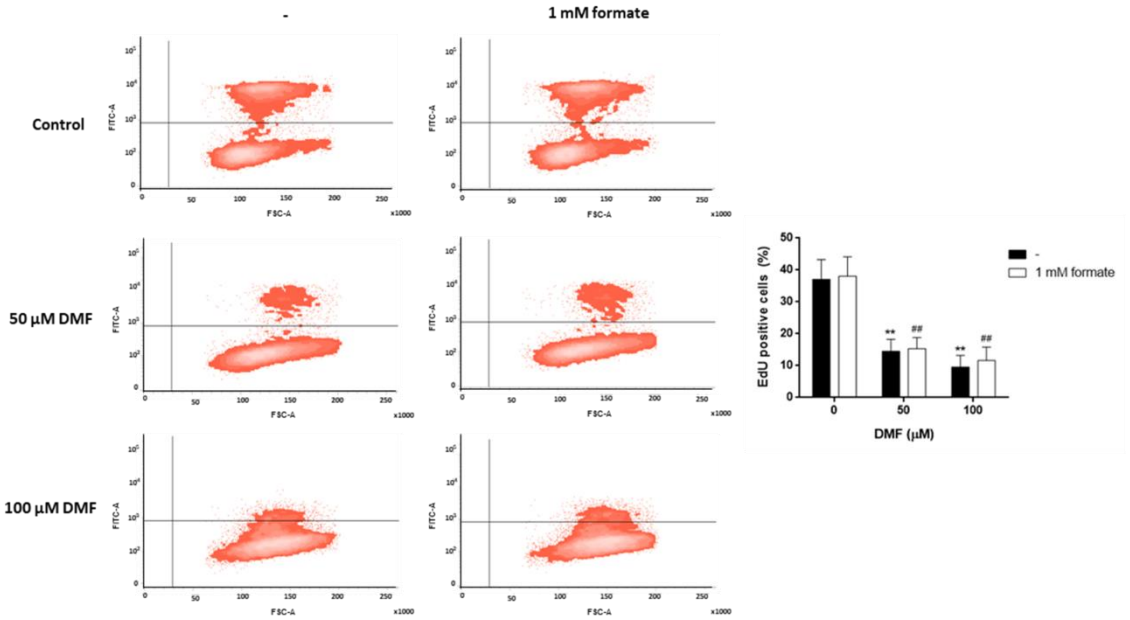

Figure 40. 10 µM EdU was added for 2 h to HMECs treated with DMF for 22 h in the presence or absence of 1 mM formate and EdU incorporation was determined using a FACS VERSE^{TM} cytometer. A representative result and the calculated values for EdU positive cells expressed as means ± SD of three independent experiments are shown. **p < 0.01 versus condition without formate; ##p < 0.01 versus condition with formate.

In order to corroborate the importance of serine and glycine synthesis on purine metabolism, cells were labeled with extracellular [U-^{13}C]-serine and [U-^{13}C]-glycine (**Figures 41 and 42**). Cells labeled with [U-^{13}C]-glucose were used as an internal control. For the experiment with cells labeled with [U-^{13}C]-serine, no extracellular glycine was added either in samples for glucose labeling. Accordingly, for the experiment with cells labeled with [U-^{13}C]-glycine, no extracellular serine was added to these cells or the ones labeled with glucose. Due to this variant not considered in results from **Figure 36**, results from glucose labeling are also shown.

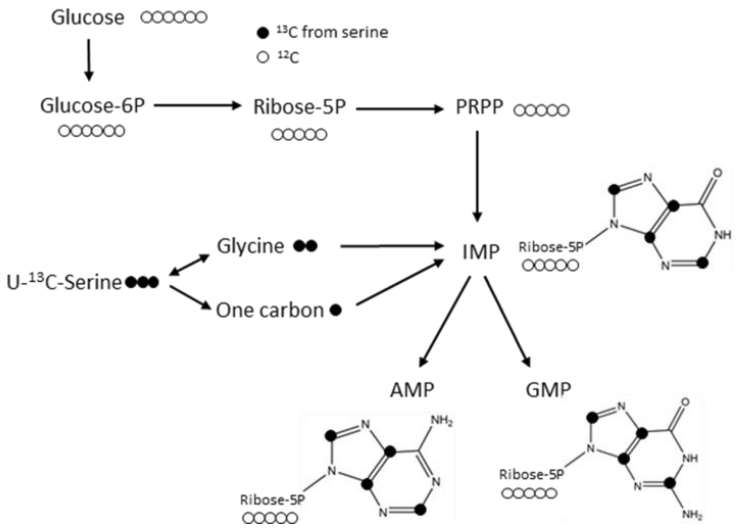

Figure 41. Scheme of *de novo* purine synthesis illustrating labeling from [U-^{13}C]-serine.

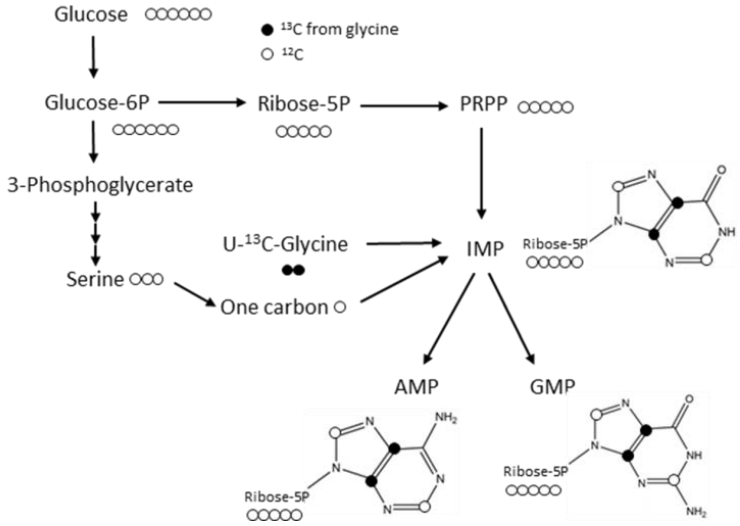

Figure 42. Scheme of *de novo* purine synthesis illustrating labeling from [U-^{13}C]-glycine.

M+1 to m+3 labeling from serine in purines was lower in DMF treated cells, whereas no change was observed in m+4 (**Figure 43A**). Similar results to those obtained in the presence of extracellular glycine were found for m+5 to m+9 labeling of purines from glucose (**Figure 43B**).

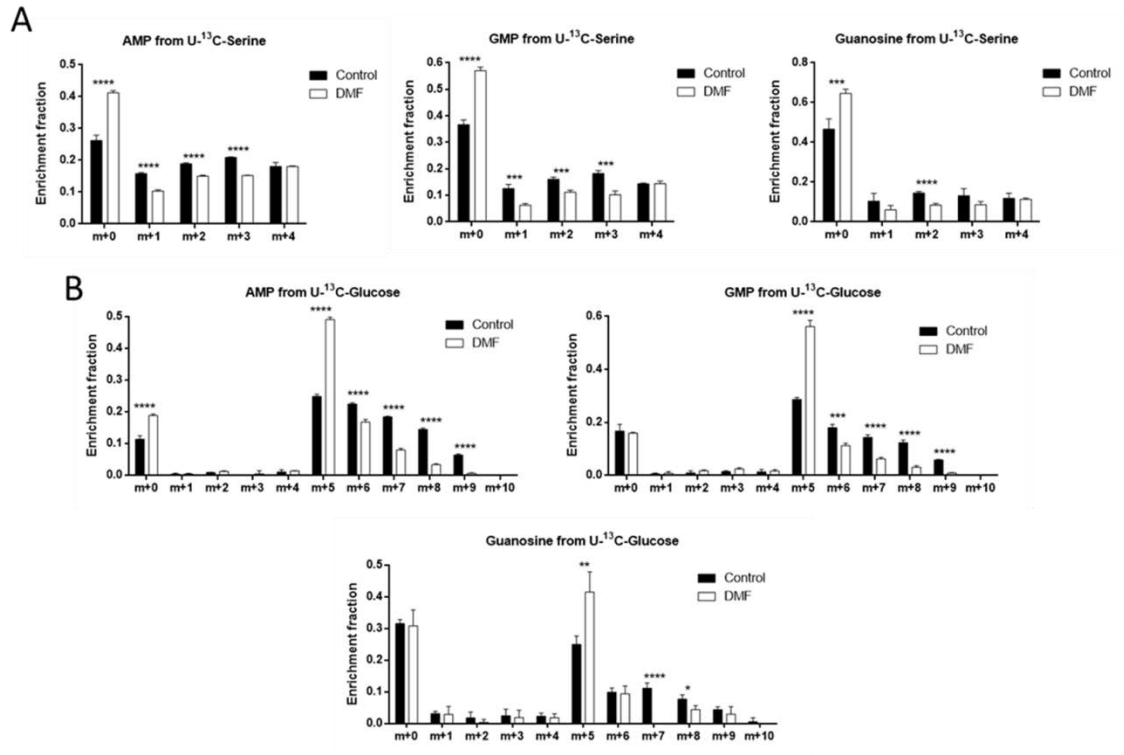

Figure 43. (A) Fractional labeling of AMP, GMP and guanosine from [U-^{13}C]-serine or (B) [U-^{13}C]-glucose in HMECs treated with 100 μM DMF for 24 h in the absence of extracellular glycine. Data are expressed as means ± SD of a unique experiment with quadruplicates. *p < 0.05, **p < 0.01, ***p < 0.001, ****p < 0.0001 versus untreated control.

Accordingly, m+2 labeling from glycine was also lower in DMF treated cells (**Figure 44A**) and similar results to those obtained in the presence of extracellular serine were found for m+5 to m+9 labeling of purines from glucose (**Figure 44B**).

These data reinforce the importance of serine and glycine synthesis for purine metabolism in contrast to their extracellular uptake.

Surprisingly, by means of the isotope labeling studies performed a slight yet consistent decrease in pyrimidines CMP and UMP m+5 from glucose, corresponding to PRPP, was observed (**Figures 45A and 45B**). Nevertheless, CMP and UMP intracellular pools were not significantly affected by DMF treatment (**Figures 45C and 45D**).

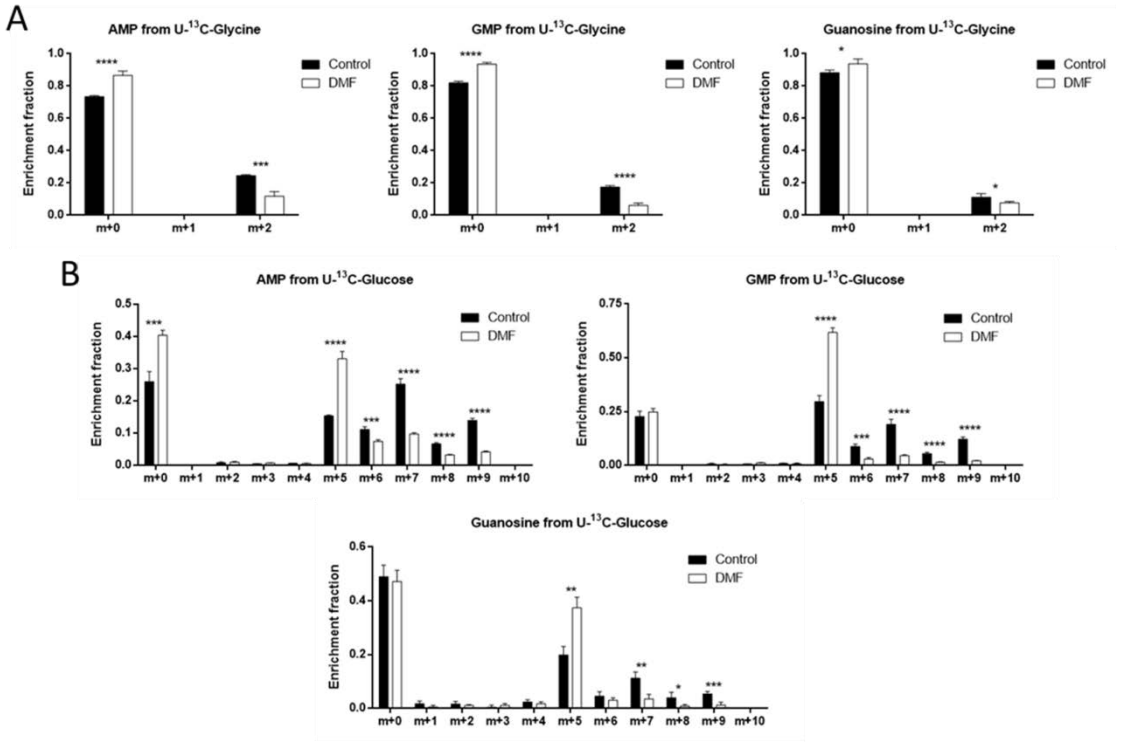

Figure 44. (A) Fractional labeling of AMP, GMP and guanosine from [U-^{13}C]-glycine or (B) [U-^{13}C]-glucose in HMECs treated with 100 μM DMF for 24 h in the absence of extracellular serine. Data are expressed as means ± SD of a unique experiment with quadruplicates. *p < 0.05, **p < 0.01, ***p < 0.001, ****p < 0.0001 versus untreated control.

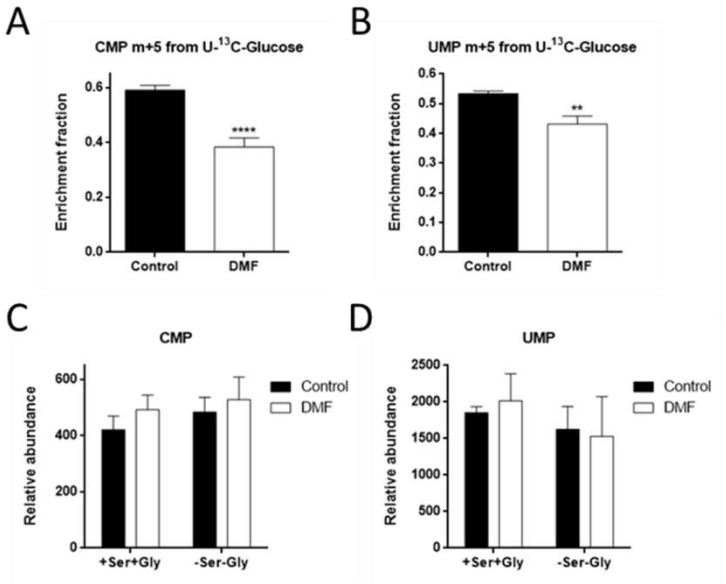

Figure 45. (A) Fractional labeling of CMP and (B) UMP from [U-^{13}C]-glucose in HMECs treated with 100 μM DMF for 24 h. (C) Intracellular CMP and (D) UMP levels in HMECs treated with 100 μM DMF for 24 h in the presence or absence of extracellular serine and glycine. Data are expressed as means ± SD of a unique experiment with quadruplicates. **p < 0.05 versus untreated control.

This decrease in m+5 labeling in pyrimidines was surprising, since pyrimidine synthesis does not depend on carbons from serine and glycine. However, it is known that PRPP must bind to orotate in order to generate UMP, the first pyrimidine in the pyrimidine synthesis pathway. Orotate is synthetized from dihydroorotate through DHODH activity. DHODH is known to be dependent on a functional mitochondrial ETC[387]. Moreover, aspartate is necessary upstream of the DHODH reaction. Therefore, DMF may affect pyrimidine synthesis through inhibition of cell respiration, even not affecting the total pool.

8. Dimethyl fumarate increases the GSH/GSSG ratio without affecting ROS levels in HMECs

It is known that DMF protects from oxidative stress in several cell lines. Hydrogen peroxide (H_2O_2) production was lower in macrovascular and microvascular ECs at low DMF concentrations[388]. Furthermore, the effect could be dependent on the incubation time, since at short incubations DMF depletes GSH from cells, whereas it increases it after 12 h[389]. This initial depletion is known to be due to conjugation of DMF with thiol-groups in GSH[390,391]. Nevertheless, DMF has been shown to reduce GSH levels after 24 h in erythrocytes, and this reduction was found to be related to an inhibition of G6PDH and GR activity[392]. Moreover, different cellular responses in the GSH levels after longer treatment with DMF were found in different cell lines, including both tumor and non-tumor cells[393-396]. Therefore, it seems likely that DMF can exert different effects in different cell types.

The oxidative response with high doses of DMF had not been tested in ECs to day. HMECs were treated with H_2O_2 in order to induce oxidative stress and test whether DMF diminished the formation of ROS. Nevertheless, 100 µM DMF failed to reduce ROS levels in HMECs in control and H_2O_2 conditions after both 4 and 24 h (**Figures 46A and 46B**).

However, after 24 h treatment with DMF GSH levels were higher compared to those of its oxidized form, GSSG, as seen by the GSH/GSSG ratio (**Figure 47**). At 6 h no GSH or GSSG were detected (data not shown), confirming the initial depletion of intracellular GSH and the later transcriptional upregulation of GSH levels in these cells.

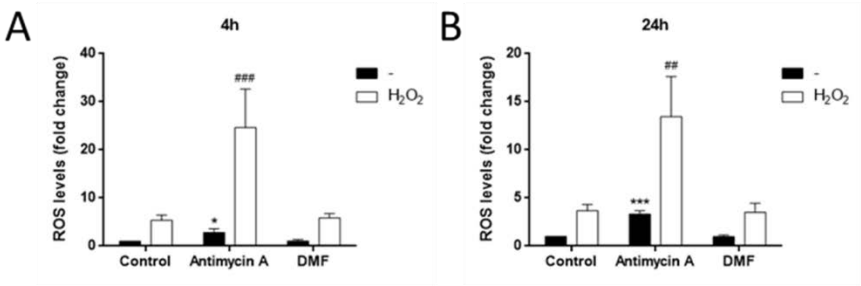

Figure 46. (A) ROS levels in HMECs incubated with or without 300 µM H_2O_2 and treated with 100 µM DMF for 4 or (B) 24 h. 200 µM antimycin A was used as positive control. Data are expressed as means ± SD of three independent experiments. *p < 0.05, ***p < 0.001 versus condition without H_2O_2; ##p < 0.01, ###p < 0.001 versus condition with H_2O_2.

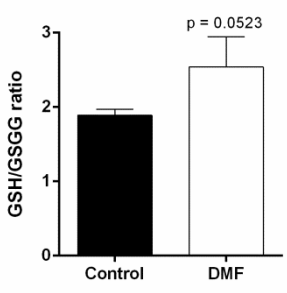

Figure 47. Intracellular GSH/GSSG ratio in HMECs treated with 100 µM DMF for 24 h. Data are expressed as means ± SD of a unique experiment with triplicates.

Serine and glycine, as well as glutamate, are also important for GSH synthesis. For this reason, the labeling of GSH from glucose and glutamine was followed in DMF treated cells (**Figure 48**).

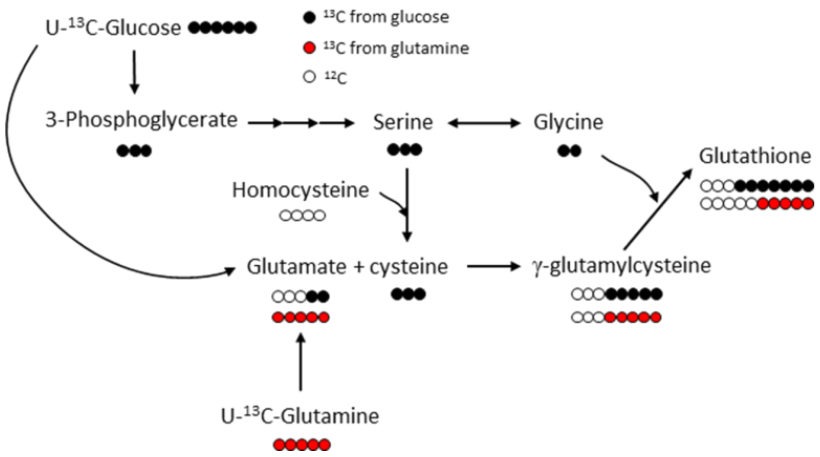

Figure 48. Scheme of glutathione synthesis illustrating labeling from [U-^{13}C]-glucose and from [U-^{13}C]-glutamine.

Surprisingly, DMF did not affect GSH labeling from glucose (**Figure 49A**). However, GSH m+5 labeling from glutamine, corresponding to glutamate incorporated into the GSH backbone, was slightly decreased with DMF treatment (**Figure 49B**).

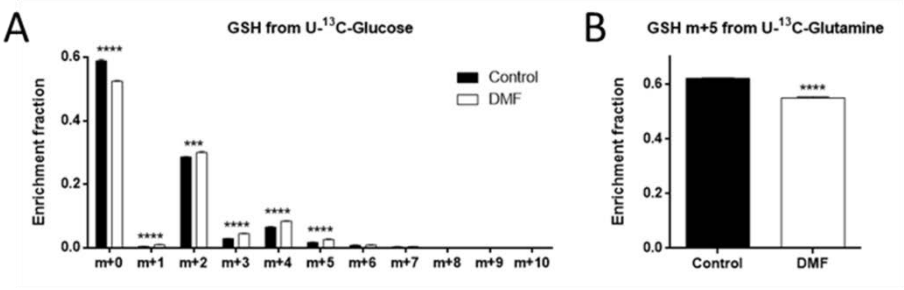

Figure 49. (A) Fractional labeling of GSH from [U-^{13}C]-glucose or (B) [U-^{13}C]-glutamine in HMECs treated with 100 μM DMF for 24 h. Data are expressed as means ± SD of a unique experiment with quadruplicates. ***p < 0.001, ****p < 0.0001 versus untreated control.

When serine and glycine were subtracted from the media, GSH m+2 and m+4 labeling from glucose, corresponding to glycine and glutamate incorporated into the GSH backbone, were diminished after treatment with 100 μM DMF (**Figure 50A**). In addition, GSH labeling from glucose was greater when no serine and glycine were present in the medium even in control conditions (**Figure 50A**), indicating an increase in *de novo* serine and glycine utilization for GSH metabolism. Conversely, the GSH/GSSG was not affected by serine and glutamine depletion in DMF-treated cells, whereas it was decreased in control conditions (**Figure 50B**).

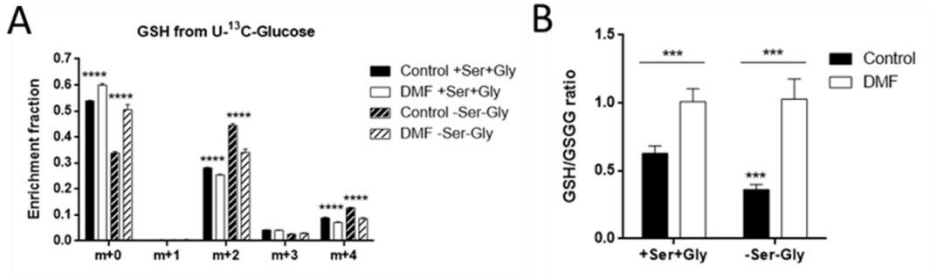

Figure 50. (A) Fractional labeling of GSH from [U-^{13}C]-glucose and (B) GSH/GSSG ratio in HMECs treated with 100 μM DMF for 24 h in the presence or absence of extracellular serine and glycine. Data are expressed as means ± SD of a unique experiment with quadruplicates. (A) ****p < 0.0001 versus untreated control or (B) ***p < 0.001 versus condition without extracellular serine and glycine.

These results suggest an additional mechanism of DMF to increase GSH in HMECs in an independent way of the modulation of serine and glycine metabolism, although no benefit in the oxidative response was found due to this increase.

Last, cells were labelled with [U-^{13}C]-serine and [U-^{13}C]-glycine in order to see whether *de novo* synthetized serine and glycine can be substituted by extracellular amino acids (**Figure 51**). Again, cells labeled with [U-^{13}C]-glucose were used as internal control.

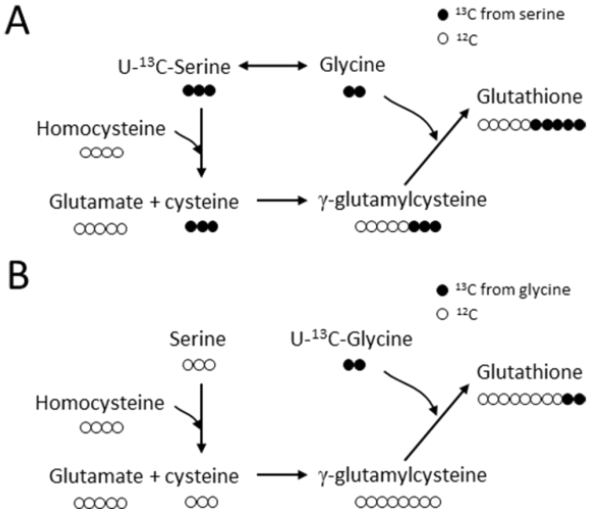

Figure 51. (A) Scheme of glutathione synthesis illustrating labeling from [U-^{13}C]-serine or (B) from [U-^{13}C]-glycine.

GSH m+2 labeling from serine was just slightly higher with DMF (**Figure 52A**). However, this was not surprising, since it was already observed that glycine labeling from extracellular serine was not much higher in cells treated with DMF compared to control condition (**Figure 29**, right panel). For this reason, it was important to add labeled glycine to the medium in order to elucidate whether extracellular glycine could compensate for the inhibition of serine/glycine synthesis affecting GSH metabolism. Results from glycine labeling showed no increase in GSH m+2 labeling from glycine in DMF treated cells (**Figure 52B**), indicating that extracellular glycine cannot support GSH synthesis in ECs.

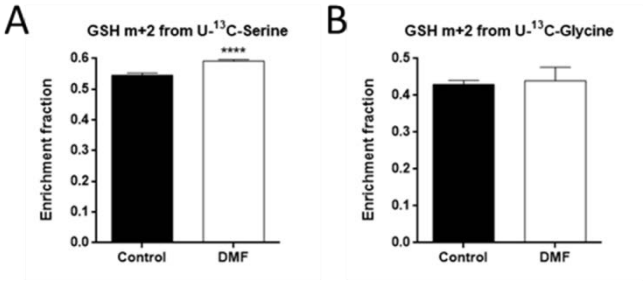

Figure 52. (A) Fractional labeling of GSH from [U-^{13}C]-serine in the absence of extracellular glycine or (B) [U-^{13}C]-glycine in the absence of extracellular serine in HMECs treated with 100 μM DMF for 24 h. Data are expressed as means ± SD of a unique experiment with quadruplicates. ****p < 0.0001 versus untreated control.

9. Dimethyl fumarate upregulates lipid metabolism in HMECs

Additionally to the previous study, by means of the AbsoluteIDQ p180 kit (Biocrates) it was found out that DMF increases the lipid profile of HMECs, especially of glycerophospholipids (**Figures 53 and 54** and **Appendix 10**). This is surprising, since glycerophospholipids are one of the main components of cell membranes, and DMF was seen to greatly inhibit proliferation of HMECs (**Figures 32 and 33**).

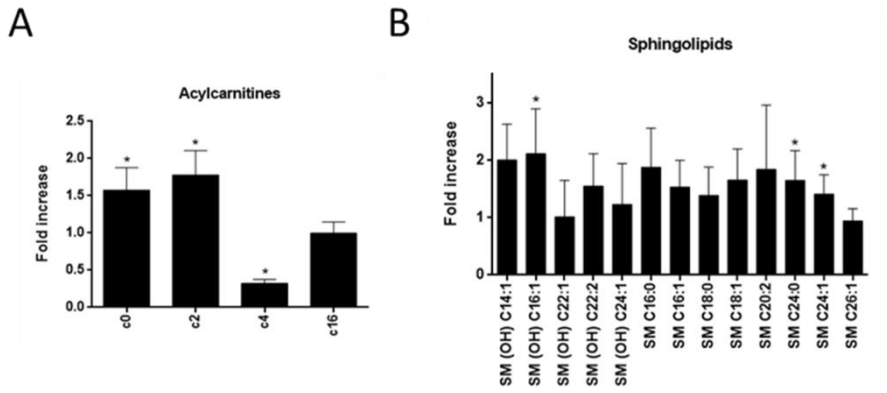

Figure 53. (A) Intracellular levels of acylcarnitines and (B) sphingolipids in HMECs treated with 100 μM DMF for 16 h. Data are expressed as means ± SD of three different experiments with triplicates. *p < 0.05 versus untreated control.

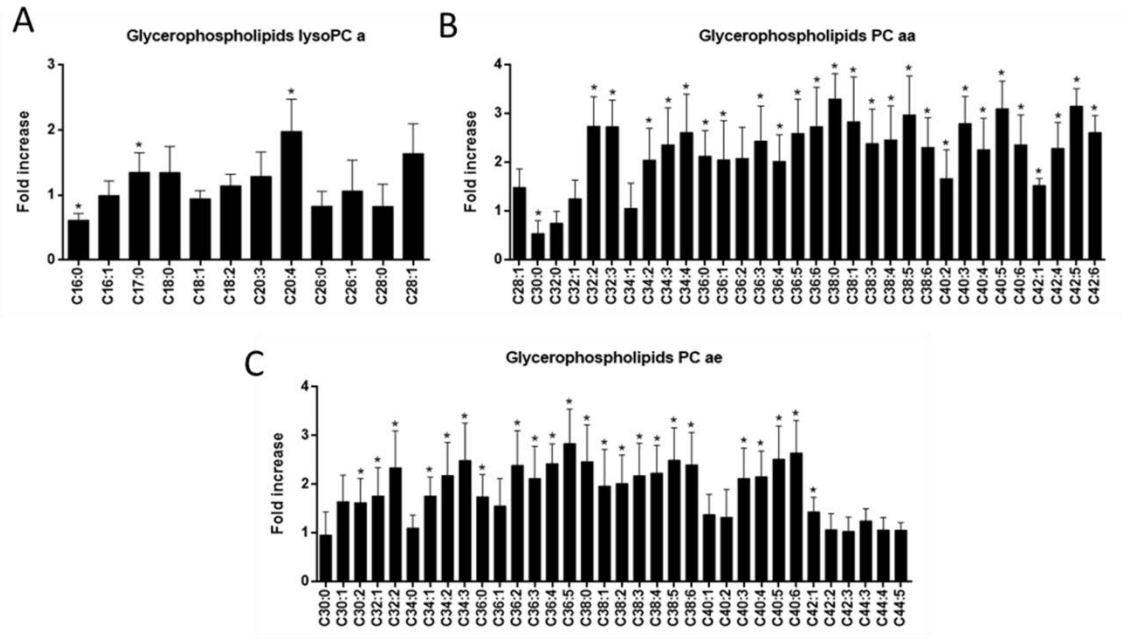

Figure 54. (A) Intracellular levels of lysophosphatidylcholines (lysoPC), (B) phosphatidylcholines aa (PC aa) and (C) phosphatidylcholines ae (PC ae) in HMECs treated with 100 µM DMF for 16 h. Data are expressed as means ± SD of three different experiments with triplicates. *p < 0.05 versus untreated control.

Accordingly, by means of a steady-state metabolite study intracellular levels of other lipids such as carnitine, deoxycarnitine, phosphorylcholine and glycerol 3-phosphate were also found to be higher in HMECs treated with DMF (**Figure 55**).

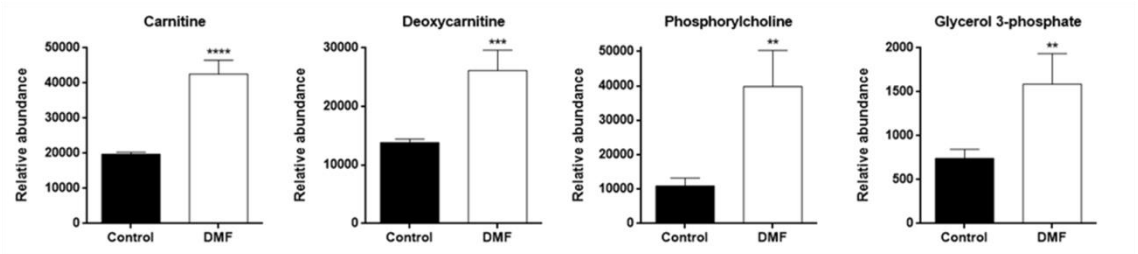

Figure 55. Intracellular levels of carnitine, deoxycarnitine, phosphorylcholine and glycerol 3-phosphate in HMECs treated or not with 100 µM DMF for 24 h. Representative data of one experiment with quadruplicates are expressed as means ± SD, although at least three independent experiments were performed with similar results. **p < 0.01, ***p < 0.001, ****p < 0.0001 versus untreated control.

Nevertheless, this compound was not able to increase palmitate uptake in these cells (**Figure 56**). Therefore, a different mechanism than lipid synthesis from extracellular fatty acids is likely to regulate lipid metabolism in cells treated with DMF.

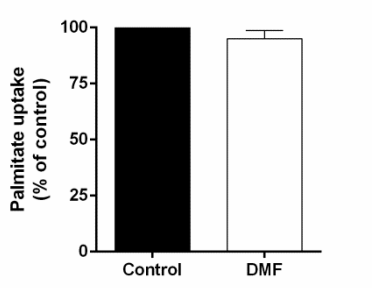

Figure 56. Palmitate uptake after 30 min incubation with 0.5 mM palmitate, 5 mM glucose and 0.5 mM glutamine in HMECs treated or not with 100 μM DMF for 16 h. Data are expressed as means ± SD of three independent experiments.

Others have also found higher lipid levels in several cell lines, such as murine oligodendrocyte cells and immune cells, after DMF treatment[397,398]. Indeed, this modulation of lipid metabolism exerted by DMF was correlated with changes in immunological parameters, which could explain the immunoregulatory role of DMF in the treatment of multiple sclerosis[397]. However, the exact mechanism by which DMF alters the lipid profile of ECs is yet to be studied.

10. Conclusions

The anti-angiogenic and anti-psoriatic compound DMF has been demonstrated to modulate EC energetic metabolism by induction of glycolysis and reduction of mitochondrial respiration. This effect may be due to an indirect mechanism or as a direct consequence of the inhibition of PHGDH activity, the rate-limiting enzyme in the serine and glycine synthesis pathway. Interestingly, this inhibition of PHGDH affects in a greater manner to glycine synthesis and intracellular levels. Since serine and glycine are important metabolites for several cellular functions, such as *de novo* purine synthesis and GSH synthesis, DMF could be considered as a potential modulator of glucose, serine and glycine metabolism in ECs. A summary of the main effects of DMF on energetic metabolism in ECs is collected in **Figure 57**. Moreover, this compound has been found to modulate the lipid profile of ECs, but its mechanism or consequences are still to be discovered.

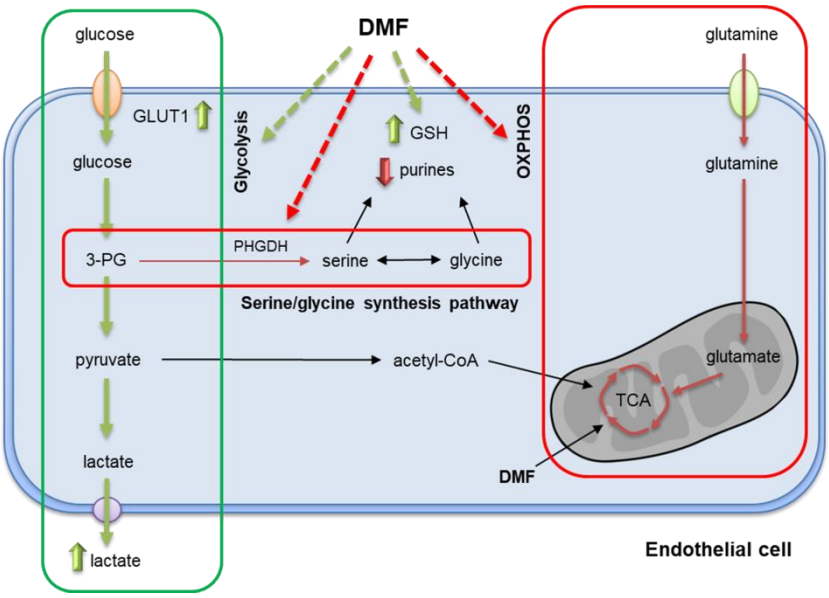

Figure 57. Summary of DMF effects on energetic EC metabolism. DMF increases glucose uptake through upregulation of GLUT1 expression. This increase in glucose uptake leads to a greater glycolytic rate and lactate secretion to the extracellular media. Conversely, glutamine uptake is diminished in cells treated with DMF, and its oxidation through the TCA cycle is reduced. DMF can also feed the TCA cycle. DMF diminishes PHGDH activity and synthesis of serine and glycine from glucose, which causes a reduction in *de novo* purine synthesis and intracellular levels. DMF increases intracellular GSH levels in ECs through a serine and glycine independent mechanism. Red arrows indicate downregulation, whereas green arrows indicate upregulation.

Elucidating the exact mechanism of action of DMF would require a vast and comprehensive experimental design, due to its high molecular reactivity and wide regulation of transcription factors. Thus, it still remains unclear whether impairment of angiogenesis through inhibition of VEGFR2 and the decrease in serine and glycine synthesis pathway by reduced PHGDH activity are correlated. Although glycolysis has been shown to be essential for angiogenesis, inhibition of PHGDH impaired the angiogenic process but increased the glycolytic rate in ECs[119,121]. Therefore, the results published by Vandekeere *et al.* and the data presented in this PhD Thesis reinforce the complexity of the metabolic regulation in ECs and its correlation with the angiogenic switch.

CONCLUSIONS

Based on the results obtained in this PhD Thesis, the following main conclusions can be drawn:

In relation to Objective 1:

- Both glucose and glutamine are essential for proliferation of all the cancer cells tested, independently of its tissue origin or invasiveness rate. Glucose has been shown to induce a different response in different tumor cells depending on their invasive capacity, reinforcing the metabolic difference between different types or even subtypes of tumors.

- Different responses to glucose deprivation have been found for the proliferation of different endothelial cell lines. Moreover, it has also been demonstrated that not all endothelial cell lines are able to incorporate lactate. These results reinforce the importance of choosing the endothelial cell line according to the goal of study.

In relation to Objective 2:

- Fasentin has been described as a weak anti-angiogenic compound, although this slight effect is most likely independent of its glucose transport modulation.

In relation to Objective 3:

- The anti-angiogenic compound dimethyl fumarate has been shown to modulate metabolism of endothelial cells through induction of glycolysis, inhibition of the serine and glycine synthesis pathway and an increase in the intracellular lipid profile of these cells.

REFERENCES

1 Wolf, K., Hu, H., Isaji, T. & Dardik, A. Molecular identity of arteries, veins, and lymphatics. *J Vasc Surg* **69**, 253-262, doi:10.1016/j.jvs.2018.06.195 (2019).

2 Munoz-Chapuli, R. Evolution of angiogenesis. *Int J Dev Biol* **55**, 345-351, doi:10.1387/ijdb.103212rm (2011).

3 Ribatti, D., Nico, B. & Crivellato, E. The development of the vascular system: a historical overview. *Methods Mol Biol* **1214**, 1-14, doi:10.1007/978-1-4939-1462-3_1 (2015).

4 Hanahan, D. & Folkman, J. Patterns and emerging mechanisms of the angiogenic switch during tumorigenesis. *Cell* **86**, 353-364, doi:10.1016/s0092-8674(00)80108-7 (1996).

5 Carmeliet, P. & Jain, R. K. Angiogenesis in cancer and other diseases. *Nature* **407**, 249-257, doi:10.1038/35025220 (2000).

6 Ribatti, D., Nico, B., Crivellato, E., Roccaro, A. M. & Vacca, A. The history of the angiogenic switch concept. *Leukemia* **21**, 44-52, doi:10.1038/sj.leu.2404402 (2007).

7 Kazerounian, S. & Lawler, J. Integration of pro- and anti-angiogenic signals by endothelial cells. *J Cell Commun Signal* **12**, 171-179, doi:10.1007/s12079-017-0433-3 (2018).

8 Carmeliet, P. Angiogenesis in life, disease and medicine. *Nature* **438**, 932-936, doi:10.1038/nature04478 (2005).

9 Folkman, J. Angiogenesis: an organizing principle for drug discovery? *Nat Rev Drug Discov* **6**, 273-286, doi:10.1038/nrd2115 (2007).

10 Quesada, A. R., Medina, M. A. & Muñoz-Chápuli, R. *Angiogénesis*. (2004).

11 Wang, G. L., Jiang, B. H., Rue, E. A. & Semenza, G. L. Hypoxia-inducible factor 1 is a basic-helix-loop-helix-PAS heterodimer regulated by cellular O2 tension. *Proc Natl Acad Sci U S A* **92**, 5510-5514, doi:10.1073/pnas.92.12.5510 (1995).

12 Semenza, G. L. Hydroxylation of HIF-1: oxygen sensing at the molecular level. *Physiology (Bethesda)* **19**, 176-182, doi:10.1152/physiol.00001.2004 (2004).

13 Hirota, K. & Semenza, G. L. Regulation of angiogenesis by hypoxia-inducible factor 1. *Crit Rev Oncol Hematol* **59**, 15-26, doi:10.1016/j.critrevonc.2005.12.003 (2006).

14 Munoz-Chapuli, R., Quesada, A. R. & Angel Medina, M. Angiogenesis and signal transduction in endothelial cells. *Cell Mol Life Sci* **61**, 2224-2243, doi:10.1007/s00018-004-4070-7 (2004).

15 Ferrara, N. & Henzel, W. J. Pituitary follicular cells secrete a novel heparin-binding growth factor specific for vascular endothelial cells. *Biochem Biophys Res Commun* **161**, 851-858, doi:10.1016/0006-291x(89)92678-8 (1989).

16 Senger, D. R. *et al.* Tumor cells secrete a vascular permeability factor that promotes accumulation of ascites fluid. *Science* **219**, 983-985, doi:10.1126/science.6823562 (1983).

17 Yamazaki, Y. & Morita, T. Molecular and functional diversity of vascular endothelial growth factors. *Mol Divers* **10**, 515-527, doi:10.1007/s11030-006-9027-3 (2006).

18 Melincovici, C. S. *et al.* Vascular endothelial growth factor (VEGF) - key factor in normal and pathological angiogenesis. *Rom J Morphol Embryol* **59**, 455-467 (2018).

19 Gille, H. *et al.* A repressor sequence in the juxtamembrane domain of Flt-1 (VEGFR-1) constitutively inhibits vascular endothelial growth factor-dependent

phosphatidylinositol 3'-kinase activation and endothelial cell migration. *EMBO J* **19**, 4064-4073, doi:10.1093/emboj/19.15.4064 (2000).

20 Terman, B. I. *et al.* Identification of the KDR tyrosine kinase as a receptor for vascular endothelial cell growth factor. *Biochem Biophys Res Commun* **187**, 1579-1586, doi:10.1016/0006-291x(92)90483-2 (1992).

21 Minchenko, A., Salceda, S., Bauer, T. & Caro, J. Hypoxia regulatory elements of the human vascular endothelial growth factor gene. *Cell Mol Biol Res* **40**, 35-39 (1994).

22 Claesson-Welsh, L. VEGF-B taken to our hearts: specific effect of VEGF-B in myocardial ischemia. *Arterioscler Thromb Vasc Biol* **28**, 1575-1576, doi:10.1161/ATVBAHA.108.170878 (2008).

23 Dashkevich, A., Hagl, C., Beyersdorf, F., Nykanen, A. I. & Lemstrom, K. B. VEGF Pathways in the Lymphatics of Healthy and Diseased Heart. *Microcirculation* **23**, 5-14, doi:10.1111/micc.12220 (2016).

24 Torry, D. S., Ahn, H., Barnes, E. L. & Torry, R. J. Placenta growth factor: potential role in pregnancy. *Am J Reprod Immunol* **41**, 79-85, doi:10.1111/j.1600-0897.1999.tb00078.x (1999).

25 Abhinand, C. S., Raju, R., Soumya, S. J., Arya, P. S. & Sudhakaran, P. R. VEGF-A/VEGFR2 signaling network in endothelial cells relevant to angiogenesis. *J Cell Commun Signal* **10**, 347-354, doi:10.1007/s12079-016-0352-8 (2016).

26 Alvarez-Aznar, A., Muhl, L. & Gaengel, K. VEGF Receptor Tyrosine Kinases: Key Regulators of Vascular Function. *Curr Top Dev Biol* **123**, 433-482, doi:10.1016/bs.ctdb.2016.10.001 (2017).

27 Guo, D., Jia, Q., Song, H. Y., Warren, R. S. & Donner, D. B. Vascular endothelial cell growth factor promotes tyrosine phosphorylation of mediators of signal transduction that contain SH2 domains. Association with endothelial cell proliferation. *J Biol Chem* **270**, 6729-6733, doi:10.1074/jbc.270.12.6729 (1995).

28 Yang, X. *et al.* Fibroblast growth factor signaling in the vasculature. *Curr Atheroscler Rep* **17**, 509, doi:10.1007/s11883-015-0509-6 (2015).

29 Good, D. J. *et al.* A tumor suppressor-dependent inhibitor of angiogenesis is immunologically and functionally indistinguishable from a fragment of thrombospondin. *Proc Natl Acad Sci U S A* **87**, 6624-6628, doi:10.1073/pnas.87.17.6624 (1990).

30 Ribatti, D. Endogenous inhibitors of angiogenesis: a historical review. *Leuk Res* **33**, 638-644, doi:10.1016/j.leukres.2008.11.019 (2009).

31 Nyberg, P., Xie, L. & Kalluri, R. Endogenous inhibitors of angiogenesis. *Cancer Res* **65**, 3967-3979, doi:10.1158/0008-5472.CAN-04-2427 (2005).

32 Arroyo, A. G. & Iruela-Arispe, M. L. Extracellular matrix, inflammation, and the angiogenic response. *Cardiovasc Res* **86**, 226-235, doi:10.1093/cvr/cvq049 (2010).

33 Oda, N., Abe, M. & Sato, Y. ETS-1 converts endothelial cells to the angiogenic phenotype by inducing the expression of matrix metalloproteinases and integrin beta3. *J Cell Physiol* **178**, 121-132, doi:10.1002/(SICI)1097-4652(199902)178:2<121::AID-JCP1>3.0.CO;2-F (1999).

34 Wang, X. & Khalil, R. A. Matrix Metalloproteinases, Vascular Remodeling, and Vascular Disease. *Adv Pharmacol* **81**, 241-330, doi:10.1016/bs.apha.2017.08.002 (2018).

35 Genersch, E., Hayess, K., Neuenfeld, Y. & Haller, H. Sustained ERK phosphorylation is necessary but not sufficient for MMP-9 regulation in

endothelial cells: involvement of Ras-dependent and -independent pathways. *J Cell Sci* **113 Pt 23**, 4319-4330 (2000).

36 Fang, J. *et al.* Matrix metalloproteinase-2 is required for the switch to the angiogenic phenotype in a tumor model. *Proc Natl Acad Sci U S A* **97**, 3884-3889, doi:10.1073/pnas.97.8.3884 (2000).

37 Lafleur, M. A., Forsyth, P. A., Atkinson, S. J., Murphy, G. & Edwards, D. R. Perivascular cells regulate endothelial membrane type-1 matrix metalloproteinase activity. *Biochem Biophys Res Commun* **282**, 463-473, doi:10.1006/bbrc.2001.4596 (2001).

38 Raffetto, J. D. & Khalil, R. A. Matrix metalloproteinases and their inhibitors in vascular remodeling and vascular disease. *Biochem Pharmacol* **75**, 346-359, doi:10.1016/j.bcp.2007.07.004 (2008).

39 Clark, J. C., Thomas, D. M., Choong, P. F. & Dass, C. R. RECK--a newly discovered inhibitor of metastasis with prognostic significance in multiple forms of cancer. *Cancer Metastasis Rev* **26**, 675-683, doi:10.1007/s10555-007-9093-8 (2007).

40 Gerhardt, H. *et al.* VEGF guides angiogenic sprouting utilizing endothelial tip cell filopodia. *J Cell Biol* **161**, 1163-1177, doi:10.1083/jcb.200302047 (2003).

41 Chen, W. *et al.* The endothelial tip-stalk cell selection and shuffling during angiogenesis. *J Cell Commun Signal* **13**, 291-301, doi:10.1007/s12079-019-00511-z (2019).

42 Benedito, R. *et al.* The notch ligands Dll4 and Jagged1 have opposing effects on angiogenesis. *Cell* **137**, 1124-1135, doi:10.1016/j.cell.2009.03.025 (2009).

43 Schimmel, L. & Gordon, E. The precise molecular signals that control endothelial cell-cell adhesion within the vessel wall. *Biochem Soc Trans* **46**, 1673-1680, doi:10.1042/BST20180377 (2018).

44 Davis, G. E. & Senger, D. R. Endothelial extracellular matrix: biosynthesis, remodeling, and functions during vascular morphogenesis and neovessel stabilization. *Circ Res* **97**, 1093-1107, doi:10.1161/01.RES.0000191547.64391.e3 (2005).

45 Davies, E. M., Gurung, R., Le, K. Q. & Mitchell, C. A. Effective angiogenesis requires regulation of phosphoinositide signaling. *Adv Biol Regul* **71**, 69-78, doi:10.1016/j.jbior.2018.11.008 (2019).

46 Ribatti, D. & Crivellato, E. "Sprouting angiogenesis", a reappraisal. *Dev Biol* **372**, 157-165, doi:10.1016/j.ydbio.2012.09.018 (2012).

47 Herbert, S. P. & Stainier, D. Y. Molecular control of endothelial cell behaviour during blood vessel morphogenesis. *Nat Rev Mol Cell Biol* **12**, 551-564, doi:10.1038/nrm3176 (2011).

48 Bautch, V. L. Endothelial cells form a phalanx to block tumor metastasis. *Cell* **136**, 810-812, doi:10.1016/j.cell.2009.02.021 (2009).

49 Iruela-Arispe, M. L. & Davis, G. E. Cellular and molecular mechanisms of vascular lumen formation. *Dev Cell* **16**, 222-231, doi:10.1016/j.devcel.2009.01.013 (2009).

50 Potente, M., Gerhardt, H. & Carmeliet, P. Basic and therapeutic aspects of angiogenesis. *Cell* **146**, 873-887, doi:10.1016/j.cell.2011.08.039 (2011).

51 Chiaverina, G. *et al.* Dynamic Interplay between Pericytes and Endothelial Cells during Sprouting Angiogenesis. *Cells* **8**, doi:10.3390/cells8091109 (2019).

52 Gaengel, K., Genove, G., Armulik, A. & Betsholtz, C. Endothelial-mural cell signaling in vascular development and angiogenesis. *Arterioscler Thromb Vasc Biol* **29**, 630-638, doi:10.1161/ATVBAHA.107.161521 (2009).

53 Jones, E. A., le Noble, F. & Eichmann, A. What determines blood vessel structure? Genetic prespecification vs. hemodynamics. *Physiology (Bethesda)* **21**, 388-395, doi:10.1152/physiol.00020.2006 (2006).

54 Chu, H. & Wang, Y. Therapeutic angiogenesis: controlled delivery of angiogenic factors. *Ther Deliv* **3**, 693-714 (2012).

55 Augustine, R., Prasad, P. & Khalaf, I. M. N. Therapeutic angiogenesis: From conventional approaches to recent nanotechnology-based interventions. *Mater Sci Eng C Mater Biol Appl* **97**, 994-1008, doi:10.1016/j.msec.2019.01.006 (2019).

56 Quesada, A. R., Munoz-Chapuli, R. & Medina, M. A. Anti-angiogenic drugs: from bench to clinical trials. *Med Res Rev* **26**, 483-530, doi:10.1002/med.20059 (2006).

57 Fallah, A. *et al.* Therapeutic targeting of angiogenesis molecular pathways in angiogenesis-dependent diseases. *Biomed Pharmacother* **110**, 775-785, doi:10.1016/j.biopha.2018.12.022 (2019).

58 Lopez-Jimenez, A. *et al.* Comparison of the anti-angiogenic potential of hydroxytyrosol and five derivatives. *Food Funct* **9**, 4310-4316, doi:10.1039/c8fo01140k (2018).

59 Carrillo, P., Martinez-Poveda, B., Medina, M. A. & Quesada, A. R. The strigolactone analog GR-24 inhibits angiogenesis in vivo and in vitro by a mechanism involving cytoskeletal reorganization and VEGFR2 signalling. *Biochem Pharmacol* **168**, 366-383, doi:10.1016/j.bcp.2019.07.019 (2019).

60 Carrillo, P. *et al.* Exploring the Antiangiogenic Potential of Solomonamide A Bioactive Precursors: In Vitro and in Vivo Evidences of the Inhibitory Activity of Solo F-OH During Angiogenesis. *Mar Drugs* **17**, doi:10.3390/md17040228 (2019).

61 Garcia-Vilas, J. A., Quesada, A. R. & Medina, M. A. Hydroxytyrosol targets extracellular matrix remodeling by endothelial cells and inhibits both ex vivo and in vivo angiogenesis. *Food Chem* **221**, 1741-1746, doi:10.1016/j.foodchem.2016.10.111 (2017).

62 Garcia-Vilas, J. A., Pino-Angeles, A., Martinez-Poveda, B., Quesada, A. R. & Medina, M. A. The noni anthraquinone damnacanthal is a multi-kinase inhibitor with potent anti-angiogenic effects. *Cancer Lett* **385**, 1-11, doi:10.1016/j.canlet.2016.10.037 (2017).

63 Garcia-Caballero, M., Canedo, L., Fernandez-Medarde, A., Medina, M. A. & Quesada, A. R. The marine fungal metabolite, AD0157, inhibits angiogenesis by targeting the Akt signaling pathway. *Mar Drugs* **12**, 279-299, doi:10.3390/md12010279 (2014).

64 Garcia-Caballero, M., Mari-Beffa, M., Canedo, L., Medina, M. A. & Quesada, A. R. Toluquinol, a marine fungus metabolite, is a new angiosuppresor that interferes with the Akt pathway. *Biochem Pharmacol* **85**, 1727-1740, doi:10.1016/j.bcp.2013.04.007 (2013).

65 Lopez-Jimenez, A., Garcia-Caballero, M., Medina, M. A. & Quesada, A. R. Anti-angiogenic properties of carnosol and carnosic acid, two major dietary compounds from rosemary. *Eur J Nutr* **52**, 85-95, doi:10.1007/s00394-011-0289-x (2013).

66 Garcia-Vilas, J. A., Quesada, A. R. & Medina, M. A. 4-methylumbelliferone inhibits angiogenesis in vitro and in vivo. *J Agric Food Chem* **61**, 4063-4071, doi:10.1021/jf303062h (2013).

67 Fortes, C., García-Vilas, J. A., Quesada, A. R. & Medina, M. A. Evaluation of the anti-angiogenic potential of hydroxytyrosol and tyrosol, two bio-active phenolic compounds of extra virgin olive oil, in endothelial cell cultures. *Food Chemistry* **134**, 134-140, doi:10.1016/j.foodchem.2012.02.079 (2012).

68 Cardenas, C., Quesada, A. R. & Medina, M. A. Anti-angiogenic and anti-inflammatory properties of kahweol, a coffee diterpene. *PLoS One* **6**, e23407, doi:10.1371/journal.pone.0023407 (2011).

69 Garcia-Caballero, M., Mari-Beffa, M., Medina, M. A. & Quesada, A. R. Dimethylfumarate inhibits angiogenesis in vitro and in vivo: a possible role for its antipsoriatic effect? *J Invest Dermatol* **131**, 1347-1355, doi:10.1038/jid.2010.416 (2011).

70 Martinez-Poveda, B., Verotta, L., Bombardelli, E., Quesada, A. R. & Medina, M. A. Tetrahydrohyperforin and octahydrohyperforin are two new potent inhibitors of angiogenesis. *PLoS One* **5**, e9558, doi:10.1371/journal.pone.0009558 (2010).

71 Martinez-Poveda, B. *et al.* DTD, an anti-inflammatory ditriazine, inhibits angiogenesis in vitro and in vivo. *J Cell Mol Med* **12**, 1211-1219, doi:10.1111/j.1582-4934.2008.00147.x (2008).

72 Martinez-Poveda, B. *et al.* IB05204, a dichloropyridodithienotriazine, inhibits angiogenesis in vitro and in vivo. *Mol Cancer Ther* **6**, 2675-2685, doi:10.1158/1535-7163.MCT-07-0136 (2007).

73 Cardenas, C., Quesada, A. R. & Medina, M. A. Evaluation of the anti-angiogenic effect of aloe-emodin. *Cell Mol Life Sci* **63**, 3083-3089, doi:10.1007/s00018-006-6399-6 (2006).

74 Martinez-Poveda, B., Quesada, A. R. & Medina, M. A. Hypericin in the dark inhibits key steps of angiogenesis in vitro. *Eur J Pharmacol* **516**, 97-103, doi:10.1016/j.ejphar.2005.03.047 (2005).

75 Cardenas, C., Quesada, A. R. & Medina, M. A. Effects of ursolic acid on different steps of the angiogenic process. *Biochem Biophys Res Commun* **320**, 402-408, doi:10.1016/j.bbrc.2004.05.183 (2004).

76 Rodriguez-Nieto, S. *et al.* Antiangiogenic activity of aeroplysinin-1, a brominated compound isolated from a marine sponge. *FASEB J* **16**, 261-263, doi:10.1096/fj.01-0427fje (2002).

77 Castro, M. E. *et al.* Study of puupehenone and related compounds as inhibitors of angiogenesis. *Int J Cancer* **110**, 31-38, doi:10.1002/ijc.20068 (2004).

78 Martinez-Poveda, B., Quesada, A. R. & Medina, M. A. Hyperforin, a bio-active compound of St. John's Wort, is a new inhibitor of angiogenesis targeting several key steps of the process. *Int J Cancer* **117**, 775-780, doi:10.1002/ijc.21246 (2005).

79 Folkman, J. Tumor angiogenesis: therapeutic implications. *N Engl J Med* **285**, 1182-1186, doi:10.1056/NEJM197111182852108 (1971).

80 Hanahan, D. & Weinberg, R. A. The hallmarks of cancer. *Cell* **100**, 57-70, doi:10.1016/s0092-8674(00)81683-9 (2000).

81 Schito, L. Hypoxia-Dependent Angiogenesis and Lymphangiogenesis in Cancer. *Adv Exp Med Biol* **1136**, 71-85, doi:10.1007/978-3-030-12734-3_5 (2019).

82 Rak, J., Yu, J. L., Klement, G. & Kerbel, R. S. Oncogenes and angiogenesis: signaling three-dimensional tumor growth. *J Investig Dermatol Symp Proc* **5**, 24-33, doi:10.1046/j.1087-0024.2000.00012.x (2000).

83 Lou, W. *et al.* MicroRNAs in cancer metastasis and angiogenesis. *Oncotarget* **8**, 115787-115802, doi:10.18632/oncotarget.23115 (2017).

84 De Palma, M., Biziato, D. & Petrova, T. V. Microenvironmental regulation of tumour angiogenesis. *Nat Rev Cancer* **17**, 457-474, doi:10.1038/nrc.2017.51 (2017).

85 Jain, R. K. Normalization of tumor vasculature: an emerging concept in antiangiogenic therapy. *Science* **307**, 58-62, doi:10.1126/science.1104819 (2005).

86 Goel, S. *et al.* Normalization of the vasculature for treatment of cancer and other diseases. *Physiol Rev* **91**, 1071-1121, doi:10.1152/physrev.00038.2010 (2011).

87 Papetti, M. & Herman, I. M. Mechanisms of normal and tumor-derived angiogenesis. *Am J Physiol Cell Physiol* **282**, C947-970, doi:10.1152/ajpcell.00389.2001 (2002).

88 Pieterse, Z., Sinha, D. & Kaur, P. Pericytes in Metastasis. *Adv Exp Med Biol* **1147**, 125-135, doi:10.1007/978-3-030-16908-4_5 (2019).

89 Valastyan, S. & Weinberg, R. A. Tumor metastasis: molecular insights and evolving paradigms. *Cell* **147**, 275-292, doi:10.1016/j.cell.2011.09.024 (2011).

90 Crum, R., Szabo, S. & Folkman, J. A new class of steroids inhibits angiogenesis in the presence of heparin or a heparin fragment. *Science* **230**, 1375-1378, doi:10.1126/science.2416056 (1985).

91 Taylor, S. & Folkman, J. Protamine is an inhibitor of angiogenesis. *Nature* **297**, 307-312, doi:10.1038/297307a0 (1982).

92 Ronca, R., Benkheil, M., Mitola, S., Struyf, S. & Liekens, S. Tumor angiogenesis revisited: Regulators and clinical implications. *Med Res Rev* **37**, 1231-1274, doi:10.1002/med.21452 (2017).

93 Jayson, G. C., Kerbel, R., Ellis, L. M. & Harris, A. L. Antiangiogenic therapy in oncology: current status and future directions. *Lancet* **388**, 518-529, doi:10.1016/S0140-6736(15)01088-0 (2016).

94 Rust, R., Gantner, C. & Schwab, M. E. Pro- and antiangiogenic therapies: current status and clinical implications. *FASEB J* **33**, 34-48, doi:10.1096/fj.201800640RR (2019).

95 Quesada, A. R., Medina, M. A. & Alba, E. Playing only one instrument may be not enough: limitations and future of the antiangiogenic treatment of cancer. *Bioessays* **29**, 1159-1168, doi:10.1002/bies.20655 (2007).

96 Ramjiawan, R. R., Griffioen, A. W. & Duda, D. G. Anti-angiogenesis for cancer revisited: Is there a role for combinations with immunotherapy? *Angiogenesis* **20**, 185-204, doi:10.1007/s10456-017-9552-y (2017).

97 Bastien, J. P., Minguy, A., Dave, V. & Roy, D. C. Cellular therapy approaches harnessing the power of the immune system for personalized cancer treatment. *Semin Immunol* **42**, 101306, doi:10.1016/j.smim.2019.101306 (2019).

98 Fukumura, D., Kloepper, J., Amoozgar, Z., Duda, D. G. & Jain, R. K. Enhancing cancer immunotherapy using antiangiogenics: opportunities and challenges. *Nat Rev Clin Oncol* **15**, 325-340, doi:10.1038/nrclinonc.2018.29 (2018).

99 Christofi, T., Baritaki, S., Falzone, L., Libra, M. & Zaravinos, A. Current Perspectives in Cancer Immunotherapy. *Cancers (Basel)* **11**, doi:10.3390/cancers11101472 (2019).

100 Jimenez-Valerio, G. & Casanovas, O. Angiogenesis and Metabolism: Entwined for Therapy Resistance. *Trends Cancer* **3**, 10-18, doi:10.1016/j.trecan.2016.11.007 (2017).

101 Missiaen, R., Morales-Rodriguez, F., Eelen, G. & Carmeliet, P. Targeting endothelial metabolism for anti-angiogenesis therapy: A pharmacological perspective. *Vascul Pharmacol* **90**, 8-18, doi:10.1016/j.vph.2017.01.001 (2017).

102 Goveia, J., Stapor, P. & Carmeliet, P. Principles of targeting endothelial cell metabolism to treat angiogenesis and endothelial cell dysfunction in disease. *EMBO Mol Med* **6**, 1105-1120, doi:10.15252/emmm.201404156 (2014).

103 Harjes, U., Kalucka, J. & Carmeliet, P. Targeting fatty acid metabolism in cancer and endothelial cells. *Crit Rev Oncol Hematol* **97**, 15-21, doi:10.1016/j.critrevonc.2015.10.011 (2016).

104 Kuczynski, E. A., Vermeulen, P. B., Pezzella, F., Kerbel, R. S. & Reynolds, A. R. Vessel co-option in cancer. *Nat Rev Clin Oncol* **16**, 469-493, doi:10.1038/s41571-019-0181-9 (2019).

105 Maniotis, A. J. *et al.* Vascular channel formation by human melanoma cells in vivo and in vitro: vasculogenic mimicry. *Am J Pathol* **155**, 739-752, doi:10.1016/S0002-9440(10)65173-5 (1999).

106 Latacz, E. *et al.* Pathological features of vessel co-option versus sprouting angiogenesis. *Angiogenesis*, doi:10.1007/s10456-019-09690-0 (2019).

107 Warburg, O. On the origin of cancer cells. *Science* **123**, 309-314, doi:10.1126/science.123.3191.309 (1956).

108 Warburg, O. The metabolism of carcinoma cells. *The Journal of Cancer Research* **9**, 148-163, doi:10.1158/jcr.1925.148 (1925).

109 Medina, M. A., Sanchez-Jimenez, F., Marquez, J., Rodriguez Quesada, A. & Nunez de Castro, I. Relevance of glutamine metabolism to tumor cell growth. *Mol Cell Biochem* **113**, 1-15, doi:10.1007/bf00230880 (1992).

110 Carrascosa, J. M., Martinez, P. & Nunez de Castro, I. Nitrogen movement between host and tumor in mice inoculated with Ehrlich ascitic tumor cells. *Cancer Res* **44**, 3831-3835 (1984).

111 Lu, W., Pelicano, H. & Huang, P. Cancer metabolism: is glutamine sweeter than glucose? *Cancer Cell* **18**, 199-200, doi:10.1016/j.ccr.2010.08.017 (2010).

112 Quesada, A. R., Medina, M. A., Marquez, J., Sanchez-Jimenez, F. M. & Nunez de Castro, I. Contribution by host tissues to circulating glutamine in mice inoculated with Ehrlich ascites tumor cells. *Cancer Res* **48**, 1551-1553 (1988).

113 Hanahan, D. & Weinberg, R. A. Hallmarks of cancer: the next generation. *Cell* **144**, 646-674, doi:10.1016/j.cell.2011.02.013 (2011).

114 Peters, K. *et al.* Changes in human endothelial cell energy metabolic capacities during in vitro cultivation. The role of "aerobic glycolysis" and proliferation. *Cell Physiol Biochem* **24**, 483-492, doi:10.1159/000257490 (2009).

115 Krutzfeldt, A., Spahr, R., Mertens, S., Siegmund, B. & Piper, H. M. Metabolism of exogenous substrates by coronary endothelial cells in culture. *J Mol Cell Cardiol* **22**, 1393-1404, doi:10.1016/0022-2828(90)90984-a (1990).

116 Leighton, B., Curi, R., Hussein, A. & Newsholme, E. A. Maximum activities of some key enzymes of glycolysis, glutaminolysis, Krebs cycle and fatty acid utilization in bovine pulmonary endothelial cells. *FEBS Lett* **225**, 93-96, doi:10.1016/0014-5793(87)81137-7 (1987).

117 Spolarics, Z., Lang, C. H., Bagby, G. J. & Spitzer, J. J. Glutamine and fatty acid oxidation are the main sources of energy for Kupffer and endothelial cells. *Am J Physiol* **261**, G185-190, doi:10.1152/ajpgi.1991.261.2.G185 (1991).

118 Dobrina, A. & Rossi, F. Metabolic properties of freshly isolated bovine endothelial cells. *Biochim Biophys Acta* **762**, 295-301, doi:10.1016/0167-4889(83)90084-8 (1983).

119 Vandekeere, S. *et al.* Serine Synthesis via PHGDH Is Essential for Heme Production in Endothelial Cells. *Cell Metab* **28**, 573-587 e513, doi:10.1016/j.cmet.2018.06.009 (2018).

120 Polet, F. & Feron, O. Endothelial cell metabolism and tumour angiogenesis: glucose and glutamine as essential fuels and lactate as the driving force. *J Intern Med* **273**, 156-165, doi:10.1111/joim.12016 (2013).

121 De Bock, K. *et al.* Role of PFKFB3-driven glycolysis in vessel sprouting. *Cell* **154**, 651-663, doi:10.1016/j.cell.2013.06.037 (2013).

122 Huang, H. *et al.* Role of glutamine and interlinked asparagine metabolism in vessel formation. *EMBO J* **36**, 2334-2352, doi:10.15252/embj.201695518 (2017).

123 Schoors, S. *et al.* Fatty acid carbon is essential for dNTP synthesis in endothelial cells. *Nature* **520**, 192-197, doi:10.1038/nature14362 (2015).

124 Pollard, T. D. & Borisy, G. G. Cellular motility driven by assembly and disassembly of actin filaments. *Cell* **112**, 453-465, doi:10.1016/s0092-8674(03)00120-x (2003).

125 Li, X., Kumar, A. & Carmeliet, P. Metabolic Pathways Fueling the Endothelial Cell Drive. *Annu Rev Physiol* **81**, 483-503, doi:10.1146/annurev-physiol-020518-114731 (2019).

126 Wilhelm, K. *et al.* FOXO1 couples metabolic activity and growth state in the vascular endothelium. *Nature* **529**, 216-220, doi:10.1038/nature16498 (2016).

127 Doddaballapur, A. *et al.* Laminar shear stress inhibits endothelial cell metabolism via KLF2-mediated repression of PFKFB3. *Arterioscler Thromb Vasc Biol* **35**, 137-145, doi:10.1161/ATVBAHA.114.304277 (2015).

128 Kalucka, J. *et al.* Quiescent Endothelial Cells Upregulate Fatty Acid beta-Oxidation for Vasculoprotection via Redox Homeostasis. *Cell Metab* **28**, 881-894 e813, doi:10.1016/j.cmet.2018.07.016 (2018).

129 Teuwen, L. A., Geldhof, V. & Carmeliet, P. How glucose, glutamine and fatty acid metabolism shape blood and lymph vessel development. *Dev Biol* **447**, 90-102, doi:10.1016/j.ydbio.2017.12.001 (2019).

130 Zecchin, A., Kalucka, J., Dubois, C. & Carmeliet, P. How Endothelial Cells Adapt Their Metabolism to Form Vessels in Tumors. *Front Immunol* **8**, 1750, doi:10.3389/fimmu.2017.01750 (2017).

131 Yetkin-Arik, B. *et al.* Endothelial tip cells in vitro are less glycolytic and have a more flexible response to metabolic stress than non-tip cells. *Sci Rep* **9**, 10414, doi:10.1038/s41598-019-46503-2 (2019).

132 Ancey, P. B., Contat, C. & Meylan, E. Glucose transporters in cancer - from tumor cells to the tumor microenvironment. *FEBS J* **285**, 2926-2943, doi:10.1111/febs.14577 (2018).

133 Thorens, B. & Mueckler, M. Glucose transporters in the 21st Century. *Am J Physiol Endocrinol Metab* **298**, E141-145, doi:10.1152/ajpendo.00712.2009 (2010).

134 Mann, G. E., Yudilevich, D. L. & Sobrevia, L. Regulation of amino acid and glucose transporters in endothelial and smooth muscle cells. *Physiol Rev* **83**, 183-252, doi:10.1152/physrev.00022.2002 (2003).

135 Blaschek, W. Natural Products as Lead Compounds for Sodium Glucose Cotransporter (SGLT) Inhibitors. *Planta Med* **83**, 985-993, doi:10.1055/s-0043-106050 (2017).

136 Yamazaki, Y., Harada, S. & Tokuyama, S. Sodium-glucose transporter as a novel therapeutic target in disease. *Eur J Pharmacol* **822**, 25-31, doi:10.1016/j.ejphar.2018.01.003 (2018).

137 Dell' Antone, P. Energy metabolism in cancer cells: how to explain the Warburg and Crabtree effects? *Med Hypotheses* **79**, 388-392, doi:10.1016/j.mehy.2012.06.002 (2012).

138 Kouidhi, S., Elgaaied, A. B. & Chouaib, S. Impact of Metabolism on T-Cell Differentiation and Function and Cross Talk with Tumor Microenvironment. *Front Immunol* **8**, 270, doi:10.3389/fimmu.2017.00270 (2017).

139 Delgoffe, G. M. & Powell, J. D. Sugar, fat, and protein: new insights into what T cells crave. *Curr Opin Immunol* **33**, 49-54, doi:10.1016/j.coi.2015.01.015 (2015).

140 Liu, Z. *et al.* Endothelial adenosine A2a receptor-mediated glycolysis is essential for pathological retinal angiogenesis. *Nat Commun* **8**, 584, doi:10.1038/s41467-017-00551-2 (2017).

141 Yu, P. *et al.* FGF-dependent metabolic control of vascular development. *Nature* **545**, 224-228, doi:10.1038/nature22322 (2017).

142 Mitchell, P. Coupling of phosphorylation to electron and hydrogen transfer by a chemi-osmotic type of mechanism. *Nature* **191**, 144-148, doi:10.1038/191144a0 (1961).

143 Pfeiffer, T., Schuster, S. & Bonhoeffer, S. Cooperation and competition in the evolution of ATP-producing pathways. *Science* **292**, 504-507, doi:10.1126/science.1058079 (2001).

144 Bhutia, Y. D. & Ganapathy, V. Glutamine transporters in mammalian cells and their functions in physiology and cancer. *Biochim Biophys Acta* **1863**, 2531-2539, doi:10.1016/j.bbamcr.2015.12.017 (2016).

145 DeBerardinis, R. J. & Cheng, T. Q's next: the diverse functions of glutamine in metabolism, cell biology and cancer. *Oncogene* **29**, 313-324, doi:10.1038/onc.2009.358 (2010).

146 Ruiz-Perez, M. V. *et al.* Glutamine, glucose and other fuels for cancer. *Curr Pharm Des* **20**, 2557-2579, doi:10.2174/13816128113199990482 (2014).

147 Mates, J. M., Campos-Sandoval, J. A. & Marquez, J. Glutaminase isoenzymes in the metabolic therapy of cancer. *Biochim Biophys Acta Rev Cancer* **1870**, 158-164, doi:10.1016/j.bbcan.2018.07.007 (2018).

148 Eelen, G. *et al.* Role of glutamine synthetase in angiogenesis beyond glutamine synthesis. *Nature* **561**, 63-69, doi:10.1038/s41586-018-0466-7 (2018).

149 Sookoian, S. & Pirola, C. J. Alanine and aspartate aminotransferase and glutamine-cycling pathway: their roles in pathogenesis of metabolic syndrome. *World J Gastroenterol* **18**, 3775-3781, doi:10.3748/wjg.v18.i29.3775 (2012).

150 Reitzer, L. J., Wice, B. M. & Kennell, D. Evidence that glutamine, not sugar, is the major energy source for cultured HeLa cells. *J Biol Chem* **254**, 2669-2676 (1979).

151 Still, E. R. & Yuneva, M. O. Hopefully devoted to Q: targeting glutamine addiction in cancer. *Br J Cancer* **116**, 1375-1381, doi:10.1038/bjc.2017.113 (2017).

152 Eagle, H. Nutrition needs of mammalian cells in tissue culture. *Science* **122**, 501-514, doi:10.1126/science.122.3168.501 (1955).

153 Glatz, J. F., Luiken, J. J. & Bonen, A. Membrane fatty acid transporters as regulators of lipid metabolism: implications for metabolic disease. *Physiol Rev* **90**, 367-417, doi:10.1152/physrev.00003.2009 (2010).

154 Son, N. H. *et al.* Endothelial cell CD36 optimizes tissue fatty acid uptake. *J Clin Invest* **128**, 4329-4342, doi:10.1172/JCI99315 (2018).
155 Beloribi-Djefaflia, S., Vasseur, S. & Guillaumond, F. Lipid metabolic reprogramming in cancer cells. *Oncogenesis* **5**, e189, doi:10.1038/oncsis.2015.49 (2016).
156 Qu, Q., Zeng, F., Liu, X., Wang, Q. J. & Deng, F. Fatty acid oxidation and carnitine palmitoyltransferase I: emerging therapeutic targets in cancer. *Cell Death Dis* **7**, e2226, doi:10.1038/cddis.2016.132 (2016).
157 Elmasri, H. *et al.* Endothelial cell-fatty acid binding protein 4 promotes angiogenesis: role of stem cell factor/c-kit pathway. *Angiogenesis* **15**, 457-468, doi:10.1007/s10456-012-9274-0 (2012).
158 Elmasri, H. *et al.* Fatty acid binding protein 4 is a target of VEGF and a regulator of cell proliferation in endothelial cells. *FASEB J* **23**, 3865-3873, doi:10.1096/fj.09-134882 (2009).
159 Sonveaux, P. *et al.* Targeting lactate-fueled respiration selectively kills hypoxic tumor cells in mice. *J Clin Invest* **118**, 3930-3942, doi:10.1172/JCI36843 (2008).
160 Perez-Escuredo, J. *et al.* Monocarboxylate transporters in the brain and in cancer. *Biochim Biophys Acta* **1863**, 2481-2497, doi:10.1016/j.bbamcr.2016.03.013 (2016).
161 Vegran, F., Boidot, R., Michiels, C., Sonveaux, P. & Feron, O. Lactate influx through the endothelial cell monocarboxylate transporter MCT1 supports an NF-kappaB/IL-8 pathway that drives tumor angiogenesis. *Cancer Res* **71**, 2550-2560, doi:10.1158/0008-5472.CAN-10-2828 (2011).
162 Sonveaux, P. *et al.* Targeting the lactate transporter MCT1 in endothelial cells inhibits lactate-induced HIF-1 activation and tumor angiogenesis. *PLoS One* **7**, e33418, doi:10.1371/journal.pone.0033418 (2012).
163 Ruan, G. X. & Kazlauskas, A. Lactate engages receptor tyrosine kinases Axl, Tie2, and vascular endothelial growth factor receptor 2 to activate phosphoinositide 3-kinase/Akt and promote angiogenesis. *J Biol Chem* **288**, 21161-21172, doi:10.1074/jbc.M113.474619 (2013).
164 Vizan, P. *et al.* Characterization of the metabolic changes underlying growth factor angiogenic activation: identification of new potential therapeutic targets. *Carcinogenesis* **30**, 946-952, doi:10.1093/carcin/bgp083 (2009).
165 Leopold, J. A. *et al.* Glucose-6-phosphate dehydrogenase modulates vascular endothelial growth factor-mediated angiogenesis. *J Biol Chem* **278**, 32100-32106, doi:10.1074/jbc.M301293200 (2003).
166 Chiaradonna, F., Ricciardiello, F. & Palorini, R. The Nutrient-Sensing Hexosamine Biosynthetic Pathway as the Hub of Cancer Metabolic Rewiring. *Cells* **7**, doi:10.3390/cells7060053 (2018).
167 de Queiroz, R. M. *et al.* Hexosamine Biosynthetic Pathway and Glycosylation Regulate Cell Migration in Melanoma Cells. *Front Oncol* **9**, 116, doi:10.3389/fonc.2019.00116 (2019).
168 Akella, N. M., Ciraku, L. & Reginato, M. J. Fueling the fire: emerging role of the hexosamine biosynthetic pathway in cancer. *BMC Biol* **17**, 52, doi:10.1186/s12915-019-0671-3 (2019).
169 Ricciardiello, F. *et al.* Inhibition of the Hexosamine Biosynthetic Pathway by targeting PGM3 causes breast cancer growth arrest and apoptosis. *Cell Death Dis* **9**, 377, doi:10.1038/s41419-018-0405-4 (2018).

170 Asano, T. *et al.* The role of N-glycosylation of GLUT1 for glucose transport activity. *J Biol Chem* **266**, 24632-24636 (1991).

171 Luo, B., Soesanto, Y. & McClain, D. A. Protein modification by O-linked GlcNAc reduces angiogenesis by inhibiting Akt activity in endothelial cells. *Arterioscler Thromb Vasc Biol* **28**, 651-657, doi:10.1161/ATVBAHA.107.159533 (2008).

172 Lynch, T. P. *et al.* Critical role of O-Linked beta-N-acetylglucosamine transferase in prostate cancer invasion, angiogenesis, and metastasis. *J Biol Chem* **287**, 11070-11081, doi:10.1074/jbc.M111.302547 (2012).

173 Chandler, K. B. *et al.* N-Glycosylation regulates ligand-dependent activation and signaling of vascular endothelial growth factor receptor 2 (VEGFR2). *J Biol Chem* **294**, 13117-13130, doi:10.1074/jbc.RA119.008643 (2019).

174 Merchan, J. R. *et al.* Antiangiogenic activity of 2-deoxy-D-glucose. *PLoS One* **5**, e13699, doi:10.1371/journal.pone.0013699 (2010).

175 Bousseau, S. *et al.* Glycosylation as new pharmacological strategies for diseases associated with excessive angiogenesis. *Pharmacol Ther* **191**, 92-122, doi:10.1016/j.pharmthera.2018.06.003 (2018).

176 Zibrova, D. *et al.* GFAT1 phosphorylation by AMPK promotes VEGF-induced angiogenesis. *Biochem J* **474**, 983-1001, doi:10.1042/BCJ20160980 (2017).

177 Zois, C. E. & Harris, A. L. Glycogen metabolism has a key role in the cancer microenvironment and provides new targets for cancer therapy. *J Mol Med (Berl)* **94**, 137-154, doi:10.1007/s00109-015-1377-9 (2016).

178 Dauer, P. & Lengyel, E. New Roles for Glycogen in Tumor Progression. *Trends Cancer* **5**, 396-399, doi:10.1016/j.trecan.2019.05.003 (2019).

179 Camus, S. *et al.* Identification of phosphorylase kinase as a novel therapeutic target through high-throughput screening for anti-angiogenesis compounds in zebrafish. *Oncogene* **31**, 4333-4342, doi:10.1038/onc.2011.594 (2012).

180 Kim, B., Li, J., Jang, C. & Arany, Z. Glutamine fuels proliferation but not migration of endothelial cells. *EMBO J* **36**, 2321-2333, doi:10.15252/embj.201796436 (2017).

181 Ghimire, K., Altmann, H. M., Straub, A. C. & Isenberg, J. S. Nitric oxide: what's new to NO? *Am J Physiol Cell Physiol* **312**, C254-C262, doi:10.1152/ajpcell.00315.2016 (2017).

182 Scerri, T. S. *et al.* Genome-wide analyses identify common variants associated with macular telangiectasia type 2. *Nat Genet* **49**, 559-567, doi:10.1038/ng.3799 (2017).

183 Guo, D. *et al.* Vascular endothelial growth factor signaling requires glycine to promote angiogenesis. *Sci Rep* **7**, 14749, doi:10.1038/s41598-017-15246-3 (2017).

184 Amin, K., Li, J., Chao, W. R., Dewhirst, M. W. & Haroon, Z. A. Dietary glycine inhibits angiogenesis during wound healing and tumor growth. *Cancer Biol Ther* **2**, 173-178, doi:10.4161/cbt.2.2.280 (2003).

185 Bruns, H. *et al.* Glycine inhibits angiogenesis in colorectal cancer: role of endothelial cells. *Amino Acids* **48**, 2549-2558, doi:10.1007/s00726-016-2278-0 (2016).

186 Ducker, G. S. & Rabinowitz, J. D. One-Carbon Metabolism in Health and Disease. *Cell Metab* **25**, 27-42, doi:10.1016/j.cmet.2016.08.009 (2017).

187 Sramek, M., Neradil, J. & Veselska, R. Much more than you expected: The non-DHFR-mediated effects of methotrexate. *Biochim Biophys Acta Gen Subj* **1861**, 499-503, doi:10.1016/j.bbagen.2016.12.014 (2017).

188 Shaker, O. G. *et al.* Antiangiogenic effect of methotrexate and PUVA on psoriasis. *Cell Biochem Biophys* **67**, 735-742, doi:10.1007/s12013-013-9563-2 (2013).
189 Joussen, A. M., Kruse, F. E., Volcker, H. E. & Kirchhof, B. Topical application of methotrexate for inhibition of corneal angiogenesis. *Graefes Arch Clin Exp Ophthalmol* **237**, 920-927, doi:10.1007/s004170050387 (1999).
190 Lu, H. *et al.* Chemotherapy triggers HIF-1-dependent glutathione synthesis and copper chelation that induces the breast cancer stem cell phenotype. *Proc Natl Acad Sci U S A* **112**, E4600-4609, doi:10.1073/pnas.1513433112 (2015).
191 Bansal, A. & Simon, M. C. Glutathione metabolism in cancer progression and treatment resistance. *J Cell Biol* **217**, 2291-2298, doi:10.1083/jcb.201804161 (2018).
192 Leopold, J. A., Zhang, Y. Y., Scribner, A. W., Stanton, R. C. & Loscalzo, J. Glucose-6-phosphate dehydrogenase overexpression decreases endothelial cell oxidant stress and increases bioavailable nitric oxide. *Arterioscler Thromb Vasc Biol* **23**, 411-417, doi:10.1161/01.ATV.0000056744.26901.BA (2003).
193 Li, B. *et al.* Fructose-1,6-bisphosphatase opposes renal carcinoma progression. *Nature* **513**, 251-255, doi:10.1038/nature13557 (2014).
194 Choi, S. J. *et al.* Isocitrate dehydrogenase 2 deficiency induces endothelial inflammation via p66sh-mediated mitochondrial oxidative stress. *Biochem Biophys Res Commun* **503**, 1805-1811, doi:10.1016/j.bbrc.2018.07.117 (2018).
195 McCarty, M. F., O'Keefe, J. H. & DiNicolantonio, J. J. Dietary Glycine Is Rate-Limiting for Glutathione Synthesis and May Have Broad Potential for Health Protection. *Ochsner J* **18**, 81-87 (2018).
196 Cui, H. *et al.* BA-12 Inhibits Angiogenesis via Glutathione Metabolism Activation. *Int J Mol Sci* **20**, doi:10.3390/ijms20164062 (2019).
197 Rohr-Udilova, N. *et al.* Impact of glutathione peroxidase 4 on cell proliferation, angiogenesis and cytokine production in hepatocellular carcinoma. *Oncotarget* **9**, 10054-10068, doi:10.18632/oncotarget.24300 (2018).
198 Yura, Y. *et al.* Endothelial cell-specific redox gene modulation inhibits angiogenesis but promotes B16F0 tumor growth in mice. *FASEB J*, fj201900786R, doi:10.1096/fj.201900786R (2019).
199 Schroder, K. Redox Control of Angiogenesis. *Antioxid Redox Signal* **30**, 960-971, doi:10.1089/ars.2017.7429 (2019).
200 Fahy, E. *et al.* A comprehensive classification system for lipids. *J Lipid Res* **46**, 839-861, doi:10.1194/jlr.E400004-JLR200 (2005).
201 Rashid, A. *et al.* Elevated expression of fatty acid synthase and fatty acid synthetic activity in colorectal neoplasia. *Am J Pathol* **150**, 201-208 (1997).
202 Shurbaji, M. S., Kalbfleisch, J. H. & Thurmond, T. S. Immunohistochemical detection of a fatty acid synthase (OA-519) as a predictor of progression of prostate cancer. *Hum Pathol* **27**, 917-921, doi:10.1016/s0046-8177(96)90218-x (1996).
203 Wang, Y. *et al.* Fatty acid synthase (FAS) expression in human breast cancer cell culture supernatants and in breast cancer patients. *Cancer Lett* **167**, 99-104, doi:10.1016/s0304-3835(01)00464-5 (2001).
204 Seguin, F. *et al.* The fatty acid synthase inhibitor orlistat reduces experimental metastases and angiogenesis in B16-F10 melanomas. *Br J Cancer* **107**, 977-987, doi:10.1038/bjc.2012.355 (2012).

205 Bruning, U. *et al.* Impairment of Angiogenesis by Fatty Acid Synthase Inhibition Involves mTOR Malonylation. *Cell Metab* **28**, 866-880 e815, doi:10.1016/j.cmet.2018.07.019 (2018).

206 Glatzel, D. K. *et al.* Acetyl-CoA carboxylase 1 regulates endothelial cell migration by shifting the phospholipid composition. *J Lipid Res* **59**, 298-311, doi:10.1194/jlr.M080101 (2018).

207 Vance, J. E. Phospholipid synthesis and transport in mammalian cells. *Traffic* **16**, 1-18, doi:10.1111/tra.12230 (2015).

208 Robinson, J. G. Lipid management beyond the guidelines. *Prog Cardiovasc Dis*, doi:10.1016/j.pcad.2019.10.004 (2019).

209 Lyu, J., Yang, E. J. & Shim, J. S. Cholesterol Trafficking: An Emerging Therapeutic Target for Angiogenesis and Cancer. *Cells* **8**, doi:10.3390/cells8050389 (2019).

210 Vander Heiden, M. G. Targeting cancer metabolism: a therapeutic window opens. *Nat Rev Drug Discov* **10**, 671-684, doi:10.1038/nrd3504 (2011).

211 Kim, J. & DeBerardinis, R. J. Mechanisms and Implications of Metabolic Heterogeneity in Cancer. *Cell Metab* **30**, 434-446, doi:10.1016/j.cmet.2019.08.013 (2019).

212 Pavlova, N. N. & Thompson, C. B. The Emerging Hallmarks of Cancer Metabolism. *Cell Metab* **23**, 27-47, doi:10.1016/j.cmet.2015.12.006 (2016).

213 Velaei, K., Samadi, N., Barazvan, B. & Soleimani Rad, J. Tumor microenvironment-mediated chemoresistance in breast cancer. *Breast* **30**, 92-100, doi:10.1016/j.breast.2016.09.002 (2016).

214 Yuan, Y., Jiang, Y. C., Sun, C. K. & Chen, Q. M. Role of the tumor microenvironment in tumor progression and the clinical applications (Review). *Oncol Rep* **35**, 2499-2515, doi:10.3892/or.2016.4660 (2016).

215 Itatani, Y., Kawada, K., Yamamoto, T. & Sakai, Y. Resistance to Anti-Angiogenic Therapy in Cancer-Alterations to Anti-VEGF Pathway. *Int J Mol Sci* **19**, doi:10.3390/ijms19041232 (2018).

216 Ebos, J. M. & Kerbel, R. S. Antiangiogenic therapy: impact on invasion, disease progression, and metastasis. *Nat Rev Clin Oncol* **8**, 210-221, doi:10.1038/nrclinonc.2011.21 (2011).

217 Parra-Bonilla, G., Alvarez, D. F., Al-Mehdi, A. B., Alexeyev, M. & Stevens, T. Critical role for lactate dehydrogenase A in aerobic glycolysis that sustains pulmonary microvascular endothelial cell proliferation. *Am J Physiol Lung Cell Mol Physiol* **299**, L513-522, doi:10.1152/ajplung.00274.2009 (2010).

218 Yetkin-Arik, B. *et al.* The role of glycolysis and mitochondrial respiration in the formation and functioning of endothelial tip cells during angiogenesis. *Sci Rep* **9**, 12608, doi:10.1038/s41598-019-48676-2 (2019).

219 Cantelmo, A. R. *et al.* Inhibition of the Glycolytic Activator PFKFB3 in Endothelium Induces Tumor Vessel Normalization, Impairs Metastasis, and Improves Chemotherapy. *Cancer Cell* **30**, 968-985, doi:10.1016/j.ccell.2016.10.006 (2016).

220 Zhang, W. *et al.* MicroRNA-153 Decreases Tryptophan Catabolism and Inhibits Angiogenesis in Bladder Cancer by Targeting Indoleamine 2,3-Dioxygenase 1. *Front Oncol* **9**, 619, doi:10.3389/fonc.2019.00619 (2019).

221 Abdel-Aziz, A. K., Shouman, S., El-Demerdash, E., Elgendy, M. & Abdel-Naim, A. B. Chloroquine synergizes sunitinib cytotoxicity via modulating autophagic, apoptotic and angiogenic machineries. *Chem Biol Interact* **217**, 28-40, doi:10.1016/j.cbi.2014.04.007 (2014).

222 Hu, Y. *et al.* Aspirin, a Potential GLUT1 Inhibitor in a Vascular Endothelial Cell Line. *Open Med (Wars)* **14**, 552-560, doi:10.1515/med-2019-0062 (2019).
223 El Sayed, S. M. *et al.* D-Amino acid oxidase-induced oxidative stress, 3-bromopyruvate and citrate inhibit angiogenesis, exhibiting potent anticancer effects. *J Bioenerg Biomembr* **44**, 513-523, doi:10.1007/s10863-012-9455-y (2012).
224 Chuang, I. C., Yang, C. M., Song, T. Y., Yang, N. C. & Hu, M. L. The anti-angiogenic action of 2-deoxyglucose involves attenuation of VEGFR2 signaling and MMP-2 expression in HUVECs. *Life Sci* **139**, 52-61, doi:10.1016/j.lfs.2015.08.002 (2015).
225 Singh, S. *et al.* Dietary 2-deoxy-D-glucose impairs tumour growth and metastasis by inhibiting angiogenesis. *Eur J Cancer* **123**, 11-24, doi:10.1016/j.ejca.2019.09.005 (2019).
226 Sutendra, G. *et al.* Mitochondrial activation by inhibition of PDKII suppresses HIF1a signaling and angiogenesis in cancer. *Oncogene* **32**, 1638-1650, doi:10.1038/onc.2012.198 (2013).
227 Jiang, J., Slivova, V., Jedinak, A. & Sliva, D. Gossypol inhibits growth, invasiveness, and angiogenesis in human prostate cancer cells by modulating NF-kappaB/AP-1 dependent- and independent-signaling. *Clin Exp Metastasis* **29**, 165-178, doi:10.1007/s10585-011-9439-z (2012).
228 Floridi, A. *et al.* Effect of lonidamine on the energy metabolism of Ehrlich ascites tumor cells. *Cancer Res* **41**, 4661-4666 (1981).
229 Del Bufalo, D. *et al.* Lonidamine causes inhibition of angiogenesis-related endothelial cell functions. *Neoplasia* **6**, 513-522, doi:10.1593/neo.04133 (2004).
230 Chen, J. *et al.* Shikonin and its analogs inhibit cancer cell glycolysis by targeting tumor pyruvate kinase-M2. *Oncogene* **30**, 4297-4306, doi:10.1038/onc.2011.137 (2011).
231 Hisa, T., Kimura, Y., Takada, K., Suzuki, F. & Takigawa, M. Shikonin, an ingredient of Lithospermum erythrorhizon, inhibits angiogenesis in vivo and in vitro. *Anticancer Res* **18**, 783-790 (1998).
232 Singh, R. P., Raina, K., Sharma, G. & Agarwal, R. Silibinin inhibits established prostate tumor growth, progression, invasion, and metastasis and suppresses tumor angiogenesis and epithelial-mesenchymal transition in transgenic adenocarcinoma of the mouse prostate model mice. *Clin Cancer Res* **14**, 7773-7780, doi:10.1158/1078-0432.CCR-08-1309 (2008).
233 Singh, R. P., Dhanalakshmi, S., Agarwal, C. & Agarwal, R. Silibinin strongly inhibits growth and survival of human endothelial cells via cell cycle arrest and downregulation of survivin, Akt and NF-kappaB: implications for angioprevention and antiangiogenic therapy. *Oncogene* **24**, 1188-1202, doi:10.1038/sj.onc.1208276 (2005).
234 Zhan, T., Digel, M., Kuch, E. M., Stremmel, W. & Fullekrug, J. Silybin and dehydrosilybin decrease glucose uptake by inhibiting GLUT proteins. *J Cell Biochem* **112**, 849-859, doi:10.1002/jcb.22984 (2011).
235 Singh, R. P., Gu, M. & Agarwal, R. Silibinin inhibits colorectal cancer growth by inhibiting tumor cell proliferation and angiogenesis. *Cancer Res* **68**, 2043-2050, doi:10.1158/0008-5472.CAN-07-6247 (2008).
236 Roy, S. & Maity, P. Effect of glutamine analogue-acivicin on tumor induced angiogenesis in Ehrlich ascites carcinoma. *Indian J Exp Biol* **43**, 407-413 (2005).

237 Araujo, F. A., Rocha, M. A., Mendes, J. B. & Andrade, S. P. Atorvastatin inhibits inflammatory angiogenesis in mice through down regulation of VEGF, TNF-alpha and TGF-beta1. *Biomed Pharmacother* **64**, 29-34, doi:10.1016/j.biopha.2009.03.003 (2010).

238 Vincent, L. *et al.* Inhibition of endothelial cell migration by cerivastatin, an HMG-CoA reductase inhibitor: contribution to its anti-angiogenic effect. *FEBS Lett* **495**, 159-166, doi:10.1016/s0014-5793(01)02337-7 (2001).

239 Araujo, F. A. *et al.* 3-Hydroxy-3-methylglutaryl coenzyme A reductase inhibitor (fluvastatin) decreases inflammatory angiogenesis in mice. *APMIS* **121**, 422-430, doi:10.1111/apm.12031 (2013).

240 Feleszko, W. *et al.* Lovastatin and tumor necrosis factor-alpha exhibit potentiated antitumor effects against Ha-ras-transformed murine tumor via inhibition of tumor-induced angiogenesis. *Int J Cancer* **81**, 560-567, doi:10.1002/(sici)1097-0215(19990517)81:4<560::aid-ijc10>3.0.co;2-7 (1999).

241 Kucharzewska, P., Welch, J. E., Svensson, K. J. & Belting, M. Ornithine decarboxylase and extracellular polyamines regulate microvascular sprouting and actin cytoskeleton dynamics in endothelial cells. *Exp Cell Res* **316**, 2683-2691, doi:10.1016/j.yexcr.2010.05.033 (2010).

242 Jasnis, M. A. *et al.* Polyamines prevent DFMO-mediated inhibition of angiogenesis. *Cancer Lett* **79**, 39-43, doi:10.1016/0304-3835(94)90060-4 (1994).

243 Takigawa, M. *et al.* Tumor angiogenesis and polyamines: alpha-difluoromethylornithine, an irreversible inhibitor of ornithine decarboxylase, inhibits B16 melanoma-induced angiogenesis in ovo and the proliferation of vascular endothelial cells in vitro. *Cancer Res* **50**, 4131-4138 (1990).

244 Huynh, F. K., Green, M. F., Koves, T. R. & Hirschey, M. D. Measurement of fatty acid oxidation rates in animal tissues and cell lines. *Methods Enzymol* **542**, 391-405, doi:10.1016/B978-0-12-416618-9.00020-0 (2014).

245 Ades, E. W. *et al.* HMEC-1: establishment of an immortalized human microvascular endothelial cell line. *J Invest Dermatol* **99**, 683-690, doi:10.1111/1523-1747.ep12613748 (1992).

246 Gospodarowicz, D., Moran, J., Braun, D. & Birdwell, C. Clonal growth of bovine vascular endothelial cells: fibroblast growth factor as a survival agent. *Proc Natl Acad Sci U S A* **73**, 4120-4124, doi:10.1073/pnas.73.11.4120 (1976).

247 Kubota, Y., Kleinman, H. K., Martin, G. R. & Lawley, T. J. Role of laminin and basement membrane in the morphological differentiation of human endothelial cells into capillary-like structures. *J Cell Biol* **107**, 1589-1598, doi:10.1083/jcb.107.4.1589 (1988).

248 Taberner, L., Banon, A. & Alsina, B. Anatomical map of the cranial vasculature and sensory ganglia. *J Anat* **232**, 431-439, doi:10.1111/joa.12762 (2018).

249 Mosmann, T. Rapid colorimetric assay for cellular growth and survival: application to proliferation and cytotoxicity assays. *J Immunol Methods* **65**, 55-63, doi:10.1016/0022-1759(83)90303-4 (1983).

250 Yue, T. L. *et al.* 2-Methoxyestradiol, an endogenous estrogen metabolite, induces apoptosis in endothelial cells and inhibits angiogenesis: possible role for stress-activated protein kinase signaling pathway and Fas expression. *Mol Pharmacol* **51**, 951-962, doi:10.1124/mol.51.6.951 (1997).

251 Nowak-Sliwinska, P. *et al.* Consensus guidelines for the use and interpretation of angiogenesis assays. *Angiogenesis* **21**, 425-532, doi:10.1007/s10456-018-9613-x (2018).

252 Benton, G., Arnaoutova, I., George, J., Kleinman, H. K. & Koblinski, J. Matrigel: from discovery and ECM mimicry to assays and models for cancer research. *Adv Drug Deliv Rev* **79-80**, 3-18, doi:10.1016/j.addr.2014.06.005 (2014).

253 Hendrix, M. J., Seftor, E. A., Seftor, R. E. & Fidler, I. J. A simple quantitative assay for studying the invasive potential of high and low human metastatic variants. *Cancer Lett* **38**, 137-147, doi:10.1016/0304-3835(87)90209-6 (1987).

254 Oikawa, T. *et al.* Inhibition of angiogenesis by staurosporine, a potent protein kinase inhibitor. *J Antibiot (Tokyo)* **45**, 1155-1160, doi:10.7164/antibiotics.45.1155 (1992).

255 Vincent, L. *et al.* Combretastatin A4 phosphate induces rapid regression of tumor neovessels and growth through interference with vascular endothelial-cadherin signaling. *J Clin Invest* **115**, 2992-3006, doi:10.1172/JCI24586 (2005).

256 Schreier, T., Degen, E. & Baschong, W. Fibroblast migration and proliferation during in vitro wound healing. A quantitative comparison between various growth factors and a low molecular weight blood dialysate used in the clinic to normalize impaired wound healing. *Res Exp Med (Berl)* **193**, 195-205, doi:10.1007/bf02576227 (1993).

257 Sun, L. *et al.* Discovery of 5-[5-fluoro-2-oxo-1,2- dihydroindol-(3Z)-ylidenemethyl]-2,4- dimethyl-1H-pyrrole-3-carboxylic acid (2-diethylaminoethyl)amide, a novel tyrosine kinase inhibitor targeting vascular endothelial and platelet-derived growth factor receptor tyrosine kinase. *J Med Chem* **46**, 1116-1119, doi:10.1021/jm0204183 (2003).

258 Mendel, D. B. *et al.* In vivo antitumor activity of SU11248, a novel tyrosine kinase inhibitor targeting vascular endothelial growth factor and platelet-derived growth factor receptors: determination of a pharmacokinetic/pharmacodynamic relationship. *Clin Cancer Res* **9**, 327-337 (2003).

259 Zhang, J. *et al.* Measuring energy metabolism in cultured cells, including human pluripotent stem cells and differentiated cells. *Nat Protoc* **7**, 1068-1085, doi:10.1038/nprot.2012.048 (2012).

260 Zou, C., Wang, Y. & Shen, Z. 2-NBDG as a fluorescent indicator for direct glucose uptake measurement. *J Biochem Biophys Methods* **64**, 207-215, doi:10.1016/j.jbbm.2005.08.001 (2005).

261 Dubikovskaya, E., Chudnovskiy, R., Karateev, G., Park, H. M. & Stahl, A. Measurement of long-chain fatty acid uptake into adipocytes. *Methods Enzymol* **538**, 107-134, doi:10.1016/B978-0-12-800280-3.00007-4 (2014).

262 Ruiz-Perez, M. V., Medina, M. A., Urdiales, J. L., Keinanen, T. A. & Sanchez-Jimenez, F. Polyamine metabolism is sensitive to glycolysis inhibition in human neuroblastoma cells. *J Biol Chem* **290**, 6106-6119, doi:10.1074/jbc.M114.619197 (2015).

263 Ribatti, D. The chick embryo chorioallantoic membrane (CAM). A multifaceted experimental model. *Mech Dev* **141**, 70-77, doi:10.1016/j.mod.2016.05.003 (2016).

264 Garcia-Caballero, M., Quesada, A. R., Medina, M. A. & Mari-Beffa, M. Fishing anti(lymph)angiogenic drugs with zebrafish. *Drug Discov Today* **23**, 366-374, doi:10.1016/j.drudis.2017.10.018 (2018).

265 Gemberling, M., Bailey, T. J., Hyde, D. R. & Poss, K. D. The zebrafish as a model for complex tissue regeneration. *Trends Genet* **29**, 611-620, doi:10.1016/j.tig.2013.07.003 (2013).

266 DeSantis, C. E. *et al.* Breast cancer statistics, 2015: Convergence of incidence rates between black and white women. *CA Cancer J Clin* **66**, 31-42, doi:10.3322/caac.21320 (2016).

267 Perou, C. M. *et al.* Molecular portraits of human breast tumours. *Nature* **406**, 747-752, doi:10.1038/35021093 (2000).

268 Foulkes, W. D., Smith, I. E. & Reis-Filho, J. S. Triple-negative breast cancer. *N Engl J Med* **363**, 1938-1948, doi:10.1056/NEJMra1001389 (2010).

269 Brouckaert, O., Wildiers, H., Floris, G. & Neven, P. Update on triple-negative breast cancer: prognosis and management strategies. *Int J Womens Health* **4**, 511-520, doi:10.2147/IJWH.S18541 (2012).

270 Kulkoyluoglu-Cotul, E., Arca, A. & Madak-Erdogan, Z. Crosstalk between Estrogen Signaling and Breast Cancer Metabolism. *Trends Endocrinol Metab* **30**, 25-38, doi:10.1016/j.tem.2018.10.006 (2019).

271 Gaglio, D. *et al.* Oncogenic K-Ras decouples glucose and glutamine metabolism to support cancer cell growth. *Mol Syst Biol* **7**, 523, doi:10.1038/msb.2011.56 (2011).

272 Hardy, S. *et al.* Saturated fatty acid-induced apoptosis in MDA-MB-231 breast cancer cells. A role for cardiolipin. *J Biol Chem* **278**, 31861-31870, doi:10.1074/jbc.M300190200 (2003).

273 Antalis, C. J., Uchida, A., Buhman, K. K. & Siddiqui, R. A. Migration of MDA-MB-231 breast cancer cells depends on the availability of exogenous lipids and cholesterol esterification. *Clin Exp Metastasis* **28**, 733-741, doi:10.1007/s10585-011-9405-9 (2011).

274 Mayers, J. R. & Vander Heiden, M. G. Famine versus feast: understanding the metabolism of tumors in vivo. *Trends Biochem Sci* **40**, 130-140, doi:10.1016/j.tibs.2015.01.004 (2015).

275 Hardy, S., Langelier, Y. & Prentki, M. Oleate activates phosphatidylinositol 3-kinase and promotes proliferation and reduces apoptosis of MDA-MB-231 breast cancer cells, whereas palmitate has opposite effects. *Cancer Res* **60**, 6353-6358 (2000).

276 Visagie, M. H. *et al.* Influence of partial and complete glutamine-and glucose deprivation of breast-and cervical tumorigenic cell lines. *Cell Biosci* **5**, 37, doi:10.1186/s13578-015-0030-1 (2015).

277 Korangath, P. *et al.* Targeting Glutamine Metabolism in Breast Cancer with Aminooxyacetate. *Clin Cancer Res* **21**, 3263-3273, doi:10.1158/1078-0432.CCR-14-1200 (2015).

278 Fu, Y. M. *et al.* Specific amino acid restriction inhibits attachment and spreading of human melanoma via modulation of the integrin/focal adhesion kinase pathway and actin cytoskeleton remodeling. *Clin Exp Metastasis* **21**, 587-598, doi:10.1007/s10585-004-5515-y (2004).

279 Mares-Perlman, J. A. & Shrago, E. Energy substrate utilization in freshly isolated Morris Hepatoma 7777 cells. *Cancer Res* **48**, 602-608 (1988).

280 Bloch-Frankenthal, L., Langan, J., Morris, H. P. & Weinhouse, S. Fatty Acid Oxidation and Ketogenesis in Transplantable Liver Tumors. *Cancer Res* **25**, 732-736 (1965).

281 Caro, P. *et al.* Metabolic signatures uncover distinct targets in molecular subsets of diffuse large B cell lymphoma. *Cancer Cell* **22**, 547-560, doi:10.1016/j.ccr.2012.08.014 (2012).

282 Deberardinis, R. J., Lum, J. J. & Thompson, C. B. Phosphatidylinositol 3-kinase-dependent modulation of carnitine palmitoyltransferase 1A expression

regulates lipid metabolism during hematopoietic cell growth. *J Biol Chem* **281**, 37372-37380, doi:10.1074/jbc.M608372200 (2006).

283 Arora, R. *et al.* Inhibition of the Warburg effect with a natural compound reveals a novel measurement for determining the metastatic potential of breast cancers. *Oncotarget* **6**, 662-678, doi:10.18632/oncotarget.2689 (2015).

284 Mookerjee, S. A., Goncalves, R. L. S., Gerencser, A. A., Nicholls, D. G. & Brand, M. D. The contributions of respiration and glycolysis to extracellular acid production. *Biochim Biophys Acta* **1847**, 171-181, doi:10.1016/j.bbabio.2014.10.005 (2015).

285 Helmlinger, G., Sckell, A., Dellian, M., Forbes, N. S. & Jain, R. K. Acid production in glycolysis-impaired tumors provides new insights into tumor metabolism. *Clin Cancer Res* **8**, 1284-1291 (2002).

286 DeBerardinis, R. J. *et al.* Beyond aerobic glycolysis: transformed cells can engage in glutamine metabolism that exceeds the requirement for protein and nucleotide synthesis. *Proc Natl Acad Sci U S A* **104**, 19345-19350, doi:10.1073/pnas.0709747104 (2007).

287 Vander Heiden, M. G., Cantley, L. C. & Thompson, C. B. Understanding the Warburg effect: the metabolic requirements of cell proliferation. *Science* **324**, 1029-1033, doi:10.1126/science.1160809 (2009).

288 Spector, A. A. & Steinberg, D. Relationship between fatty acid and glucose utilization in Ehrlich ascites tumor cells. *J Lipid Res* **7**, 657-663 (1966).

289 Nath, A., Li, I., Roberts, L. R. & Chan, C. Elevated free fatty acid uptake via CD36 promotes epithelial-mesenchymal transition in hepatocellular carcinoma. *Sci Rep* **5**, 14752, doi:10.1038/srep14752 (2015).

290 Binker-Cosen, M. J. *et al.* Palmitic acid increases invasiveness of pancreatic cancer cells AsPC-1 through TLR4/ROS/NF-kappaB/MMP-9 signaling pathway. *Biochem Biophys Res Commun* **484**, 152-158, doi:10.1016/j.bbrc.2017.01.051 (2017).

291 Turcotte, L. P., Raney, M. A. & Todd, M. K. ERK1/2 inhibition prevents contraction-induced increase in plasma membrane FAT/CD36 content and FA uptake in rodent muscle. *Acta Physiol Scand* **184**, 131-139, doi:10.1111/j.1365-201X.2005.01445.x (2005).

292 Uray, I. P., Liang, Y. & Hyder, S. M. Estradiol down-regulates CD36 expression in human breast cancer cells. *Cancer Lett* **207**, 101-107, doi:10.1016/j.canlet.2003.10.021 (2004).

293 Kannan-Thulasiraman, P., Seachrist, D. D., Mahabeleshwar, G. H., Jain, M. K. & Noy, N. Fatty acid-binding protein 5 and PPARbeta/delta are critical mediators of epidermal growth factor receptor-induced carcinoma cell growth. *J Biol Chem* **285**, 19106-19115, doi:10.1074/jbc.M109.099770 (2010).

294 Pellon-Maison, M. *et al.* Glycerol-3-phosphate acyltranferase-2 behaves as a cancer testis gene and promotes growth and tumorigenicity of the breast cancer MDA-MB-231 cell line. *PLoS One* **9**, e100896, doi:10.1371/journal.pone.0100896 (2014).

295 Mracek, T., Drahota, Z. & Houstek, J. The function and the role of the mitochondrial glycerol-3-phosphate dehydrogenase in mammalian tissues. *Biochim Biophys Acta* **1827**, 401-410, doi:10.1016/j.bbabio.2012.11.014 (2013).

296 Cattaneo, E. R. *et al.* Glycerol-3-phosphate acyltransferase 2 expression modulates cell roughness and membrane permeability: An atomic force microscopy study. *PLoS One* **12**, e0189031, doi:10.1371/journal.pone.0189031 (2017).

297 Lane, A. N. *et al.* Probing the metabolic phenotype of breast cancer cells by multiple tracer stable isotope resolved metabolomics. *Metab Eng* **43**, 125-136, doi:10.1016/j.ymben.2017.01.010 (2017).
298 Balaban, S. *et al.* Heterogeneity of fatty acid metabolism in breast cancer cells underlies differential sensitivity to palmitate-induced apoptosis. *Mol Oncol* **12**, 1623-1638, doi:10.1002/1878-0261.12368 (2018).
299 Hopperton, K. E., Duncan, R. E., Bazinet, R. P. & Archer, M. C. Fatty acid synthase plays a role in cancer metabolism beyond providing fatty acids for phospholipid synthesis or sustaining elevations in glycolytic activity. *Exp Cell Res* **320**, 302-310, doi:10.1016/j.yexcr.2013.10.016 (2014).
300 Przybytkowski, E. *et al.* Upregulation of cellular triacylglycerol - free fatty acid cycling by oleate is associated with long-term serum-free survival of human breast cancer cells. *Biochem Cell Biol* **85**, 301-310, doi:10.1139/o07-001 (2007).
301 Schoors, S. *et al.* Partial and transient reduction of glycolysis by PFKFB3 blockade reduces pathological angiogenesis. *Cell Metab* **19**, 37-48, doi:10.1016/j.cmet.2013.11.008 (2014).
302 Koziel, A., Woyda-Ploszczyca, A., Kicinska, A. & Jarmuszkiewicz, W. The influence of high glucose on the aerobic metabolism of endothelial EA.hy926 cells. *Pflugers Arch* **464**, 657-669, doi:10.1007/s00424-012-1156-1 (2012).
303 Loader, J. *et al.* Acute Hyperglycemia Impairs Vascular Function in Healthy and Cardiometabolic Diseased Subjects: Systematic Review and Meta-Analysis. *Arterioscler Thromb Vasc Biol* **35**, 2060-2072, doi:10.1161/ATVBAHA.115.305530 (2015).
304 Heeneman, S., Deutz, N. E. & Buurman, W. A. The concentrations of glutamine and ammonia in commercially available cell culture media. *J Immunol Methods* **166**, 85-91, doi:10.1016/0022-1759(93)90331-z (1993).
305 Karbach, S. *et al.* Hyperglycemia and oxidative stress in cultured endothelial cells--a comparison of primary endothelial cells with an immortalized endothelial cell line. *J Diabetes Complications* **26**, 155-162, doi:10.1016/j.jdiacomp.2012.03.011 (2012).
306 Zhang, J., Shan, Y., Li, Y., Luo, X. & Shi, H. Palmitate impairs angiogenesis via suppression of cathepsin activity. *Mol Med Rep* **15**, 3644-3650, doi:10.3892/mmr.2017.6463 (2017).
307 Geng, Y. *et al.* Protective effect of metformin against palmitate-induced hepatic cell death. *Biochim Biophys Acta Mol Basis Dis*, 165621, doi:10.1016/j.bbadis.2019.165621 (2019).
308 Haywood, J. & Yammani, R. R. Free fatty acid palmitate activates unfolded protein response pathway and promotes apoptosis in meniscus cells. *Osteoarthritis Cartilage* **24**, 942-945, doi:10.1016/j.joca.2015.11.020 (2016).
309 Du, J. Y. *et al.* Suppression of Kv1.5 protects against endothelial apoptosis induced by palmitate and in type 2 diabetes mice. *Life Sci* **168**, 28-37, doi:10.1016/j.lfs.2015.12.054 (2017).
310 Kim, D. H., Cho, Y. M., Lee, K. H., Jeong, S. W. & Kwon, O. J. Oleate protects macrophages from palmitate-induced apoptosis through the downregulation of CD36 expression. *Biochem Biophys Res Commun* **488**, 477-482, doi:10.1016/j.bbrc.2017.05.066 (2017).
311 Yamagishi, S. *et al.* Palmitate-induced apoptosis of microvascular endothelial cells and pericytes. *Mol Med* **8**, 179-184 (2002).

312 Sera, R. K., McBride, J. H., Higgins, S. A. & Rodgerson, D. O. Evaluation of reference ranges for fatty acids in serum. *J Clin Lab Anal* **8**, 81-85, doi:10.1002/jcla.1860080205 (1994).
313 Abdelmagid, S. A. *et al.* Comprehensive profiling of plasma fatty acid concentrations in young healthy Canadian adults. *PLoS One* **10**, e0116195, doi:10.1371/journal.pone.0116195 (2015).
314 Arreola, A., Cowey, C. L., Coloff, J. L., Rathmell, J. C. & Rathmell, W. K. HIF1alpha and HIF2alpha exert distinct nutrient preferences in renal cells. *PLoS One* **9**, e98705, doi:10.1371/journal.pone.0098705 (2014).
315 Fan, J. *et al.* Glutamine-driven oxidative phosphorylation is a major ATP source in transformed mammalian cells in both normoxia and hypoxia. *Mol Syst Biol* **9**, 712, doi:10.1038/msb.2013.65 (2013).
316 Birsoy, K. *et al.* An Essential Role of the Mitochondrial Electron Transport Chain in Cell Proliferation Is to Enable Aspartate Synthesis. *Cell* **162**, 540-551, doi:10.1016/j.cell.2015.07.016 (2015).
317 Sullivan, L. B. *et al.* Supporting Aspartate Biosynthesis Is an Essential Function of Respiration in Proliferating Cells. *Cell* **162**, 552-563, doi:10.1016/j.cell.2015.07.017 (2015).
318 Makita, J., Hosoya, K., Zhang, P. & Kador, P. F. Response of rat retinal capillary pericytes and endothelial cells to glucose. *J Ocul Pharmacol Ther* **27**, 7-15, doi:10.1089/jop.2010.0051 (2011).
319 Galluzzi, L., Pietrocola, F., Levine, B. & Kroemer, G. Metabolic control of autophagy. *Cell* **159**, 1263-1276, doi:10.1016/j.cell.2014.11.006 (2014).
320 Samuel, S. M. *et al.* Metformin represses glucose starvation induced autophagic response in microvascular endothelial cells and promotes cell death. *Biochem Pharmacol* **132**, 118-132, doi:10.1016/j.bcp.2017.03.001 (2017).
321 Schaaf, M. B., Keulers, T. G., Vooijs, M. A. & Rouschop, K. M. LC3/GABARAP family proteins: autophagy-(un)related functions. *FASEB J* **30**, 3961-3978, doi:10.1096/fj.201600698R (2016).
322 Culic, O., Decking, U. K. & Schrader, J. Metabolic adaptation of endothelial cells to substrate deprivation. *Am J Physiol* **276**, C1061-1068, doi:10.1152/ajpcell.1999.276.5.C1061 (1999).
323 Artwohl, M. *et al.* Insulin does not regulate glucose transport and metabolism in human endothelium. *Eur J Clin Invest* **37**, 643-650, doi:10.1111/j.1365-2362.2007.01838.x (2007).
324 Marchut, E., Guminska, M. & Kedryna, T. The inhibitory effect of various fatty acids on aerobic glycolysis in Ehrlich ascites tumour cells. *Acta Biochim Pol* **33**, 7-16 (1986).
325 Medina, M. A. *et al.* Glutamine and glucose as energy substrates for Ehrlich ascites tumour cells. *Biochem Int* **16**, 339-347 (1988).
326 Medina, M. A., Sanchez-Jimenez, F., Quesada, A. R., Marquez, F. J. & Nunez de Castro, I. Effect of palmitate, acetate and glucose on glutamine metabolism in Ehrlich ascites tumor cells. *Biochimie* **70**, 833-834, doi:10.1016/0300-9084(88)90114-9 (1988).
327 Spahr, R., Krutzfeldt, A., Mertens, S., Siegmund, B. & Piper, H. M. Fatty acids are not an important fuel for coronary microvascular endothelial cells. *Mol Cell Biochem* **88**, 59-64, doi:10.1007/bf00223424 (1989).
328 Dagher, Z., Ruderman, N., Tornheim, K. & Ido, Y. Acute regulation of fatty acid oxidation and amp-activated protein kinase in human umbilical vein endothelial cells. *Circ Res* **88**, 1276-1282, doi:10.1161/hh1201.092998 (2001).

329 Rattigan, Y. I. *et al.* Lactate is a mediator of metabolic cooperation between stromal carcinoma associated fibroblasts and glycolytic tumor cells in the tumor microenvironment. *Exp Cell Res* **318**, 326-335, doi:10.1016/j.yexcr.2011.11.014 (2012).

330 Romero-Garcia, S., Moreno-Altamirano, M. M., Prado-Garcia, H. & Sanchez-Garcia, F. J. Lactate Contribution to the Tumor Microenvironment: Mechanisms, Effects on Immune Cells and Therapeutic Relevance. *Front Immunol* **7**, 52, doi:10.3389/fimmu.2016.00052 (2016).

331 Kishimoto, A., Takahashi-Iwanaga, H., Watanabe, M. M. & Iwanaga, T. Differential expression of endothelial nutrient transporters (MCT1 and GLUT1) in the developing eyes of mice. *Exp Eye Res* **153**, 170-177, doi:10.1016/j.exer.2016.10.019 (2016).

332 Miranda-Goncalves, V. *et al.* Monocarboxylate transporter 1 is a key player in glioma-endothelial cell crosstalk. *Mol Carcinog* **56**, 2630-2642, doi:10.1002/mc.22707 (2017).

333 Kennedy, K. M. *et al.* Catabolism of exogenous lactate reveals it as a legitimate metabolic substrate in breast cancer. *PLoS One* **8**, e75154, doi:10.1371/journal.pone.0075154 (2013).

334 Ullah, M. S., Davies, A. J. & Halestrap, A. P. The plasma membrane lactate transporter MCT4, but not MCT1, is up-regulated by hypoxia through a HIF-1alpha-dependent mechanism. *J Biol Chem* **281**, 9030-9037, doi:10.1074/jbc.M511397200 (2006).

335 Saraswati, S., Guo, Y., Atkinson, J. & Young, P. P. Prolonged hypoxia induces monocarboxylate transporter-4 expression in mesenchymal stem cells resulting in a secretome that is deleterious to cardiovascular repair. *Stem Cells* **33**, 1333-1344, doi:10.1002/stem.1935 (2015).

336 Lopes-Coelho, F. *et al.* Monocarboxylate transporter 1 (MCT1), a tool to stratify acute myeloid leukemia (AML) patients and a vehicle to kill cancer cells. *Oncotarget* **8**, 82803-82823, doi:10.18632/oncotarget.20294 (2017).

337 Halestrap, A. P. The SLC16 gene family - structure, role and regulation in health and disease. *Mol Aspects Med* **34**, 337-349, doi:10.1016/j.mam.2012.05.003 (2013).

338 Lang, I. *et al.* Heterogeneity of microvascular endothelial cells isolated from human term placenta and macrovascular umbilical vein endothelial cells. *Eur J Cell Biol* **82**, 163-173, doi:10.1078/0171-9335-00306 (2003).

339 Jackson, C. J. & Nguyen, M. Human microvascular endothelial cells differ from macrovascular endothelial cells in their expression of matrix metalloproteinases. *Int J Biochem Cell Biol* **29**, 1167-1177, doi:10.1016/s1357-2725(97)00061-7 (1997).

340 Wood, T. E. *et al.* A novel inhibitor of glucose uptake sensitizes cells to FAS-induced cell death. *Mol Cancer Ther* **7**, 3546-3555, doi:10.1158/1535-7163.MCT-08-0569 (2008).

341 Carriere, V. *et al.* Hypoxia and CYP1A1 induction-dependent regulation of proteins involved in glucose utilization in Caco-2 cells. *Am J Physiol* **274**, G1101-1108, doi:10.1152/ajpgi.1998.274.6.G1101 (1998).

342 Kraus, D. *et al.* Targeting glucose transport and the NAD pathway in tumor cells with STF-31: a re-evaluation. *Cell Oncol (Dordr)* **41**, 485-494, doi:10.1007/s13402-018-0385-5 (2018).

343 Fumarola, C. *et al.* Effects of sorafenib on energy metabolism in breast cancer cells: role of AMPK-mTORC1 signaling. *Breast Cancer Res Treat* **141**, 67-78, doi:10.1007/s10549-013-2668-x (2013).
344 Lu, J. *et al.* Corticotropin releasing hormone can selectively stimulate glucose uptake in corticotropinoma via glucose transporter 1. *Mol Cell Endocrinol* **470**, 105-114, doi:10.1016/j.mce.2017.10.003 (2018).
345 Zheng, P. P. *et al.* Glut1/SLC2A1 is crucial for the development of the blood-brain barrier in vivo. *Ann Neurol* **68**, 835-844, doi:10.1002/ana.22318 (2010).
346 Jensen, P. J., Gitlin, J. D. & Carayannopoulos, M. O. GLUT1 deficiency links nutrient availability and apoptosis during embryonic development. *J Biol Chem* **281**, 13382-13387, doi:10.1074/jbc.M601881200 (2006).
347 Zheng, P. P., van der Spek, P. J., Dirven, C. M., Willemsen, R. & Kros, J. M. Sinus venosus defect (SVD) identified in zebrafish Glut1 morphants by video imaging. *Int J Cardiol* **154**, e60-61, doi:10.1016/j.ijcard.2011.06.029 (2012).
348 Song, G., Ouyang, G. & Bao, S. The activation of Akt/PKB signaling pathway and cell survival. *J Cell Mol Med* **9**, 59-71, doi:10.1111/j.1582-4934.2005.tb00337.x (2005).
349 Beg, M., Abdullah, N., Thowfeik, F. S., Altorki, N. K. & McGraw, T. E. Distinct Akt phosphorylation states are required for insulin regulated Glut4 and Glut1-mediated glucose uptake. *Elife* **6**, doi:10.7554/eLife.26896 (2017).
350 Basu, S., Hubbard, B. & Shevach, E. M. Foxp3-mediated inhibition of Akt inhibits Glut1 (glucose transporter 1) expression in human T regulatory cells. *J Leukoc Biol* **97**, 279-283, doi:10.1189/jlb.2AB0514-273RR (2015).
351 Hammer, A. *et al.* The NRF2 pathway as potential biomarker for dimethyl fumarate treatment in multiple sclerosis. *Ann Clin Transl Neurol* **5**, 668-676, doi:10.1002/acn3.553 (2018).
352 Schulze-Topphoff, U. *et al.* Dimethyl fumarate treatment induces adaptive and innate immune modulation independent of Nrf2. *Proc Natl Acad Sci U S A* **113**, 4777-4782, doi:10.1073/pnas.1603907113 (2016).
353 Linker, R. A. & Haghikia, A. Dimethyl fumarate in multiple sclerosis: latest developments, evidence and place in therapy. *Ther Adv Chronic Dis* **7**, 198-207, doi:10.1177/2040622316653307 (2016).
354 Mrowietz, U. *et al.* Clinical use of dimethyl fumarate in moderate-to-severe plaque-type psoriasis: a European expert consensus. *J Eur Acad Dermatol Venereol* **32 Suppl 3**, 3-14, doi:10.1111/jdv.15218 (2018).
355 Nestle, F. O., Kaplan, D. H. & Barker, J. Psoriasis. *N Engl J Med* **361**, 496-509, doi:10.1056/NEJMra0804595 (2009).
356 Peng, H. *et al.* Dimethyl fumarate inhibits dendritic cell maturation via nuclear factor kappaB (NF-kappaB) and extracellular signal-regulated kinase 1 and 2 (ERK1/2) and mitogen stress-activated kinase 1 (MSK1) signaling. *J Biol Chem* **287**, 28017-28026, doi:10.1074/jbc.M112.383380 (2012).
357 Loewe, R. *et al.* Dimethylfumarate inhibits TNF-induced nuclear entry of NF-kappa B/p65 in human endothelial cells. *J Immunol* **168**, 4781-4787, doi:10.4049/jimmunol.168.9.4781 (2002).
358 Heidenreich, R., Rocken, M. & Ghoreschi, K. Angiogenesis drives psoriasis pathogenesis. *Int J Exp Pathol* **90**, 232-248, doi:10.1111/j.1365-2613.2009.00669.x (2009).
359 Meissner, M. *et al.* Suppression of VEGFR2 expression in human endothelial cells by dimethylfumarate treatment: evidence for anti-angiogenic action. *J Invest Dermatol* **131**, 1356-1364, doi:10.1038/jid.2011.46 (2011).

360 Huang, Y., Mao, Y., Li, H., Shen, G. & Nan, G. Knockdown of Nrf2 inhibits angiogenesis by downregulating VEGF expression through PI3K/Akt signaling pathway in cerebral microvascular endothelial cells under hypoxic conditions. *Biochem Cell Biol* **96**, 475-482, doi:10.1139/bcb-2017-0291 (2018).

361 Florczyk, U. *et al.* Nrf2 regulates angiogenesis: effect on endothelial cells, bone marrow-derived proangiogenic cells and hind limb ischemia. *Antioxid Redox Signal* **20**, 1693-1708, doi:10.1089/ars.2013.5219 (2014).

362 Wei, Y. *et al.* Nrf2 acts cell-autonomously in endothelium to regulate tip cell formation and vascular branching. *Proc Natl Acad Sci U S A* **110**, E3910-3918, doi:10.1073/pnas.1309276110 (2013).

363 Arbiser, J. L. Fumarate esters as angiogenesis inhibitors: key to action in psoriasis? *J Invest Dermatol* **131**, 1189-1191, doi:10.1038/jid.2011.45 (2011).

364 Yates, M. S. *et al.* Genetic versus chemoprotective activation of Nrf2 signaling: overlapping yet distinct gene expression profiles between Keap1 knockout and triterpenoid-treated mice. *Carcinogenesis* **30**, 1024-1031, doi:10.1093/carcin/bgp100 (2009).

365 Mitsuishi, Y. *et al.* Nrf2 redirects glucose and glutamine into anabolic pathways in metabolic reprogramming. *Cancer Cell* **22**, 66-79, doi:10.1016/j.ccr.2012.05.016 (2012).

366 Kornberg, M. D. *et al.* Dimethyl fumarate targets GAPDH and aerobic glycolysis to modulate immunity. *Science* **360**, 449-453, doi:10.1126/science.aan4665 (2018).

367 Diebold, M. *et al.* Dimethyl fumarate influences innate and adaptive immunity in multiple sclerosis. *J Autoimmun* **86**, 39-50, doi:10.1016/j.jaut.2017.09.009 (2018).

368 Ahuja, M. *et al.* Distinct Nrf2 Signaling Mechanisms of Fumaric Acid Esters and Their Role in Neuroprotection against 1-Methyl-4-Phenyl-1,2,3,6-Tetrahydropyridine-Induced Experimental Parkinson's-Like Disease. *J Neurosci* **36**, 6332-6351, doi:10.1523/JNEUROSCI.0426-16.2016 (2016).

369 Foresti, R. *et al.* Nrf2 activators modulate oxidative stress responses and bioenergetic profiles of human retinal epithelial cells cultured in normal or high glucose conditions. *Pharmacol Res* **99**, 296-307, doi:10.1016/j.phrs.2015.07.006 (2015).

370 Kuosmanen, S. M. *et al.* NRF2 regulates endothelial glycolysis and proliferation with miR-93 and mediates the effects of oxidized phospholipids on endothelial activation. *Nucleic Acids Res* **46**, 1124-1138, doi:10.1093/nar/gkx1155 (2018).

371 Vizcaino, J. A. *et al.* ProteomeXchange provides globally coordinated proteomics data submission and dissemination. *Nat Biotechnol* **32**, 223-226, doi:10.1038/nbt.2839 (2014).

372 Koivunen, P. *et al.* Inhibition of hypoxia-inducible factor (HIF) hydroxylases by citric acid cycle intermediates: possible links between cell metabolism and stabilization of HIF. *J Biol Chem* **282**, 4524-4532, doi:10.1074/jbc.M610415200 (2007).

373 Babicki, S. *et al.* Heatmapper: web-enabled heat mapping for all. *Nucleic Acids Res* **44**, W147-153, doi:10.1093/nar/gkw419 (2016).

374 Ravez, S., Spillier, Q., Marteau, R., Feron, O. & Frederick, R. Challenges and Opportunities in the Development of Serine Synthetic Pathway Inhibitors for Cancer Therapy. *J Med Chem* **60**, 1227-1237, doi:10.1021/acs.jmedchem.6b01167 (2017).

375 Possemato, R. *et al.* Functional genomics reveal that the serine synthesis pathway is essential in breast cancer. *Nature* **476**, 346-350, doi:10.1038/nature10350 (2011).
376 DeNicola, G. M. *et al.* NRF2 regulates serine biosynthesis in non-small cell lung cancer. *Nat Genet* **47**, 1475-1481, doi:10.1038/ng.3421 (2015).
377 Liu, S. *et al.* Glyceraldehyde-3-phosphate dehydrogenase promotes liver tumorigenesis by modulating phosphoglycerate dehydrogenase. *Hepatology* **66**, 631-645, doi:10.1002/hep.29202 (2017).
378 Ou, Y., Wang, S. J., Jiang, L., Zheng, B. & Gu, W. p53 Protein-mediated regulation of phosphoglycerate dehydrogenase (PHGDH) is crucial for the apoptotic response upon serine starvation. *J Biol Chem* **290**, 457-466, doi:10.1074/jbc.M114.616359 (2015).
379 Ma, L. *et al.* Control of nutrient stress-induced metabolic reprogramming by PKCzeta in tumorigenesis. *Cell* **152**, 599-611, doi:10.1016/j.cell.2012.12.028 (2013).
380 Frycak, P., Zdrahal, Z., Ulrichova, J., Wiegrebe, W. & Lemr, K. Evidence of covalent interaction of fumaric acid esters with sulfhydryl groups in peptides. *J Mass Spectrom* **40**, 1309-1318, doi:10.1002/jms.910 (2005).
381 Saidu, N. E. B. *et al.* Dimethyl fumarate, a two-edged drug: Current status and future directions. *Med Res Rev* **39**, 1923-1952, doi:10.1002/med.21567 (2019).
382 Bar-Peled, L. *et al.* Chemical Proteomics Identifies Druggable Vulnerabilities in a Genetically Defined Cancer. *Cell* **171**, 696-709 e623, doi:10.1016/j.cell.2017.08.051 (2017).
383 Hitzel, J. *et al.* Oxidized phospholipids regulate amino acid metabolism through MTHFD2 to facilitate nucleotide release in endothelial cells. *Nat Commun* **9**, 2292, doi:10.1038/s41467-018-04602-0 (2018).
384 Oh, C. J. *et al.* Dimethylfumarate attenuates restenosis after acute vascular injury by cell-specific and Nrf2-dependent mechanisms. *Redox Biol* **2**, 855-864, doi:10.1016/j.redox.2014.06.003 (2014).
385 Kalhan, S. C. & Hanson, R. W. Resurgence of serine: an often neglected but indispensable amino Acid. *J Biol Chem* **287**, 19786-19791, doi:10.1074/jbc.R112.357194 (2012).
386 Ducker, G. S. *et al.* Human SHMT inhibitors reveal defective glycine import as a targetable metabolic vulnerability of diffuse large B-cell lymphoma. *Proc Natl Acad Sci U S A* **114**, 11404-11409, doi:10.1073/pnas.1706617114 (2017).
387 Fang, J. *et al.* Dihydro-orotate dehydrogenase is physically associated with the respiratory complex and its loss leads to mitochondrial dysfunction. *Biosci Rep* **33**, e00021, doi:10.1042/BSR20120097 (2013).
388 Kavian, N. *et al.* The Nrf2-Antioxidant Response Element Signaling Pathway Controls Fibrosis and Autoimmunity in Scleroderma. *Front Immunol* **9**, 1896, doi:10.3389/fimmu.2018.01896 (2018).
389 Brennan, M. S. *et al.* Dimethyl fumarate and monoethyl fumarate exhibit differential effects on KEAP1, NRF2 activation, and glutathione depletion in vitro. *PLoS One* **10**, e0120254, doi:10.1371/journal.pone.0120254 (2015).
390 Held, K. D., Epp, E. R., Clark, E. P. & Biaglow, J. E. Effect of dimethyl fumarate on the radiation sensitivity of mammalian cells in vitro. *Radiat Res* **115**, 495-502 (1988).
391 Schmidt, T. J., Ak, M. & Mrowietz, U. Reactivity of dimethyl fumarate and methylhydrogen fumarate towards glutathione and N-acetyl-L-cysteine--

preparation of S-substituted thiosuccinic acid esters. *Bioorg Med Chem* **15**, 333-342, doi:10.1016/j.bmc.2006.09.053 (2007).

392 Ghashghaeinia, M. *et al.* Pharmacological targeting of glucose-6-phosphate dehydrogenase in human erythrocytes by Bay 11-7082, parthenolide and dimethyl fumarate. *Sci Rep* **6**, 28754, doi:10.1038/srep28754 (2016).

393 Odom, R. Y., Dansby, M. Y., Rollins-Hairston, A. M., Jackson, K. M. & Kirlin, W. G. Phytochemical induction of cell cycle arrest by glutathione oxidation and reversal by N-acetylcysteine in human colon carcinoma cells. *Nutr Cancer* **61**, 332-339, doi:10.1080/01635580802549982 (2009).

394 Han, G. & Zhou, Q. Dimethylfumarate induces cell cycle arrest and apoptosis via regulating intracellular redox systems in HeLa cells. *In Vitro Cell Dev Biol Anim* **52**, 1034-1041, doi:10.1007/s11626-016-0069-2 (2016).

395 Bennett Saidu, N. E. *et al.* Dimethyl fumarate is highly cytotoxic in KRAS mutated cancer cells but spares non-tumorigenic cells. *Oncotarget* **9**, 9088-9099, doi:10.18632/oncotarget.24144 (2018).

396 Boivin, A. *et al.* Transient alteration of cellular redox buffering before irradiation triggers apoptosis in head and neck carcinoma stem and non-stem cells. *PLoS One* **6**, e14558, doi:10.1371/journal.pone.0014558 (2011).

397 Bhargava, P. *et al.* Dimethyl fumarate treatment induces lipid metabolism alterations that are linked to immunological changes. *Ann Clin Transl Neurol* **6**, 33-45, doi:10.1002/acn3.676 (2019).

398 Sghaier, R. *et al.* Dimethyl fumarate and monomethyl fumarate attenuate oxidative stress and mitochondrial alterations leading to oxiapoptophagy in 158N murine oligodendrocytes treated with 7beta-hydroxycholesterol. *J Steroid Biochem Mol Biol* **194**, 105432, doi:10.1016/j.jsbmb.2019.105432 (2019).

APPENDICES

APPENDIX 1

The Mediterranean diet, a rich source of angiopreventive compounds in cancer

Beatriz Martínez-Poveda, José Antonio Torres-Vargas, **Mª Carmen Ocaña**, Melissa García-Caballero, Miguel Ángel Medina, Ana R. Quesada

Nutrients 11:2036 (2019)

DOI:10.3390/nu11092036

Review article

IF: 4.171, ranked 16/87 in Nutrients & Diabetics, Q1 in JCR2018

nutrients

MDPI

Review

The Mediterranean Diet, a Rich Source of Angiopreventive Compounds in Cancer

Beatriz Martínez-Poveda [1,2,*], José Antonio Torres-Vargas [1], María del Carmen Ocaña [1], Melissa García-Caballero [3,4], Miguel Ángel Medina [1,2,5] and Ana R. Quesada [1,2,5,*]

1 Department of Molecular Biology and Biochemistry, Faculty of Sciences, University of Málaga, Andalucía Tech, 29071 Málaga, Spain
2 IBIMA (Biomedical Research Institute of Málaga), 29071 Málaga, Spain
3 Laboratory of Angiogenesis and Vascular Metabolism, VIB Center for Cancer Biology, VIB, 3000 Leuven, Belgium
4 Laboratory of Angiogenesis and Vascular Metabolism, Department of Oncology, Leuven Cancer Institute, KU Leuven, 3000 Leuven, Belgium
5 CIBER of Rare Diseases, Group U741 (CB06/07/0046), 29071 Málaga, Spain
* Correspondence: bmpoveda@uma.es (B.M.-P.); quesada@uma.es (A.R.Q.); Tel.: +34-952131674 (B.M.-P.); +34-952137128 (A.R.Q.)

Received: 19 August 2019; Accepted: 25 August 2019; Published: 31 August 2019

APPENDIX 2

Metabolism in the tumor microenvironment: What is known about stromal and immune cells?

Mª Carmen Ocaña, Beatriz Martínez-Poveda, Ana R. Quesada, Miguel Ángel Medina.

Clinical Immunology, Endocrine & Metabolic Drugs 4:33-36 (2017)

DOI:10.2174/2212707004666170818164513

Review article

Not indexed journal

Clinical Immunology, Endocrine & Metabolic Drugs, 2017, *4*, 33-36

REVIEW ARTICLE

Metabolism in the Tumor Microenvironment: What is Known about Stromal and Immune Cells?

Mª Carmen Ocaña[1], Beatriz Martínez-Poveda[1], Ana R. Quesada[1,2] and Miguel Ángel Medina[1,2,*]

[1] *Departamento de Biología Molecular y Bioquímica, Facultad de Ciencias e IBIMA (instituto de Biomedicina de Málaga), Universidad de Málaga, Andalucía Tech, Málaga, Spain and* [2]*Unidad 741, CIBER de Enfermedades Raras (CIBERER), Málaga, Spain*

ARTICLE HISTORY

Received: December 07, 2016
Revised: June 05, 2017
Accepted: August 08, 2017

DOI:
10.2174/2212707004666170818164513

Abstract: ***Background***: In the 20th century, cancer metabolism has been studied from different aspects. In the last decade, the interest in this issue has been renewed and many studies have been carried out on tumor and endothelial metabolism. Although tumor metabolism is well recognized, there are some discrepancies between what we knew and what has been studied lately about the metabolism of endothelial cells. Moreover, cancer and endothelial cells are not alone in their microenvironment. Immune cells and fibroblasts are also present and have a crucial role in tumor-associated inflammation, as well as in tumor progression, metastasis and angiogenesis. Nevertheless, metabolism of these cells is poorly understood.

Conclusion: In the present mini-review, information about metabolic characteristics of these cells is summarized and compared with our knowledge about cancer and endothelial cell metabolism. This knowledge could contribute to open up innovative approaches to the treatment of cancer.

APPENDIX 3

Metabolism within the tumor microenvironment and its implication on cancer progression: An ongoing therapeutic target

Mª Carmen Ocaña, Beatriz Martínez-Poveda, Ana R. Quesada, Miguel Ángel Medina

Medicinal Research Reviews 39:70-113 (2019)

DOI:10.1002/med.21511

Review article

IF: 9.791, ranked 2/61 in Medicinal Chemistry, D1 in JCR2018

Received: 19 January 2018 | Revised: 30 April 2018 | Accepted: 1 May 2018

DOI: 10.1002/med.21511

WILEY

REVIEW ARTICLE

Metabolism within the tumor microenvironment and its implication on cancer progression: An ongoing therapeutic target

Mª Carmen Ocaña[1] | Beatriz Martínez-Poveda[1] | Ana R. Quesada[1,2] | Miguel Ángel Medina[1,2]

[1]Departamento de Biología Molecular y Bioquímica, Facultad de Ciencias, and IBIMA (Biomedical Research Institute of Málaga), Andalucía Tech, Universidad de Málaga, Málaga, Spain

[2]CIBER de Enfermedades Raras (CIBERER), Málaga, Spain

APPENDIX 4

Glucose favors lipid anabolic metabolism in the invasive breast cancer cell line MDA-MB-231

Mª Carmen Ocaña, Beatriz Martínez-Poveda, Ana R. Quesada, Miguel Ángel Medina

Biology 9(1), 16 (2020)

DOI:10.3390/biology9010016

Original research article

IF: 4.42, ranked 9/185 in General Agricultural and Biological Sciences, D1 in Scopus2018

biology

MDPI

Article

Glucose Favors Lipid Anabolic Metabolism in the Invasive Breast Cancer Cell Line MDA-MB-231

Mª Carmen Ocaña [1,2], Beatriz Martínez-Poveda [1,2], Ana R. Quesada [1,2,3] and Miguel Ángel Medina [1,2,3,*]

1 Departamento de Biología Molecular y Bioquímica, Facultad de Ciencias, Andalucía Tech, Universidad de Málaga, E-29071 Málaga, Spain; mc.ocanaf@gmail.com (M.C.O.); bmpoveda@uma.es (B.M.-P.); quesada@uma.es (A.R.Q.)
2 IBIMA (Biomedical Research Institute of Málaga), E-29071 Málaga, Spain
3 CIBER de Enfermedades Raras (CIBERER), E-29071 Málaga, Spain
* Correspondence: medina@uma.es; Tel.: +34-952137132

Received: 20 November 2019; Accepted: 9 January 2020; Published: 10 January 2020

check for updates

APPENDIX 5

Highly glycolytic immortalized human dermal microvascular endothelial cells are able to grow in glucose-starved conditions.

Mª Carmen Ocaña, Beatriz Martínez-Poveda, Ana R. Quesada, Miguel Ángel Medina

Biomolecules 9:332 (2019)

DOI:10.3390/biom9080332

Original research article

IF: 4.694, ranked 58/298 in Biochemistry & Molecular Biology, Q1 in JCR2018

biomolecules

MDPI

Article

Highly Glycolytic Immortalized Human Dermal Microvascular Endothelial Cells are Able to Grow in Glucose-Starved Conditions

Mª Carmen Ocaña [1,2], Beatriz Martínez-Poveda [1,2], Ana R. Quesada [1,2,3] and Miguel Ángel Medina [1,2,3,*]

[1] Universidad de Málaga, Andalucía Tech, Departamento de Biología Molecular y Bioquímica, Facultad de Ciencias, E-29071 Málaga, Spain
[2] IBIMA (Biomedical Research Institute of Málaga), E-29071 Málaga, Spain
[3] CIBER de Enfermedades Raras (CIBERER), E-29071 Málaga, Spain
* Correspondence: medina@uma.es; Tel.: +34 952137132

Received: 26 June 2019; Accepted: 30 July 2019; Published: 1 August 2019

APPENDIX 6

Fasentin diminishes endothelial cell proliferation, differentiation and invasion in a glucose metabolism-independent manner

Mª Carmen Ocaña, Beatriz Martínez-Poveda, Manuel Marí-Beffa, Ana R. Quesada, Miguel Ángel Medina

Manuscript

APPENDIX 7

The anti-angiogenic compound dimethyl fumarate inhibits the serine synthesis pathway and increases glycolysis in endothelial cells

Mª Carmen Ocaña, Chendong Yang, Beatriz Martínez-Poveda, Hieu S. Vu, Casimiro Cárdenas, José Antonio Torres-Vargas, Alba Subiri-Verdugo, Ralph DeBerardinis, Ana R. Quesada, Miguel Ángel Medina

Manuscript

APPENDIX 8

Proteins detected with the proteomics analysis in HMECs treated with 100 μM DMF for 24 h with an abundance ratio (DMF/DMSO) > 1.5 and p-value < 0.01.

Los datos contenidos en este anexo están sujetos a derechos de *copyright* por estar en vías de publicación.

APPENDIX 9

Proteins detected with the proteomics analysis in HMECs treated with 100 µM DMF for 24 h with an abundance ratio (DMF/DMSO) < 0.75 and p-value < 0.01.

Los datos contenidos en este anexo están sujetos a derechos de *copyright* por estar en vías de publicación.

APPENDIX 10

Results from the AbsoluteIDQ p180 kit (Biocrates) in HMECs treated with 100 µM for 16 h.